Investigating the Dissolution and Permeation Properties of Flufenamic Acid Cocrystals

PhD Thesis

Minshan Guo

This thesis is submitted in partial fulfilment of the requirements of De Montfort University for the award of Doctor of Philosophy

June 2018

Faculty of Health and Life Sciences

De Montfort University, Leicester

CONTENTS

DECLARATION

I declare that the words described in this thesis is original work undertaken by myself for the Doctor of Philosophy degree, at the School of Pharmacy, Faculty of Health and Life Sciences, De Montfort University, Leicester, United Kingdom.

No part of the material described in this thesis has been submitted for the award of any other degree or qualification in this or any other university or college of advanced education.

Minshan Guo

ABSTRACT

The purpose of this study is to improve the solubility, dissolution rate and permeability of poorly water-soluble drugs by investigating the dissolution and permeation properties of flufenamic acid cocrystals in the presence of polymers. This study was separated into four tasks:

(1) Formation of pharmaceutical cocrystals:

Two pharmaceutical cocrystals of poorly water soluble active pharmaceutical ingredient (API) flufenamic acid (FFA) were synthesized, including 1:1 flufenamic acid-nicotinamide cocrystal (FFA-NIC CO) and 1:1 flufenamic acid-theophylline cocrystal (FFA-TP CO). The results of infrared spectroscopy (IR), differential scanner calorimetry (DSC) and x-ray powder diffraction (XRPD) confirmed the formation of cocrystals.

(2) Effect of polymers on cocrystals supersaturated solution:

The influence of three polymers (polyethylene glycol (PEG), polyvinylpyrrolidone (PVP), and a copolymer of *N*-vinly-2-pyrrolidone (60%) and vinyl acetate (40%) (PVP-VA)) on FFA crystallization from FFA and FFA cocrystals supersaturated solutions was studied by measuring the nucleation induction time and desupersaturation rates of the supersaturated solutions in the absence or presence of crystals seeds. It was found that the competition of intermolecular hydrogen bonding among drug/coformer, drug/polymer and coformer/polymer was the key factor for maintaining the supersaturated state in cocrystal solution.

(3) Study the mechanism of cocrystals dissolution:

The dissolution mechanism of cocrystals in absence or presence of polymers was investigated by carrying out different dissolution experiments of both single and powdered cocrystals at multiple length scales, including molecular level, macroscopic level and bulk experiment. According to the results, FFA-NIC CO and FFA-TP CO have different dissolution mechanisms. The addition of polymers can alter the dissolution property of cocrystals by interacting with crystal face.

(4) Investigation of permeation property of cocrystals:

The key processes (kinetics of FFA cocrystals supersaturation and subsequent drug permeation) during cocrystals dissolution in the absence or presence of different concentration of polymers (PVP and PVP-VA) were systematically evaluated by using dissolution/permeation system in a side-by-side cell. Furthermore, the insight mechanism of the supersaturated solution and permeation behavior was explored by ^{1}H NMR. We found that the permeation property of cocrystals is highly depended on the polymer type, coformer type and polymer concentration.

.

ACKNOWLEDGEMENTS

I would like to extent my thanks to the people that support and encourage me to complete my PhD study.

Firstly, I would like to express my sincere appreciation to my respectful supervisor Dr Mingzhong Li. It was my honor to become his PhD student. During my PhD study, he gave greatly support, guidance, and encouragement to me. I appreciate all his contributions of funding, ideas, suggestions and time to help me do my research. I am also thankful for that he gave me a lot of opportunities to build up my confidence and broaden my knowledge by attending different international conferences to present my work. The enthusiasm he has for his research motivate me.

Secondly, I wish to extent my thanks to my second supervisor Dr David Armitage and all technicians in faculty of Health and Life Science. Thanks for their technical support and professional advises for my research.

I am grateful to my colleges Manreet Kaur, Preyanthiny Kirubakaran and Linzie Bolus. Thanks for their accompany, friendship, collaboration and suggestions. I really had a good time to work with them.

I would like to acknowledge De Montfort University and Great Britain-China Educational Trust for the financial support.

I wish to thank my dear family for their endless love and support to help me pursue my dream.

Finally, a note for the readers, some parts of the chapters that presented in this dissertation has been published.

LIST OF FIGURES

LIST OF TABLES

ABBREVIATIONS

^{1}H NMR.	One Dimensional Proton Nuclear Magnetic Resonance
AFM	Atomic Force Microscopy
API	Active Pharmaceutical Ingredients
ATR-FTIR	Attenuated Total Reflectance-Fourier Transform Infrared Spectroscopy
AUC	Area Under the Curve
BCS	Biopharmaceutics Classification System
CD	Cyclodextrins
$CDCl_3$	Chloroform-d
CMC	Critical Micelle Concentration
CSD	Cambridge Structural Database
D/P	Dissolution/Permeation
DMF	N,N-Dimethylformamide
DMSO	Dimethyl Sulfoxide
DPP	Dissolution Performance Parameter
DSC	Differential Scanning Calorimetry
FFA	Flufenamic Acid
FFA I	Flufenamic Acid Form I
FFA III	Flufenamic Acid Form III
FFA-BP CO	1:0.5 Flufenamic acid -4,4'-bipyridine (BP) Cocrystal
FFA-CNB CO	1:1 Flufenamic acid- 2-Chloro-4-Nitrobenzoic Acid Cocrystal
FFA-ETZ CO	1:1 Flufenamic acid- Ethenzamide Cocrystal
FFA-NIC CO	1:1 Flufenamic acid-Nicotinamide Cocrystal
FFA-PYR CO	1:1 Flufenamic acid -2-Pyridone Cocrystal
FFA-TP CO	1:1 Flufenamic acid -Theophylline Cocrystal
FTIR	Fourier Transform Infrared Spectroscopy
GI	Gastrointestinal

HEC	2-Hydroxyethyl Cellulose
HPC	Hydroxypropyl Cellulose
HPLC	High Performance Liquid Chromatography
HPMC	Hydroxypropyl Methylcellulose
HPMCAS	Hypromellose Acetate Succinate
IR	Infrared Spectroscopy
LLPS	Liquid-Liquid Phase Separation
NIC	Nicotinamide
OLM	Optical Light Microscopy
PBS	Phosphate Buffer Solution
PEG	Polyethylene Glycol
PPG	Poly(Propylene Glycol)
PVA	Poly(Vinyl Alcohol)
PVP	Polyvinylpyrrolidone
PVP-VA	Copolymer of N-Vinyl-2-Pyrrolidone (60%) and Vinyl Acetate (40%)
SEM	Scanning Electron Microscope
SLS	Sodium Lauryl Sulphate
SMPT	Solution Mediated Phase Transformation
SP	Solubility Parameter
SSR	Supersaturated Ratio
SSNMR	Solid State Nuclear Magnetic Resonance Spectroscopy
SSP	Supersaturated Parameter
SXRD	Single Crystal X-ray Diffraction
TP	Theophylline
UV	Ultraviolet
XRPD	X-Ray Powder Diffraction

Chapter 1 Introduction

1.1 Research Background

In systemic circulation, the desired (anticipated) pharmacological response could be achieved when the desired drug concentration reached [1]. The reality in pharmaceutical industries is that 99% Active Pharmaceutical Ingredients (API) failed to develop as a commercial drugs because of their poor water solubility [2], which limit the applications of the highly potent drugs [3, 4]. Hence, it is essential to improve the solubility of the poorly water-soluble drugs to maximize their therapeutic values. Many techniques have emerged to enhance the solubility and dissolution rate of poorly water-soluble drugs, such as particle size reduction, solid dispersion, hot-melt extrusion and nanomaterials [1]. These approaches have shown the benefits on increasing solubility and dissolution rate of APIs [5-8].

Recently, cocrystals have attracted numerous attention due to its ability to improve the bioavailability of poorly water-soluble APIs by combining them with coformers at a specific stoichiometric ratio [2, 9, 10]. Cocrystals are physicochemically stable at room temperature and have been proved to be highly potential methods to modulate the physicochemical properties of APIs for overcoming the insufficient bioavailability of drugs [2, 11-15].

For cocrystal formulations, the ability to generate and maintain the supersaturated state in solution is the key factor of oral drug delivery [16, 17]. Nevertheless, crystallization of the stable form from the supersaturation would simultaneously occur during cocrystals dissolution, which would diminish the dissolution and solubility advantages of cocrystals. Especially, the surface of dissolving cocrystal could be covered when the crystallization happens on the cocrystal surface [18-20]. This problem of crystallization also causes no effective permeation of drugs [16]. Based on the literatures, the addition of crystallization inhibitor (e.g. polymers) in a solubility-enable formulation can maintain the supersaturation state by preventing the crystallization, subsequently for adequate drugs absorption. The reported polymers include PVP, PVP-VA, HPMC and HPMC-AS [21, 22]. For example, the previous work in our lab shown that HPMCAS

polymer can maintain the supersaturated solution of carbamazepine-cinnamic acid cocrystals [10]. The effect of the polymeric crystallization inhibitors on supersaturated state in other systems have been extensively studied, in particular amorphous solid dispersions [23, 24]. However, such studies are still rare for cocrystal based formulations. Therefore, a full understanding of the polymers influence on cocrystal products is significant. Firstly, the effect of polymers on the key processes (kinetics of nucleation and crystal growth) of crystallization in supersaturated solution needs to be considered. Furthermore, the additional polymers in solution not only impact the crystallization process of APIs but also influence the dissolution behaviors of cocrystals during dissolution. Hence, revealing the dissolution mechanism of cocrystal in solution in the absence and presence of pre-dissolved polymers is essential. The therapeutic effect of oral administration drug products is strongly depended on both dissolution and permeation steps. If the drug molecules in the gastrointestinal (GI) tract cannot across the, the drug would fail to be absorbed by the body. Furthermore, based on solid dispersion systems, the introduced polymers would influence the supersaturated state and reduce or enhance the capability of drug molecules to permeate across the membrane [25]. Other work also showed that polymers can reduce the permeability of drug, such as cyclodextrins, micellar solubilization [26, 27], because the drug encapsulated in the solubilizing agent reduces free fraction of the drug available for membrane permeation. For a cocrystal formulation, it has been reported that cocrystal can alter the permeability property of API due to the API-coformer interaction [28-30]. Thus, to successfully develop a cocrystal formulation, the underlying relationship between the supersaturated solution and drug permeation in the presence of polymers during cocrystals dissolution need to be discreetly considered.

1.2. Research Aim and Objectives

The aim of this study is to improve the water solubility of flufenamic acid by using cocrystal method and investigate the dissolution and permeation properties of corresponding cocrystals in the presence of polymers. The properties of cocrystals can be disclosed by studying the crystallization process of cocrystal supersaturated solution, investigating the dissolution mechanism of cocrystals and examining the permeation properties of cocrystals in the presence of polymers.

Objective 1: review the pharmaceutical cocrystals definition, synthesis methods, characterization techniques, advantages and disadvantages of cocrystals and find out methods of avoiding cocrystals drawbacks.

Objective 2: synthesize two cocrystals of 1:1 flufenamic acid-nicotinamide cocrystal (FFA-NIC CO) and 1:1 flufenamic acid-theophylline cocrystal (FFA-TP CO) in both powdered and single crystal form and characterize these two cocrystals by using FTIR, Raman, DSC and XRPD.

Objective 3: investigate the influence of polymers on supersaturated FFA cocrystals solutions by studying the crystallization kinetics of both nucleation and crystal growth of supersaturated solution in the absence or presence of polymers.

Objective 4: understand the dissolution mechanisms of cocrystals in solution in the absence and presence of pre-dissolved polymers by examining dissolution properties of cocrystal in different dissolution experiments of both single and powdered cocrystals at multiple length scales, including the molecular level, macroscopic level and bulk experiments in both sink and nonsink condition.

Objective 5: study the polymers influence on the kinetics of cocrystals supersaturation and subsequent drug permeation during dissolution by using dissolution/permeation system in side-by-side cell and explore the insight mechanism of the supersaturated solution and permeation behavior by applying one dimensional proton nuclear magnetic resonance (^{1}H NMR) to study the interaction between API, coformers and polymers in solution.

1.3 Thesis Structure

This thesis includes 8 chapters:

Chapter 1: Brief introduction of research background, research aims, objectives and thesis structure.

Chapter 2: Literature reviews on pharmaceutical cocrystals, additives effect on recrystallization, dissolution and permeation properties of drugs. Brief introduction about FFA cocrystals, pharmaceutical coformers and polymers used in this study.

Chapter 3: Description of the materials, analytical techniques, experimental methods, preparation methods and calculation equations that used in this research. Comprehensive introduction about analytical methods including principles, operation procedures and parameters setting.

Chapter 4: Samples characterization of FFA I, NIC, TP, FFA-NIC CO and FFA-TP CO by using DSC, ATR and XRPD. The molecular structures of FFA-NIC CO and FFA-TP CO were displayed in this chapter.

Chapter 5: The influence of polymers of polyethylene glycol (PEG), polyvinylpyrrolidone (PVP) and Copolymer of *N*-Vinyl-2-Pyrrolidone (60%) and Vinyl Acetate (40%) (PVP-VA) on recrystallization from cocrystals supersaturated solution was discussed in this chapter. The nucleation process and crystal growth of FFA stable form in FFA and FFA cocrystals supersaturated solution were fully examined. The molecular interactions among FFA, coformers and polymers were also investigated by applying liquid ATR-FTIR.

Chapter 6: The dissolution mechanisms of FFA cocrystals in the presence of PEG, PVP and PVP-VA were disclosed in multiple length scales. At molecular level, atomic force microscopy (AFM) was used to detect the etching pattern of crystal surface to find out how polymers interact with crystal faces during dissolution. At macroscopic level, optical light microscopy (OLM) was employed to monitor the dissolution rate of the specific faces of single crystals. In bulk experiments, dissolution tests of pure FFA and FFA cocrystals were conducted in both sink and non-sink condition.

Chapter 7: The permeation property of FFA cocrystals in the absence or presence of different concentration of polymers (PVP and PVP-VA) was investigated using dissolution and permeation system in side-by-side cell. The insight mechanism between supersaturated state and permeation property was examined by ^{1}H NMR.

Chapter 8: Conclusions of the present work and brief introduction of the future work.

Chapter 2 Literature Reviews

2.1 Chapter Review

Firstly, a brief introduction of current approaches for improving the bioavailability of poorly water-soluble drugs was given. Then, a comprehensive introduction of pharmaceutical cocrystals including cocrystals definition, cocrystals design strategies, cocrystals screening methods and physicochemical properties of cocrystals were presented. After that, detailed reviews about the problems of cocrystals and the additives effect on crystallization of drug stable form, dissolution behavior and permeation property of drugs were described. Finally, the basic information about materials used in this study was introduced, including FFA, FFA cocrystals, NIC, TP, PEG, PVP and PVP-VA.

2.2 Biopharmaceutics Classification System (BCS)

Biopharmaceutics Classification System (BCS) (Figure 2. 1) is a scientific approach to classify drug substances into different classes according to drug's aqueous solubility and intestinal permeability [31]. Based on BCS system, drugs are classified into four classes: **Class I**: high solubility-high permeability; **Class II**: low solubility-high permeability; **Class III**: high solubility-low permeability; **Class IV**: low solubility-low permeability [32]. Most of newly developed APIs belong to BCS class II with the properties of low solubility but high permeability [33]. The low water solubility of APIs causes low drug dissolution and oral absorption. Therefore, it is important to improve the solubility of Class II drugs to achieve the drug therapeutic efficacy. Various techniques have been successfully used to conquer the solubility problem, such as cocrystals [11, 34], solid dispersion [35], cyclodextrin complexation [36].

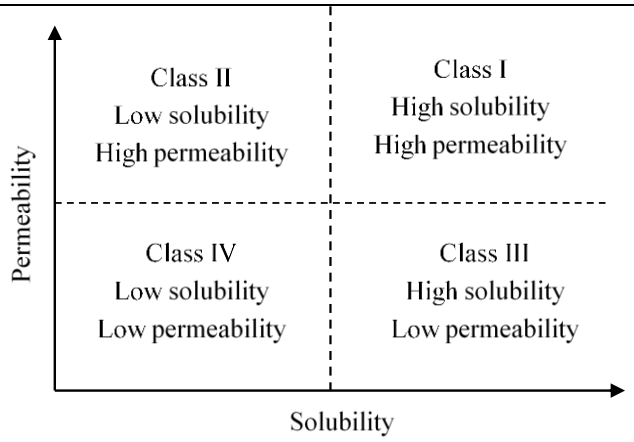

Figure 2. 1 Biopharmaceutics Classification System (BCS)

2.3 Enabling Formulations for Poorly Water-Soluble Drug

Generally, improving the performance of dissolution and solubility of Class II drug can be obtained by three techniques including physical modifications (such as particle size reduction like micronization, crystal engineering like pharmaceutical cocrystal and amorphous like solid dispersion), chemical modifications (such as salt formation, pH modification) and miscellaneous methods (such as co-solvency and surfactant solubilization) [1].

2.3.1 Micronization

Micronization is a conventional approach of particle size reduction, which can rise the dissolution rate of API by increasing the surface area, but cannot increase the equilibrium solubility of API [37]. Micronization of a drug can be achieved by employing jet mill, rotor stator colloid mills *et al.* Micronization has been widely used to improve the bioavailability of poorly water-soluble drugs, such as griseofulvin [38-43], progesterone [44-47], danazol [48] and digoxin [49]. For example, micronized danazol showed around 16-fold (5.1% to 82.3%) increasing bioavailability. The problems of micronized particles are the reduced wettability and their handling [50].

2.3.2 Salt Formation

Salt formation has been commonly used to enhance the properties of solubility and dissolution for the basic and acidic APIs [51]. In general, a stable salt can be formed if

the difference of pKa between base and acid is greater than 3 [52].In early 1950s, salt formation had been employed to improve the dissolution rate of several weakly acidic compounds [53, 54]. Different absorption rates and extents of novobiocin [55] and tolbutamide [56] were found with a combination of sodium salt formation. An enhanced dissolution rate and oral bioavailability were observed for celecoxib-sodium salt with respect to pure celecoxib [57].

2.3.3 Solid Dispersion

Solid dispersion is an effective pharmaceutical approach for increasing the solubility, dissolution and bioavailability of drugs by loading the hydrophobic drug into a hydrophilic polymer matrix. Enormous studies have shown that solid dispersion can enhance the drug release rate [58-62]. Chiou and Riegelman found that insoluble griseofulvin would be almost completely absorbed by man and dog by using solid dispersion [63].

2.3.4 Cyclodextrin Complexation

Cyclodextrins (CD) are oligosaccharides, formed as a hydrophobic cavity interior with a hydrophilic exterior surface [64]. Cyclodextrins have shown its potential ability to increase the oral absorption of poorly water-soluble API by forming inclusion complexes [65-68]. Examples of such formation include acetazolamide, [69] carbamazepine [70], cyclosporine [71], finasteride [72], oxazepam [73] and propofol [74]. Tonnesen *et al* used cyclodextrin complex to increase the solubility of curcumin by a factor of at least 104 under pH 5 buffer [75]. The solubility of camptothecin was171-fold higher compared with crystalline camptothecin by applying cyclodextrin method in 0.02M HCl at 25°C [36]. Currently, around 35 commercial formulations of cyclodextrin have appeared into the market [76], including pansporin T, opalmon, meiact, transillium and more [76].

2.3.5 Pharmaceutical Cocrystals

Historically, the first reported cocrystal was described as a “complex” or “compound” in 1844 [77]. Quinhydrone is the earliest reported cocrystal, a 1:1 molar ratio compound of quinone and hydroquinone which was discovered by Friedrich Wöhler in 1844 [78].

To date, there is no universal and uniform definition of cocrystal based on the scientific literatures [79]. Most of the literatures defined cocrystals as crystals, which composes at least two components. A restrictive definition of cocrystals was introduced by Michael J. Zaworotko group [80], *"a cocrystal is a multicomponent crystalline material at a defined stoichiometric ratio, which is solid under ambient temperature and all components are discrete neutral molecules"*. The difference between a salt and a cocrystal is that there is proton transfer during salt formation but no proton transfer within a cocrystal formation. Compared with salts formation, there are at least two inherent benefit of cocrystal method: (1) all APIs including weakly ionizable and non-ionizable molecules can form cocrystal. But for salt, only strong ionizable molecules can form salt; (2) Due to toxicity issues, only about 12 basic or acidic counter-molecules can be used for salt screening but abundant potential counterions are explored in cocrystal formation [81].

For pharmaceutical cocrystals, one of the components is drug molecule. The early reported pharmaceutical cocrystals were sulphonamides cocrystals [82]. In the past 30 years, pharmaceutical cocrystals have been effectively applied to improve the physicochemical property of poorly water soluble drugs, such as lamivudine [83], AMG 517 [84], gabapentin [85], piroxicam [86], celecoxib [20] and norfloxacin [87]. Currently, 3 pharmaceutical cocrystals have been approved, Entresto® (sacubitril-valsartan), • Lexapro® (escitalopram oxalate) and Depakote® (valproate sodium cocrystal with valproic acid) [88].

2.3.5.1 Cocrystals Design Strategies

Cocrystal design and formation is based on the fundamental principle of crystal engineering, referring to construction or engineering of a new solid crystalline material with the desirable property of designed molecule based on the intermolecular interactions and non-covalent interactions (e.g. hydrogen bonding) between molecules, which control the supramolecular assemblies and molecular recognitions [89, 90]. The bioavailability and chemical stability of cocrystals are depended on the non-covalent interactions in the crystal structures, like hydrogen bonding, van der Waals interactions, π–π stacking and electrostatic interactions [90]. Among these mentioned non-covalent interactions, hydrogen bonding is the most important and popular interaction in the

synthesis of cocrystal system due to its directionality and strength [2, 91, 92]. Three hydrogen bonding rules were introduced by Etter and Donohue [93-95].

(1) All good hydrogen bonding acceptors and donors can be used in hydrogen bonding;

(2) Intramolecular hydrogen bonds are easier to form within six-membered-ring than intermolecular hydrogen bonds;

(3) The best hydrogen bonding donors and acceptors still can form intermolecular hydrogen bonds with others after the formation of intramolecular hydrogen bonds.

Based on these rules, synthon formation and hydrogen bonding between the functional groups can be predicted and cocrystal strategies can be proposed [96-98].Figure 2. 2 shows the common hydrogen bonds used in crystals.

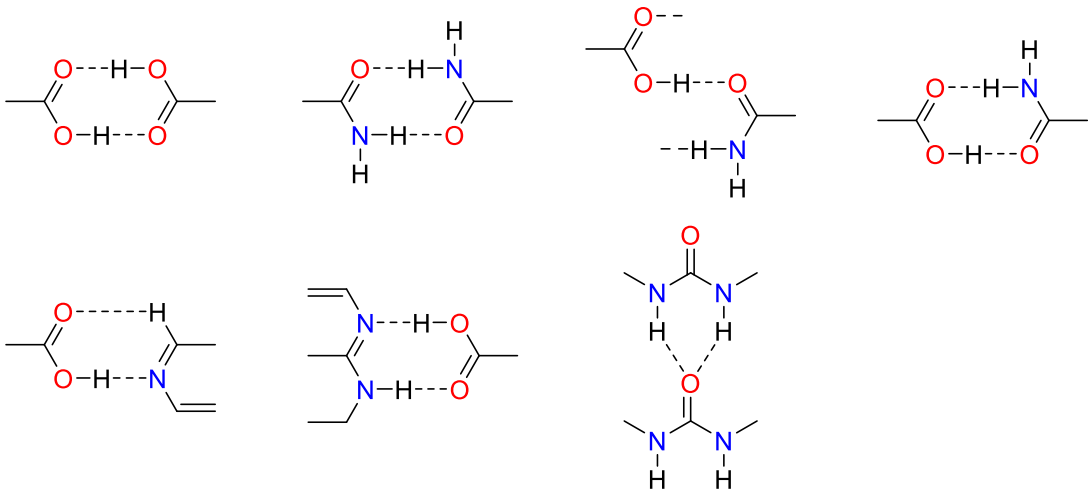

Figure 2. 2 Common synthon used in crystals

In order to get an ideal cocrystal, it is important to have a design strategy of cocrystal formation. There are several steps to design a pharmaceutical cocrystal [99], Figure 2. 3 represents the diagram of stages for cocrystal design.

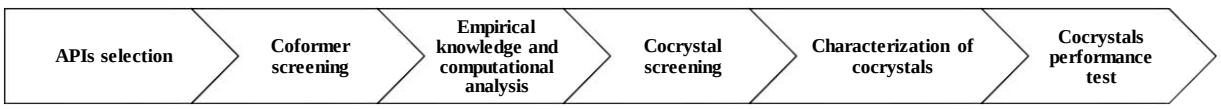

Figure 2. 3 Diagram of stages for cocrystal design [99]

2.3.5.2 Coformer Selection

For cocrystal formation, the first step is the coformer selection. In this process, the formation of supramolecular synthons or non-covalent bonds between molecules is a crucial parameter [100]. Before starting coformer selection, it is vital to understand structure and functional groups of APIs and determine which functional groups can form stable intermolecular interaction with the coformer. Then computational methods such as Cambridge Structural Database (CSD) can be applied to identify a stable and common supramolecular synthon for the APIs. Isostar search allows to discover the common arrangement of hydrogen bonding within crystals [101]. Coformers selection can base on the following standards [101]:

(1) All coformers are commercial drug products and pharmaceutically acceptable;

(2) All coformers are non-toxic;

2.3.5.3 Cocrystal Screening Methodology

At present, the main techniques that have been used for cocrystal screening are solution-based methods like antisolvent addition, solvent evaporation and cooling crystallization and solid-based methods like crystallization form melting, solvent drop grinding and neat grinding [102, 103]. Compared with solid-based methods, solution-based methods are more common to prepare cocrystals [104] and majority of the single cocrystals can only be prepared by solution-based method.

2.3.5.3.1 Solution-Based Method

In practice, cocrystal screening using solution-based method needs to follow one of following two strategies [105]: (1) application of solvents or co-solvents in which all starting components have similar solubility and the cocrystals congruently saturates; (2) reaching the cocrystal stability region in noncongruently saturating solvents by applying non-equivalent reactant concentration. For designing a successful cocrystal, it is useful to construct ternary phase diagrams to describe the three-phase behaviors of reactants, solvent and cocrystal, and predict the pathway of cocrystal formation [13]. Particularly, solubility of reactants is a significant factor in these diagrams based on previous studies

because differences would change the location of thermodynamically stable cocrystal phase regions. Two possible phase diagrams of cocrystal are illustrated in Figure 2. 4. In Figure 2. 4(a) the solubility of A and B is similar in solvent and solution crystallization with equimolar reactants results in 1:1 AB cocrystal from solvent evaporation. From Figure 2. 4(b) (components with non-equivalent solubility in solvent), cocrystal from solution by solvent evaporation may lead pure starting crystalline materials, or mixture of cocrystals and single component crystal. This situation can be developed by reaction crystallization, adding B into a component A saturated or nearly saturated solution cause a AB cocrystal supersaturated solution, which crystallization pathway would pass either through region 5 or 4. Therefore, a rational design of cocrystal method can be selected by using ternary phase diagram.

Compared with other cocrystallization methods, there are several factors for popularity of solution-based method, including high yield, high purity, more easily evaluated surface features and crystal habit single crystal [106].

Figure 2. 4 Isothermal ternary phase diagram of cocrystal: (a) similar solubility of API and coformer in solvent; (b) different solubility of API and coformer in solvent; 1: A and solvent; 2: A and cocrystal; 3: cocrystal; 4: mixture of B and cocrystal; 5: B and solvent and 6: solution [13].

2.3.5.3.2 Solid-Based Method

Solid-based method is alternative to solution-based method when the cocrystal components solubility in a given solvent is not concerned [106-109], which provided an significantly more efficient method for cocrystals screening and synthesis [110]. To date, a lot of cocrystals have been successfully formed by solid-based method, as listed in Table 2. 1.

Crystallization from melting using hot-melting microscopy is a thermal method for cocrystal screening by recognizing cocrystal phases then to determine the binary phase diagrams (composition–temperature plots) of molecular complexes [111]. In thermal method (Figure 2. 5): (1) Both higher melting point cocrystal component A and low melting point cocrystal component B melt; (2) Component A recrystallizes before component B encounters component A; (3) Liquid component B contacts and solubilizes a part of component A. Furthermore, all components solidify and form a mixing zone [112] where cocrystal can be possibly formed.

Solid-state grinding can trigger chemical change (mechanochemical reaction) resulting in cocrystal formation [106]. Solid-state grinding method comprises neat and liquid-assisted grinding. In neat grinding method, the stoichiometric cocrystals components are mixed by using mortar and pestle or ball mill. Whereas, for liquid-assisted grinding, a small amount of solvent is added to the cocrystal components. Etter and coworkers suggested that there were two determined factors related to cocrystal formation by using solid-based grinding method, including (1) at least one of the cocrystal components have volatile property at the operating temperature of grinding process; (2) The intermolecular hydrogen bonding within cocrystals should be stronger than the hydrogen bonding with the starting materials [113].

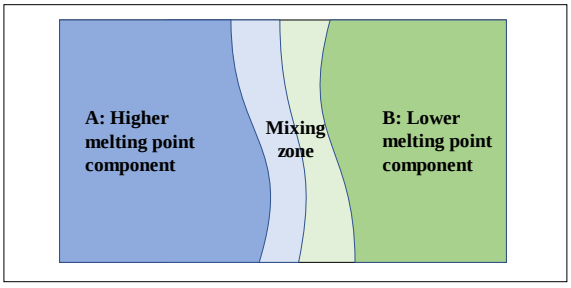

Figure 2. 5 Diagram of crystallization from melting [112]

Table 2. 1 Example of cocrystals synthesis by solid-state grinding

Solid-based method	Cocrystals	Reference
Neat grinding	4-aminobenzonic aicd-3,5-dinitrobenzoic acid cocrystal; Anhydrous theophylline-citric acid cocrystal, theophylline anhydrate-citric acid cocrystal, caffeine	[92, 114]

	hydrate-citric acid cocrystal,	
Liquid-assisted grinding	theophylline anhydrate-citric acid cocrystal, caffeine hydrate-citric acid cocrystal, adefovir dipovoxil-glutaric acid cocrystal	[114, 115]
Crystallization from melting	Nicotinamide-ibuprofen cocrystal; salicylic acid-nicotinamide cocrystal, flurbiprofen-nicotinamide and fenbufen-nicotinamide cocrystal. Carbamazepine-nicotinamide cocrystal	[99, 112, 116]

2.3.5.4 Cocrystal Characterization Techiniques

It is important to understand the structural information and physiochemical properties of cocrystals. Various analytical apparatuses have been used to characterize cocrystals. For identifying the structure of cocrystals, analytical techniques like infrared spectroscopy (IR), Raman spectroscopy, single crystal X-ray diffraction (SXRD), X-ray powder diffraction (XRPD), and solid state nuclear magnetic resonance spectroscopy (SSNMR) has been broadly applied. For determining the thermal properties of cocrystal, differential scanning calorimetry (DSC) have been widely employed.

X-ray diffraction is a useful technique to determine the crystal structure of the molecules in three dimensions and has been used to study the structure data from the twentieth century [117]. The electron density and periodic assembly of molecules or atoms of a crystal can be rebuilt according to the X-ray diffraction data. The data obtained from single crystal X-ray Diffraction (SXRD) can expose the regularly repeating arrangement of molecules and the packing pattern of the single crystal. SXRD can promise to provide very accurate parameters of cell dimensions if there are less than 100 atoms in the asymmetric unit in the structures [118]. However, it is difficult to prepare a single crystal with sufficient size for SXRD testing. Therefore, X-ray powder diffraction (XRPD) has become an essential equipment for studying the structure of cocrystal. However, XRPD is not capable of differentiating between hydrates, polymorphs or solvates from cocrystals, especially for isostructural phases [99].

Raman Spectroscopy is an effective technique for distinguishing polymorphs of APIs and isostructural phases based on bond vibrational energies of crystal structure [119]. Furthermore, the testing of Raman is rapid and non-destructive.

IR spectroscopy is a common tool to confirm the cocrystal formation, especially when a carboxylic acid is involved in hydrogen bonding formation between an API and coformer because of the strong stretching at C=O band (~1700cm^{-1}), C-O (~1200cm^{-1}) and O-H (~3000cm^{-1}) [120].

SSNMR is a helpful technique to provide detailed information about the cocrystal structure, especially for cocrystals synthesized by grinding methods. Hydrogen bonding, spin diffusion and intermolecular contacts can be studied by application of ^{1}H-^{1}H, ^{1}H-^{13}C and ^{19}F-^{13}C experiments by SSNMR [121].

DSC is a particularly convenient method to characterize thermal properties of cocrystals, including melting point data, enthalpy of melting, heat of fusion and transition temperature [122], which can be compared with individual cocrystal components to confirm the formation of cocrystal. The only drawback of DSC is that the low heating rate would cause overlap of the melting event of metastable form and recrystallization of stable form in DSC graph [123].

2.3.5.5 Physicochemical Properties of Cocrystals

The key benefit of cocrystals is the ability to change physicochemical properties of APIs, for improving the solubility, bioavailability, dissolution rate and melting point. These properties would directly or indirectly impact the stability and efficacy of the API dosage form.

Melting point

Meting point is the temperature where the solid phase change to the liquid phase, depending on the crystal structure. Generally, cocrystals have a distinct melting point as compared to individual components because of the different intermolecular interactions, crystal structure and composition. Analysis of 50 cocrystals of different API shows that melting point of cocrystal can be higher, lower or between that of cocrystal formers [120]. The fusion information of carbamazepine cocrystals is not sufficient to predict

the solubility behaviors of cocrystal, which is more related with solute-solvent interaction [124].

Stability

Stability is a vital factor to evaluate the properties of a new chemical, which depend on the molecular arrangement in crystal lattice. In terms of hygroscopicity, cocrystals have shown a stable property under typical manufacturing and storage state and an improved stability compared with the individual components [11, 125, 126]. In the attempt to improve the physical stability of theophylline, cocrystallization of theophylline was investigated. Over 7-week study at 98% RH (relative humidity), cocrystal of theophylline-oxalic acid was stable while theophylline anhydrate was transferred to theophylline monohydrate [127]. Indomethacin-saccharin cocrystal sorbed negligible water (<0.05%), less than γ-form indomethacin at 95% RH at 25°C [128]. In order to evaluated the chemical stability of 2-[4-(4-chloro-2-fluorophenoxy)phenyl] pyrimidine-4-carboxamide cocrystal (glutaric acid as coformer), the samples was putted in a glass bottles at 40°C/75% RH and 60°C for 2 months. Cocrystal samples were measured by DSC, XRPD and HPLC after stored. The results of DS, XRPD and HPLC did not find out any know degradants during storage [11]. For analyzing the photochemical stability of crystalline carbamazepine (III), carbamazepine-saccharin cocrystal and carbamazepine-nicotinamide cocrystal, the samples were exposed at 98% RH at room temperature under fluorescent/ambient light up to 9 months. After 9 months, the samples were detected by HPLC, DSC and FTIR. The crystalline carbamazepine (III) transferred to carbamazepine (dihydrate) after absorbing moisture and slowly turned to yellow-orange after 4 months storage due to photochemical instability. Conversely, the carbamazepine cocrystals did not show degradation after 9 months [125].

Solubility

An improved solubility of poorly water-soluble drug is one of the two main reasons to study cocrystals. The potential application of cocrystal as a solubility improvement approach was realized since early 1900s and number of pharmaceutical application was reported in the late 20th century [77]. For instance, Kranz *et al.* disclosed that sodium theophyllinate-glycine cocrystal could enhance the solubility of theophylline in 1947 [129]. In 1950s, cocrystals of sulfa drug with homosulfamine showed an increased

solubility relative to sulfa drugs [130]. Additionally, other Japanese group revealed that glucuronic acid-caffeine cocrystal and glucuronic acid-theobromine cocrystal generated a higher solubility compared to caffeine and theobromine [77]. Aakeröy *et al.* found that five anticancer drug cocrystals formed with different dicarboxylic acids as coformers had enhanced or reduced aqueous solubility compared with the pure anticancer drug [131]. Based on these results, it can be realized that the solubility of cocrystal has a relationship with the molecular structure of coformers.

Dissolution rate

An enhanced dissolution rate is one of the key properties of cocrystals. Remenar's research group found that itraconazole cocrystals with malic acid, succinic acid and tartaric acid showed 4-20 times enhanced drug concentration during dissolution testing as compared to the crystalline drug [132]. An 1:1 molar ratio cocrystal of a potential API with glutaric acid demonstrated an eighteen folds dissolution rate relative to pure crystalline API [11]. Thus, these studies indicated that cocrystals have the potential to increase the dissolution rate of API to achieve a therapeutic effect.

Bioavailability

Animal bioavailability is a method to evaluate the pharmacokinetic data of a new drug candidate by measuring the rate and amount of an API that reach the systemic circulation of animals. Various studies have exposed that cocrystals have the potential ability to develop the drug absorption. For example, about 10-fold bioavailability improvement of cocrystals of quercetin over pure quercetin [34]. Chen *et al.* studied the mean $AUC_{0\text{-}24}$ of apixaban-oxalic acid cocrystal in beagle dogs, showing the cocrystal outperformed apixaban with a growth mean $AUC_{0\text{-}24}$ up to 2.7 folds [133]. Other cocrystals also shown an enhanced bioavailability such as in danazol cocrystal [134], cilostazol cocrystal [17], AMG 517 sorbic acid cocrystal [135] and indomethacin-saccharin cocrystal [136].

2.4 Development of Pharmaceutical Cocrystal Formulation

2.4.1 Solution Mediated Phase Transformation (SMPT)

Improving the solubility of poorly water-soluble drug is the key stage to successfully develop a new drug candidate and obtain the desired therapeutic performance. Pharmaceutical cocrystals have been demonstrated to be an effective tool for enhancing the solubility and create a supersaturated state of poorly water-soluble drugs [11, 137, 138]. However, cocrystals is not thermodynamically stable in solution, leading to a phenomenon called solution-mediated phase transformation (SMPT) due to the crystallization of stable solid phase from the metastable phase from supersaturated condition in bulk solution or around the surface of dissolving solid during dissolution [128, 139-142]. Such transformation is a challenge for cocrystals, which may reduce the advantages of the cocrystals and consequently decrease the bioavailability [143]. In our group, this phenomenon on flufenamic acid cocrystals and carbamazepine cocrystals has been systematically investigated [9, 10, 144-146]. For instance, the intrinsic dissolution behaviors of carbamazepine-nicotinamide cocrystal were studied using UV-imaging techniques by Qiao *et al* [145]. The intrinsic dissolution rate of carbamazepine-nicotinamide cocrystal reached a maximum value of 0.0123 mg/min/cm^2 then slowly decreased during dissolution. The precipitation with lower free energy state, carbamazepine dihydrate, was found on the surface of sample compact after dissolution test and analyzed by Raman and SEM. Other groups also reported that the supersaturated state generated by cocrystal has the trend back to the equilibrium state of the stable form [20, 139, 140]. For example, the dissolution of fluoxetine hydrochloride-succinic acid cocrystal in water at 20°C shown that a maximum fluoxetine hydrochloride concentration with 1.7-fold higher with respect to pure API was achieved first, followed by a decreased concentration after 2 min. The results of solid residues obtained after dissolution indicated that recrystallization of fluoxetine hydrochloride from cocrystal occurred, which was confirmed by XRPD [139].

There are several factors influencing the phase transformation of a cocrystal during dissolution, such as the type of coformers [144, 146], dissolution condition (e.g. pH and buffer strength) [128, 139, 142, 147]. In terms of coformers, the

carbamazepine-cinnamic acid cocrystal was more stable than carbamazepine-saccharin cocrystal in 1% SLS aqueous solution [146]. For different dissolution conditions, the dissolution behaviors of indomethacin-saccharin cocrystal in 60mM and 200mM phosphate buffer (pH 7.4) at 26°C were different [128]. The results of indomethacin-saccharin cocrystal powder dissolution showed that the peak concentration of indomethacin was maintained for several hours in 200mM buffer with no evidence of precipitation from the dissolution profile. On the other hand, precipitation was found in 60mins in 60mM buffer because of the drop of the pH from 7.4 to 6.8. Although no precipitation observed in 200mM buffer, the results of XRPD indicated that the solid residues were not cocrystal. Therefore, it is important to characterize the solid residues after dissolution to completely understand the SMPT phenomenon.

In a SMPT process, there are three steps: (1) supersaturated condition created by dissolving metastable solid; (2) nucleation of stable form; and (3) crystal growth of the formed nucleus.

2.4.1.1 Nucleation

Nucleation is a process of formation of new crystal nuclei by self-association of the solute molecules, including primary nucleation (nuclei spontaneously from clear supersaturated solution) and secondary nucleation (nuclei from supersaturated solution in presence of seeded crystals). Therefore, it is significant to disturb the self-association of molecules for preventing nucleation. There are two nucleation types in primary nucleation: homogeneous and heterogeneous nucleation [148]. Homogenous nucleation happens randomly and spontaneously in a medium without any foreign bodies. However, it is rare to obtain homogenous nucleation because of its rigor requirements. Heterogeneous nucleation takes place in presence of foreign bodies in the supersaturated solution, such as residues or dust from last batch. The nucleation occurs in supersaturated solution in the presence of crystals, called secondary nucleation. The presence of extra substances (impurity or crystals) would promote the formation of the nuclei. Hence, secondary nucleation and heterogenous nucleation could happen in lower supersaturated solution compared with the homogenous nucleation.

The size of the aggregates or clusters is one of the key factors in nucleation process. Stable aggregates or clusters can be formed only when the size of weak aggregates or clusters are larger than critical size. Otherwise, the unstable clusters would re-dissolve. The possibility of forming a stable aggregates or critical nuclei is dependent on the energy of the nucleus' formation and the subsequent growth [149, 150].

2.4.1.2 Crystal Growth

Crystal growth is the process of subsequent growth of the nuclei. The crystal growth of nucleus occurs if the rate of growth is greater than the rate of dissolving nuclei. In supersaturated solution, nucleation or crystal growth rate will be high if the $\Delta\mu$ (chemical potential) is high and ΔG (the difference of free energy between solid-sate of solute and solution-state solute) is low. According to Hartman and Perdock theory [151], for a three dimensional crystal face, the capture of growth units can be classified into three types based on how many bond contacts formed between the absorbed growth unit and the crystal surface (Figure 2. 6), including kinked faces (three attachment), stepped faces (two attachment) and flat faces (one attachment). In general, the ranking of ΔG of three crystal faces is kinked<stepped<flat [152]. The more interaction sites free on the crystal face, the faster it will grow. Therefore, the growth rate of kinked faces is faster than stepped face while the flat face is the slowest. The crystal shape is mainly determined by the slow growing face. Therefore, it is important to block the interaction site for inhibiting the crystal growth.

Figure 2. 6 Types of growth faces [149]

2.4.2 Additives Effect on SMPT

A method called "spring and parachute" (Figure 2. 7) has been widely used on promoting and maintaining supersaturated state for poorly water-soluble drug in solution to improve the oral absorption [118]. "Spring" refers to the high energy form of the drug (cocrystals, crystalline salt or amorphous), which may rapidly dissolve and generate a supersaturated solution with a higher concentration than the equilibrium solubility of API and then cause the crystallization of API. In this condition, additives (parachute) can maintain the supersaturated solution for a physiologically relevant type period to allow adequate drug absorption in the body and improve the bioavailability. Vast of studies proved that additives could be effective crystallization inhibitors in high energy form formulations for delaying the crystallization of stable form [153].

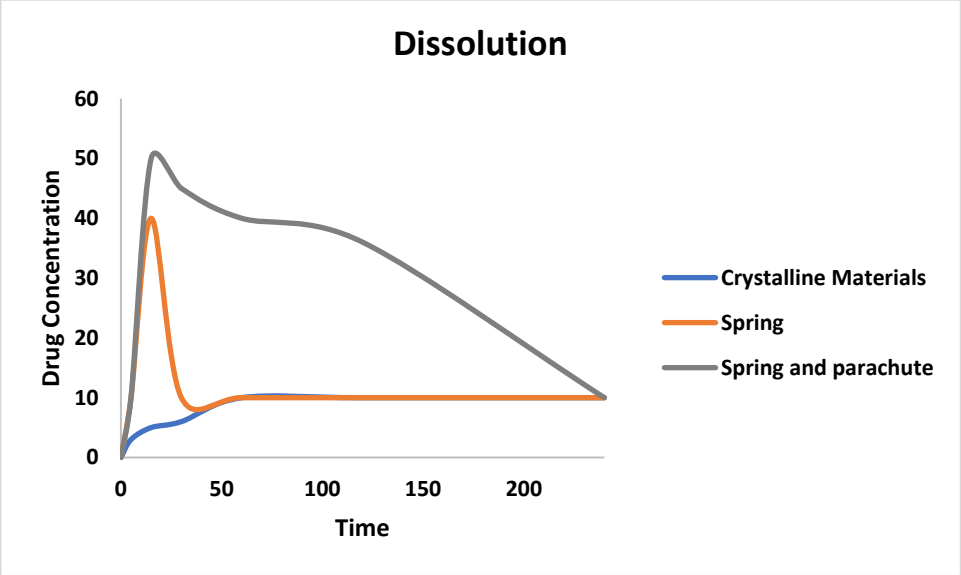

Figure 2. 7 Spring and parachute approach

2.4.2.1 Precipitation Inhibitors

The ability of additives on slowing down the crystallization from supersaturated solution is mainly going through two aspects: (1) effect on the system's thermodynamic (equilibrium state of API) properties; (2) effect on the kinetics of crystallization (nucleation and crystal growth) [153].

In terms of thermodynamic properties, massive works have been demonstrated that additives can enhance the solubility of API [154, 155]. Polymers, including

polyvinylpyrrolidone (PVPK30), polyvinylpyrrolidone K90 (PVPK90), polyethylene glycol (PEG6000), polyethylene-polypropylene glycol 188 (F-68) and hydroxypropylmethyl cellulose (HPMC), have been reported to enhance the solubility of pioglitazone hydrochloride in water [154]. Surfactants also have been established to promote the drug solubility (e.g. Kolliphor TPGS and sodium Lauretha sulfate (SLES)) [134]. Generally, the mechanism of this solubilizing effect of additives is due to the formation of a micelle between the additive and API (Figure 2. 8) [155].

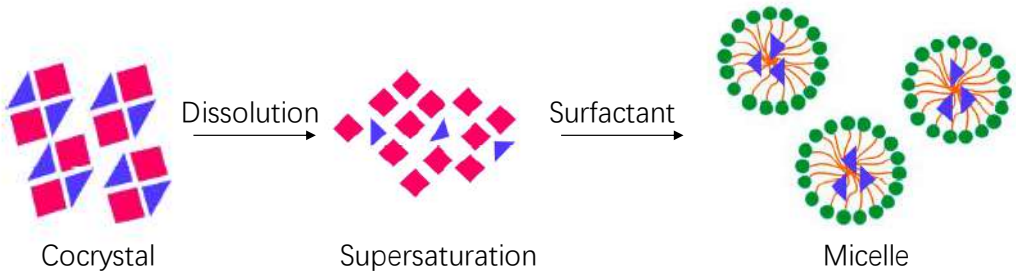

Figure 2. 8 Diagram of surfactant effect on supersaturation [155]

The ability of additives on inhibiting crystallization by changing the kinetics of nucleation and crystal growth process is based on the specific intermolecular interaction between polymers and APIs in solution (hydrogen bonding or hydrophobic interaction) or steric hindrance of polymers on crystallization process [156]. The key factors influencing the inhibitory effect of additives include (1) hydrophobic level of additives [157, 158] and (2) the ability of the polymers to interact with drugs via hydrogen bonds [159]. In our group, Qiu *et al.* has enclosed the effect of polymers in carbamazepine cocrystals powder dissolution [10]. In the presence of 2mg/mL HPMCAS, carbamazepine-nicotinamide cocrystal and carbamazepine-cinnamic acid cocrystal showed about 8-fold increased drug release with respect to pure carbamazepine III in pH 6.8 phosphate buffer. In the meantime, HPMCAS showed a great stabilizing effect on carbamazepine-saccharin cocrystal and carbamazepine-cinnamic acid cocrystal with smallest eutectic constant (Keu=$\frac{Coformer_{eu}}{API_{eu}}$, the ratio of concentrations of the coformer and drug at the eutectic point in dissolution medium). It suggested the significant effect of preventing crystallization of carbamazepine if Keu value is below the stoichiometric ratio (such as Keu $\leqslant$ 0.5 for 2:1 cocrystals or Keu $\leqslant$ 1 for 1:1 cocrystals), indicating

that the cocrystals are stable in dissolution medium [160]. The inhibition effect of HPMCAS is due to its dual role on inhibiting crystallization of carbamazepine, acted as a nucleation inhibitor and also a crystal growth retardant [161]. Ozaki *et al.* also exposed that amorphous griseofulvin and danazol had higher degree of supersaturated solution in the presence of PVP and HPMC compared to the polymers-free solution because of their inhibition effect on both kinetics of nucleation and crystal growth. Without polymers, only around 1.5-fold increased supersaturation for griseofulvin and 3-fold increased supersaturation for danazol compared with crystalline materials, respectively. In contrast, amorphous griseofulvin showed about 8-fold and 3-fold increased supersaturation in the presence of HPMC and PVP. For danazol, 15-fold and 9-fold increased supersaturation in the presence of HPMC and PVP, respectively [162].

Additives Effect on Nucleation

The inhibition effect of additives on nucleation are mainly attributed to the intermolecular interactions between APIs and polymers during the embryo formation phase and then disturbs the self-assembly of solute molecules. In nucleation system, determination of the induction time is a useful method for evaluating the kinetics of nucleus formation. Induction time, also called nucleation time, is the time span from the creation of supersaturated solution to the first nuclei formed [163]. In the presence of additives, the length of induction time for the nucleation is depended on the strength of the interactions between drugs and additives, which is determined on both hydrogen bonding functional groups of drugs and additives [159]. For example, in the presence of HPMC, the induction time of hydrocortisone acetate nucleation was longer than that in the presence of PVP, due to stronger interactions between hydrocortisone acetate and HPMC as HPMC has more hydrogen bonding functional groups per monomer unit [159]. The polymers HPMCAS and HPMC significantly retarded the nucleation of acetaminophen due to the intermolecular interactions between APIs and polymers [164]. Similar effect of HPMC on nucleation of felodipine from felodipine supersaturated solution was reported [165]. HPMCAS HF suppressed the nucleation of supersaturated carbamazepine solution due to strong hydrophobic interaction between HPMCAS and carbamazepine [161].

Additives Effect on Crystal Growth

The additives can be absorbed on the growth site and act as a mechanical barrier and thus inhibit the crystal growth [166]. The de-supersaturated rate would be significantly reduced when the additive attaches on the faster growing faces [164]. There are two types of attachments on the crystal surface, including reversibly physical absorption (van der Waals forces and electrostatic force) and irreversibly chemical absorption (covalent bonding) [157]. The interactions of hydrophobic [167], electrostatic interaction [168] and hydrogen bonding [169] between polymers and crystal faces are the key factors in absorption process as these interaction can drive the polymer absorption on the crystal surface [169]. The electrostatic interaction would be considered only when the additive and absorbent bear groups have opposite charges [170]. For un-ionized components, hydrophobic interactions and intermolecular interactions (e.g. hydrogen bonding) are important for inhibiting crystal growth. For instance, the intermolecular interaction between drugs of celecoxib and efavirenz and polymer PVP-VA promoted the polymer to absorb on the crystal surface for preventing crystal growth [169]. It has been also reported that the absorption of HPMC on different crystal faces of hydrocortisone acetate can modify the crystal habit by forming hydrogen bonds with the functional groups of API which are exposed at the surface of crystal [159]. Cellulose derivatives inhibited the crystal growth of ritonavir, which was contributed by the following properties of polymers: moderate level hydrophobicity and rigidity of polymer structure [157]. The absorption of polymers on crystal surface also can be influenced by the solution properties. For example, HPMCAS has different conformation when it absorbed on the crystal surface of felodipine in different pH solutions [166]. HPMCAS unevenly absorbed on the crystal surface in pH 3 while HPMCAS uniformly adsorbed on the surface in pH 6.8 and effectively covered the crystal growth sites [166].

2.4.2.2 Additives Screening

It is obviously significant for selecting effective additives to prevent nucleation and crystal growth for maximizing the period of the supersaturated state of high energy drugs. There are two steps for screening potential additives, including generation of supersaturated solution and de-supersaturated process analysis.

Generation of Supersaturated Solution

There are several techniques to generate a supersaturated solution, such as, solvent shift, pH change, temperature change, dissolving of high energy solid phases, and the addition of antisolvent that reduces the solubility of the solute [171]. The most commonly methods used are solvent shift [154, 163, 172] and dissolving a high energy solid form in solution [20, 134, 173, 174].

The solvent shift method is the most frequent technique to employ for polymer screening [175]. In this method, drug is dissolved in a water-miscible solvent as a stock solution, in which the drug has a high solubility. Supersaturated solution can be created by diffusing suitable fraction of stock solution of high drug concertation into dissolution media. The commonly used solvents included dimethyl sulfoxide (DMSO) [173, 176], methanol [154, 177], *N*,*N*-dimethylformamide (DMF) [178] and ethanol [179, 180]. For example, Sun and Lee used solvent shift method to create indomethacin, naproxen and piroxicam supersaturated solution [179]. Supersaturated loviride solutions with different supersaturation ratios were obtained via solvent shift method, for evaluating the inhibitory effect of HPMC-E5 on precipitation of loviride [181].

A supersaturated solution also can be formed by dissolving a high energy form in solution, such as amorphous forms, crystalline salts, or cocrystals. Many works has investigated the effect of additives on supersaturated solution by dissolving a metastable form, such as solid dispersion [156, 182].

Methods for De-Supersaturation Analysis

To determine additives effect on supersaturated solution, induction time of nucleation, the changes of drug concentration with time, mass and morphology of the precipitates in pre-dissolved additive solution need to be analyzed.

In general, for simply determine the overall effect of additives on inhibiting API crystallization kinetics (nucleation and crystal growth) from a supersaturated solution, the rate of de-supersaturation in unseeded de-supersaturation experiment is measured by detecting the changes of drug concentration [183]. As for determining the induction time, there are several apparatuses, such as optical microscopy, UV and turbidity detector. For example, a 20 mL supersaturation (supersaturation ratio of 1.5) solution of

acetaminophen was prepared in 10mM pH 6.8 sodium phosphate buffer at 70 °C with stirring rate of 700 rpm, followed by reduction of temperature to 20°C. When the new nucleus appeared, the laser transmission through sample decreased. The nucleation induction time was taken as the time difference between the initial decrease in transmission and the zero-time point [164]. The induction time of diprophylline during nucleation was detected by light transmission, which would be reduced once the nucleus appears [184]. Ozaki *et al.* used UV absorption to detect the induction time of danazol and griseofulvin. A supersaturated solution was firstly prepared by adding an aliquot of DMSO solution with high drug concentration into a 2ml fasted state simulated intestinal fluid (FaSSIF) in the absence or presence of polymers in a quartz cuvette at 300 rpm stirring rate. Finally, the induction time was detected by monitoring the UV absorption at 320nm (danazol) and 350nm (griseofulvin) and measuring the sharp change in the absorption-time curve. Different from laser or light transmission, a steep increased absorption happened when nucleus came out [173]. Furthermore, polarizing microscopy was also used to determine the induction time via detecting of firstly appeared crystals, such as nucleation of tripalmitin [185] and di- and metasilicate glasses [186]. In terms of crystal growth, the ability of additives can be determined by measuring the rate of de-supersaturation in presence of seed crystal using HPLC and UV to measure the changes of drug concentration with time [157].

To evaluate the additives (polymers) effect on crystal habit (e.g. morphology and size of new growth crystals) during crystallization, optical microscopy [164, 187, 188] and scanning electron microscopy [10] are widely used. For example, the solid residuals of acetaminophen after seeded crystal growth experiment were observed by microscope with a 40x magnification and found that polymers altered the morphology of crystals. Without polymers, the crystals were thin, flat and elongated. However, the crystals were large, prismatic and polyhedral in the presence of polymer poly(acrylic acid) [164].

2.4.3 Additives Effect on Crystal Dissolution

2.4.3.1 Methods for Determining Crystal Dissolution Mechanism in The Presence of Additives

In cocrystals dissolution process, the pre-dissolved additives in solution not only influence the crystallization of supersaturated condition but also the dissolution properties of the solid crystals. The performance of cocrystal-based product is depended on additives effect and cocrystal dissolution behaviors. Therefore, it is essential to understand the dissolution rate and dissolution mechanism of cocrystals in the presence of additives, which can lead to strategies for developing cocrystal enabling formulations [189].

The process of crystal dissolution is a specific type of heterogeneous reaction between the solid and solvent, including three steps: (1) absorption: solvent molecules absorb on the surface of crystal; (2) interaction or reaction: the crystal molecules interact/react with absorbed solvent molecules; (3) detachment and diffusion: the molecules detach and diffuse away from the crystal surface [189].

Atomic force microscopy (AFM) has been widely used for observation of the crystal dissolution at molecular level by analyzing the etching pattern changes of crystal surface during dissolution. The etching pattern is impacted by the crystal interaction network and the interaction between the crystal molecules in the lattice and solvent molecules [190-196]. The presence of additives in solution, would form an absorbed additive layer on the dissolving crystal surface that affect the solute bulk diffusion and surface diffusion during dissolution [197]. There are many factors that would impact the absorption of polymers on crystal surface, including crystal structure (i.e. functional group exposed on face [198]), polymer properties (i.e. chain rigidity and chain length [199]) and attachment energy between polymer and crystal surface [199]. For example, Wen *et al*. investigated the hydrogen bonding interaction between polymers and crystal face (010) of acetaminophen through detecting the etching pattern changes by applying AFM [200]. The presence of hydroxypropyl cellulose (HPC), 2-hydroxyethyl cellulose (HEC), poly(vinyl alcohol) (PVA) and hydroxypropyl methylcellulose (HPMC) changed the etching patterns of acetaminophen crystal surface in the direction of a-axis

due to the formation of hydrogen bonds between polymers and crystal surface. However, in the case of dextran, poly(ethylene glycol) (PEG) and poly(propylene glycol) (PPG) did not change the etching pattern in the direction of a-axis (crystal cell edge) because no hydrogen bonding was formed between polymers and crystal face.

As a crystal dissolves, the dissolution rate of each face is distinct because different function groups are exposed on each crystal face. Optical light microscopy (OLM) has been used to determine the dissolution rate of particular face of a single crystal by measuring the physical retreated velocities of different faces at a macroscopic scale [198, 201-203]. Adobes-Vidal *et al*. measured the dissolution rate of (010) and (101) faces of furosemide in 4 mL KCl (50mM) aqueous solution in a Petri dish by measuring the displacement of the width and length of (001) face with time using optical microcopy [198].

2.4.4 Additives Effect on Permeability

Based on the Biopharmaceutical Classification System, the ability of drug molecules to pass through the intestinal mucosa is a key factor for administrating the extent of oral absorption of a drug [26]. However, the enhanced drug concentration of solid form in gastrointestinal tract cannot always improve the drug absorption. Higuchi has mentioned that diffusion flux relies on thermodynamic activity/chemical potential instead of the concertation gradient [204]. In the presence of low concentration of polymers, enhanced permeation of drug could be obtained in supersaturated solutions due to polymers' inhibition effect on crystallization of stable form [205-210]. For example, the permeation of fentanyl was improved in propylene glycol/ethanol formulation because of the enhanced drug thermodynamic activity of fentanyl [209]. However, an increasing equilibrium solubility of API due to the additives' solubilization effect (i.e. surfactant), would reduce the permeation performance of API. This reduced permeability results from the formation of micelle between additive and drug, which would decrease the free fraction of drug available for membrane permeation [211, 212]. This observation is supported by the studies of Dahan *et al* [26], Miller *et al* [27, 213-215]. Raina *et al* [212] also showed that when additives concentration was higher than critical micelle concentration (CMC) the diffusive flux of

felodipine and nifedipine decreased. Besides, there is a maximum value of flux of drug, which could be achieved in a supersaturated solution when liquid-liquid phase separation (LLPS) take place.

The insight mechanism of stabilized and solubilized effect of additives on supersaturation and permeation behaviors can be revealed by using nuclear magnetic resonance (NMR) [216, 217]. For example, the mechanism underlying additives effect on permeation properties of carbamazepine were determined by NMR by observing the chemical shift and spin−lattice relaxation time (T_1) over spin−spin relaxation time (T_2) of carbamazepine in presence of HPMC-AS and P407 [216].

2.5 Flufenamic Acid Cocrystals Studies

2.5.1 Introduction of Flufenamic Acid (FFA)

In 1948, flufenamic acid (2-[[3-(trifluoromethyl)phenyl]amino] benzoic acid, FFA) was first synthesed by Wilkinson and Finar [218] and discovered it as a useful anti-inflammatory drug in 1963 [219]. Its anti-inflammatory property is due to the inhibition of the prostaglandin synthesis [220]. In 1996, FFA was used to treat the problems of arthritis and inflammation associated with muscular-skeletal [221]. Its acute (oral) potency was 16-folds as aspirin, 12-folds as aminopyrene, 3.2-folds as mefenamic acid and 1.6-folds as phenybutazole [222]. Furthermore, it has been discovered that FFA can act as an ion channel modulator where it not only impacts the non-selective cation channels and chloride channels but also modifies the potassium calcium and sodium channels [223]. Recently, it has been found that FFA has effect/activity on neuroprotection [224] and antitumor therapy [225]. There are nine reported polymorphs of FFA but only FFA I (white) and FFA III (yellow) has been used as commercial solid forms [226]. The transition point of FFA I and FFA III is 42°C: FFA III is the stable form and FFA I is the metastable form at room temperature [227]. It is a Class II drug with low water solubility (0.0067mg/mL in 22°C) and high permeability (logP =5.62) in BCS system [228, 229]. The poor water solubility leads to the low oral bioavailability of FFA, which restricts their applications on oral and parenteral pharmaceutical formulations. Many approaches have been used to enhance

the solubility of FFA, such as amorphous materials [230], solid dispersion with PVP [231] and Cyclodextrins [232].

2.5.2 FFA Cocrystals Research

As mentioned in Section 2.3.5, cocrystal is an effective approach to modulate the solubility, dissolution and other physiochemical properties of low water-soluble APIs via forming hydrogen bonds with high water-soluble components. Only 7 FFA cocrystals have been reported as summarized in Table 2. 2.

Table 2. 2 Summary of known FFA cocrystals

FFA cocrystal	Reference
FFA-transthyretin	[233]
1:1 FFA-nicotinamide (NIC)	[229, 234, 235]
1:1 FFA-Theophylline (TP), 1:1 FFA-2-Pyridone (PYR) and 1:0.5 FFA-4,4'-bipyridine (BP)	[229]
1:1 FFA- 2-chloro-4-nitrobenzoic acid (CNB) and 1:1 FFA- ethenzamide (ETZ)	[236]

2.5.3 FFA Cocrystals Design Strategies and Synthesis

To date, hydrogen bonds are the most frequently used strategy in FFA cocrystals design. The structure of FFA (Figure 2. 9a) composes of two aromatic rings with -NH bridge, CF_3 and carboxylic acid that has a strong hydrogen bond donor and acceptor. Based on the hydrogen bonding pattern (Figure 2. 9) of 6 FFA cocrystals, there are two cocrystal design strategies for designing FFA cocrystals. One is to use both C=O and C-OH of carboxylic acid to from hydrogen bonds with other coformers, such as NIC (Figure 2. 9b), PRY (Figure 2. 9d), CNB (Figure 2. 9f) and ETZ (Figure 2. 9g). The other strategy is to employ the OH of carboxylic acid to form hydrogen bonds with other coformers, such as TP (Figure 2. 9c), and BP (Figure 2. 9e).

FFA cocrystals have been successfully prepared by both solution-based and solid-based methods. In a study by Fabian *et al*, FFA-nicotinamide cocrystal was synthesized by liquid-assisted grinding and solution crystallization methods [234]. Aitipamula *et al.*

used solvent evaporation and liquid-assisted grinding to prepare FFA-theophylline cocrystal, FFA-2-pyridone cocrystal and FFA- 4,4′-bipyridine cocrystal [229].

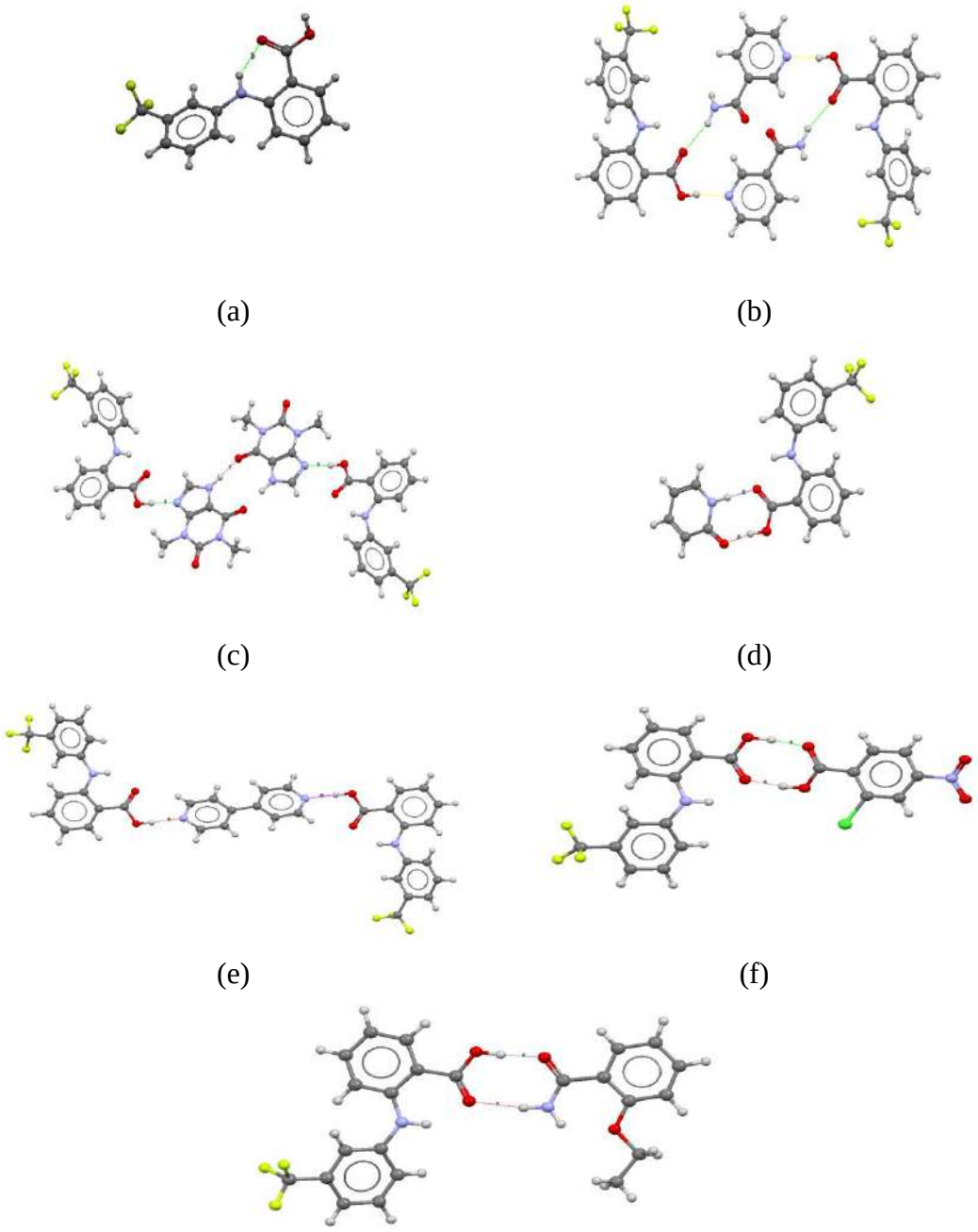

Figure 2. 9 Structures of (a) FFA I; (b) FFA-NIC CO, (c) FFA-TP CO, (d) FFA-PRY CO; (e) FFA-BP CO; (f) FFA-CNB CO and (g) FFA-ETZ CO.

2.5.4 Introduction of Pharmaceutical Cocrystal Coformers: Nicotinamide and Theophylline

Nicotinamide (NIC) (Figure 2. 10) is amide of niacin and belongs to vitamin B group (B_3), which has ability to restore cognition in Alzheimer's disease transgenic mice by employing sirtuin inhibition and selective reduction of Thr231-Phosphotau [237]. There are four reported polymorphs of NIC with different melting points, including NIC I (126-128°C), NIC II (112-117°C), NIC III (107-111°C) and NIC IV (101-103°C) [238]. Form I is the stable form at room temperature. NIC has been reported as a popular coformer in synthesis of pharmaceutical cocrystal [239], contributing to by its high water solubility and amide group for forming hydrogen bonding [235]. Table 2. 3 shows a list of cocrystals containing NIC.

Theophylline (TP) (Figure 2. 10) is an active pharmaceutical ingredient for treating respiratory diseases (e.g. asthma) with melting point at around 271°C [240, 241]. TP (Figure 2. 10) has been reported as a coformer for cocrystals because it can act as both hydrogen-bonding donor (imidazole NH and CH group) and hydrogen-boning acceptor (two carbonyl oxygen atoms) [242]. The cocrystals containing APIs and theophylline are drug-drug cocrystals, which have potential for developing combination drugs [243, 244]. Table 2. 3 shows a list of cocrystals containing TP.

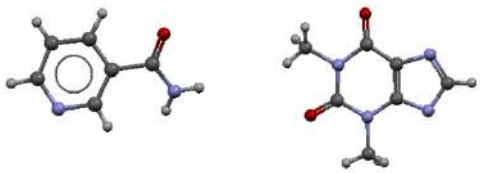

NIC TP

Figure 2. 10 Structures of NIC and TP

Table 2. 3 list of cocrystals containing NIC and TP

Coformer	Cocrystal	References
NIC	Flufenamic acid-NIC cocrystal, niflumic acid-NIC cocrystal, tolfenamic acid-NIC cocrystal and mefenamic acid-NIC cocrystal	[234]
	Naproxen-NIC cocrystal	[245]

	Carbamazepine-NIC cocrystal	[145]
	Celecoxib-NIC cocrystal	[246]
	Baicalein-NIC cocrystal	[247]
	Ibuprofen-NIC cocrystal	[248]
	α-lipoic acid-NIC cocrystal	[249]
	Simvastatin-NIC cocrystal	[250]
	Flurbiprofen-NIC cocrystal	[251]
	Salicylic acid-NIC cocrystal	[252]
	Diflunisal-NIC cocrystal	[253]
	Indomethacin-NIC cocrystal	[254]
	Protocatechuic acid-NIC cocrystal	[255]
	Curcumin-NIC cocrystal	[256]
	Dasatinib-NIC cocrystal	[257]
	Aspirin-NIC cocrystal	[258]
	Furosemide-NIC cocrystal	[259]
	P-coumaric acid-NIC cocrystal	[260]
	Rebamipide-NIC cocrystal	[261]
	Adefovir dipivoxil-NIC cocrystal	[262]
	Olanzapine-NIC cocrystal	[263]
	Propiconazole-NIC cocrystal	[264]
	Theophylline-NIC cocrystal	[265]
TP	Caffeine-TP cocrystal and	[266]
	Flufenamic acid-TP cocrystal	[229]
	Acetaminophen-TP cocrystal	[267]
	Glibenclamide-TP cocrytsal	[268]
	Sulfacetamide-TP cocrystal	[269]
	Diflunisal-TP cocrystal and diclofenac-TP cocrystal	[270]

2.5.5 Introduction of Polymers

Polyethylene Glycol (PEG)

PEG (Figure 2. 11) is a semi-crystalline polymer that contains different numbers of ethylene glycol unit with a molecular weight ranging from 200 to 300000. PEG is a non-toxic, colorless, odorless and non-irritating polymer. The viscosity of PEG would increase as increasing molecular weight. PEG 4000 is a frequently used polymer in pharmaceutical industry because of its high water solubility (50mg/mL at 25°C) and suitable melting point (50-58°C) [271]. It is a hydrophilic polymer that can improve dissolution, solubility and inhibit the crystallization of drug by forming hydrogen boning with drug [272],[273]. For example, PEG can reduce the crystallization rate of benzocaine and increase induction time for crystallization of ibuprofen and fenofibrate [273].

Polyvinylpyrrolidone (PVP)

PVP (Figure 2. 11) is an amorphous polymer which contains varying number of vinylpyrrolidone units with molecular weights falling in the range of 2500-3000000. The average molecular weight of PVP K30 is 40000 with Tg at 165.03°C. An increase in molecular weight of PVP would increase the viscosity resulting in lower dissolution rate of drug due to the formation of diffusion boundary layer on the dissolving surface [271]. PVPs are widely applied in pharmaceutical manufacturing as excipients [271]. PVP has also been found to stabilize the supersaturated condition of drugs by forming hydrogen bonding, such as norethindrone acetate [274], bicalutamide [275], indomethacin [276] and ketoconazole [277]. There are two functional groups (=N- and C=O) that are likely to form hydrogen bonding in each PVP unit. The carbonyl group is preferred for hydrogen bonding because the steric hindrance interrupts the intermolecular interaction with nitrogen atom [278].

Plasdone S630 (PVP-VA)

PVP-VA (Figure 2. 11) is an amorphous copolymer of *N*-vinyl-2-pyrrolidone (60%) and vinyl acetate (40%). It is white and odorless powder with an average molecular weight of 51000 [279]. PVP-VA is more hydrophobic than PVP but with a lower Tg (106°C) due to the presence of vinyl acetate groups and dissolves in water and a lot of organic

solvent. PVP-VA is a good binder for direct-compression tablet/drug granulation/coating materials of control release drug [280] and a stabilizer for drug crystallization. Each monomer unit of PVP-VA contains two strong hydrogen bonding acceptors of C=O of vinylpyrrolidone group and C=O vinyl acetate group. PVP-VA has been reported as an inhibitor of crystal growth rate of amorphous felodipine [281] and stabilizer for amorphous solid dispersion of ketoconazole [282], itraconazole [282] and dipyridamole [283].

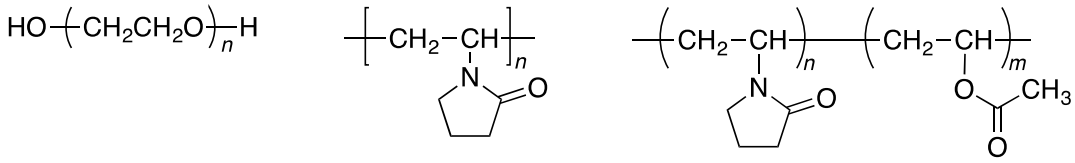

PEG PVP PVP-VA

Figure 2. 11 Molecular structures of polymers

2.6 Chapter Conclusion

In this chapter, a brief introduction about pharmaceutical cocrystals was given. Firstly, description and several key issues about cocrystals were presented, including cocrystal design strategies, coformer selection, cocrystal screening methods, cocrystal characterization techniques and cocrystal physicochemical properties. Secondly, the key problem of cocrystal during dissolution, solution media phase transformation, was mentioned. The additives effect on recrystallization, dissolution and permeation behaviors of cocrystals also was introduced in 2.4.2 and 2.4.3 section. The methods that applied for screening additives and determining the dissolution mechanism of cocrystals were discussed. Finally, some information about the materials that used in this study were introduced, including FFA, FFA cocrystals, NIC, TP, PEG, PVP and PVP-VA.

Chapter 3 Materials and Methods

3.1 Chapter Overview

The materials, analytical techniques and calculation methods used in this study were fully described in this chapter.

Firstly, the formulas, purity and manufacturers of materials were mentioned. Then, the analytical techniques applied to characterize the cocrystals formation and determine the physicochemical properties of cocrystals were presented, including infrared spectroscopy (IR), Raman spectroscopy, differential scanner calorimetry (DSC), high performance liquid chromatography (HPLC), atomic force microscopy (AFM), optical light microscopy (OLM), X-ray diffraction (XRD) and nuclear magnetic resonance (NMR). The working principle, instrumental models, parameter setting and operation procedures of these analytical techniques were comprehensively discussed. Then, the experimental and preparation methods were also mentioned. The calculation methods were presented, containing the equation of solubility parameter (SP), supersaturated ratio (SSR), supersaturated parameter (SSP), cocrystal solubility, dissolution performance parameter (DPP) and flux rate.

3.2 Materials

All materials were used as received, without further processing. The details of materials were presented in Table 3. 1.

Table 3. 1 Lists of raw materials for experiments

Materials	Formula	Purity/grade	Manufacturer
Flufenamic Acid	$C_{14}H_{10}F_3NO_2$	97%	Sigma-Aldrich Company Ltd., Dorset, UK
Nicotinamide	$C_6H_6N_2O$	≥99.5%	Sigma-Aldrich Company Ltd., Dorset, UK
Theophylline	$C_7H_8N_4O_2$	≥99.5%	Sigma-Aldrich Company Ltd.,

			Dorset, UK
Methanol	CH_3OH	HPLC grade	Fisher Scientific Loughborough, U.K.
Ethanol	CH_3CH_2OH	Lab grade	Fisher Scientific Loughborough, U.K.
Acetonitrile	CH_3CN	HPLC grade	Fisher Scientific Loughborough, U.K.
Chloroform-d	$CDCl_3$	99.8%	Cambridge Isotope Laboratories, Inc, USA
Double distilled water	H2O	Double distilled	Lab made by Bi-Distiller (WSC044.MH3.7, Fistreem International Limited, Loughborough, UK)
Potassium phosphate monobasic	KH_2PO_4	≥99.0%	Sigma-Aldrich Company Ltd., Dorset, UK
Sodium hydroxide	NaOH	0.2M	Fisher Scientific Loughborough, U.K.
PEG 4000	$C_{2n}H_{4n+2}O_{n+1}$	`	Sigma-Aldrich Company Ltd., Dorset, UK
PVP K30	$(C_6H_9NO)_n$		Ashland Inc. (Schaffhausen, Switzerland)
PVP-VA	$(C_6H_9NO)_n(C_4H_6O_2)_m$		Ashland Inc. (Schaffhausen, Switzerland)

3.3 Methods

3.3.1 Analytical Techniques

3.3.1.1 Vibrational Spectroscopy

Vibrational spectroscopy is a useful and energy sensitive approach to identify the structure of organic chemicals via detecting the functional groups or finger print. Its working principle is based on the variation of dipole moment (IR) or polarizabilities

(Raman) of samples because of the molecular vibration (stretching, blending). When the radiation shines on the sample, the electromagnetic radiation would be absorbed (IR) or scattered (Raman).

3.3.1.1.1 Infrared (IR) Spectroscopy

IR spectroscopy is an analytical method to identify chemical samples (solid, gas or liquid) by detecting the interaction between a molecule and radiation in the IR regions from 2.5μm to 25μm (4000 to 400cm^{-1}).

The underlying principle behind IR spectroscopy is the absorption will only take place in resonant frequencies, referring to the frequency (energy) of incident radiation/photon matches the frequency of the molecular vibration or the energy gap from the ground state to excited state. The samples could be motivated to an excited state by absorbing energy from incident radiation, causing the radiation loses energy. There are three factors impact the energy gap including shape of the molecular potential energy surface, the associate vibronic coupling and masses of the atoms.

Fourier transform infrared (FTIR) spectroscopy is for recording the infrared spectra based on the emission or absorption of radiation when the radiation hits a solid or liquid sample. All wavelengths would be simultaneously measured by FTIR via applying a Michelson interferometer (Figure 3. 1) In Michelson interferometer, the source radiation passes through a beamsplitter, which splits the source into two separated beams and send them to two mirrors. One beam is reflected from the fixed mirror and the other from movable mirror. The total path length of movable beam is different compared with the fixed mirror beam, this because of the movement of movable mirror. Then two beams recombine when they meet again at the beamsplitter and the different in path length creates a destructive and constructive interference, called interferogram. The recombined beam then passes through the sample, in which the beam will be absorbed, reflected, transmitted or scattered. The variation of the transmitted light is a function of the position of the moving mirror. Only transmitted light would be detected and reported as a signal of variation in transmitted light versus time. Then a mathematical Fourier-transform is used to convert the raw data (intensity vs time) into desired result (intensity vs frequency).

In this study, the spectra of solid and liquid sample were determined by an ALPHA A4 interferometer (Bruker UK Limited, Coventry, UK) by conjunction with IR. The samples can be observed directly without further preparation. A universal attenuates total reflectance (ATR) accessory is horizontally equipped with the ALPHA interferometer for measuring the solid sample. A small number of samples were putted on the surface of the diamond ATR plate and the ATR assembly were clamped to ensure good contact. The solution spectra were collected using the same spectrometer fitted with a transmission accessory and the Bruker 6500S Circular Aperture liquid cell with size of 32 × 3 mm CaF_2 window. The path length was 0.05 mm. In each measurement, 30 scans were collected per spectrum with a resolution of 2 cm^{-1} in the spectral region of 400 to 4000 cm^{-1} using OPUS software. All the spectral data were collected at an ambient temperature, between 20 to 23°C [183].

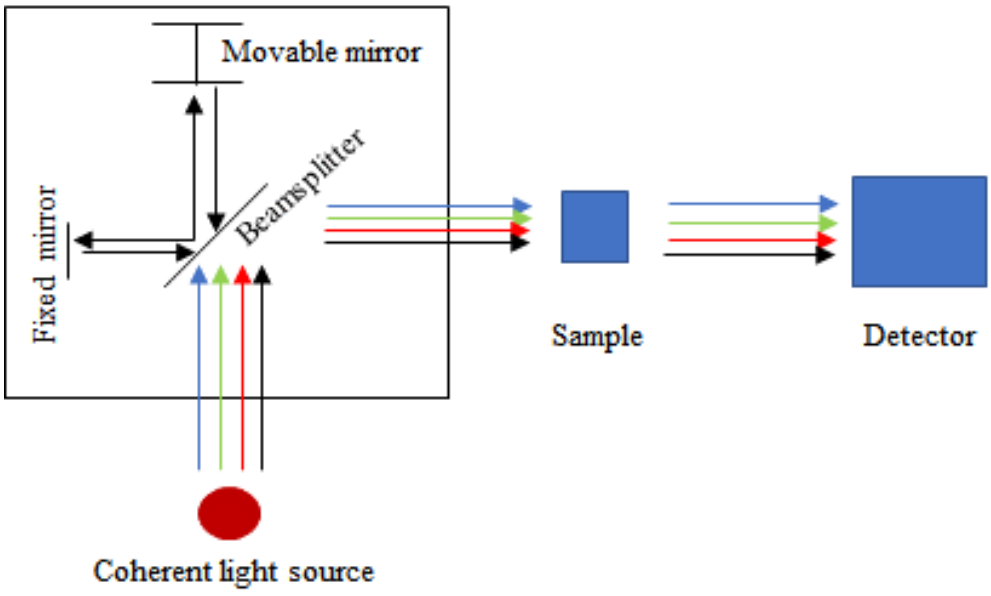

Figure 3. 1 Schematic diagram of Michelson Interferometer.

3.3.1.1.2 Raman Spectroscopy

Raman spectroscopy relies on inelastic scattering/Raman scattering of photons by samples, which was initial observed experimentally by C.V. Raman and K.S. Krishnan in 1928.

Raman spectroscopy is a common analytical equipment for detecting the molecules structure, as the vibrational information can be obtained from scattering the radiation by the molecules. Raman spectroscopy is specifically relevant to the chemical bonds and symmetry of molecules. In Raman system, it is not necessarily for the photons that have the same energy as the energy gap between ground state and excited state. The working principle of Raman spectroscopy is that variations of polarizability of the molecule in the electric field, in which radiation would change the electron cloud around the nuclei of a molecule.

When photons impinge on a sample, majority of the scattering is elastic without loss of energy thus no change of frequency, this scattering is known as Rayleigh scattering (Figure 3. 2). However, Raman scattering is an inelastic scattering, meaning that the energy/frequency of scattering photons is changeable because energy of photons is transferred or accepted from molecule of a sample when the molecule vibrated. If the incident protons transfer energy to the sample, the incident photon will have a redshift (lower frequency), also called stokes shift (Figure 3. 2). In the contrast, if the incident proton accepted energy from a sample, it is scattered with a blueshift (higher frequency) and referred as anti-stokes shift (Figure 3. 2). In most of cases, stokes scattering is the most common type of scattering as only small number of molecules are exited in an excited state. Typically, Raman scattering is recorded in the wavenumber ranges of 100-4000cm^{-1}.

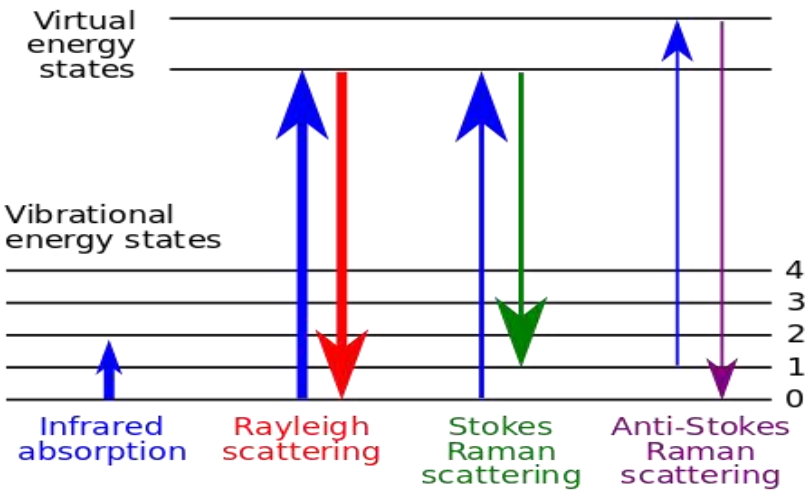

Figure 3. 2 Energy-level diagram showing the states involved in Raman[284]

Enspectcter R532® Raman spectrometer (Figure 3. 3) is applied to measure the Raman spectra of solid or liquid sample directly without further sample preparation in room temperature. This equipment is comprised three parts: (1) 20-30mW an output power laser source with a wavelength of 532nm; (2) Czerny-Turner spectrometer; (3) scattered light collection and analysis system. The ranges of wavenumber of the spectra is recorded from 140 to 6000cm^{-1}, covering the vibration ranges of inorganic and organic molecules and photoluminescence visible range. In this study, for solid measurement, the parameter of the integration time was 200 milliseconds and each spectrum was achieved in an average of 100 scans.

Figure 3. 3 Enspectcter R532® Raman spectrometer

3.3.1.2 Differential Scanner Calorimetry (DSC)

DSC is the most used thermal analysis technique applied to determine enthalpy changes of a sample, such as melting point temperature, crystalline phase transition temperature and glass transition temperature. The fundamental principle of DSC is that when phase transformation of the sample occurs, the amount of the heat flow will change for maintaining the same temperature of the sample and reference. In an endothermic process, more heat need to flow to the sample for increasing the temperature, such as the melting of solid into liquid. In contrast, in an exothermic process, less amount of heat flow is required for the sample to produce the same temperature of reference, like crystallization. The DSC equipment can measure the amount of heat absorbed or released during the phase transition by detecting the difference in heat flow between the sample and reference. An example of DSC curve is shown in Figure 3. 4.

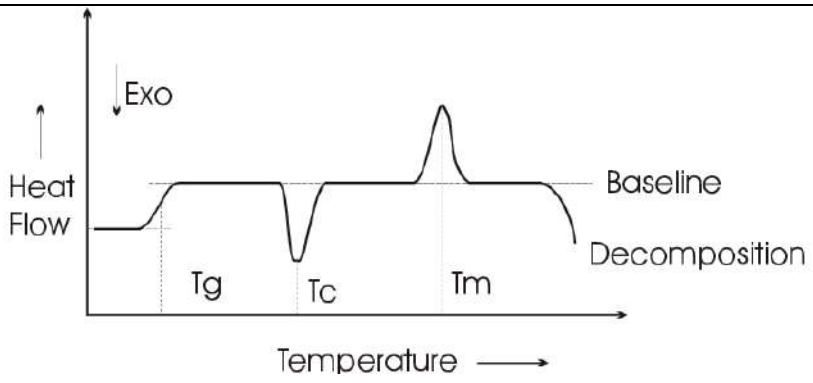

Figure 3. 4 DSC curve [285]

In this study, the melting point of solids was measured by a PerkinElmer Jade DSC (PerkinElmer Ltd., Beaconsfield, U.K.) controlled by Pyris Software. The temperature and heat flow of the instrument were calibrated using indium and zinc standards. A test sample (8−10 mg) was analyzed in crimped aluminum pan with a pinhole pierced lid. Measurements were carried out at a heating rate of 20 °C/min under a nitrogen flow rate of 20mL/min [183].

3.3.1.3 High Performance Liquid Chromatography (HPLC)

HPLC is a liquid chromatographic technique to separate mixture sample into the individual component to identify, quantify and purify the mixture based on molecular composition and structure. HPLC instrumentation consist of a solvent reservoir, degasser, pump, sample injector, column, detector and data collection devise. A small volume sample (0.1-100μL) is injected into the flow stream of the mobile phase and flows through a column with a stationary phase. If a component has stronger interaction with stationary phase, then it will move slower than other components thus has longer retention time (the time point that specific analyte elutes from the column). There are different types of stationary phase including normal phase (silica gel), reverse phase (silica gel-C18), ion-exchange (stationary phase contains ion group) and size exclusion. In reverse phase HPLC, the stationary phase is non-polar and the mobile phase (mixture of water and methanol/acetonitrile) is polar. Therefore, the component with less polarity has longer retention time. A chromatography detector, lied at the end of the column, is used to detect separated analytes that eluted from the column then convert the physical/chemical property of effluents into an electric signal associated with the

concentration or identity of effluents. The UV detector is the most frequently used to measure the sample that absorb UV light at a specific wavelength (190-400nm) [286]. If the wavelength is shorter than 210nm, it is not suitable for HPLC system because every organic chemical can absorb when the wavelength is less than 210nm. HPLC technique is one of most important techniques which has been used in lots quantitative analysis work for cocrystal solubility measurement. In cocrystal system, UV method cannot determine the individual concentrations of each components. In contrast, HPLC can separate mixture components into individual components hence can determine the individual concentration for cocrystal components.

In chapter 5 and chapter 6, A Perkin-Elmer series 200 HPLC system (PerkinElmer Ltd., Beaconsfield, U.K.) equipped A HAISLL 100 C18 column (5μm, 250 × 4.6 mm) (Higgins Analytical Inc., Mountain View, CA, USA) was utilized to measure FFA, NIC and TP concentration in solution at room temperature. All samples were detected by a UV absorption detection. For determining the HPLC methods of FFA, NIC and TP, we tried different percentages of mobile phase (Table 3. 2). We found out that the following parameters were the best conditions for FFA, NIC and TP. The method that applied for detecting FFA was used mobile phase with 15% water (including 0.5% formic acid) and 85% methanol at 1.5 mL/min flow rate and 286 nm wavelength. Both NIC and TP concentrations were identified by an isocratic method with 55% methanol and 45% water at 1mL/min flow rate and 265 nm. The injection volume was 20 μL.

In chapter 7, A HEWLETT PACKARD series 1100 automatic HPLC with a Luna@ Omega PS C18 100A LC column (5μm, 150× 4.6 mm) (Phenomenex, Inc., Macclesfield, UK) at 40°C was employed. An isocratic method was used to detect FFA, NIC and TP concentration. The method with 15% water (including 0.5% formic acid) and 85% methanol at 1.5mL/min flow rate and 286 nm wavelength with 50 μL injection volume was used for detecting FFA concentration. NIC concentrations were identified by a method with 10% methanol and 90% water at 1mL/min flow rate and 265 nm. TP concentrations were determined by a method with 40% methanol and 60% water at 1mL/min flow rate and 265nm. The injection volume of NIC and TP was 20 μL.

The series of concentrations for building calibration curves of FFA, NIC and TP was listed in Table 3. 3. Calibration graphs (Table 3. 4) of FFA, NIC and TP were produced using peak areas verse concentration. Three replicated injection of each sample were injected into machine. The final peak area was the average of 3 peak areas. Low concentration calibration curve was for permeation test and high concentration calibration curve was for dissolution test, solubility test and desupersaturated experiments. HPLC calibration curves were validated by known concertation standard solution of FFA, NIC and TP. The validation results of calibration curve were listed in Table 3. 5, showing that all standard deviation (SD: to evaluate the difference between real and measuring concentration) less than 5%, meaning the accuracy of all calibration curve were high.

Table 3. 2 HPLC methods

Components	Mobile Phases		Flow rate (mL/min)	Detection Wavelength (nm)
	Water (V/V%)	Methanol (V/V%)		
FFA	50 (with 0.5% formic acid)	50	1.5	286
	30 (with 0.5% formic acid)	70	1.5	286
	15 (with 0.5% formic acid)	85	1.5	286
NIC	50	50	1	265
	65	35	1	265
	55	45	1	265
TP	50	50	1	265
	55	45	1	265

Table 3. 3 Concentrations for calibration curve

Components	Calibration curve range	Concentration points (μg/mL)
FFA	0.1-1(μg/mL)	0.01, 0.05, 0.1, 0.5 and 1
	1-50(μg/mL)	1, 5, 10, 20, and 50
NIC	0.1-1(μg/mL)	0.1, 0.2, 0.5 and 1
	1-50(μg/mL)	1, 5, 10, 20, and 50
TP	0.1-1(μg/mL)	0.1, 0.2, 0.5 and 1
	1-50(μg/mL)	1, 5, 10, 20, and 50

Table 3. 4 Calibration curves of FFA, NIC and TP

Compoments	Calibration Curve	
	0.1-1 μg/mL	1-50 μg/mL
FFA	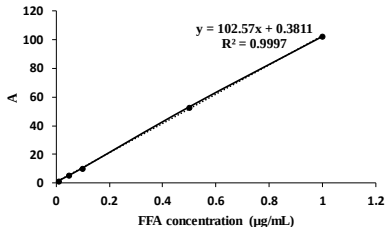	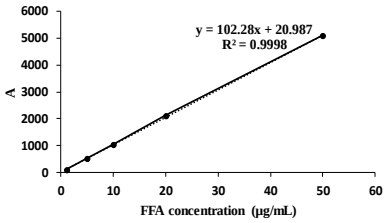
NIC	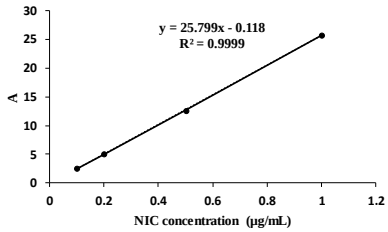	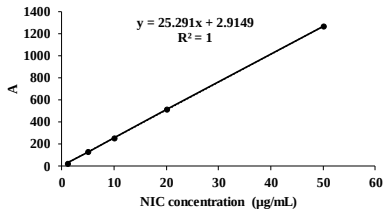
	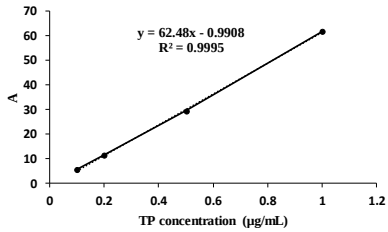	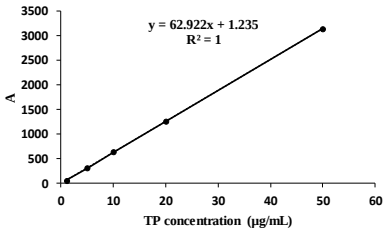

Table 3. 5 Validation of calibration curve x: in unit of μg/mL; C_r: validation solution of real concentration, μg/mL and C_m: validation solution of measured concentration, μg/mL

Testing samples		Calibration equations		Validation		
Components	Concentration range (μg/mL)			C_r	C_m	$\frac{\lvert C_m - C_r \rvert}{C_r}$%
FFA	0.1-1	y=102.57x+0.3811	R^2=0.9997	0.8	0.81	1.25
	1-50	y=102.28x+20.987	R^2=0.9998	30	29.84	0.53
NIC	0.1-1	y=25.799x-0.118	R^2=0.9999	0.8	0.78	2.50
	1-50	y=25.191x+2.9149	R^2=1	30	29.68	1.07
TP	0.1-1	y=62.48x-0.9908	R^2=0.9995	0.8	0.82	2.50
	1-50	y=62.622x+1.235	R^2=1	30	29.54	1.53

3.3.1.4 Atomic Force Microscopy (AFM)

AFM is a type of scanning probe microscopy, one of the important techniques for measuring, manipulating and imaging sample on the atomic level with a high resolution

at nanoscale. Its first time used in experiment was in 1986 and original commercial version was introduced in 1989.

AFM (Figure 3. 5) comprises several configurations, including cantilever, support for cantilever, piezoelectric element, tip, detector of deflection and motion of cantilever, xyz driver and sample stage. Practically, an ultra-fine tip (probe) with needle shape approaches the sample and scans the surface and the movement (up and down) of the tips causes a deflection of the cantilever. Then a laser irradiates on the cantilever at an oblique angle and is reflected from the back of cantilever. The incidence angle of the laser beam will be altered as a function of the deflection of cantilever. The reflected laser beam strikes a position-sensitive photo-detector, which can translate the deflection of cantilever into an electrical signal and the intensity of the signal is proportional to the displacement of the cantilever. The position of sample needs to be under the tip, adjusted by xyz driver.

AFM operation is classified into three modes based on the way of tip motion: non-contact mode, contact mode and tapping mode. Contact mode (static mode) is the simplest and most forthright imaging mode. In contact mode, the tip continuously drags cross the surface of the sample in a well-defined scan area with a repulsive interaction force. The cantilever deflection is directly used as a feedback signal for maintaining the cantilever in a constant position which is set by the user. Low stiffness cantilevers need to be used for strengthening the deflection signal due to the measurement of static signal is influenced by the noise and drift. The lateral force that exerted on the surface is high, could damage the surface structure of the sample. Therefore, contact mode is not suitable for the sample with soft surface.

In this study, AFM (Agilent 5420 SPM, USA) measurements were carried out in contact mode at room temperature using a J-type piezo-scanner with a standard silicon nitride tip (Windsor Scientific Ltd., UK). The resolution of a measurement was 512 × 512 points (nm × nm) with equal steps along the x and y directions. The images created by AFM system software were saved as the deflection mode, which was the derivative along the scan directions of the surface profile.

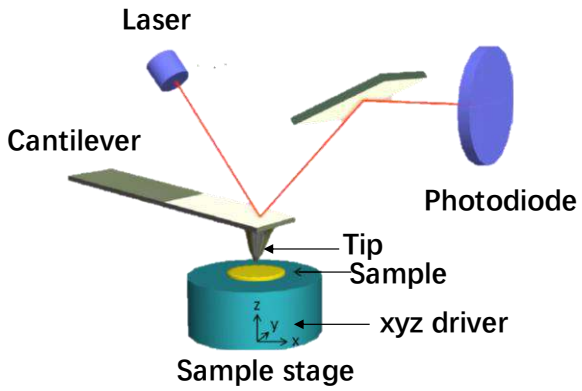

Figure 3. 5 Diagram of AFM [287]

3.3.1.5 Optical Light Microscopy (OLM)

Optical microscopy (light microscopy) is a type of microcopy that employs visible light and lenses to magnify image of small samples which cannot be observed by naked eye. There are several configurations in an optical microscopy, including eyepieces, objective turret, objective lenses, focus knobs (coarse and fine adjustment), sample stage, light source, diaphragm and condenser and mechanical stage (moving the sample). The principle of the optical microscopy is that the sample will be magnified by an objective lens to create a magnified image. The magnified image will be further magnified by eyepiece to allow the user to observe the sample.

In this study, a LEICA DM 750 polarizing microscope (Leica Microsystem Ltd., Milton Keynes, U.K.) with a 200× or 100× objective equipped with a version 4.0 studio capture for monitoring the FFA crystallization behavior from a supersaturated solution and displacement of different faces of a single crystal during dissolution.

3.3.1.6 X-ray Diffraction (XRD)

X-rays are electromagnetic waves with very short wavelengths, ranging from 0.001 to 10 nanometers. The X-rays diffraction can happen in crystal due to several reasons: (1) the atoms are periodically arranged in a crystal that can diffracted the X-rays; (2) the wavelength of X-rays is similar as the distances between crystal planes. X-ray diffraction is a non-destructive and common analytical technique for understanding the atomic spacing and crystal structure of a crystal. When a monochromatic X-ray beam

shines a crystal, the incidence beam will be diffracted into many specific directions by crystalline atoms. A three-dimensional X-ray crystallography of the electron density in the crystal can be calculated by detecting the intensities of diffracted spots and angles of the diffracted beams. The average positions of the atom and chemical bonds within the crystal can be measured based on the electron density

A constructive interference of the diffracted beam can occur when the conditions satisfy Bragg's Law:

$$n\lambda = 2d\sin\theta \qquad \text{(Equ.3-1)}$$

Where n is any integer, λ is the wavelength of the incidence beam, d is the distance between crystal planes and θ is the incidence angle (Figure 3. 6).

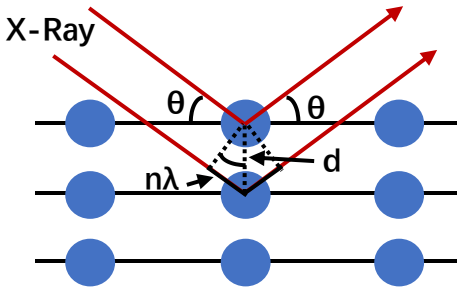

Figure 3. 6 Extra distance (2dsinθ) of x-Rays for penetrating deeper into the sample

The samples used in X-ray diffraction experiments can be single crystal or powdered sample. Single crystal X-ray diffraction is used to detect the unit cell, including position of the atoms within the crystal and cell dimension. In this diffraction, the intensity of diffraction spots is a function of the Miller indices (hkl), which used to determine the planes of atoms. In X-ray powder diffraction (XRPD), all possible diffraction directions of the lattice can be detected by scanning the powdered sample. The crystalline materials can be identified by conversing the diffraction peak into d-spacings according to the Bragg's Law.

In this study, X-ray powder diffraction pattern of solids was recorded from 5° to 35° at a scanning rate of 0.3° (2θ) min^{-1} by D2 PHASER diffractometer (Bruker U.K. Limited,

Coventry, UK). Cu-Kβ radiation was used with a voltage of 30 kV and current of 10 mA.

3.3.1.7 Nuclear Magnetic Resonance (NMR) Spectroscopy

NMR is a spectroscopy technique for studying chemical, physical and structure information of molecule by absorbing and re-emitting electromagnet radiation in a magnate field. In a molecule, all nuclei are charged and some of them have spin. Only the atom with odd mass or odd atomic number (such as ^{1}H and ^{13}C), the nuclei will have spin. Practically, a magnetic field is created due to the spin of nucleus. without an extra applied magnetic field, nucleus spin in different directions. When nucleus in an extra magnetic field, they will be parallel with the extra magnetic field and an energy transfer will happen between the ground state and excited state of nuclei. The energy gap (between ground state to exited state) of different nuclei is distinct. An energy transfer takes place from ground state to exited state by absorbing radio frequency, which would be emitted when exited state is back to the ground state. A NMR spectrum obtaining based on the emitted frequency, is a plot of intensity of signal as a function of emitted frequency.

Normally, the emitted frequency is converted to chemical shift (ppm) in a spectrum, referring to the difference in parts per million between the emitted frequency of the evaluated nuclei and frequency of reference. For proton NMR, the chemical shift of tetramethysilane (TMS) is 0 ppm, thus it is always used as reference. The chemical shift is changed when the electron density is altered around the nucleus. High electron density around the nucleus will shield the nucleus and the signal would locate in upfield (low chemical shift) and vice versa. There are several factors that impact the chemical shift, including electronegative group, magnetic anisotropy of π system.

In this study, a Bruker AV400 NMR Spectrometer (Bruker UK Limited, Coventry, UK). was used to measure the ^{1}H NMR for probing interaction among drug, coformer and polymer in a ternary solution. Samples were prepared in deuterated chloroform ($CDCl_3$) using standard 5 mm NMR tubes and TMS as an internal standard. For each ^{1}H NMR measurement, 64 scans with a relaxation delay of 1s were set, a spectral with 8278Hz

and a time domain of 32k data points. All analyses were carried out using software MestReNova V11.0 (Mestrelab Research, Escondido, CA 92027, USA).

3.3.2 Experimental Methods

3.3.2.1 Apparent Equilibrium Solubility Test

Equilibrium solubility test is used to measure the amount of materials that can dissolve into a specific solvent to generate a saturated solution under specific temperature and pressure.

In this study, all samples solubility was determined by suspending an excess amount of crystalline materials in small vials with 20mL dissolution media. The suspension was kept at specific temperature with specific well-defined shaking rate for 24h. The supernatant was separated from excess solids in solution by MSE Micro Centaur at 13000RPM for 1min in a MSB 010.CX2.5 centrifuge (MSE Ltd., London, U.K.). Subsequently, the supernatant was diluted, and the concentrations of FFA and coformers were determined using HPLC. The solid residues were retrieved from the tests, dried for 24h at ambient temperature, and analyzed by DSC, FTIR, and XRPD. All experiments were conducted in triplicate, and data were reported as an average concentration in solution.

3.3.2.2 Desupersaturation Experiments

Desupersaturation experiments is used to evaluate the polymers effect on the kinetics of nucleation and crystal growth in a cocrystal supersaturated system. Seeded desupersaturation experiment is applied for examining the polymers effect on crystal growth. A low supersaturation ratio should be used in the crystal growth experiments for avoiding secondary nucleation. The overall effect of polymers of crystallization of supersaturated solution can be studied by using unseeded supersaturated solution.

In this study, all supersaturated solutions were generated by solvent shift method. In seeded desupersaturation experiments, 50mg of milled FFA I crystal seeds (size $\leq$ 250μm) were placed into 50mL dissolution media and reached to FFA equilibrium state at 37°C for 24 h. A supersaturated solution was created by diffusing 0.3mL of a 5

mg/mL FFA stock solution of pure FFA, FFA-NIC CO or 0.6mL of 2.5mg/mL FFA-TP CO into the FFA equilibrium solution. The amount of ethanol added to the medium was small and had a negligible impact on the apparent FFA equilibrium solubility. In unseeded desupersaturation experiments, a supersaturated solution was generated by diffusing 20mL of 500μg/mL FFA stock solution of pure FFA, FFA-NIC CO or FFA-TP CO to 80mL of water, resulting in 100 μg/mL FFA in the cosolvent of 1:4 ethanol and water.

Each sample (1mL) was withdrawn from the solution at six predetermined time intervals, i.e. 5, 15, 30, 60, 120 and 240min. The supernatant was separated from excess solids by centrifugation at 13000RPM for 1min in a MSE Micro Centaur. The supernatant was diluted to determine the concentrations of FFA and coformer of NIC or TP by HPLC. The solid residues obtained from the desupersaturation experiments were examined by DSC, FTIR and OLM. All experiments were conducted in triplicate and data were reported as the average of the experiments.

3.3.2.3 Cocrystal Solubility Test

The cocrystals solubility cannot be measured by using the normal solubility test method because of their unstable thermodynamic in solution. A method called eutectic point measurement is applied to successfully measure the solubility of cocrystal, in which two solid phases of drug and cocrystal coexisted in an equilibrium state.

The transition concentrations of FFA and a coformer in PBS were measured to determine the solubility of cocrystal. A series of the coformer solutions with different concentrations were prepared. Excess amount of FFA I crystalline materials was added into a small vial with 20mL of each of the prepared coformer solutions in a shaking water bath at 250RPM shaking rate at 23 ± 0.5 °C for 24 h. The samples were separated from excess solids by centrifugation at 13000RPM for 1min in a MSE Micro Centaur. The concentrations of FFA and coformers were determined by HPLC and the solid residues were analyzed by XRPD, DSC, and FTIR. The transition concentrations (or an eutectic point) of a cocrystal were determined in the lowest coformer solution prepared where two solid phases of the solid drug and cocrystal coexisted in equilibrium with solution. All experiments were repeated in triplicate.

3.3.2.4 Powder Dissolution Test

The powder dissolution test can be conducted under both in-sink and non-sink condition to examine the effect of polymers on dissolution behaviors of drug by analyzing the concentration changes of drug with time in dissolution medium. In sink condition, the dissolution medium volume should be three to ten times greater than the volume required to saturate a drug in solution. For non-sink condition, the needed volume of dissolution medium is three to ten times less than the saturation volume of drug.

Under sink condition, the effect of polymers on the dissolution rate of cocrystals can be evaluated. In this condition, the changes of the dissolution rate of cocrystals in different polymers solution is relevant to the interaction between the pre-dissolved polymer and dissolving crystal surface. Under non-sink condition, the capability of polymers on generating and maintaining the supersaturated state of cocrystals would be examined during dissolution. Additionally, assessment of the supersaturated system under non-sink condition can mimic in vivo conditions in the gastrointestinal tract.

All samples that used in powder dissolution tests were slightly grinded by a mortar and pestle and sieved by a 60mesh sieve (below 250μm) to diminish the influence of particle size on the dissolution rates. Dissolution media (400mL) in a flat bottom beaker was used in each of the experiments. For sink condition experiments, cocrystal powders with equivalent 40mg of FFA I were used. While powders with equivalent 400mg of FFA I were used for non-sink condition tests. The dissolution tests were conducted at 23 ± 0.5°C with the aid of magnetic stirring at 250 RPM. Samples of 1 ± 0.1mL were withdrawn from the dissolution vessel at predefined time points of 5, 15, 30, 60, 120, and 240min. The supernatant was separated from excess solids by centrifugation at 13000RPM for 1min in a MSE Micro Centaur. HPLC was used to determine the concentrations of FFA and coformers of NIC or TP. Solid residues obtained from the non-sink condition experiments were dried at room temperature and analyzed by DSC, FTIR, and XRPD. All experiments were repeated in triplicate.

3.3.2.5 OLM Monitoring Single Crystal Dissolution and Analysis

OLM with video camera at 200× magnification and version 4.0 of the Studio Capture software were used to monitor the displacement of different faces of a single crystal during dissolution. The size of single crystals ranges from millimeters to one centimeter. A single crystal was horizontally placed inside a Petri dish with one end fixed by blue tack and then followed by addition of 20mL of PBS in the absence or presence of a 200μg/mL pre-dissolved polymer. Data were collected at 0, 2, 4, and 6h.

The specific faces' dissolution rates of single crystals (FFA I, FFA-NIC CO and FFA-TP CO) were determined by measuring the retreated velocity of the faces. Figure 3.7 represents a model showing the temporal change in the lateral dimensions of single crystals. The retreated rate of the crystal length represents for the dissolution rate of the (100) and the retreated velocity of crystal width represents for the dissolution rate of the (001). The dissolution rate of (100) and (0-11) for FFA I, (01-1) and (100) for FFA-NIC CO and (001) and (100) for FFA-TP CO was monitored by OLM. All experiments were repeated in triplicate.

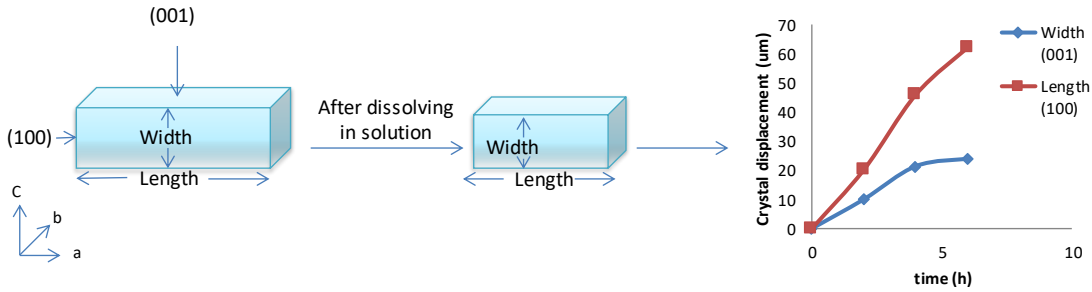

Figure 3.7 Model of dissolving a single crystal

3.3.2.6 Dissolution and Permeation Measurements

In order to determine in vitro behavior of a cocrystal formulation, a dissolution/permeation (D/P) system was used to evaluate the dissolution and permeation behavior of cocrystals simultaneously. The D/P system consists of side-by-side chambers with a regenerated cellulose membrane of a MWCO of 6-8 KDa (Spectrum Labs, USA) mounted between the donor and acceptor sides as a model membrane of the human intestine shown in Figure 3. 8. Each compartment has a capacity of 10mL and orifice diameter of 0.9 cm corresponding to 0.671 cm^2 surface

area of the membrane. A small amount of crystalline materials (size below 250µm) was added into a donor compartment and then 9mL of 0.01M pH 4.5 PBS was filled into the receptor cell. Finally, 9mL of 0.01M pH 4.5 PBS without and with a pre-dissolved polymer solution was added into the donor cell to start the experiment. The temperature of the cells was maintained at 37°C using a circulating water bath. The samples from donor was withdrawn using a syringe and immediately replaced the same amount of the fresh dissolution media into the donor cell to keep the constant dissolution volume in the cell at pre-determined time. The samples from donor need to be separated from excess solids by centrifugation at 13000RPM for 1min in a MSE Micro Centaur. The sample concentration measurement from donor cell mainly showed the dissolution profile. The sample was taken from the acceptor cell using a 100 µL Gilson pipette. Concentrations measured from acceptor represented the permeation profile. The FFA, NIC and TP concentration was determined by an automatic HPLC. All experiments were repeated in triplicate.

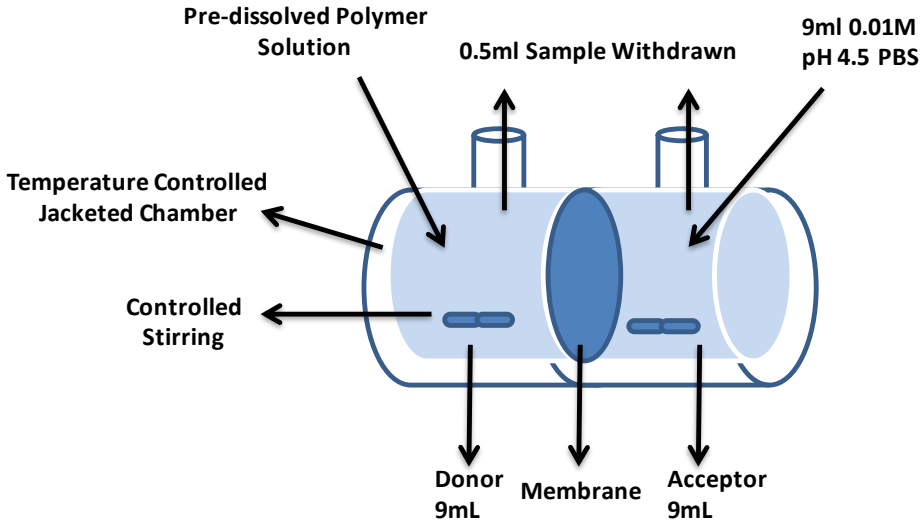

Figure 3. 8 Schematic illustration of a D/P system

3.4 Preparation

3.4.1 Buffer Preparation

pH 6.8 (0.01M) phosphate buffer solution (PBS) was prepared as a dissolution medium according to British Pharmacopoeia 2018. 50mL of 0.2M potassium dihydrogen phosphate (KH_2PO_4) and 22.4mL of 0.2M sodium hydroxide (NaOH) were mixed and diluted to 1000mL with double distilled water.

pH4.5 PBS (0.01M) was used as a dissolution medium in this study, which was prepared according to British Pharmacopoeia 2018. 1.361g potassium phosphate monobase dissolved in 1L double distilled water and pH value of the solution was adjusted using sodium hydroxide solution if necessary

3.4.2 Cocrystals Preparation

3.4.2.1 Powdered Cocrystals Formation

FFA-NIC CO was prepared by a solvent evaporation method. A 1:1 equimolar mixture of FFA I and NIC was dissolved in acetonitrile with stirring at 80°C. The solution was placed in a fume cabinet overnight for solvent evaporation. FFA-TP CO was synthesized by a cooling crystallization method. A 1:1 molar ratio of FFA and TP was dissolved in a cosolvent (7:3 acetonitrile and water) with stirring at 90 °C and then the solution was placed into an ice bath for 2h until the crystals were separated out from the solution. Both FFA-NIC CO and FFA-TP CO were characterized and confirmed by DSC, FTIR, and XRPD.

3.4.2.2 Single Cocrystals Formation

The single cocrystals of FFA-NIC CO and FFA-TP CO were grown from a saturated 1:1 equimolar mixture solution of FFA and coformers in cosolvent (7:3 mixture of acetonitrile and water) by slow evaporation at room temperature over a period of 3−4 days. FFA cocrystals were harvested from the mother solutions by vacuum filtration. The phase identities of single crystals were confirmed by DSC, FTIR, and XRPD.

3.5 Calculation Equations

3.5.1 Solubility Parameter (SP)

Solubility parameter (SP) is used to compare the relative hydrophobicity of polymers, FFA, and coformers in solution. The SP of an organic compound is estimated by Fedors [288] as

$$\mathrm{SP} = \delta = \sqrt{\delta_d^2 + \delta_p^2 + \delta_h^2} \qquad \text{(Equ.3- 2)}$$

$$\delta_d = \sum F_{di} \ / V_m \qquad \text{(Equ.3- 3)}$$

$$\delta_p = \sqrt{\sum F_{pi}^2} \ / V_m \qquad \text{(Equ.3- 4)}$$

$$\delta_h = \sqrt{\sum E_{hi} / V_m} \qquad \text{(Equ.3- 5)}$$

$$V_m = \frac{M}{P} \qquad \text{(Equ.3- 6)}$$

where δ is total solubility parameter, δ_d is dispersion Hansen solubility parameter, δ_p is the polar Hansen solubility parameter, δ_h is the hydrogen-bonding Hansen solubility parameter, F_{di} are the group contributions to the dispersion component F_d (the molar attraction constant), F_{pi} are the group contributions to the polar component, F_p, E_{hi} is the hydrogen-bonding energy per structural group i, V_m is the corresponding molar volume, M is molecular weight, p is density, The method is based on group additive constants; therefore, it requires only knowledge of the structural formula of the compounds. The unit of solubility parameter is $(\mathrm{MPa})^{(1/2)}$, representing twice the number of $(\text{calories per cm}^3)^{1/2}$ [289].

Table 3. 6 shows the solubility parameter calculation of FFA. All the values of F_{di}, F_{pi} and E_{hi} of different function groups at 25°C are given in Ref [290]. The detailed

calculations about the SP of TP, NIC PEG, PVP and PVP-VA were listed in Table A2. 1.

Table 3. 6 Solubility parameter calculation of FFA.

FFA		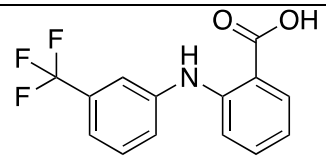	
Group	F_{di}	F_{pi}^2	E_{hi}
=CH- (8)	1600	0	0
=C-(4)	280	0	0
NH (1)	160	44100	3100
COOH (1)	530	176400	10000
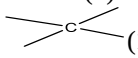 (1)	-70	0	0
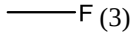 (3)	660	--------	--------
sum	3160	220500	13100

Vm=M/ρ=281.22(g/mol)/1.47(g/cm^3) =191 (cm^3/mol)

$\delta_d = \frac{\sum F_{di}}{V_m} = \frac{3160}{191}$ =16.5 MPa$^{(1/2)}$

$\delta_p = \frac{\sqrt{\sum F_{pi}^2}}{V_m} = \frac{\sqrt{220500}}{191}$ =2.5 MPa$^{(1/2)}$

$\delta_h = \sqrt{\sum E_{hi}/V_m} = \sqrt{\frac{13100}{191}}$ = 8.28 MPa$^{(1/2)}$

$\delta = \sqrt{\delta_d^2 + \delta_p^2 + \delta_h^2}$ = (16.5^2+2.5^2+8.28^2) $^{(1/2)}$ =18.62 MPa$^{(1/2)}$

3.5.2 Supersaturation Ratio (SSR)

Supersaturation is the driving force for crystallization. Supersaturation ratio (SSR) defined as the ratio of the supersaturation concentration to is thermodynamic solubility in the same medium and temperature. SSR can be calculated using the following equation:

$$\text{SSR} = C_{supersaturation}/C_{eq} \qquad \text{(Equ.3- 7)}$$

where C is the concentration of supersaturation solution and C_{eq} is the concentration of solute equilibrium saturated value respectively. Crystallization will only occur when SSR>1.

3.5.3 Supersaturation Parameter (SSP)

Supersaturation parameter (SSP) is used to evaluate the drug precipitation behavior from a supersaturated system in comparison to a reference system based on the work by Chen *et al* [291].

Figure 3.9 shows the concentration-time curves of a supersaturation system in a dissolution medium. The reference system (curve $\boldsymbol{C_0C_R(t)}$) and the investigated system (curve $\boldsymbol{C_0C(t)}$ or curve $\boldsymbol{C_0C'}$(t)) were compared. Curve $\boldsymbol{C_0C_R(t)}$ represents the desupersaturated curve of the pure API supersaturated solution in the absence of polymers. The C_0 is the initial concentration of the supersaturated solution, which is higher than API's equilibrium solubility. Curve $\boldsymbol{C_0C_0(t)}$ represents an ideal situation where the drug still dissolved in the medium and no crystallization happens over the period of time (t). An integration area of $\boldsymbol{A_{C_0C_R(t)C_0(t)}}$ can be used to indicate *"the amount of drug precipitated from the pure API supersaturated solution over time (t)"* in the absence of polymers. An integration area of $\boldsymbol{A_{C_0C(t)C_0(t)}}$ or $\boldsymbol{A_{C_0C'(t)C_0(t)}}$ illustrates *"the amount of drug precipitated from the investigated system over time (t)"* in the presence of coformers or polymers. An integration area of $\boldsymbol{A_{C_0C_R(t)C(t)}}$ and $\boldsymbol{A_{C_0C'(t)C_R(t)}}$ conceptually considered as *"the amount difference of precipitation between the reference and the investigated system"*. For a supersaturated system with the desupersaturation curve of $\boldsymbol{C_0C(t)}$, the integration area of $\boldsymbol{A_{C_0C(t)C_0(t)}}$ is smaller than that of the reference system, indicating less drug precipitation. Compared with the reference system, a supersaturated system with the desupersaturation curve of $\boldsymbol{C_0C'}$(t) has more precipitated drug solids because of a larger integration area of $\boldsymbol{A_{C_0C'(t)C_0(t)}}$. To quantitatively compare the abilities of different systems on inhibiting the drug precipitation, *SSP* is defined as [291]

$$\mathrm{SSP(t)} = \frac{\boldsymbol{A_{C_0C_R(t)C(t)}}}{\boldsymbol{A_{C_0C_R(t)C_0(t)}}} = \frac{\boldsymbol{A_{C_0C_R(t)C_0(t)}} - \boldsymbol{A_{C_0C(t)C_0(t)}}}{\boldsymbol{A_{C_0C_R(t)C_0(t)}}} \times 100\% \qquad \text{(Equ.3-8)}$$

OR

$$\mathrm{SSP(t)} = \frac{\boldsymbol{A_{C_0C'(t)C_R(t)}}}{\boldsymbol{A_{C_0C_R(t)C_0(t)}}} = \frac{\boldsymbol{A_{C_0C_R(t)C_0(t)}} - \boldsymbol{A_{C_0C'(t)C_0(t)}}}{\boldsymbol{A_{C_0C_R(t)C_0(t)}}} \times 100\% \qquad \text{(Equ.3-9)}$$

SSP is a dimensionless parameter. A system with a positive *SSP* value shows an ability to prolong drug supersaturation while a negative *SSP* value indicates no ability to maintain the drug supersaturation.

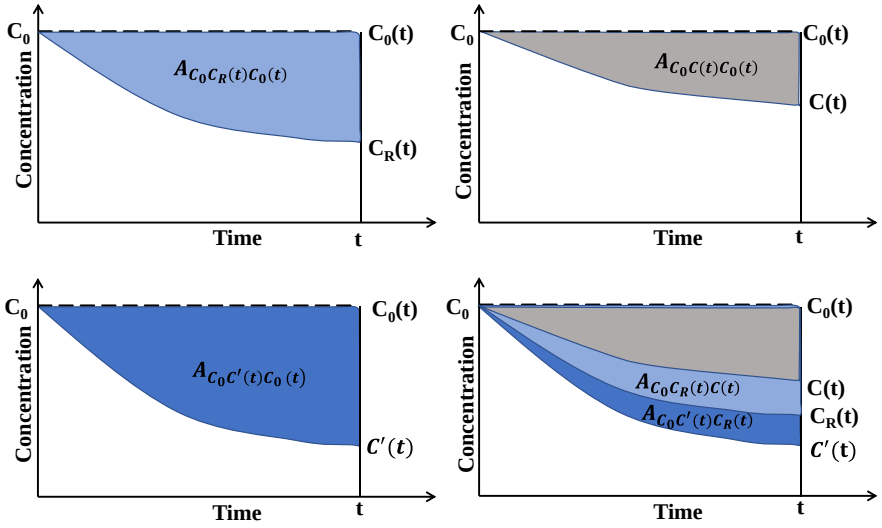

Figure 3. 9 Illustration of supersaturation parameter

3.5.4 Dissolution Performance Parameter (DPP)

Dissolution performance parameter (DPP), was used to evaluate the dissolution profile of cocrystal powders in the absence or presence of a pre-dissolved polymer in comparison to a reference system. Figure 3. 10 shows the dissolution profiles of different solid powders in which C_{eq} is the equilibrium crystalline API concentration in the dissolution medium and specific temperature. The area under the curve (AUC) $\boldsymbol{AUC_{C(t)}}$ of a dissolution profile $C(t)$ indicates *"the amount of drug dissolved"* and is maintained over the period of the dissolution time from 0 to t [291]. A higher AUC of the dissolution profile indicates a better dissolution performance. A curve $\boldsymbol{C_R(t)}$ is the reference dissolution profile of solids R with $\boldsymbol{AUC_{C_R(t)}}$. For solid with a dissolution curve $C(t)$, its concentration passes the equilibrium value at T_{eq} and reaches the maximum concentration (C_{max}). The $\boldsymbol{AUC_{C(t)}}$ is significantly higher than that of the reference solids R, indicating more solid dissolves. Compared with the reference solid R,

the solid with a smaller value of $\boldsymbol{AUC_{C'(t)}}$ dissolved less. In order to quantitatively compare the dissolution performance of two solids, DPP is defined as

$$\mathrm{DPP(t)} = \frac{\boldsymbol{AUC_{C(t)}} - \boldsymbol{AUC_{C_R(t)}}}{\boldsymbol{AUC_{C_R(t)}}} \times 100\% \qquad \text{(Equ.3-10)}$$

OR

$$\mathrm{DPP(t)} = \frac{\boldsymbol{AUC_{C'(t)}} - \boldsymbol{AUC_{C_R(t)}}}{\boldsymbol{AUC_{C_R(t)}}} \times 100\% \qquad \text{(Equ.3-11)}$$

Solids with a positive DPP value show an increased ability to dissolve and to be maintained in a dissolution medium, while as a negative DPP value indicates that solids have a less ability to dissolve and to be maintained in solution.

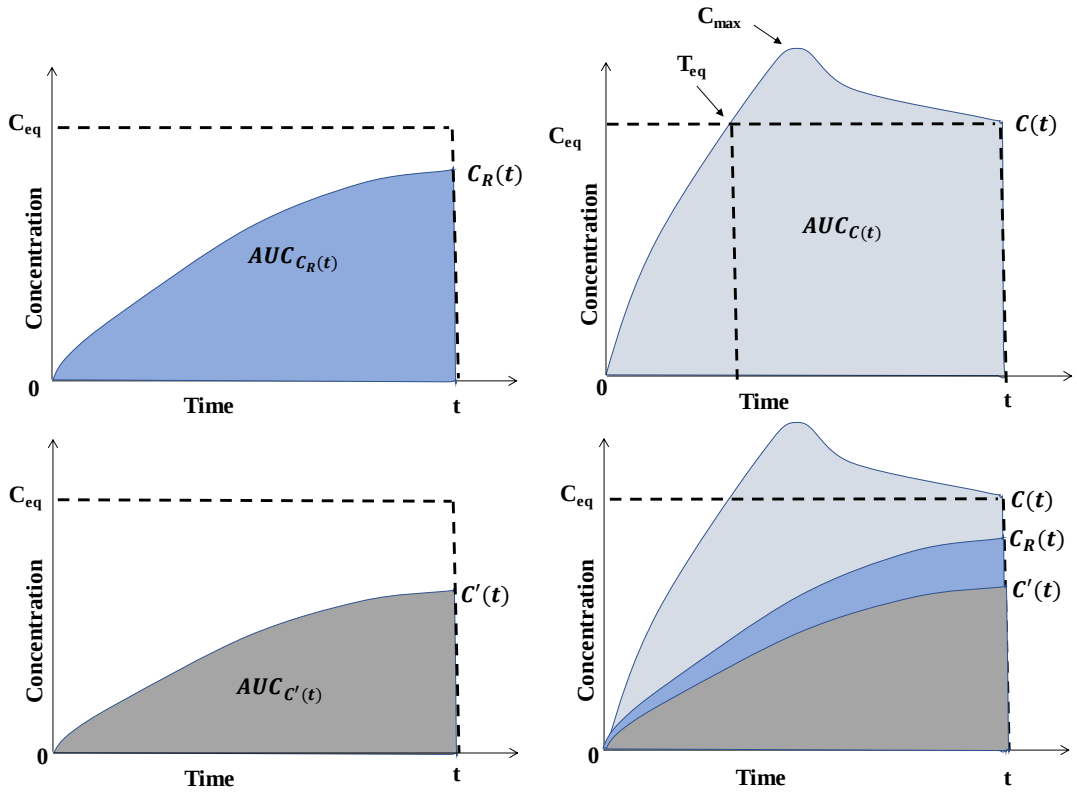

Figure 3. 10 Illustration of dissolution performance parameter.

3.5.5 Flux Rate

Figure 3. 11 represents a permeation profile. The flux of a drug through a membrane, is defined as *"the amount of drug crossing a unit area perpendicular to its flow direction per unit time (t)"*, calculated using the following equation [292]:

$$J(t) = \frac{\left(C(t) - C_{t_1}\right)}{A(t - t_1)} V \qquad \text{(Equ.3-12)}$$

where $J(t)$ is the flux of a drug; C_{t_1} is the drug concentration (μg/mL) in acceptor cell (Figure 3. 8) at t_1 (min); C_{t_2} is the drug concentration (μg/mL) in acceptor at t_2 (min); *V* is the solution volume (mL) in the acceptor cell and *A* is the area of exposed membrane in cm^2. Unit of flux rate is μg/(cm^2*min).

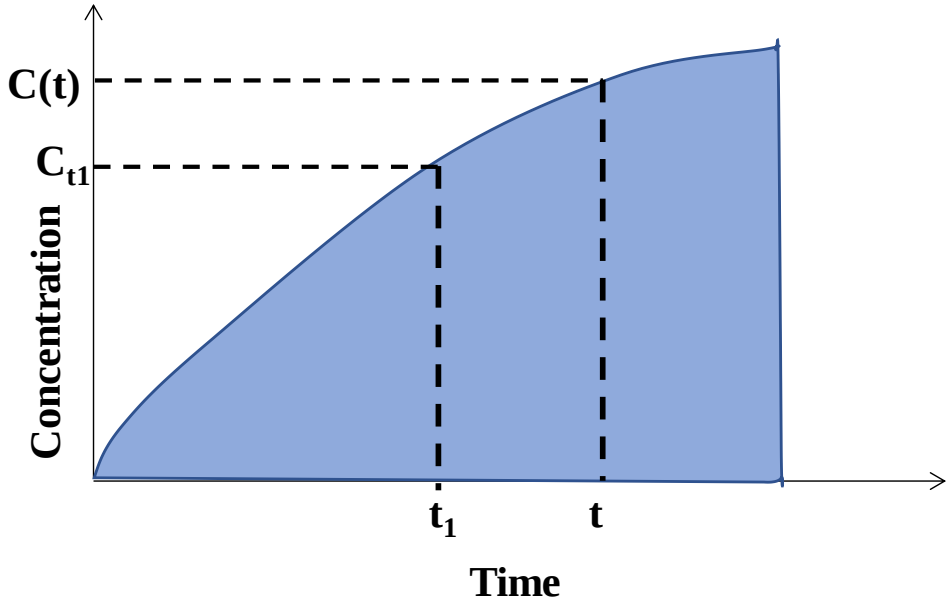

Figure 3. 11 Illustration of permeation profile

3.6 Chapter Conclusion

This chapter introduced the materials, analytical techniques, experimental methods, preparation methods and calculation equations used in this study. The name, formula, purity and manufacturer of materials were presented. The working principle, application, instrumental setting, operation procedure and instrumental models of analytical

techniques were shown, including IR, Raman, DSC, HPLC, AFM, optical microscopy, XRD and NMR. The experimental methods of solubility tests, desupersaturation experiments, eutectic point of cocrystal, powder dissolution and D/P measurement were described. Then, the preparation methods of dissolution buffer (0.01M pH 6.8 PBS and 0.01M pH 4.5 PBS) and cocrystals (single and powdered FFA-NIC CO and FFA-TP CO) were described. Finally, the calculation equations that used to calculate SP, SSR, SSP, cocrystal solubility, DPP and flux rate were mentioned.

Chapter 4 Samples Characterization

4.1 Chapter Overview

In this chapter, FFA-NIC CO and FFA-TP CO were prepared by using solvent evaporation and cooling crystallization respectively. Different analytical techniques were used for confirming the formation of cocrystals by comparing the spectra of individual components (FFA I, NIC and TP), FFA-NIC CO and FFA-TP CO, including DSC, ATR-IR and XRPD. The results of these analytical techniques show that both of FFA-NIC CO and FFA-TP CO were successfully synthesized. The structures of FFA-NIC CO and FFA-TP CO were presented in this chapter.

4.2 Materials and Methods

4.2.1 Materials

FFA I, NIC, TP, acetonitrile and double distilled water were used in this chapter and detailed introduction of this materials can be found in chapter 3.

4.2.2 Methods

FFA-NIC CO and FFA-TP CO were formed by solvent evaporation and cooling crystallization respectively. ATR-FTIR, DSC, XRPD and Raman have been used to characterize the formation of cocrystals. Details of cocrystals synthesis methods and these techniques were described in Chapter 3.

4.3 Results

4.3.1 DSC Analysis of FFA I, FFA-NIC CO and FFA-TP CO

The DSC curve in Figure 4. 1 shows that the melting point of FFA-NIC CO was around 136.4^{o}C which was higher than the melting points of FFA I (133.5^{o}C) and NIC (128.1^{o}C). In contrast, the melting point of FFA-TP CO was 185.6^{o}C which was in the middle of the melting points of FFA I and the TP melting point at 272.8^{o}C.

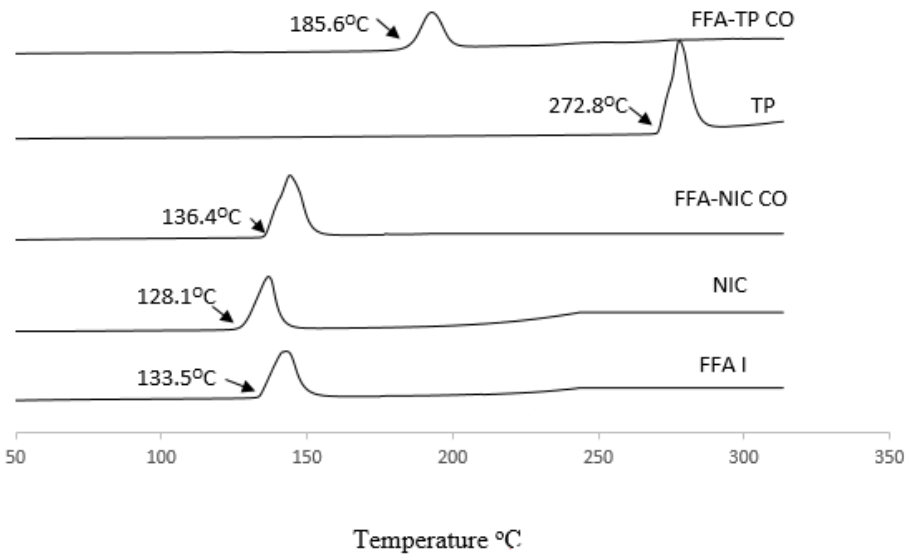

Figure 4. 1 DSC thermograms for FFA I, NIC, FFA-NIC CO, TP and FFA-TP CO

4.3.2 IR Spectroscopy Analysis of FFA I, FFA-NIC CO and FFA-TP CO

The structures of FFA, NIC, TP, FFA-NIC CO and FFA-TP CO have been studied in the published literatures [229] shown in Figure 4. 2.

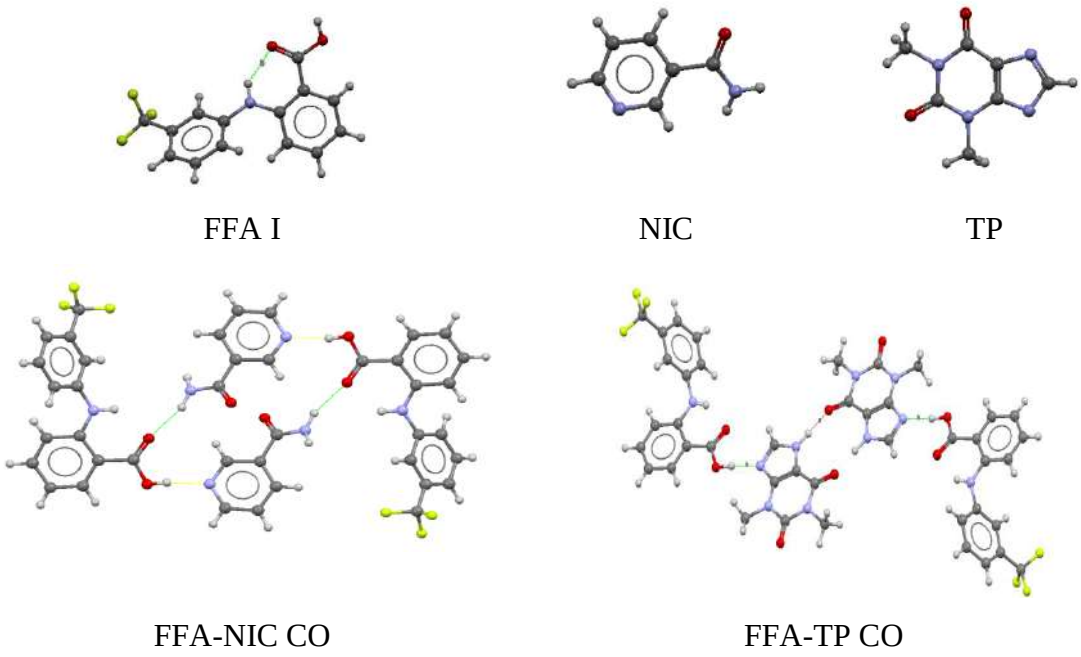

Figure 4. 2 Molecular structures of FFA I, NIC, TP, FFA-NIC CO and FFA-TP CO

The structures of FFA-NIC CO and FFA-TP CO have been confirmed by the measured IR spectra in Figure 4. 3 [229, 234]. FFA-NIC CO is formed through an acid-pyridine heterosynthon involving FFA and NIC molecules [234]. The IR spectrum of FFA I has peaks at 3318 cm^{-1} and 1651 cm^{-1}, corresponding to N-H and C=O stretching frequencies [293]. The spectra of NIC has 2 peaks at 3353 cm^{-1} and 1592 cm^{-1}, corresponding to N-H and pyridine ring C=N stretching [294]. In the spectrum of FFA-NIC CO, the frequencies of N-H stretching and C=O stretching of FFA are shifted to 3324 cm^{-1} and 1660 cm^{-1} while the peaks of N-H stretching and pyridine ring C=N stretching of NIC shifted to 1608 cm^{-1} from 1592 cm^{-1} and to 3395 cm^{-1} from 3353 cm^{-1}. FFA-TP CO is formed through an O-H···N hydrogen bond involving the carboxylic acid of FFA and unsaturated N atom of the imidazole ring of TP [295]. The IR spectrum of TP has peaks at 3119 cm^{-1}, 1660 cm^{-1} and 1561 cm^{-1}, corresponding to N-H, C=O and C=N stretching frequencies which are shifted to 3068cm^{-1}, 1669 cm^{-1} and 1558 cm^{-1} in FFA-TP CO spectrum, respectively. In the spectrum of FFA-TP CO, FFA's N-H stretching and C=O stretching frequencies are shifted to 3280cm^{-1} and 1647 cm^{-1} respectively. The summary of IR peak identities of FFA I, NIC, TP and cocrystals are shown in Table A1.1 in the appendixes. The summary of Raman results in Figure A1. 1 and Figure A1. 2, showing new peaks of FFA-NIC CO at 3321 cm^{-1}, 1402cm^{-1} and 1158 cm^{-1} and FFA-TP CO at 3269 cm^{-1}, 3077 cm^{-1}, 1423 cm^{-1} and double peak (1161 cm^{-1} and 1165 cm^{-1}).

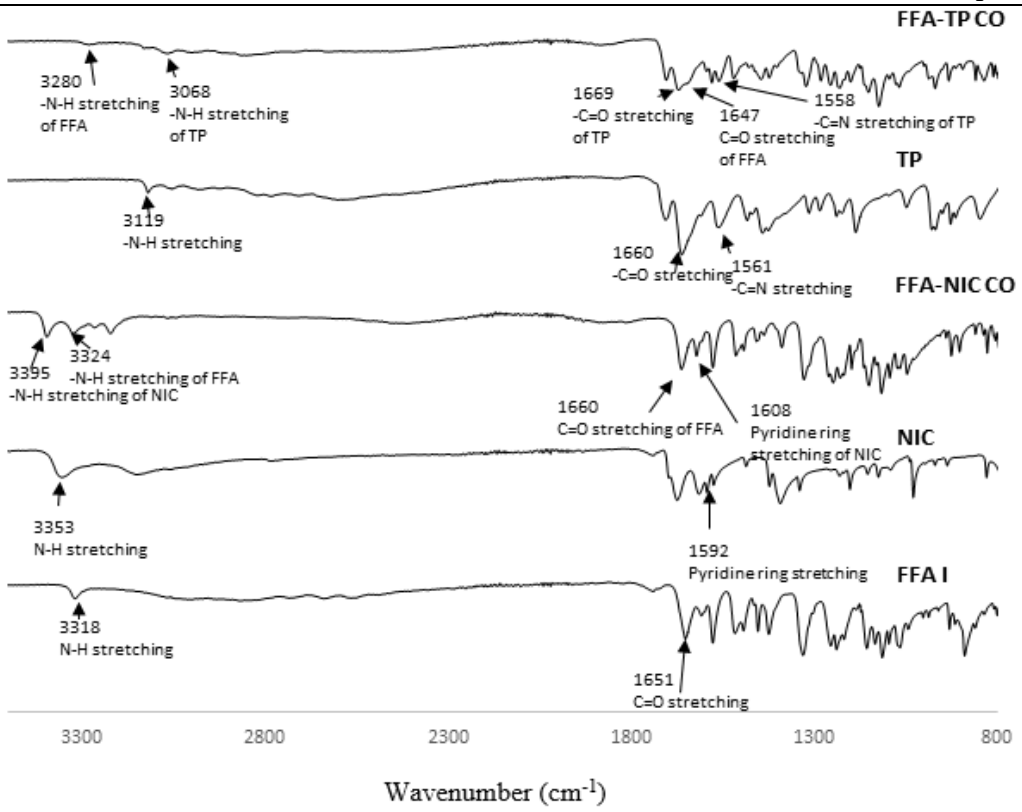

Figure 4. 3 IR spectrum of FFA I, NIC, FFA-NIC CO, TP and FFA-TP CO

4.3.3 XRPD Spectroscopy Analysis of FFA, FFA-NIC CO and FFA-TP CO

Figure 4. 4 shows the XRPD patterns of individual component of FFA I, NIC, TP, FFA-NIC CO and FFA-TP CO. The significant characteristic diffraction peaks of FFA I are at 2θ=7.1º, 14.2º, 21.4º and 24.6º. Key characteristic diffraction peaks of NIC are at 2θ=14.9º and 23.5º. After co-evaporation of FFA and NIC in acetonitrile, the new materials of FFA-NIC CO have been formed, showing the characteristic diffraction peaks at 2θ=6.7º, 9.6 º, 16.2º, 16.8º and 21.9º ,which are in agreement with those of published data [234]. The characteristic diffraction peaks of TP are at 2θ=7.2º, 12.7º and 14.5º. Through the cooling crystallization method described in chapter 3, FFA-TP CO was generated, indicated by the characteristic diffraction peaks at 2θ=5.9º, 11.3º, 15.6º and 26.8º [295].

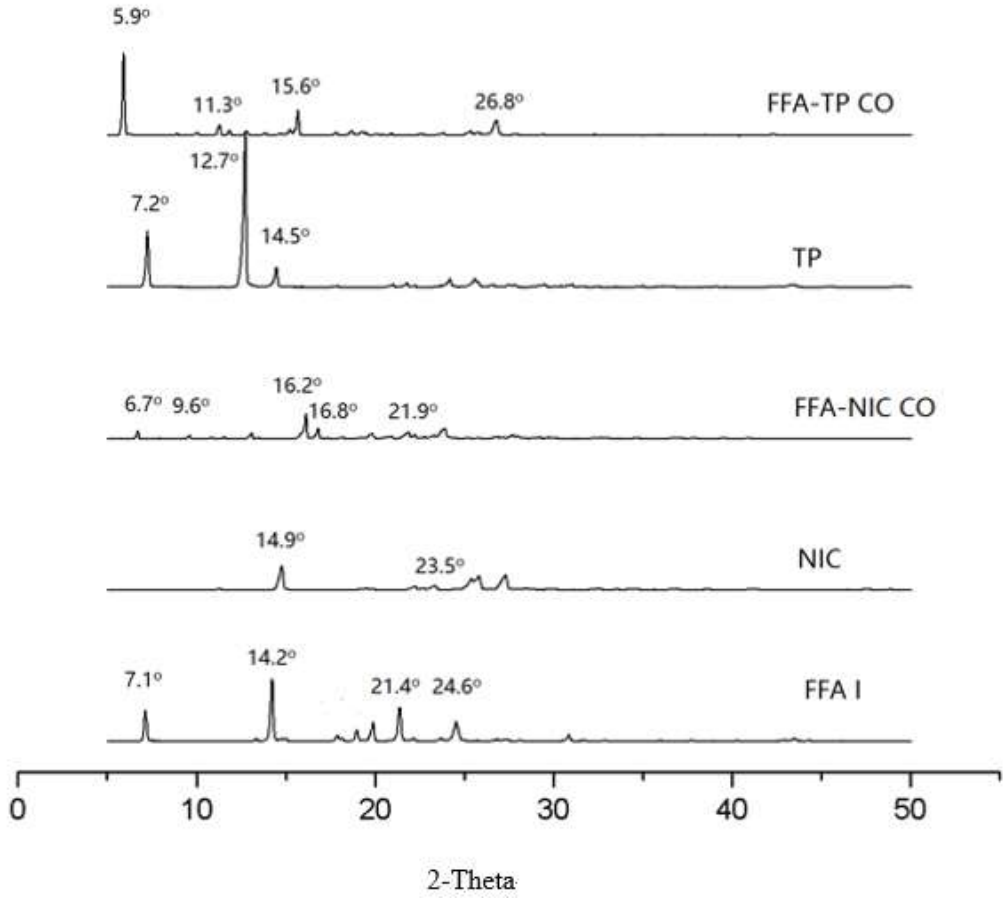

Figure 4. 4 XRPD spectra of FFA I, NIC, FFA-NIC CO, TP and FFA-TP CO

4.4 Chapter Conclusion

In this chapter, samples of FFA I, NIC, TP, 1:1 FFA-NIC CO and 1:1 FFA-TP CO were characterized by DSC, IR and XRPD. All characterized results demonstrated that both of FFA-NIC CO and FFA-TP CO were formed. Based on DSC spectra, FFA-NIC CO and FFA-TP CO has distinct melting point compared to individual components. FTIR spectra show the hydrogen bonding formation between FFA with NIC or TP during cocrystals formation. XRPD spectra demonstrated new characteristic diffraction peaks existing in cocrystals compared with the pure FFA I, NIC and TP.

Chapter 5 Investigating the Influence of Polymers on Supersaturated Flufenamic Acid Cocrystal Solutions

(This work has been published. Citation: Guo, M., et al., Investigating the Influence of Polymers on Supersaturated Flufenamic Acid Cocrystal Solutions. Molecular Pharmaceutics, 2016. 13(9): p. 3292-3307.)

5.1 Chapter Overview

In this chapter, it is the first time to carry out a systematic investigation for exploring the influence of different polymeric additives in cocrystal formulations to illuminate the molecular mechanism of the interplay among the polymer/drug/coformer that impacts the cocrystal parent drug crystallization kinetics of nucleation and growth. Chemical structures of the model drug, coformers and monomer unit of the polymers are shown in Table 5. 1.

Firstly, equilibrium solubility tests were conducted to assess the effect of polymers in changing the apparent FFA solubility in solution. Then, a solvent shift approach was used to generate an initial FFA supersaturation condition to study crystallization kinetics of both nucleation and growth [296]. OLM was used to determine the induction time for quantifying the drug nucleation from a supersaturated solution in the absence and presence of different pre-dissolved polymers (PEG, PVP and PVP-VA). Measuring the desupersaturation curve in the presence of seeds of pure FFA I crystals for evaluating the impact of different polymers on growth. The overall impact of polymers on inhibiting FFA crystallization from a supersaturated solution was characterized and evaluated by measuring desupersaturation curves in the absence of the crystal seeds. SSP in different supersaturated solutions were calculated and compared for quantifying a polymer inhibition ability to prolong drug supersaturation [291]. DSC, XRPD, ATR-FTIR and OLM was used to examine the solid residuals after the solubility and the desupersaturation experiments with and without seeds. To further explore the intermolecular interaction mechanisms among a polymer, drug and coformer in solution, infrared spectra of the parent drug FFA I and coformers of NIC and TP in combination with different polymers were collected and compared.

Table 5. 1 Structure and SP values of FFA, NIC, TP, and polymers

Molecular structure		SP ($MPa^{1/2}$)
FFA	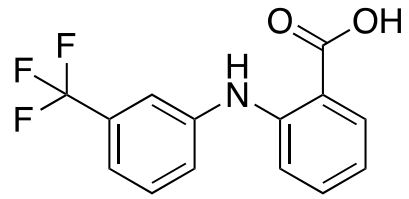	18.62
NIC	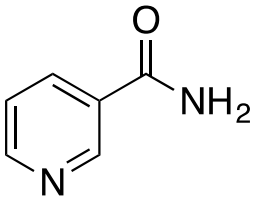	30
TP	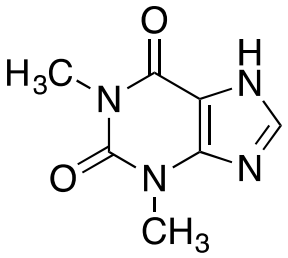	29
PEG	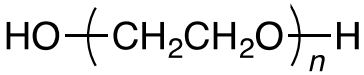	21.94
PVP	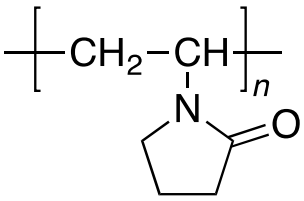	21.24
PVP-VA	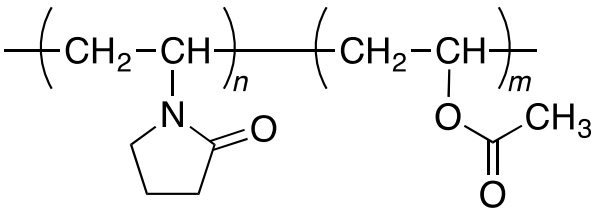	20.98

The unit of solubility parameter is $(MPa)^{(1/2)}$, representing twice the number of $(calories\ per\ cm^3)^{1/2}$ [289].

5.2 Materials and Methods

5.2.1 Materials

FFA I, NIC, TP, FFA-NIC CO, FFA-TP CO, PEG, PVP, PVP-VA, methanol, ethanol, acetonitrile and double distilled water were used in this study. Detailed information of these materials can be found in Chapter 3.

5.2.2 Methods

5.2.2.1 Preparation of FFA-NIC CO and FFA-TP CO

FFA-NIC CO and FFA-TP CO were used in this chapter, detailed synthesized methods can be found in chapter 3.

5.2.2.2 Apparent Equilibrium Solubility Determination

The apparent equilibrium solubility of FFA I, FFA-NIC CO and FFA-TP CO was determined in the cosolvent (1:4 ethanol and water) in the absence or presence of 200 µg/mL of a pre-dissolved polymer (PEG, PVP or PVP-VA). The cosolvent of 1:4 ethanol and water were used in this study to increase the apparent FFA equilibrium solubility and thus avoid immediate crystallization of FFA in media through maintaining slower kinetics of nucleation and growth. The detailed solubility test method can be found in chapter 3.

5.2.2.3 Nucleation Induction Time Monitoring by OLM

Nucleation induction times were determined from desupersaturation experiments monitored by a OLM. The FFA stock concentration of pure FFA I, FFA-NIC CO or FFA-TP CO dissolved in ethanol was 1mg/mL. Different initial supersaturated solutions of 50, 100 and 200µg/mL were generated by adding the appropriate amount of the stock solution into a small quartz cell filled with 0.5mL of the cosolvent in the absence or presence of 200µg/mL of different polymers. The FFA crystallization behavior from a supersaturated solution was monitored by OLM. Data collection started immediately after addition of the drug stock solution to the test medium. The induction time was

determined by observing the onset of the FFA crystal formation. Detailed information about the OLM can be found in chapter 3

5.2.2.4 Effect of Polymers on Supersaturated FFA and Cocrystal Solutions

To decouple the nucleation process, the inhibition effect of a polymer on the growth of FFA crystals was assessed from the seeded experiments by measuring the desupersaturation curve of a supersaturated solution of pure FFA, FFA cocrystals in the absence and presence of 200μg/mL of a pre-dissolved polymer, either PEG, PVP or PVP-VA.

To evaluate the overall inhibition effect of a polymer on FFA crystallization kinetics from a supersaturated solution, unseeded desupersaturation experiments were conducted.

Detailed methods of seeded, unseeded desupersaturated experiments can be found in chapter 3.

5.2.2.5 IR for studying intermolecular interaction

The investigation of the intermolecular interaction among FFA, NIC, TP and polymers (PEG, PVP and PVP-VA) in solution was carried out by solution IR. Methanol was selected for the intermolecular interaction study of FFA, NIC and polymers, in which concentrations of individual components were 50, 21.7 and 20mg/mL respectively. A cosolvent of 1M HCl and methanol at a ratio of 1:6 were selected for the intermolecular interaction study of FFA, TP and polymers, in which concentrations of individual components were 14.3, 9.14 and 20mg/mL respectively. The detailed setting about IR can be found in chapter 3.

5.2.2.6 Physical Property Characterization Techniques

HPLC was used to study the solubility and the effect of polymers on supersaturated FFA I and FFA cocrystals solutions. DSC, FITR and XRPD were used for characterization. The detailed information about these techniques can be found in chapter 3.

5.2.2.7 Solubility Parameter (SP) and Supersaturated Parameter (SSP) Calculation

In this chapter, solubility parameter (SP) is used to compare the relative hydrophobicity of polymers, FFA and coformers in solution. Supersaturation parameters (SSP) were calculated and compared for both seeded and unseeded experiments to quantify different polymer inhibition abilities [291]. The equations that used to calculate SP and SSP can be found in chapter 3.

5.3 Results

5.3.1 Apparent FFA Equilibrium Solubility of FFA I, FFA Cocrystals in Cosolvent in the Absence and Presence of Different Polymers

Figure 5. 1 (a) demonstrates the apparent equilibrium solubility of FFA I, FFA-NIC CO and FFA-TP CO in cosolvent media in the absence or presence of predissolved polymers of PVP, PEG and PVP-VA at equilibrium after 24 h. In the absence of a polymer, the apparent FFA equilibrium solubility of FFA-NIC CO (41.9±2.1µg/mL) was slightly higher than those of FFA I and FFA-TP CO which were comparable (36.0±0.5µg/mL for FFA-TP CO and 36.8±2.1µg/mL for the pure FFA I). In the presence of 200µg/mL polymer, PEG, PVP or PVP-VA, the apparent FFA equilibrium solubility of FFA I or FFA cocrystals does not change, indicating that none of the polymers changed the solution properties.

Solid residues collected after the solubility tests were analyzed by DSC in Figure 5. 1b. For pure FFA I, the resultant solid residues were the same as the starting materials after the solubility test in the absence or presence of polymers, indicated by identical DSC thermographs in Figure 5. 1b. Following the solubility tests of FFA-NIC CO and FFA-TP CO in presence or absence of polymers, the solid residues were yellow FFA III crystals, indicating the cocrystals of FFA-NIC CO or FFA-TP CO had transformed into FFA III. This was confirmed by DSC thermographs of the solid residues in Figure 5. 1b, in which the same thermal events occurred as that of the pure FFA III. Under DSC heating conditions, FFA III melted at 123.1 °C and recrystallized to FFA I, which then melted at 134.4°C [297] However, morphologies of FFA III particles collected from the two cocrystal tests in Figure 5. 1c were significantly different. FFA III crystals from

FFA-NIC CO tests were needle-shaped, whereas those from FFA-TP CO tests were rod/disc-shaped. FTIR data of the solid residues are shown in Figure A2. 1 in the appendixes, showing that resultant solid residues had the same IR peak at 1607cm^{-1}, 1598 cm^{-1} and 1652 cm^{-1} as pure FFA I [298]. While the resultant solid residues from FFA-NIC CO and FFA-TP CO samples shows same characterized IR peak as FFA III at 1601 cm^{-1}, 1581 cm^{-1} and double peaks (1670 cm^{-1} and 1655 cm^{-1}) [298]. The IR results indicate that phase transformation occurred in cocrystal system during dissolution.

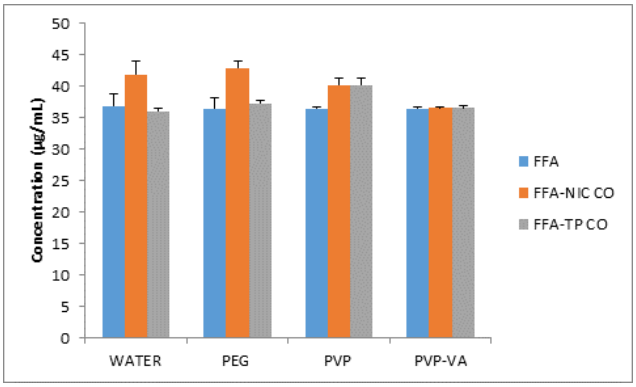

(a)

FFA FFA-NIC CO FFA-TP CO

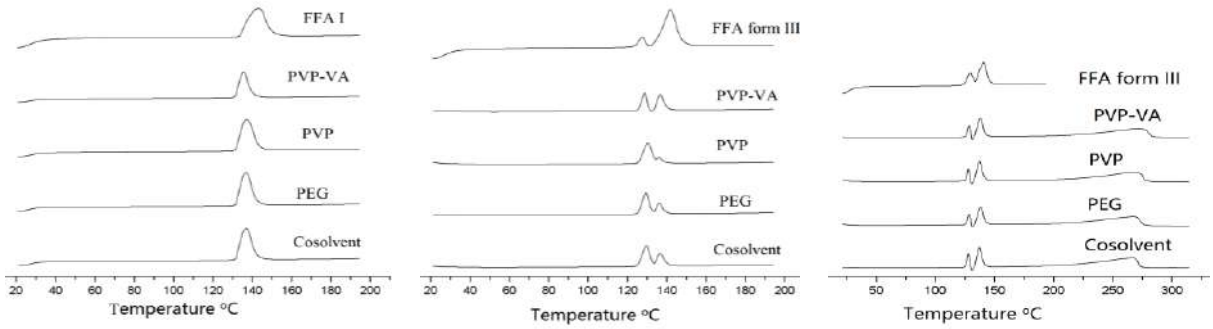

(b)

	FFA	FFA-NIC CO	FFA-TP CO
Starting materials	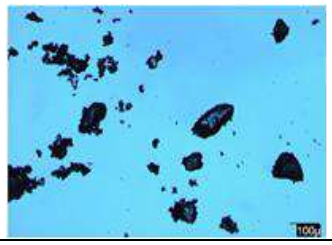	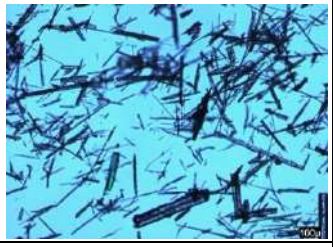	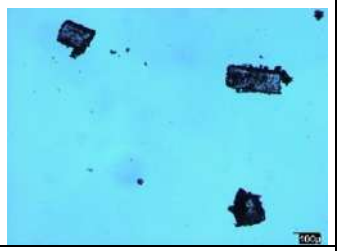
Cosolvent	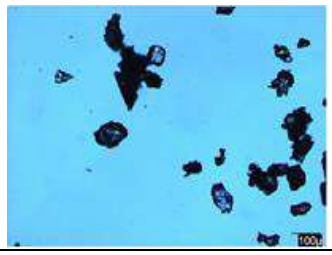	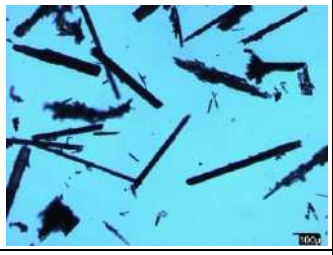	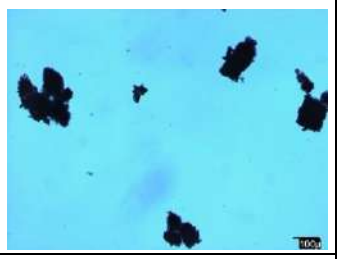
Cosolvent with predissolved PEG	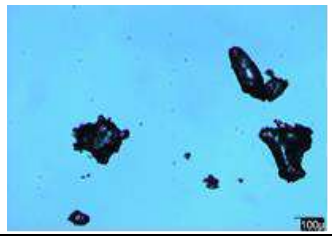		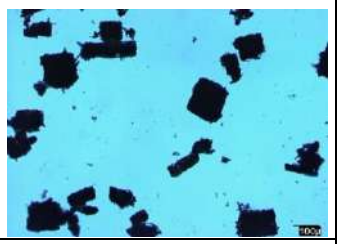
Cosolvent with predissolved PVP	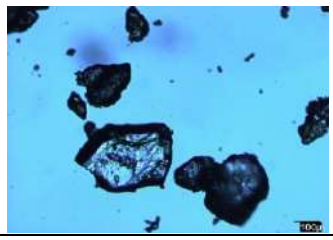		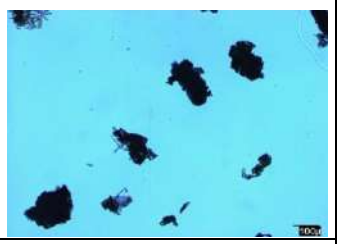
Cossolvent with predissolved PVP-VA	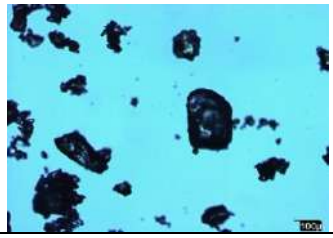		

(c)

Figure 5. 1 Solubility test results after 24h: (a) apparent equilibrium solubility; (b) DSC results of solid residues; (c) imaging of solid residues: All scale bars were 100μm.

5.3.2 Effect of Polymers on the Nucleation Induction Time of FFA Crystallization in Solution

According to the measured equilibrium solubility of FFA I in the previous section, the initial supersaturated solutions of 50, 100, and 200μg/mL corresponded to the SSR

values of 1.36, 2.72, and 5.44, respectively. The nucleation induction times in Table 5. 2 are based on the initial observation times of FFA crystals detectable by OLM. Without a predissolved polymer in the cosolvent media, the precipitation of FFA from the pure FFA and two cocrystal solutions occurred rapidly at the low SSR of 1.36. The induction times of FFA, FFA cocrystals supersaturated solution were significantly distinct in the presence of different polymers, PEG, PVP, and PVP-VA. With predissolved PEG in solution, its induction times were increased slightly for all test solutions at the low SSR of 1.36. No FFA crystals were found for all test solutions in the presence of 200μg/mL of predissolved PVP or PVP-VA at an SSR 1.36, indicating that PVP or PVP-VA can completely inhibit the crystallization of FFA during the 30min experiment. In order to differentiate the inhibition abilities of PVP and PVP-VA, the experiments were proceeded with a higher initial degree of supersaturation SSR 2.72. From the recorded images, it was observed that dense liquid particles appeared immediately in the experiments with the predissolved PVP or PVP-VA and then the formation of the crystal nuclei within the dense liquid clusters. It is in excellent agreement with the two-step mechanism of nucleation of crystals in solution [299]. In the presence of predissolved PVP in solution, the order of the induction times was $T_{FFA\text{-}TP\ CO} < T_{FFA\text{-}NIC\ CO} < T_{FFA}$. In contrast, PVP-VA can completely inhibit the crystallization of FFA from the three test solutions. Further tests were conducted at the supersaturation level of SSR = 5.44 with predissolved PVP-VA. It was shown that the induction times were comparable for the two cocrystal solutions, with the longest induction time being 446 s for the pure FFA solution.

Figure 5. 2 shows the images of a representative part of the quartz cell, indicating the morphology of the FFA crystals after tests. In cosolvent without a predissolved polymer, the needle shape morphology of FFA crystals from both the FFA-NIC CO and pure FFA solution was similar. In contrast, the FFA crystals from the FFA-TP CO solution were significantly smaller and rod-shaped. In the presence of PEG in solution, the FFA crystals precipitated from the three test samples became smaller. In the presence of PVP or PVP-VA in solution, all crystals precipitated from three test solutions were a similar shape, lacking any distinctive crystal morphology.

Table 5. 2 Nucleation induction time (30mins controlled experiments)

		Cosolvent	Cosolvent with predissolved PEG	Cosolvent with predissolved PVP	Cosolvent with predissolved PVP-VA
SSR=1.36	FFA	9± 2(sec)	176 ±37 (sec)	No crystal appeared	No crystal appeared
	FFA-NIC CO	15±7(sec)	288± 172(sec)	No crystal appeared	No crystal appeared
	FFA-TP CO	24±10(sec)	218± 161(sec)	No crystal appeared	No crystal appeared
SSR=2.72	FFA	n.m.[1,2]	n.m.[2]	658±47 (sec)	No crystal appeared
	FFA-NIC CO	n.m. [2]	n.m. [2]	555±93 (sec)	No crystal appeared
	FFA-TP CO	n.m. [2]	n.m. [2]	510±166 (sec)	No crystal appeared
SSR=5.44	FFA	n.m. [2]	n.m. [2]	n.m. [3]	446±73 (sec)
	FFA-NIC CO	n.m. [2]	n.m. [2]	n.m. [3]	392± 93(sec)
	FFA-TP CO	n.m. [2]	n.m. [2]	n.m. [3]	397± 63(sec)

1: not measured; 2: Nucleation experiments not measured when SSR=2.72 as the induction time of FFA in the absence or the presence of PEG has been detected at SSR=1.36; 3: Nucleation experiments not measured when SSR=5.44 because the induction time of FFA in the presence of PVP has been detected at SSR=2.72.

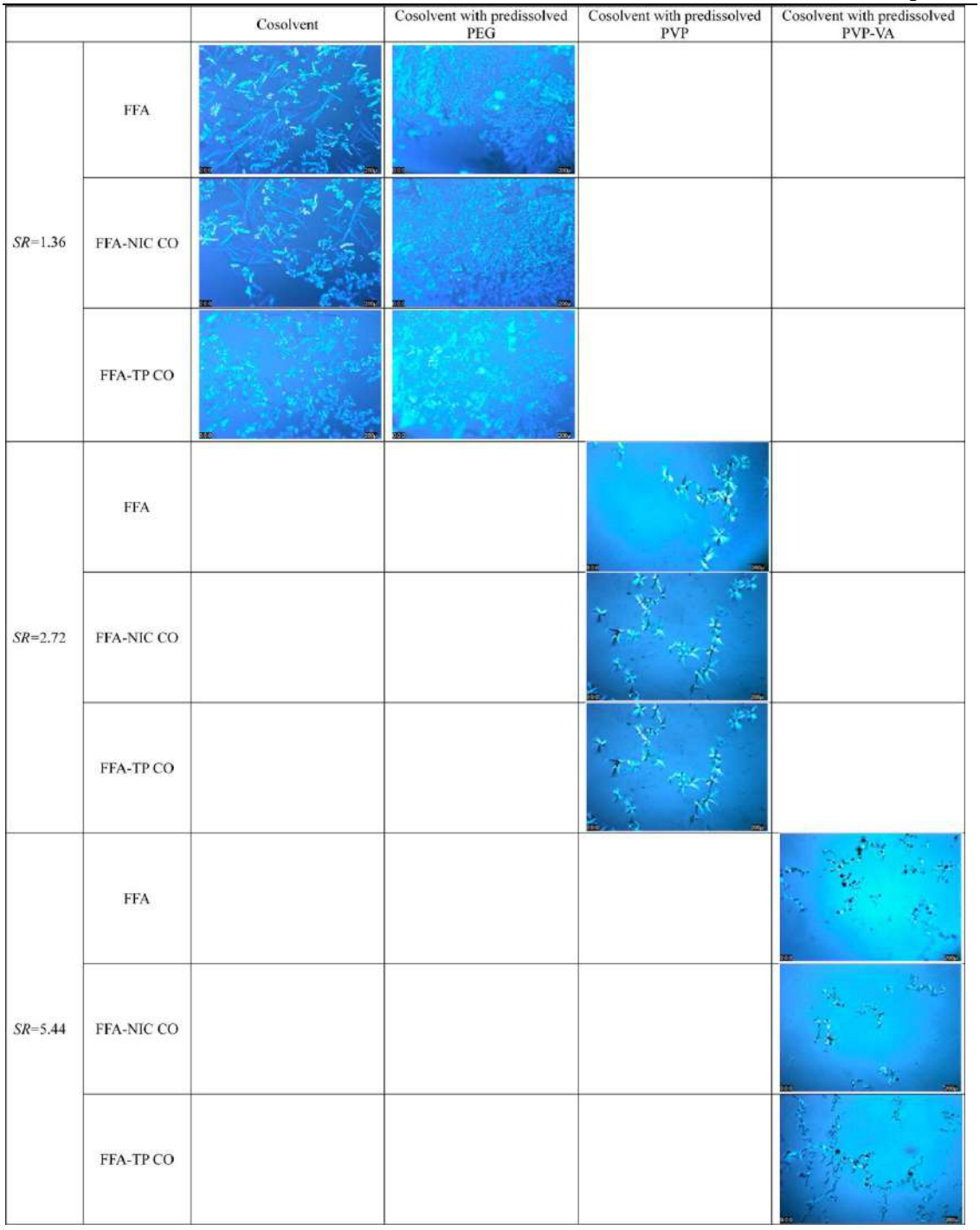

Figure 5. 2 Images of FFA crystals after induction time tests after 30mins; All scale bars were 200μm.

5.3.3 Effect of Polymers on the FFA Crystal Growth in Solution

Due to the variation of the initial FFA concentrations in the seeded solutions, the desupersaturation curve is represented by the normalized value of $C_{norm}(t)$ which is the ratio of the measured FFA concentration via the initial FFA concentration in solution as:

$$C_{norm}(t) = \frac{C(t)}{C_0 + C_{stock}} \qquad \text{(Equ5-1)}$$

where $C(t)$ is the measured FFA concentration at sampling time *t*, C_0 is the initial FFA concentration in the seeded solution without adding the stock solution and C_{stock} is the FFA concentration of the stock solution.

Figure 5. 3 shows the desupersaturation curves of the different test samples. The gradient of a FFA desupersaturation curve is directly related to bulk growth rate of FFA crystals in solution. Without a polymer, the growth rate of FFA crystals of the FFA-NIC CO and FFA-TP CO solutions was slower than that of the pure FFA solution, indicating the coformer of NIC or TP can inhibit the growth of FFA crystals, with NIC being more effective at 12% of SSP. PEG can slightly reduce the growth rate of the FFA crystals in the pure FFA solution with 4% of SSP. In contrast, PEG reduced the inhibition ability of NIC for the growth of FFA crystals in FFA-NIC CO solution in which SSP was reduced to 1% from 12% shown in Figure 5. 3e. Surprisingly, both PVP and PVP-VA were ineffective in inhibiting the growth of FFA crystals and instead accelerated the FFA crystal growth rates, indicating that the FFA concentrations in solution quickly decreased to the equilibrium solubility, shown in Figure 5. 3c, d. With predissolved PVP, the SSP dropped to −17% in the pure FFA solution, to −28% in the FFA-NIC CO solution and to −12% in the FFA-TP CO solution. In the presence of PVP-VA in solution, the crystal growth rates in cocrystal solutions SSP values, −27% in the FFA-NIC CO solution, and −24% in FFA-TP CO solution, were faster than that of the pure FFA solution, SSP of −13%. DSC thermographs and images of the solids isolated from the experiments were the same as that of initial seeds of FFA I, shown in Figure A2. 2 in the appendixes. However, when closely examining the FTIR data of the solids

collected in Figure 5. 3f, it was found that a shift of the carbonyl peak (1651 cm^{-1}) of FFA I was observed in all the experiments, suggesting that a coformer or polymer was integrated in the solids.

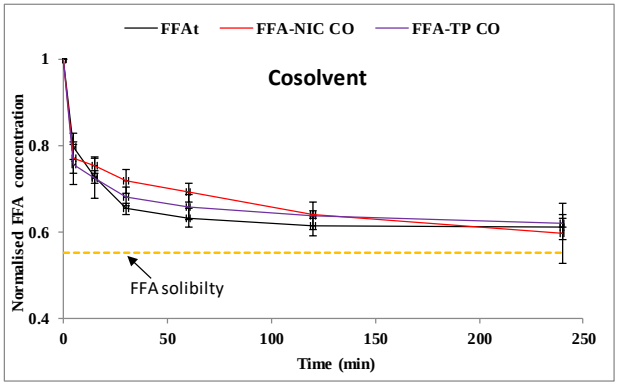

(a)

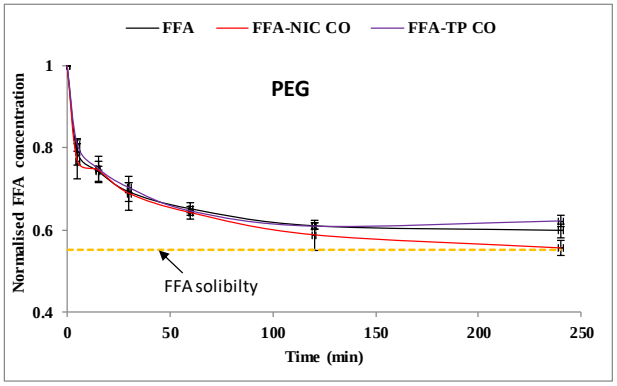

(b)

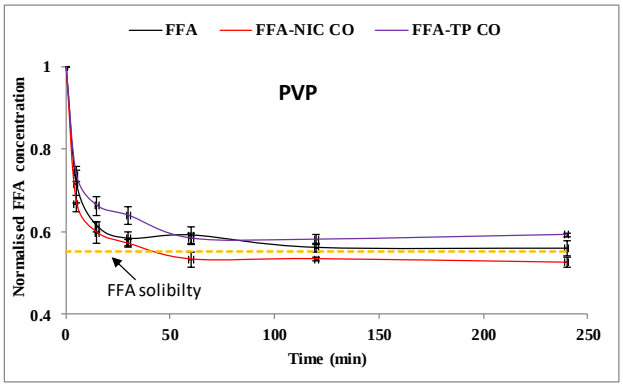

(c)

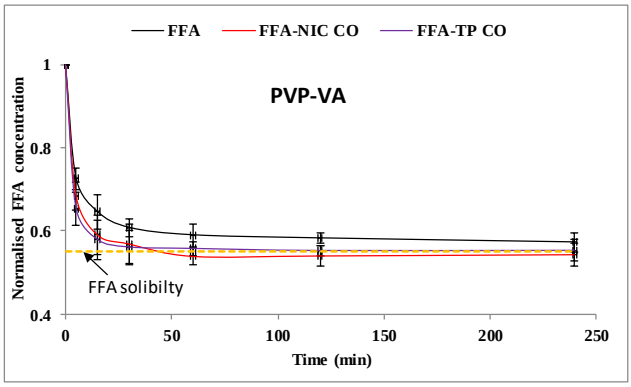

(d)

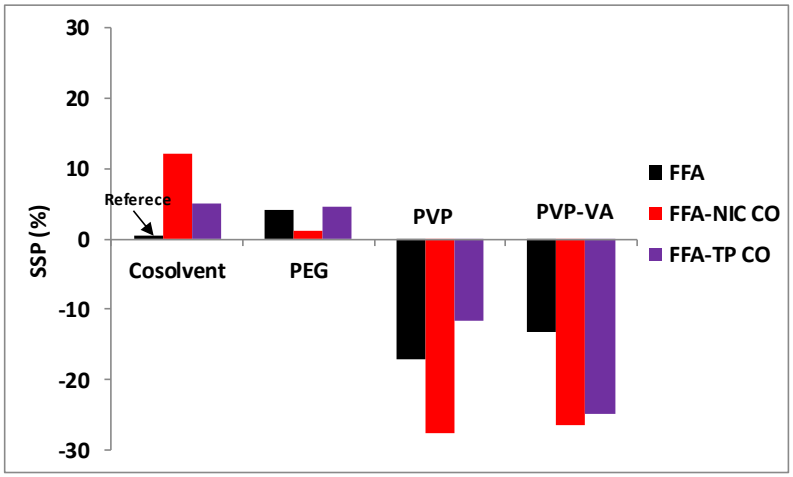

(e)

FFA	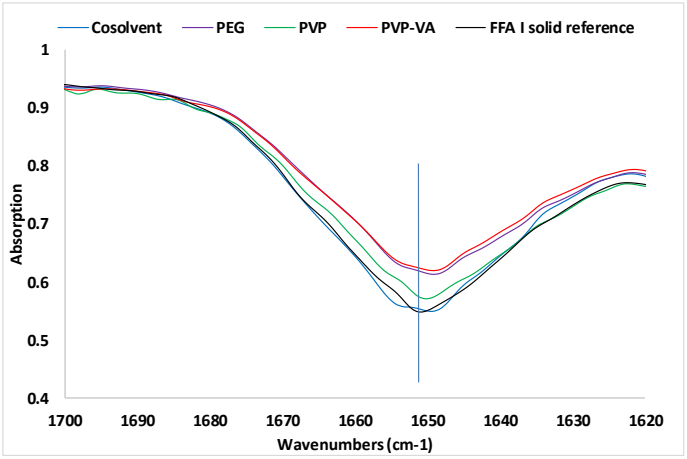
FFA-NIC CO	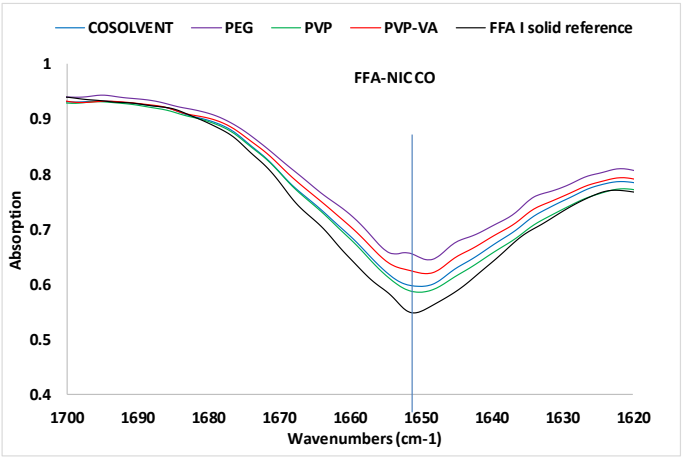
FFA-TP CO	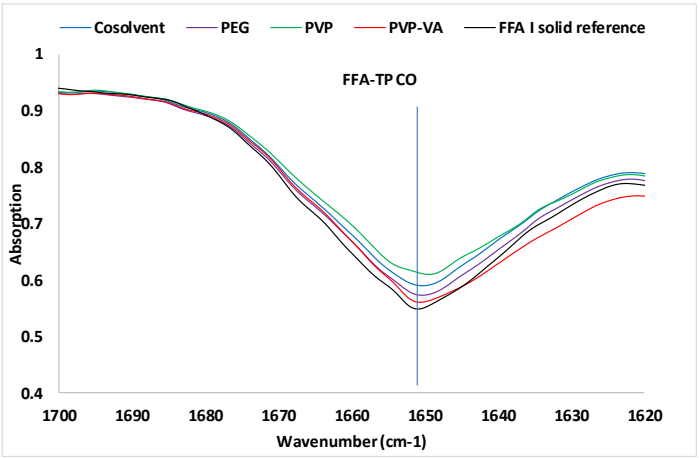

(f)

Figure 5. 3 Seeded desupersaturation curves in the absence or presence of polymers: (a) cosolvent; (b) Cosolvent with predissolved PEG ;(c) Cosolvent with predissolved PVP; (d) Cosolvent with predissolved PVP-VA; (e) Comparison of supersaturation parameters (reference is the pure API in cosolvent); (f) FTIR data of solids

5.3.4 Overall Polymer Inhibition Ability on Maintaining FFA Supersaturation

The overall effect of a polymer on inhibition of FFA crystallization from a supersaturated solution was evaluated by unseeded desupersaturation experiments in the absence or presence of 200μg/mL of a predissolved polymer of PEG, PVP, or PVP-VA, as described in the previous section. The initial FFA concentration was 100μg/mL corresponding to SSR = 2.72. Figure 5. 4 shows the desupersaturation curves of the different test samples. The FFA concentrations from different test samples decreased rapidly in the cosolvent media without a predissolved polymer in Figure 5. 4a. The FFA-NIC CO and FFA-TP CO solutions show a comparable performance in which the rate of desupersaturation was slower than that of the pure FFA solution. The FFA concentrations in all three test solutions were reduced to the same static level of 42μg/mL within 2h, which was slightly higher than its solubility. In the predissolved PEG media, the decreasing rates of the supersaturated FFA concentrations in the FFA-NIC CO and FFA-TP CO solutions are significantly slower in comparison with that of the pure FFA solution, showing an increased SSP of 13.4% for FFA-NIC CO solution, 12.2% for FFA-TP CO, and just 3.2% for the pure FFA solution in Figure 5. 4b. Among the three solutions with predissolved PVP, Figure 5. 4c demonstrates that PVP is the effective inhibitor for the pure FFA solution as seen by a 15.9% increase in inhibition of FFA. Compared with PEG, PVP has a reduced ability on maintaining FFA in either the FFA-NIC CO or FFA-TP CO solutions. PVP-VA predissolved in solution can significantly reduce the rate of the FFA precipitation from both supersaturated FFA and FFA-NIC CO solutions, showing 27.4% and 26.4% increases of SSP values in Figure 5. 4d,e. However, there is no difference between PVP and PVP-VA in maintaining the supersaturated FFA in FFA-TP CO solution in Figure 5. 4e. The solids precipitated from all the experiments were yellow needle-shape FFA III crystals confirmed by the DSC results and images in Figure A2. 3 in the appendixes. The FTIR data showed that a shift of the carbonyl peak (1655 cm^{-1}) of FFA III at was observed in all the experiments, suggesting that a coformer or polymer was coprecipitated in the solids in Figure 5. 4f.

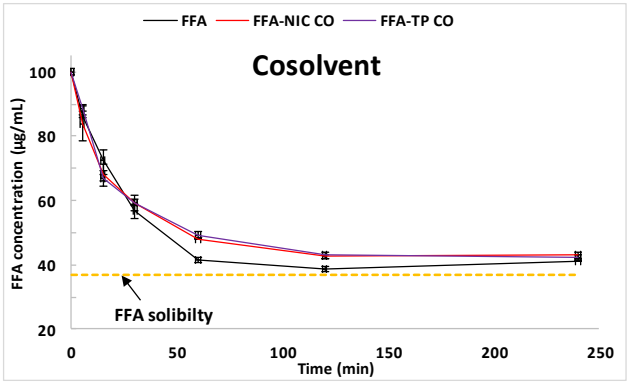
FFA
FFA-NIC CO
FFA-TP CO
Cosolvent
FFA concentration (μg/mL)
Time (min)
FFA solibilty

(a)

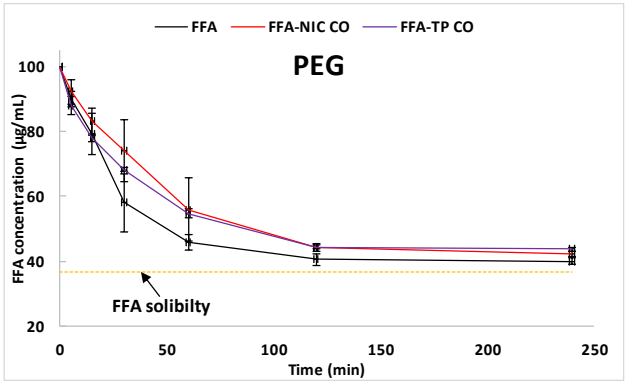
FFA
FFA-NIC CO
FFA-TP CO
PEG
FFA concentration (μg/mL)
Time (min)
FFA solibilty

(b)

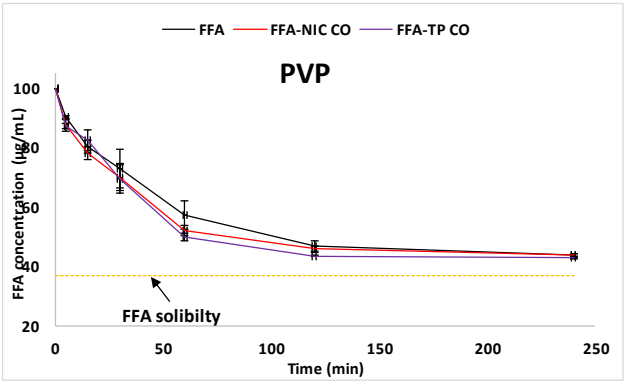
FFA
FFA-NIC CO
FFA-TP CO
PVP
FFA concentration (μg/mL)
Time (min)
FFA solibilty

(c)

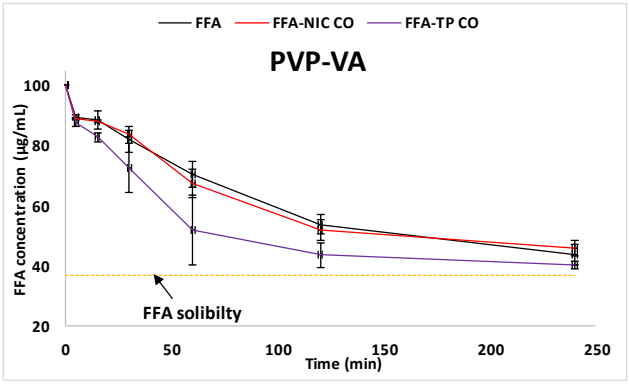
FFA
FFA-NIC CO
FFA-TP CO
PVP-VA
FFA concentration (μg/mL)
Time (min)
FFA solibilty

(d)

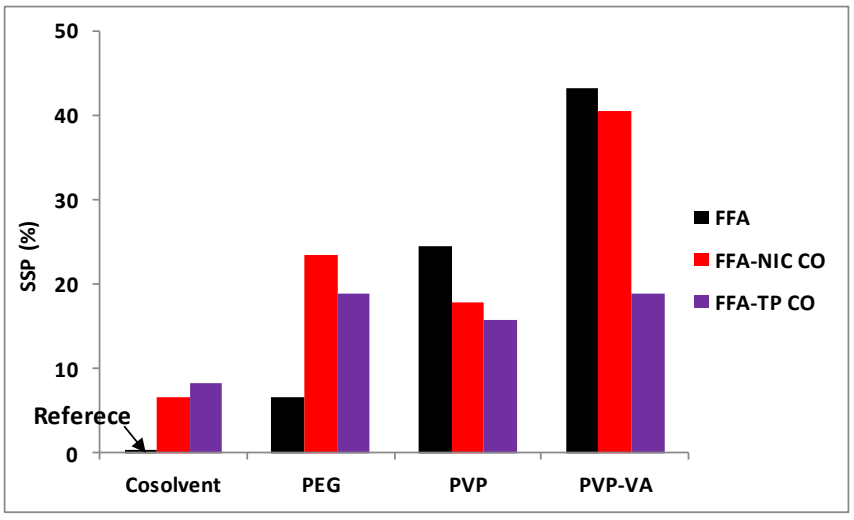
SSP (%)
Referece
Cosolvent
PEG
PVP
PVP-VA
FFA
FFA-NIC CO
FFA-TP CO

(e)

FFA	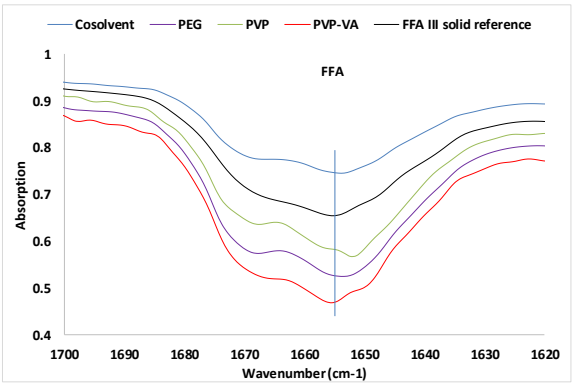
FFA-NIC CO	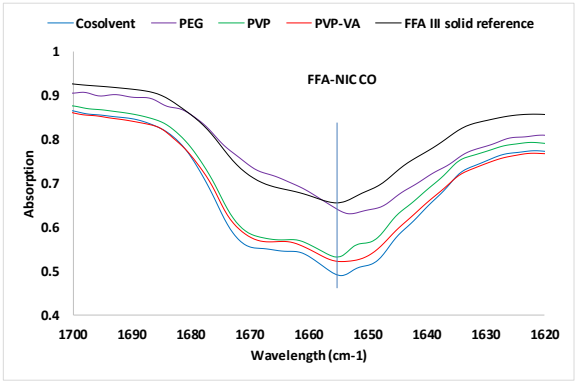
FFA-TP CO	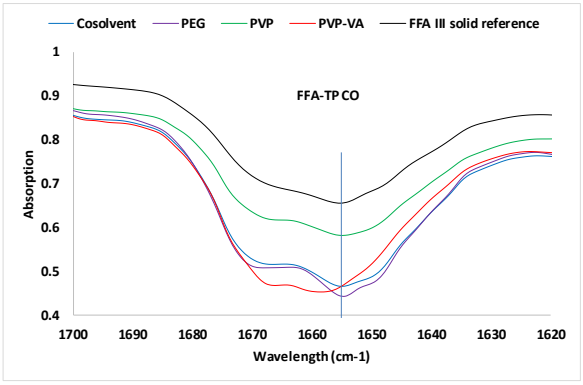

(f)

Figure 5. 4 Unseeded desupersaturation curves in the absence or presence of polymers: (a) cosolvent; (b) Cosolvent with predissolved PEG; (c) Cosolvent with predissolved PVP; (d) Cosolvent with predissolved PVP-VA; (e) Comparison of supersaturation parameters; (f) FTIR data of solids

5.3.5 IR Spectroscopic Investigation of Intermolecular Interactions among FFA, Coformer, and Polymer in Solution

Figure 5. 5 shows the comparison of the solution IR spectra of individual components of FFA, NIC, TP, and mixtures of FFA and coformers in the absence and presence of different polymers. In Figure 5. 5a, strong peak of FFA in methanol was found at 1686

cm^{-1}, indicating C=O stretching [293]. When a component of NIC, PVP, or PVP-VA was added in the solution, this FFA characteristic peak was shifted to a smaller wavelength number of 1684 cm^{-1}, indicating an intermolecular interaction between them in solution. In contrast, there is no change in the FFA C=O peak in the PEG solution, suggesting no interaction between these two components. NIC can interact with FFA or PVP in solution, demonstrated by a change in the characteristic peak of NIC at 1625 cm^{-1}, corresponding to N−H stretching [294], to 1617 cm^{-1} in the presence of FFA and to 1631 cm^{-1} in the presence of PVP in Figure 5. 5b. Surprisingly there is no interaction between NIC with PVP-VA or PEG in solution, confirmed by no change in the characteristic peak of NIC at 1625 cm^{-1}. The IR characteristic peak of TP (Figure 5. 5c) at 925 cm^{-1}, corresponding to N-H symmetric stretching [300], has been shifted to a lower wavenumber by inclusion of PVP or PVA-VA and to a higher wavenumber by adding PEG or FFA in solution, indicating TP can interact with any of the components, FFA, PEG, PVP, or PVP-VA in solution.

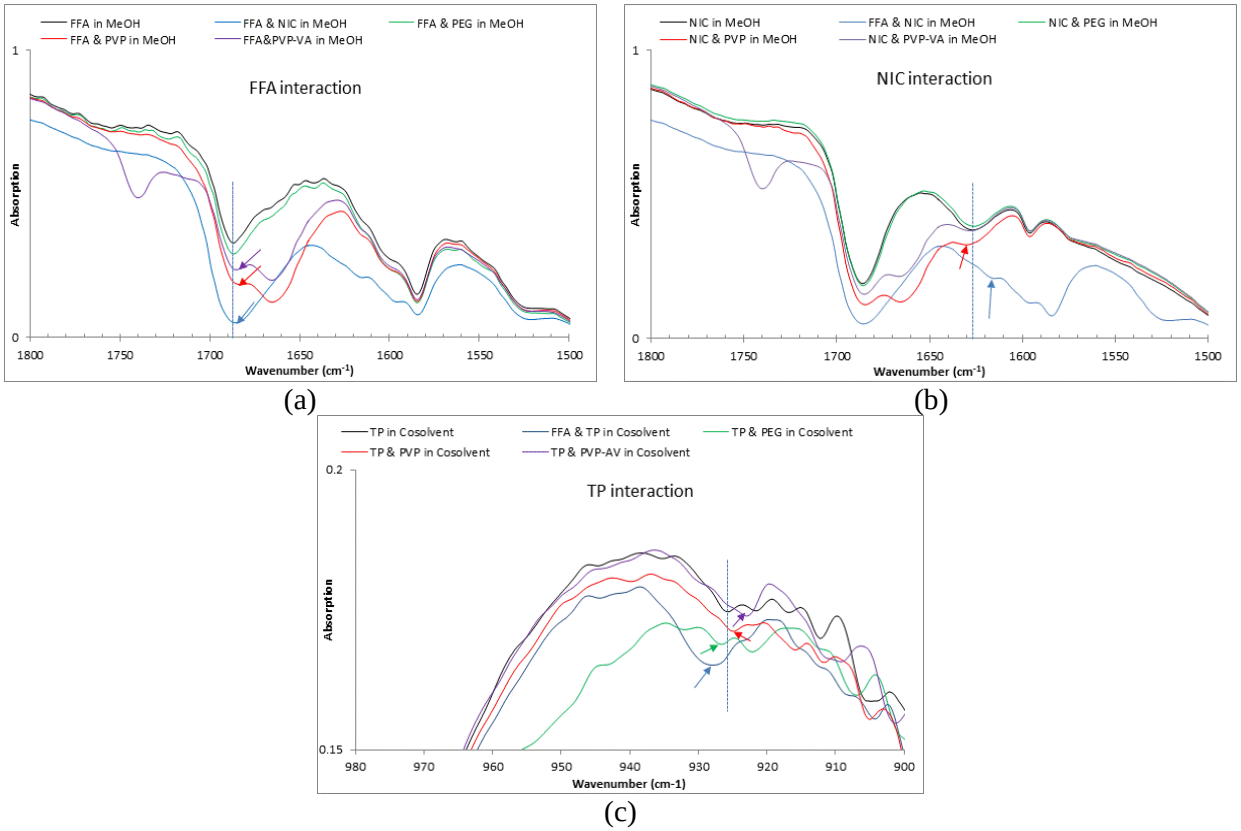

Figure 5. 5 IR spectroscopic investigation of molecular interaction in solution: (a) FFA interaction with NIC and polymers; (b) NIC interaction with FFA and polymers; (c) TP interaction with FFA and polymers

5.4 Discussion

5.4.1 Effect of a Polymer on the Apparent FFA Equilibrium Solubility of FFA I, FFA-NIC CO, and FFA-TP CO in Cosolvent

There is widespread acceptance that the crystalline nature of pharmaceutical cocrystals can offer advantages over amorphous materials to formulate drug compounds with limited solubility and bioavailability, due to superior thermodynamic stability and purity. Although significant advances in design and discovery have been made, little work has been conducted to formulate cocrystals into a drug product. Therefore, the behavior of a cocrystal in a formulated product is largely unknown. To offer the most desired in vivo performance with the highest bioavailability for many life-saving drugs with poor biopharmaceutical properties, a fundamental understanding of critical factors that control the dissolution and absorption performance of a cocrystal formulated product is required. In this work, the focus was on understanding the parent drug crystallization kinetics from a supersaturated cocrystal solution in the presence of a polymeric excipient. It aimed to provide the mechanistic understanding of the properties of a polymer as a good inhibitor of crystallization for a given drug cocrystal. Two FFA cocrystals, FFA-NIC CO and FFA-TP CO, were chosen due to significant differences in their physicochemical properties. The low polymer concentration of 200μg/mL used in the investigation was based on the rational consideration of a 500mg tablet containing 250mg of stabilizing polymer, in which 20% of the polymer was released in 250mL of the GI tract at the beginning stage of dissolution. According to the equilibrium solubility results in Figure 5. 1a, FFA concentrations of FFA I, FFA-NIC CO, or FFA-TP CO were constant in solution in the absence and presence of 200μg/mL polymer of PEG, PVP, or PVP-VA, indicating that the impact of a polymer on FFA supersaturation is due to the stabilization effect on crystallization rather than solubilization effect of polymer. Furthermore, due to the low molecular weight of the polymer used in the study, the viscosity of the 200μg/mL polymer solution was essentially the same as that of the dissolution medium without a predissolved polymer. Therefore, the interplay of API-coformer, API-polymer, and coformer-polymer elucidated in this study was not affected by the changes of solution bulk properties of solubility and mass transport.

5.4.2 Effect of Intermolecular Interactions of Drug/Coformer, Drug/Polymer, and Coformer/Polymer on Parent Drug Nucleation and Growth Kinetics in Solution

This study has clearly demonstrated that a cocrystal coformer can interfere with a polymer to alter its ability to maintain the parent drug supersaturation in solution. This property involves both nucleation and growth through competition of the intermolecular interactions of drug/coformer, drug/polymer, and coformer/polymer in solution.

In the solid state, cocrystals are formed through hydrogen bonding between an API and coformer. Once cocrystals are dissolved in solution, they could be regarded as completely separate individual molecules. For example, US FDA has elected to classify cocrystals within their framework as dissociable "API-excipient" molecular complexes. However, in this study it was found that hydrogen bonds between FFA and coformers, NIC, or TP, were not broken completely, indicated by changes in their characteristic peaks of the solution spectra in Figure 5. 5(a). This API/coformer interaction in solution certainly affected the formation of nuclei by hindering the reorganization of a cluster of FFA molecules into its ordered structure. Therefore, the coformer of NIC or TP can be regarded as a nucleation inhibitor for FFA crystallization, generating slightly longer induction time (15s for FFA-NIC CO solution and 24s for FFA-TP CO solution) compared with the pure FFA supersaturated solution (9s of induction time) in the absence of a polymer, as shown in Table 5. 2.The FFA molecule, shown in Table 5. 1, has the very strong hydrogen bond donor of O−H combined with a middle strength acceptor of C=O, thus displaying higher hydrophobicity with a low value of SP (18.62 $MPa^{1/2}$). Therefore, FFA self-association should be disrupted by a polymer with strong acceptor groups that can effectively compete with the acceptor group C=O [301]. Indeed, the formation of the hydrogen bonding between the polymer of PVP or PVP-VA with FFA in solution was demonstrated by the IR spectroscopic investigation in Figure 5. 5a, as both polymers (N−C=O in PVP and N−C=O and O−C=O in PVP-VA) have strong acceptors. This suggested that both PVP and PVP-VA were able to act as effective nucleation inhibitors, indicated by the significantly increased nucleation induction times at different degrees of supersaturation. A higher level of inhibition effectiveness of PVP-VA in comparison with PVP was due to the presence of carbonyl oxygens C=O on the side chain, which contributed to a more hydrophobic nature and

flexibility to interact with FFA molecules in solution. Therefore, evidence for a two-step mechanism of cocrystal nucleation was revealed in the presence of PVP-VA. During two-step mechanism nucleation, a droplet of a dense liquid (metastable zone with respect to the crystalline state) is formed in the homogeneous solutions prior to nucleation. Then clusters order inside the droplet to produce a crystal[299]. The precipitated solids in Figure 5. 2 show a lack of birefringence under polarized light and no distinct particle morphology, indicating the amorphous nature of the particles was due to the integration of PVP or PVP-VA in the FFA crystal structure and/or rapid desupersaturation. The amorphous nature of the precipitated particles could be also related to liquid−liquid phase separation (LLPS), which was observed in amorphous solid dispersion systems (ASDs) in recent publications [302, 303]. The high supersaturation generated by ASDs can lead to a two-phase system wherein one phase is an initially nanodimensioned drug-rich phase and the other is a drug-lean continuous aqueous phase. In those studies, the stronger nucleation inhibitors PVP/PVP-VA allowed the system to reach supersaturation levels such that the system underwent LLPS. The excess drug then precipitated forming a dispersed, colloidal amorphous drug-rich phase, which resulted in the absence of birefringence in the precipitated particles.

The ineffectiveness of PEG as a nucleation inhibitor was probably due to its structural rigidity in which the hydrogen acceptor, C−O−C, on the main chain had been prevented from interacting with FFA molecules in solution. Thus, no change was observed in the characteristic peak of FFA in solution with the predissolved PEG (Figure 5. 5a). The limited inhibition ability of PEG may be due to the steric barrier for the formation of nuclei via the adsorption of the polymer on the surface of pre-nuclear clusters [304]. It has to be stressed that although all three polymers of PEG, PVP, and PVP-VA interacted with FFA with different mechanisms, they were all integrated into the FFA crystal lattices, showing as a variation of the FFA III characteristic peak, which corresponds to its C=O stretching frequency (1655 cm^{-1}) in Figure 5. 4f. The results are in good agreement with previous studies, which have shown that multicomponent molecular complexes in solution lead to a metastable form precipitating preferentially

[305, 306]. A change in crystal morphologies, seen in Figure A2. 3 in the appendixes, also supported this.

It was not surprising that the nucleation induction time was reduced for FFA-NIC CO solution in the presence of PVP compared to the pure FFA solution because the competition between NIC and FFA with PVP weakened the polymer inhibition ability. There was no interaction between NIC with PVP-VA in solution shown in Figure 5. 5b. Therefore, the nucleation induction time from the FFA-NIC CO solution was almost the same as that of the pure FFA solution, in the presence of PVP-VA. As TP can interact with both polymers of PVP and PVP-VA in solution, the nucleation induction time reduced in the FFA-TP CO solution compared to the pure FFA solution in the presence of the polymers, as shown in Table 5. 2. PEG inhibits FFA crystallization using a different mechanism in comparison with PVP or PVP-VA, for reasons outlined above. The nucleation induction time increased in both the FFA-NIC CO and FFA-TP CO solutions in the presence of PEG due to the accumulated inhibition effects of both the coformer and polymer on FFA.

In order to study the effectiveness of the polymers on inhibiting FFA crystal growth after nucleation, desupersaturation experiments were conducted including the addition of the FFA seeds. A low SSR of 1.27 (based on 36.6μg/mL of the solubility of FFA I measured in this study) was used in the growth experiments to avoid secondary nucleation. It was observed that polymer effectiveness at reducing crystal growth rates was not found to have a similar impact on nucleation. In the nucleation induction time study, PVP and PVP-VA were effective nucleation inhibiting agents in the pure FFA solution. In contrast, they were poor at inhibiting growth and actually accelerated the growth of FFA crystal seeds, as seen by the negative values of SSP in Figure 5. 3e. It is known that the alteration of crystal growth by additives can be achieved through modifying the step speed or altering the step edge energy, which is classified as step pinning, incorporation, kink block, and step edge adsorption mechanisms [307]. To occur, the additives must be adsorbed on the surface of the crystals to block active crystal growth sites. There are a number of interactive forces responsible for the adsorption of additive molecules on the solid surface including electrostatic, hydrogen

bonding, and hydrophobic interactions. The electrostatic force was not considered because of the neutral natures of the solution and drug components used in this study.

The coformer molecules of NIC or TP in a cocrystal solution were most likely adsorbed on the FFA crystal surface due to hydrogen bonding attraction as the growth rate inhibitor. This led to moderately increased SSP values of 12% for FFA-NIC cocrystal solution and 5% for FFA-TP CO solution, as shown in Figure 5. 3e. In the pure FFA solution with the predissolved PEG, hydrogen bonding was not promoted between PEG and FFA as shown in the IR spectroscopic investigation in Figure 5. 5a. Therefore, hydrophobic interaction was the main interactive force to drive PEG molecules to be adsorbed on the surfaces of the FFA crystal seeds. A large difference in their SP values in Table 5. 1 suggests a weak interactive force between FFA and PEG in solution. It was not surprising that PEG was neither an effective FFA nucleation nor growth inhibitor. The decrease in the growth inhibition in the FFA-NIC CO solution in the predissolved PEG can most likely be the reduced NIC, being a more effective inhibitor in comparison to PEG, when adsorbed on the solid surface due to competition by PEG for the same adsorption sites. In the FFA-TP CO solution in the presence of PEG, there was no noticeable change in the extent of growth inhibition as both TP and PEG were equally effective on an individual basis shown in Figure 5. 3e.

In the pure FFA solution in the presence of PVP or PVP-VA, acceleration of crystal growth occurred, indicated by the negative SSP values of −17% for PVP and −13% for PVP-VA. Similar phenomena were found in other studies when one or more surfactants were predissolved in the solution in which it was believed that the adsorbed additives could lead to a decrease in interfacial tension to be favorable to growth [308]. However, in this study the enhanced crystal growth was not likely to be caused by the reduced interfacial tension between the crystal and solution due to the polymer adsorption. It is known that strong intermolecular hydrogen bonding was occurring between FFA and PVP or PVP-VA in solution. When polymer molecules were adsorbed on the surface of the FFA seeds, the bound FFA molecules were driven around the FFA seeds, leading to increase local supersaturation at the surface and contributing to the acceleration in crystal growth.

In the FFA-NIC CO solution with the predissolved PVP or PVP-VA, acceleration of crystal growth was enhanced in comparison to the pure FFA solution in the presence of the same polymer. In the FFA-TP CO solution with the predissolved PVP, acceleration of crystal growth was reduced in contrast to PVP-VA where growth was promoted. These results demonstrated that the combination of PVP or PVP-VA in the presence of either coformer (NIC or TP) can either enhance or reduce the rate of the crystal growth. Overall, the effect was to accelerate the growth. Thus, rational selection of a polymer is required to enhance the inhibition ability in a cocrystal supersaturation solution.

The comparison of the overall desupersaturation profiles of three supersaturation solutions in the absence and presence of a polymer of PEG, PVP, or PVP-VA is given in Figure 5. 4. In the absence of a polymer, a cocrystal solution showed a better performance to maintain the FFA in solution in comparison to the pure FFA solution due to the enhanced combination effects of the nucleation and growth inhibition abilities of the coformers. In the predissolved PEG, a cocrystal solution showed an increased ability to maintain supersaturation for extended time periods, which was most likely due to the enhanced combination effects of the individual nucleation and growth inhibition abilities of the coformer and PEG. Clearly the polymer nucleation inhibition effect outweighed its growth acceleration ability for FFA in solution, indicating that the rate of desupersaturation was reduced dramatically in the presence of PVP or PVP-VA. The desupersaturation behavior of FFA cocrystal solutions in the presence of PVP or PVP-VA depends on different interaction mechanisms of the polymer and coformer and on the competition effect of the polymer and coformer for formation of hydrogen bonding with FFA molecules, in which PVP-VA was a good crystallization inhibitor for FFA-NIC CO solution.

It is worth noting that the study has shown the coformers and polymers have been integrated in the solid particles recovered from the seeded and unseeded experiments based on the measured IR spectra. However, the IR data cannot quantify the relative proportion of coformer/polymer coprecipitated in the desupersaturated solids, which could be determined by solid state NMR or other techniques. In the meantime, more fundamental research is required to guide the selection of polymers in cocrystal formulation systems through understanding the parent drug crystallization kinetics.

5.5 Chapter Conclusion

The development of enabling formulations is a key stage when demonstrating the effectiveness of pharmaceutical cocrystals is applied to maximize the oral bioavailability for poorly water-soluble drugs. It is important to have a fundamental understanding of nucleation and crystal growth for evaluating the inhibition effect of polymers on the drug crystallization from cocrystals' supersaturation. In this study, the influence of three polymers PEG, PVP, and PVP-VA on the FFA crystallization in three different supersaturated solutions of the pure FFA and two cocrystals of FFA-NIC CO and FFA-TP CO has been investigated by measuring nucleation induction times and desupersaturation rates in the presence and absence of seed crystals.

It was found that the competition of intermolecular hydrogen bonding among drug/coformer, drug/polymer, and coformer/polymer was a key factor responsible for maintaining the supersaturation through nucleation inhibition and crystal growth modification in a cocrystal solution. The supersaturated cocrystal solutions with predissolved PEG demonstrated effectiveness at stabilizing supersaturated solution compared to pure FFA in the presence of the same polymer. In contrast, the two cocrystal solutions in the presence of PVP or PVP-VA did not perform as well as pure FFA with the same predissolved polymer. The study suggested that the selection of a polymeric excipient in a cocrystal formulation should not be solely dependent on the interplay of the parent drug and polymer without considering the coformer effects.

Chapter 6 Insight into Flufenamic Acid Cocrystal Dissolution in the Presence of a Polymer in Solution: from Single Crystal to Powder Dissolution

*(This work has been published. Citation: Guo, M., et al., Insight into Flufenamic Acid Cocrystal Dissolution in the Presence of a Polymer in Solution: from Single Crystal to Powder Dissolution. Molecular Pharmaceutics, 2017. **14**(12): p. 4583-4596.)*

6.1 Chapter Overview

In this study, the aim is to understand the dissolution mechanisms of cocrystals in solution in the absence and presence of a predissolved polymer. We conducted different dissolution experiments of both single and powdered cocrystals to evaluate the dissolution behaviors at multiple length scales. At the molecular level, we studied how a cocrystal surface interacted with a polymer by investigating the changes of the etching pattern observed by using AFM. At the macroscopic scale, dissolution rates of particular faces of a single crystal were determined by measurement of the physical retreated velocities of different faces using optical light microscopy (OLM). In the bulk experiments, the concentration of a drug in a dissolution medium in the absence or presence of a polymer was measured under both sink and non-sink conditions and the dissolution rate was deduced from the evolution of this concentration. Sink condition experiments were performed to evaluate the effect of a polymer on the dissolution rate of cocrystals, and non-sink condition was to evaluate the ability of a polymer to generate and maintain supersaturated drug solutions. Under sink conditions the change of a cocrystal dissolution rate during dissolution should be directly related to the interaction between the predissolved polymer in solution with the dissolving crystal surface. Evaluation of the supersaturating systems benefits from the use of non-sink conditions that mimic the in vivo conditions in the gastrointestinal tract. The FFA-NIC CO and FFA-TP CO with PEG, PVP, and PVP-VA were selected, with the aim to identify the different influences of these polymers on cocrystal dissolution. The chemical structures of the model drug, the coformers, and the monomer units of the polymers and their detailed description can be found in our previous publication [183].

In order to eliminate the effect of viscosity, a low polymer concentration of 200μg/mL was used in the study. At this polymer concentration, the equilibrium solubility of FFA remained virtually the same as without the presence of the polymers. Because of the thermodynamically unstable nature of a cocrystal in solution, the solubility of FFA-TP CO and FFA-NIC CO was determined by their eutectic points through measuring their solubility curves [309]. The faces of FFA I, FFA-TP CO, and FFA-NIC CO single crystals were indexed using X-ray diffraction and nanometer-scale models of their morphologies which were created using Mercury 3.9 (The Cambridge crystallographic Data Centre, Cambridge, UK). These morphology models were also used to explain the properties of each face of a single crystal in the AFM and OLM dissolution experiments. In order to quantify the effect of a predissolved polymer on the powder dissolution performance, the dissolution performance parameters (DPPs) in different condition experiments were calculated and compared. The solid residues after the solubility and powder dissolution experiments were examined by DSC, XRPD and IR.

6.2 Materials and Methods

6.2.1 Materials

FFA I, NIC, TP, KH_2PO_4, NaOH, PEG, PVP, PVP-VA, methanol, acetonitrile, double distilled water was used in this chapter. Detailed information about these materials can be found in Chapter 3.

6.2.2 Methods

6.2.2.1 Preparation of 0.01M pH 6.8 PBS

The detailed method for preparing 0.01M pH 6.8 buffer can be found in Chapter 3.

6.2.2.2 Powdered and Single FFA Cocrystals preparation

Powdered and single FFA-NIC CO and FFA-TP CO was used in this chapter. The detailed methods for forming FFA cocrystals can be found in Chapter 3.

6.2.2.3 Single Crystal Face Indexing and Morphology Models

To identify the exposed crystal faces of single crystal during AFM and OLM dissolution experiments, representative crystals of each type were mounted on an Oxford Diffraction XCalibur diffractometer. Only a few X-ray images were collected for each crystal, which allowed determination of the unit cell parameters and the orientation matrix. The major faces could then be identified by orienting the crystals in specific crystallographic directions on the diffractometer, while observing them through the built-in camera. Models of the observed morphologies were created in Mercury 3.9 (The Cambridge crystallographic Data Centre, Cambridge, UK) by manually adjusting the list of faces and face-to- centroid distances to match those observed experimentally on the diffractometer. A summary of these results is given in Figure 6. 1, with the single crystal indexing data in Table A3.1 in the appendixes

6.2.2.4 Apparent Equilibrium Solubility of FFA I

The Apparent equilibrium solubility of FFA I was determined in 0.01M pH 6.8 PBS with or without 200μg/mL of a polymer (PEG, PVP or PVP-VA) in a shaking water bath at 250RPM sharking rate and 23 ± 0.5°C for 24h. The detailed information about solubility tests can be found in Chapter 3.

6.2.2.5 Cocrystal Solubility

For a 1:1 cocrystal of AB without consideration of ionization of each component, its solubility is calculated as[309]

$$S_{AB} = \sqrt{K_{sp}} = \sqrt{A_{eu}B_{eu}} \qquad \text{(Equ. 6- 1)}$$

where K_{sp} is the solubility product of the AB cocrystal and concentrations of A_{eu} and B_{eu} are transient concentrations of drug and coformer where the solution is in equilibrium with solid drug and cocrystal.

To measure transition concentrations of FFA and a coformers of TP or NIC in PBS, a series of coformer solutions were prepared: 0.0, 7.1, 8.9, 10.7, 12.4, 14.2mmol/L for TP

solutions and 0.0, 17.8, 57.4, 61.8, 66.2, 71.1, 142.3, and 213.4mmol/L for NIC solutions, respectively. The details of the measurement can be found in chapter 3.

6.2.2.6 Atomic Force Microscopy (AFM) Measurements

Single crystals with well-defined and visually flat faces were selected for dissolution study. The size of single crystal was from millimeters to one centimeter. In order to correlate the etching pits with the crystal structure, the axis directions were determined by comparing the observed crystal face with the indexed crystal morphology created by Mercury 3.9. A single crystal was first mounted onto an AFM sample disk using double-sided seal tape, in which the studied face was up. The prepared sample disk was then immersed in a Petri dish with 20mL of 0.01M pH 6.8 PBS in the absence or presence of a polymer at room temperature for a period of time varying from 2 to 10min as shown in Table 6. 1. After a predetermined time interval, the disk was taken from the solution and the remaining solution on the crystal surface was removed with filter paper. Finally, the sample was air-dried for at least 0.5h before AFM observation.

The surfaces of single crystals of FFA I, FFA-TP CO and FFANIC CO before and after the immersing dissolution tests (Table 6. 1) were observed with an AFM. The detailed information and setting of AFM can be found in chapter 3.

Table 6. 1 AFM measurements.

Crystal	Face	Dissolution time (min)			
		PBS	PBS with pre-dissolved PEG	PBS with pre-dissolved PVP	PBS with pre-dissolved PVP-VA
FFA I	(100)	10	10	10	10
FFA-TP CO	(001)	10	10	10	10
FFA-NIC CO	(01-1)	2	2	3	4

6.2.2.7 Optical Light Microscopy (OLM) Dissolution Monitoring for Single Crystals of FFA I and FFA Cocrystals

In this study, the dissolution rate of specific faces of single crystal of FFAI, FFA-NIC CO and FFA-TP CO was monitored by OLM. The detailed information and setting of OLM can be found in chapter 3.

6.2.2.8 Powder Dissolution Tests

Powder dissolution experiments of FFA I, FFA-TP CO, and FFA-NIC CO were performed under both sink and non-sink conditions and conducted in 0.01M pH6.8 PBS in the absence or presence of 200μg/mL of a polymer (i.e., PEG, PVP, or PVP-VA). The detailed method can be found in chapter 3.

6.2.2.9 Dissolution Performance Parameter (DPP)

The equation that used to calculate DPP can be found chapter 3.

6.2.2.10 Analytical Techniques

HPLC was applied to determine the solubility and dissolution properties of FFA I, FFA cocrystals. DSC, XRPD and AIR was employed for characterization. The details about these techniques can be found in chapter 3.

Crystal	Unit cell & supramolecular network	Comparison of predicted morphology and XRPD with measurements	Structure of crystal face	
			Structure of each face	Functional group exposed on plane
FFA I	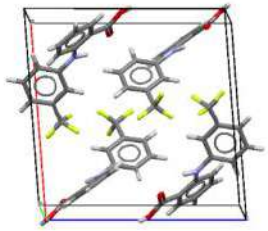	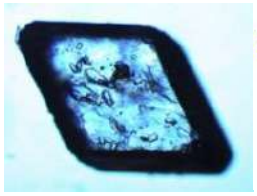 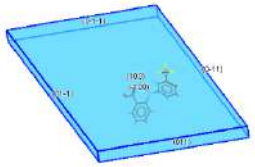 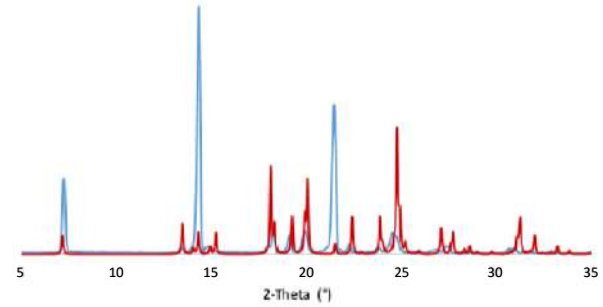	(100) 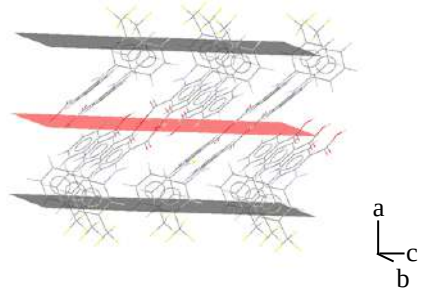	CF_3 (see top) or CF_3 (see bottom)
			(0-11) 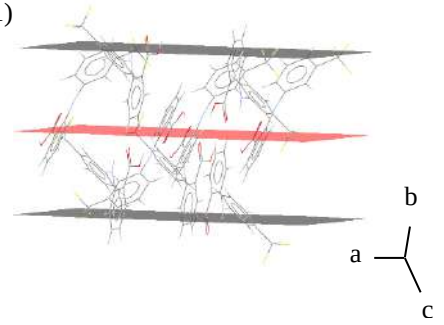	CF_3, COOH, and the aromatic rings of FFA

<table>
<tr>
<td>FFA-TP CO</td>
<td> 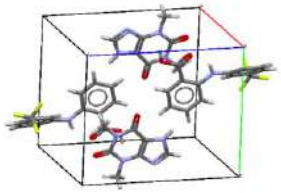
 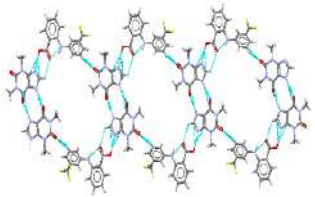 </td>
<td> 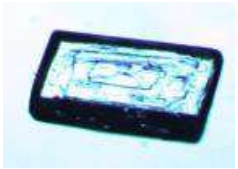 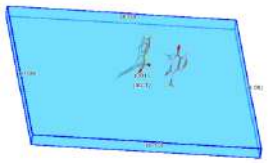
 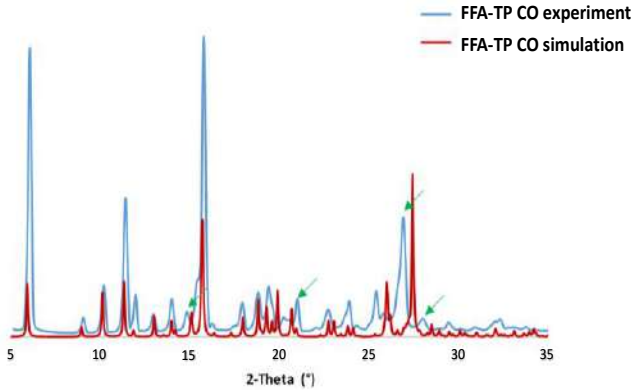
</td>
<td>(001)
 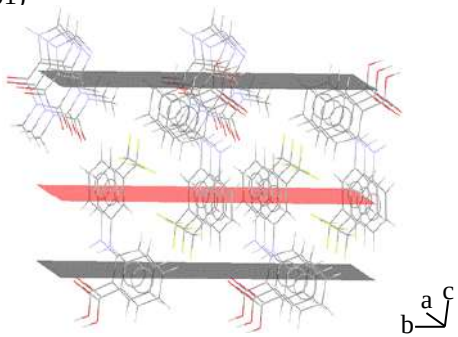
</td>
<td>COOH, aromatic rings and CF_3 (both FFA) or COOH (FFA) and NH and C=O (TP)</td>
</tr>
<tr>
<td></td>
<td></td>
<td></td>
<td>(100)
 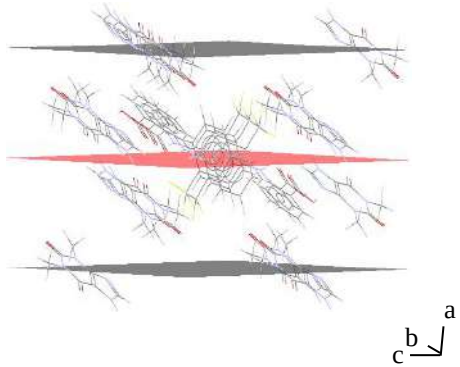
</td>
<td>Plane is approximately parallel with mean plane of molecules, so can expose any part of the molecules on the surface.</td>
</tr>
</table>

FFA-NIC CO	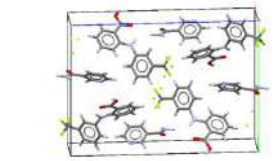 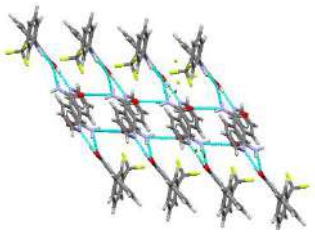	 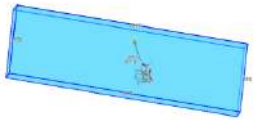	(01-1) 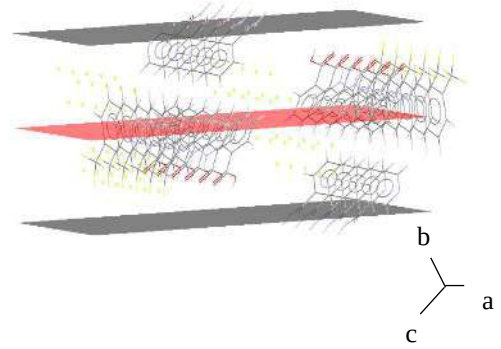	Aromatic rings (both molecules) and CF3 or aromatic rings, amide and pyridine N (NIC)
			(100) 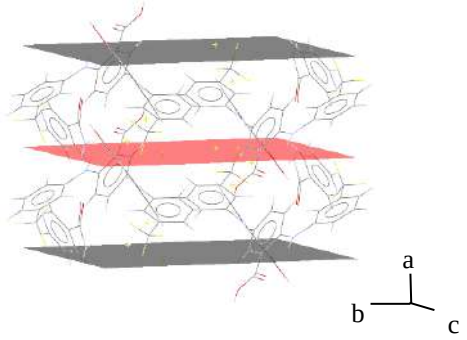	CF_3 and aromatic rings with COOH and NH

Figure 6. 1 Crystal morphologies and molecular packings at crystal faces used in experiments.

6.3 Results

6.3.1 FFA I and FFA Cocrystals Characterization, Morphology Prediction and Face Indices

Single cocrystals of FFA-NIC CO and FFA-TP CO were grown using the slow solvent evaporation technique described in the chapter 3. The identities of the crystals have been confirmed by XRPD, DSC, and FTIR measurements (Figure A3. 1 in the appendixes). Single FFA-NIC COs harvested were thin, brick-shaped and single FFA-TP COs were chunky, with sizes ranging from millimeters up to one centimeter. The single crystals of FFA I from the received materials were plate-like with a wider size range from millimeters up to one centimeter. Representative microscopy images of these single crystals are shown in Figure 6. 1. Models of the crystal morphologies were created using Mercury 3.9 based on the crystal structures of each material obtained from the Cambridge Structural Database (CSD refcodes: FPAMCA18 for FFA I; EXAQAW for FFA-NIC CO; ZIQDUA for FFA-TP CO, details in Table A3.1 in the appendixes) and face indexing of representative single crystals using an X-ray diffractometer (Figure 6. 1).

The FFA I structure is formed with hydrogen-bonded dimers between the carboxyl groups of two FFA molecules [310]. In the FFA-NIC CO structure, hydrogen-bonded rings are formed by two FFA and two NIC molecules. These four-molecule rings are linked into infinite tubes by the amide chain motif [234]. Regarding the FFA-TP CO structure, TP molecules form a dimer via N−H···O hydrogen bonds involving the saturated N atom of the imidazole ring and one of the carbonyl groups. An O−H···N hydrogen bond involving the carboxylic acid of the FFA and unsaturated N atom of the imidazole ring of TP results in a four- component supramolecular unit [295]. The identity of each powdered sample was confirmed by comparison of the measured and predicted XRPD patterns shown in Figure 6. 1. The calculated XRPD patterns were in good agreement with the experimental data for all crystals. All main XRPD peaks of FFA I were predicted accurately. Some mismatched peak positions in the predicted and measured XRPD patterns of cocrystals of FFA-NIC CO and FFA-TP CO were found in Figure 6. 1 (indicated by arrows). These differences were likely to come from the

different temperatures of the measurements, i.e., room temperature for XRPD measurements and around 100 K for the single crystal data [234, 295]. At different temperatures the size of the unit cell will be (slightly) different, leading to the shifts of the XRPD peak positions.

In comparison with the observed single crystal images in Figure 6. 1, the crystal morphologies of FFA I, FFA-TP CO, and FFA-NIC CO are represented accurately by the models created by the software of Mercury 3.9. Therefore, each surface of a single crystal can be assigned through directly comparing the measured image with its morphology model.

Six well-defined planes of a single FFA I crystal were identified, with a pair of major faces, (100) and (−100), bounded by two pairs of the less prominent side faces (011), (0−1−1), (01−1), and (0−11). The (100) plane could expose either the COOH or the CF3 groups (Figure 6. 1). The (0−11) face, on the other hand, exposes the COOH and CF3 groups simultaneously, along with the aromatic rings (Figure 6. 1). Based on this structural inspection, it is expected that subsequent (100) layers with dominant CF3⋯ CF3 contacts should have lower attachment energy than the (0−11) faces and have a slow growth rate normal to the surface, leading to a large face.

The rectangular shape of FFA-TP CO is formed with a pair of the dominant (001) and (00−1) faces, larger side faces (0−10) and (010), and smaller side faces (100) and (−100). The (001) face could again have a more hydrophobic nature, because the trifluoromethylbenzene rings of FFA are exposed almost perpendicularly out of this surface. In contrast, the crystal faces (0−10) and (100) are more hydrophilic, because they expose more hydrogen-bond donors and acceptors.

The dominant pair of FFA-NIC CO faces are (0−11) and (01−1), with less prominent faces (011) and (0−1−1) and the smallest pair of (−100) and (100). On the (100) face, both COOH groups of FFA and $CONH_2$ groups of NIC are exposed, resulting in a polar surface. The (01−1) plane is less polar, carbon, fluorine, and hydrogen atoms are dominating the exposed area.

6.3.2 Solubility Study

The apparent FFA I equilibrium solubility at 23°C was 373.3 ± 4.2μg/mL in pH 6.8 PBS and was comparable of those of FFA I in the presence of 200μg/mL PEG (376.3 ± 6.7μg/mL), PVP (387.7 ± 5.9μg/mL), or PVP-VA (398.8 ± 2.3μg/mL) shown in Table 6. 2, indicating that none of the polymers changed the equilibrium solution properties. The solid residues collected after the experiments were analyzed by DSC, AIR, and XRPD, and indicated that they were the same as the starting materials (Figure A3. 2, appendixes).

The concentrations of FFA and TP after equilibration for 24h when excess amount of FFA I was added into each of the prepared TP solutions are shown in Figure 6. 2a. The solubility of FFA I initially increased slightly with increasing the TP concentration due to soluble complex formation between the two compounds. When the TP concentration exceeded 8.9mM, it was found that the apparent solubility of FFA I reached a plateau, because the solubility limit of the complex formed was did not change significantly. Only an averaged 1.2-fold increase in the apparent solubility of FFA I was observed in the presence of TP in comparison to FFA I solubility in PBS alone. Precipitation of the FFA-TP CO was observed based on XRPD analysis (DSC and IR results in Figure A3. 3 in the appendixes) of the solid residues, which indicated the presence of two solid phases, FFA-TP CO and FFA I as shown in Figure 6. 2b. Therefore, the measured concentrations of FFA and TP in this solution represent the FFA-TP CO transition concentration (Table 6. 2). The molar ratio of FFA to TP at the transition point was 0.26:1, indicating that the system is incongruently saturating. The solubility of FFA-TP CO was calculated as 2.99mmol/mL using (Equ. 6- 1), which is a 2.25-fold increase compared to the solubility of FFA I alone.

The apparent concentration of FFA I as a function of NIC concentration is shown in Figure 6. 2c, which is similar to a previous work [311]. The apparent solubility of FFA I increased with increasing NIC concentration up to 61.8mM, indicating complex formation of FFA and NIC in solution. In this region, the solubility limit of the complex formed was not exceeded, therefore the solid residues were FFA I alone, confirmed by XRPD results in Figure 6. 2d (DSC and FTIR results in Figure A3. 4 in the appendix).

In solutions with a NIC concentration of 66.2mM or above, the solid residues indicated the presence of two phases: FFA-NIC CO and FFA I solids, again confirmed by XRPD results in Figure 6. 2d (DSC and FTIR results in Figure A3. 4 in the appendix). Therefore, the measured concentrations of FFA and NIC in the 66.2mM NIC solution represent the FFA-NIC CO transition concentration shown in Table 6. 2. The molar ratio of FFA to NIC at the transition point was 0.026:1. The solubility of FFA-NIC CO was determined to be 10.4mM, which is 7.83 folds increase compared to the solubility of FFA I alone.

Table 6. 2 Solubility test results.

FFA I equilibrium solubility (μg/mL)	In PBS	373.3±4.2
	In PBS with pre-dissolved PEG	376.3±6.7
	In PBS with pre-dissolved PVP	387.7±5.9
	In PBS with Pre-dissolved PVP-VA	398.8±2.3
FFA-TP CO transition concentration (μg/mL)	FFA concentration in 8.9mM (1600μg/mL) of TP solution	439.9±2.0
	TP concentration in 8.9mM (1600μg/mL) of TP solution	1028.9±25.3
FFA-NIC CO transition concentration (μg/mL)	FFA concentration in 66.2mM (8080μg/mL) of NIC solution	474.3±15.6
	NIC concentration in 66.2mM (8080μg/mL) of NIC solution	7812.5±300.6

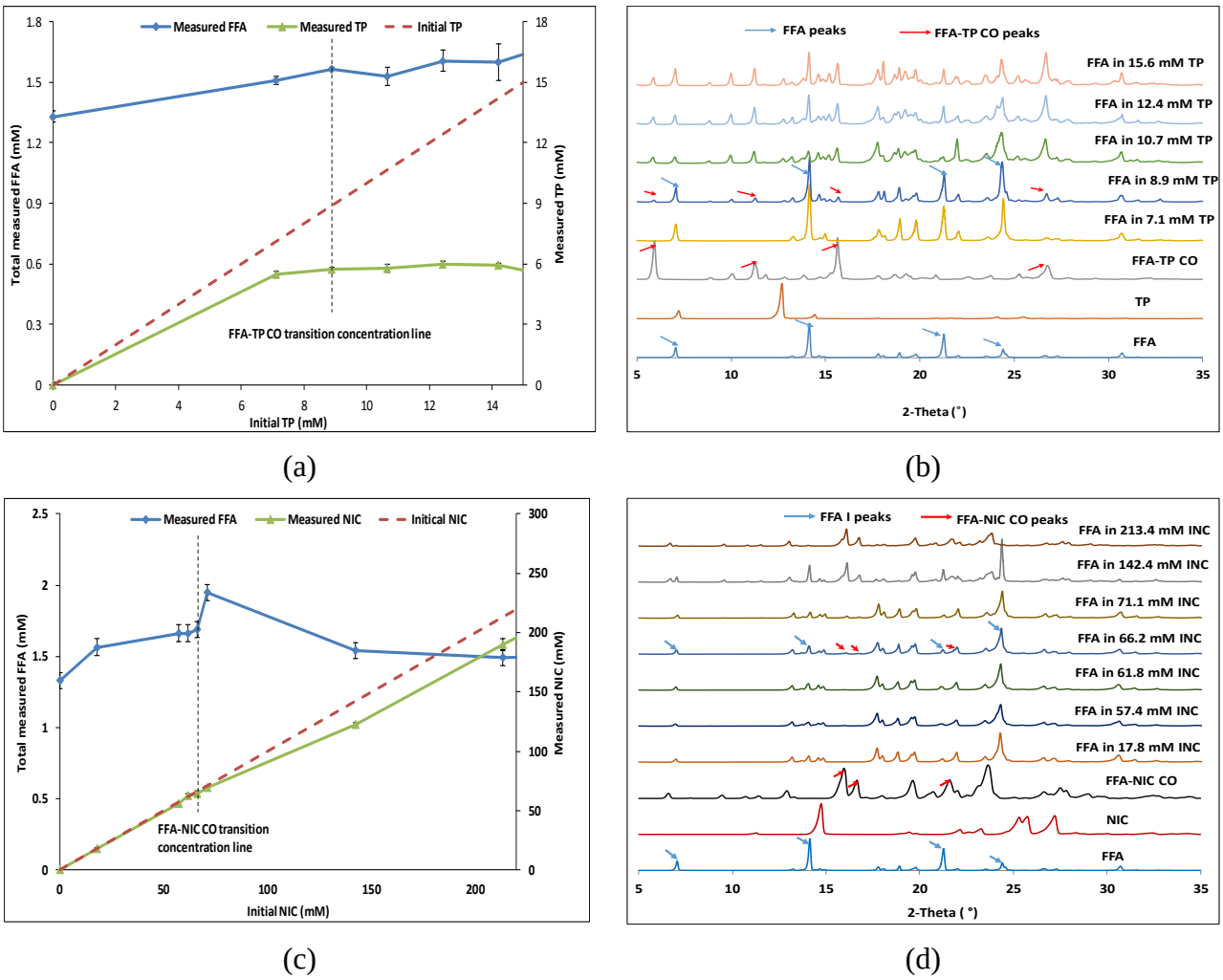

Figure 6. 2 Apparent solubility of FFA I in a coformer solution: (a) FFA and TP concentrations as a function of TP concentration; (b) XRPD results of solid residues after the tests in TP solutions; (c) FFA and NIC concentrations as a function of NIC concentration; (d) XRPD results of solid residues after the tests in NIC solutions.

6.3.3 AFM Measurements of Single Crystals

Figure 6. 3 shows the representative AFM images of the faces of single crystals at a 40 × 40 μm^2 scan area after exposure to PBS in the absence and presence of PEG, PVP, or PVP-VA. The AFM images at other scans can be found in Figure A3. 5 in the appendixes. Before the etching experiments, the surfaces of FFA I and FFA-TP CO studied were generally flat and smooth, but with clear defects shown in Figure 6. 3a and f. In contrast, the FFA-NIC CO (01−1) face was not smooth but was marked with many parallel strips (Figure 6. 3k).

After being etched by PBS, clear etching patterns appeared on the FFA I (100) face shown in Figure 6. 3b. The pits observed were roughly circular in shape and were randomly distributed on the surface. Their diameters ranged from 1 to 10μm with depths of up to 0.5μm shown in three-dimensional AFM images in Figure A3. 6 in the appendixes. When the FFA I (100) face was etched using PBS in the presence of PEG, bigger and deeper pits were obtained in comparison with those etched by PBS alone (Figure 6. 3c and Figure A3. 6 in the appendixes). Similar pits were also obtained by etching in the presence of PVP, but they appeared at a much smaller in diameter. In contrast, the pattern etched by PBS in the presence of PVP-VA was less regular, with pits of varied shapes and sizes.

When the FFA-TP CO (001) face was etched by PBS, many small interpenetrating trapezium pits with some isolated pits were formed with diameters of less than 1μm (Figure 6. 3g). At the same time, several long ditches were observed, with depth of about 1.3μm (Figure A3. 6 in the appendixes). In the presence of PEG in PBS, similar etching patterns were obtained to that etched by PBS alone (Figure 6. 3h). The sizes of the well-defined separate pits in Figure 6. 3i, etched by PBS in the presence of PVP, were much larger than those by PBS alone or in the presence of PEG. The etching pattern by PBS in the presence of PVP-VA, shown in Figure 6. 3j, was very different, with less clearly defined ditches than in PBS alone.

The etching patterns in Figure 6. 3l-o on the FFA-NIC CO (01−1) face etched by PBS in the absence and presence of PEG, PVP, or PVP-VA were very similar to the original surface (Figure 6. 3k), showing striped patterns with lines in the direction of the a-axis. However, the roughness of the FFA-NIC CO (01−1) face was different after etching dissolution in different dissolution media in Figure A3. 6 in the appendixes. In PBS with the predissolved PVP-VA the roughness of the etching surface is pretty much same as the original one while the surface is roughest etched by PBS in the predissolved PEG.

6.3.4 Face Dissolution Rate Determination of Single Crystals

The temporal change in the lateral dimensions of a single crystal was recorded by measurements of the retreating face using OLM. The measurements were made for two

faces of each single crystal: (100) and (0−11) faces of FFA I, (001) and (100) faces of FFA-TP CO, and (01−1) and (100) faces of FFA-NIC CO.

Representative images of a single crystal during dissolution recorded by OLM are shown in Figure 6. 4a (all other images can be found in Figure A3. 7 in the appendixes) and the face dissolution profiles of each single crystal are shown in Figure 6. 4b. A linear relationship for different faces of both FFA I and FFA-TP CO single crystals in PBS in the absence or presence of a polymer was observed in Figure 6. 4b1-b8, indicating a constant dissolution rate. The face dependent dissolution rate was determined from the gradient of a plot of displacement of the edge of a face versus dissolution time. It can be seen in Figure 6. 5 that the dissolution rates of different faces for the same crystal are distinctly different. It was found that for the same crystal the bigger face had a lower dissolution rate. In the presence of PEG in PBS, the dissolution rates of the faces of FFA I or FFA-TP CO increased slightly except the FFA-TP CO (100) face, indicating PEG can enhance the crystal dissolution. In contrast, in the presence of PVP or PVP-VA, the retreating rates of the faces of FFA I or FFA-TP CO decreased, indicating PVP or PVP-VA can retard the face dissolution.

FFA-NIC CO shows complicated face dependent dissolution behavior in Figure 6. 4b9-b12. In contrast to FFA I and FFA-TP CO, the dissolution rate increased rapidly on both faces in the presence of PVP or PVP-VA in PBS. The variation of the dissolution rate on the small (100) face was significantly higher than the big face (01−1). It was interesting to note that the predissolved PEG in solution decreased the dissolution of the small face (100) and increased the dissolution of the big face (01−1), leading to close to isotropic dissolution behavior of FFA-NIC CO faces. Furthermore, FFA-NIC CO faces showed good linear dissolution behavior in PBS in the presence of a polymer of PEG. In pure PBS, a nonlinear relationship of the crystal displacement vs time data for the FFA-NIC CO (01−1) face in Figure 6. 4b9 due to precipitation of FFA III solids on the dissolving FFA-NIC CO crystal surface.

Crystal	Before Dissolution	PBS	PBS with pre-dissolved PEG	PBS with pre-dissolved PVP	PBS with pre-dissolved PVP-VA
FFA	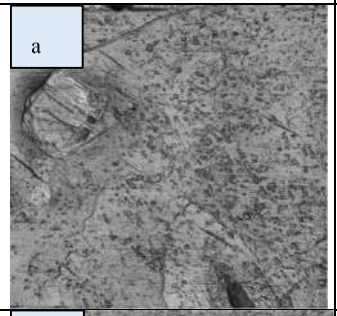	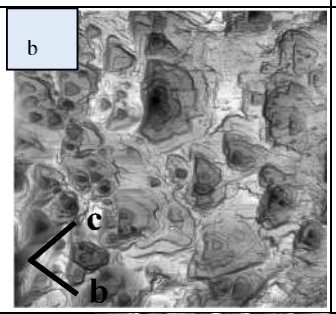	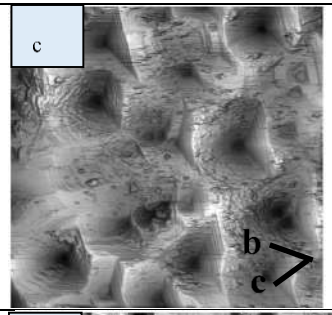	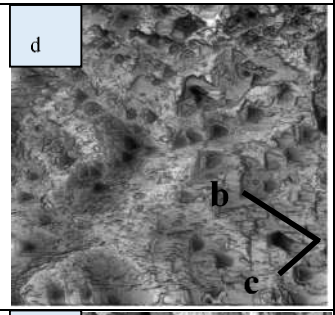	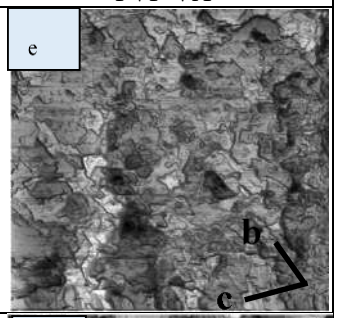
FFA-TP CO	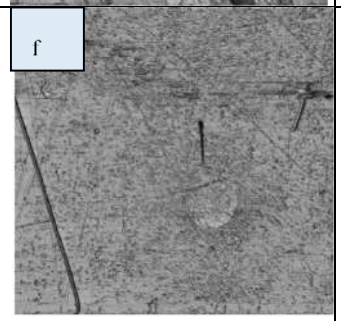	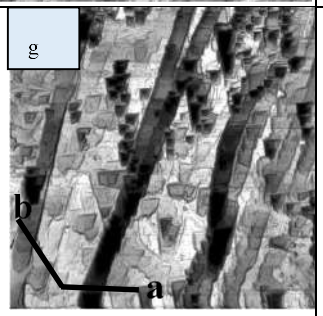	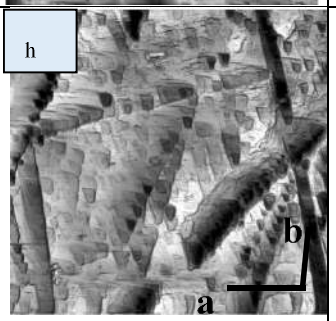	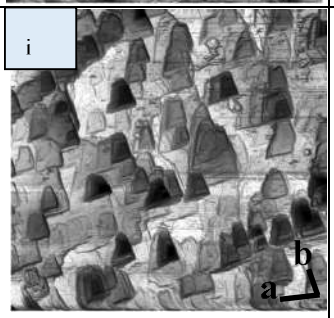	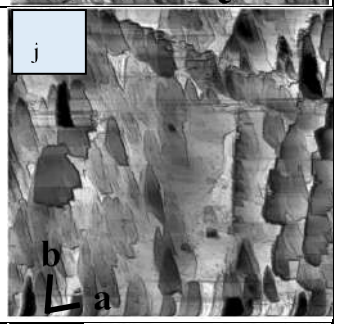
FFA-NIC CO	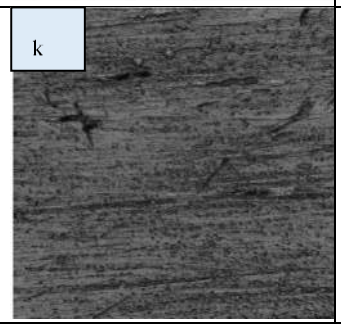	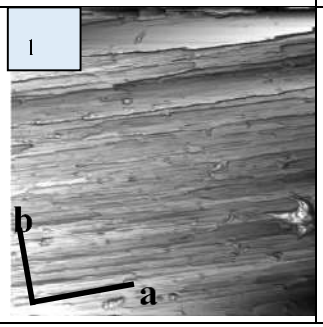	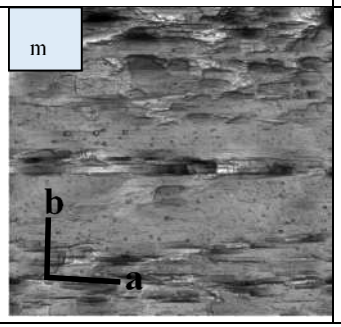	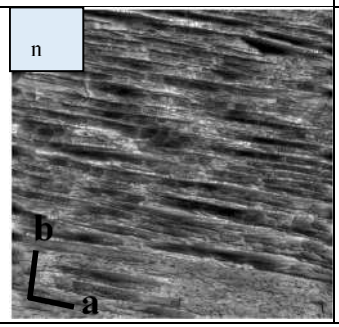	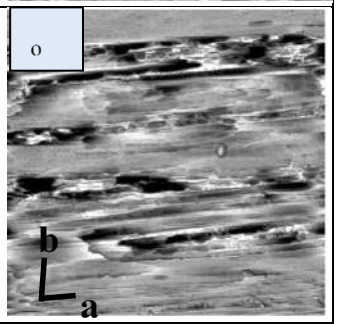

Figure 6. 3 AFM images of results at a 40x40μm^2 scan area.

Crystal	0	2h	4h	6h
FFA-NIC CO in PBS	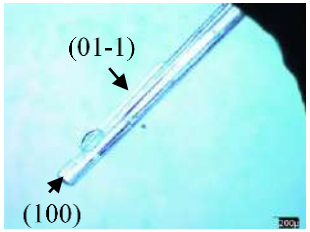	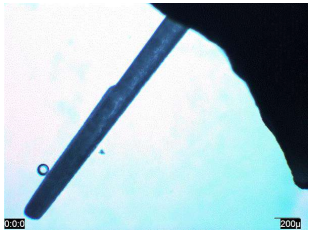	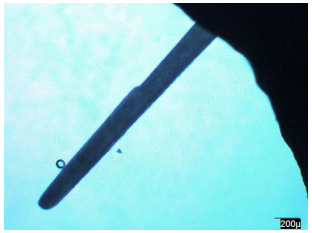	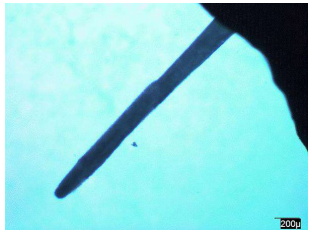

(a)

Crystals	PBS	PBS with pre-dissolved PEG	PBS with pre-dissolved PVP	PBS with pre-dissolved PVP-VA
FFA I	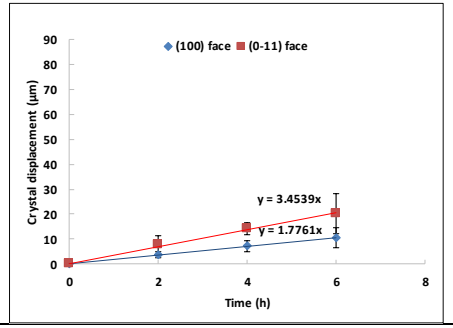	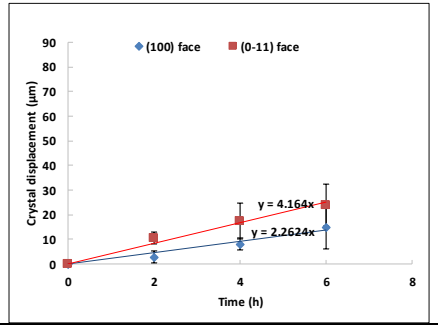	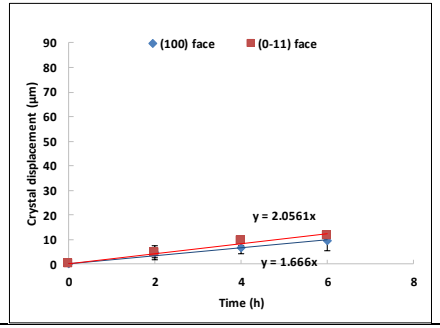	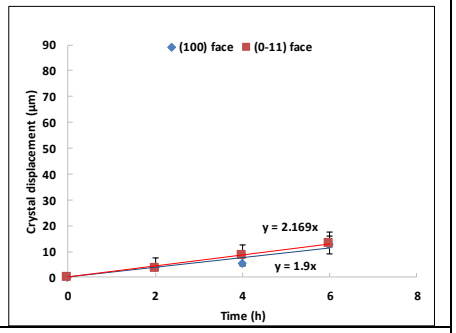
	b1	b2	b3	b4

FFA-TPCO	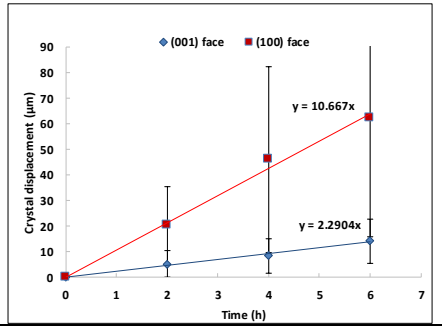	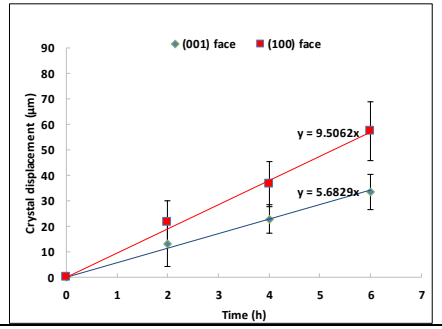	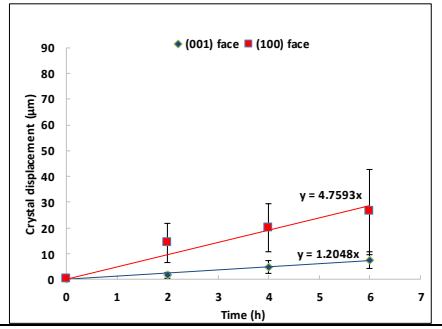	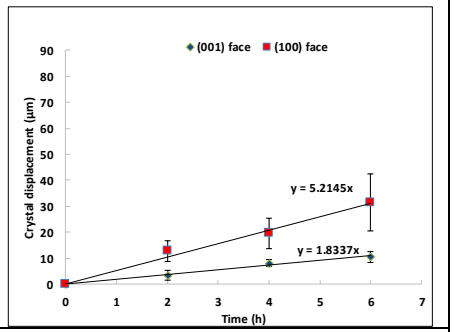
	b5	b6	b7	b8
FFA-NICCO	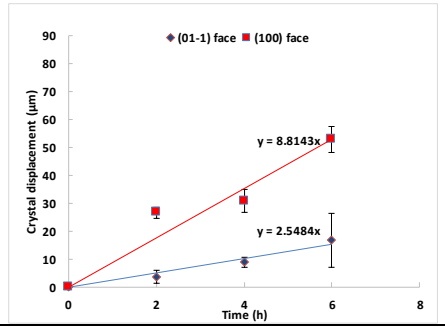	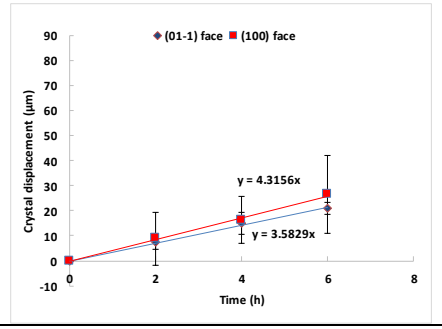	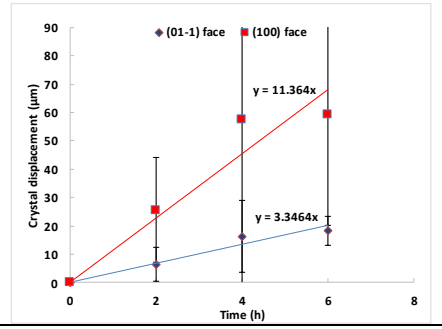	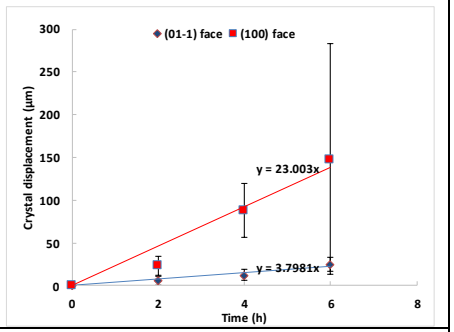
	b9	b10	b11	b12

(b)

Figure 6. 4 OLM dissolution experiments: a) representative OLM images of single crystal during dissolution; b) displacements of the edge of a crystal face as a function of dissolution time.

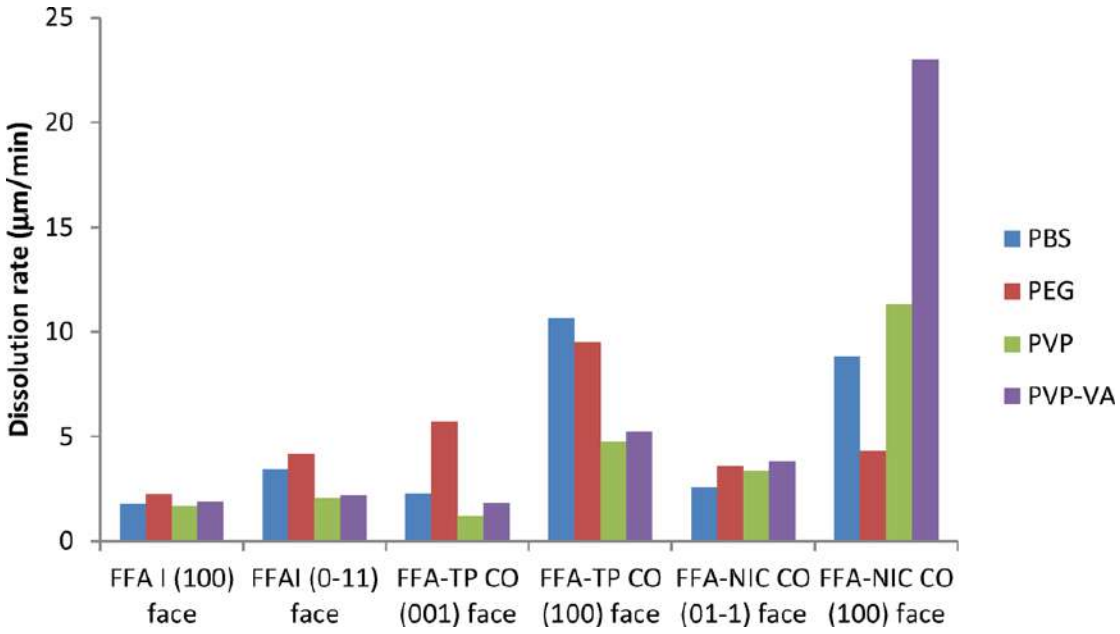

Figure 6. 5 Face dependent dissolution rate of a single crystal in PBS in the absence and presence of a polymer

6.3.5 Powder Dissolution Under Sink and Non-Sink Conditions

Figure 6. 6 shows the dissolution profiles of FFA I, FFA-TP CO, and FFA-NIC CO in the absence and presence of a polymer under sink conditions in which $C_{equilibrium}$ was 100μg/mL (based on all the materials dissolved in solution). The gradient of a dissolution curve indicates the solid dissolution rate. Without a predissolved polymer in solution, FFA-TP CO was shown to dissolve fastest, with 24% increase of AUC in comparison with that of pure FFA I solids. FFA-NIC COs dissolved rapidly in the first 5min, but after that their dissolution rate slowed and became comparable with FFA I, indicating that a phase transformation to FFA III occurred. Overall the AUC of FFA-NIC COs was 11% higher than that of FFA I. There was no significant change (within ±2%) of DPP and dissolution rate of FFA I, FFA-TP COs, or FFA-NIC COs in the predissolved PEG solution. With predissolved PVP or PVP-VA, the dissolution performance of FFA-NIC COs improved remarkably, i.e., in the predissolved PVP solution 75% of solids dissolved within 15 min and AUC increased by 34%, while in the predissolved PVP-VA solution 89% of solids dissolved within 15 min and AUC increased by 38%. In contrast, both PVP and PVP-VA reduced the dissolution rate and DPP of FFA-TP COs and FFA I solids as shown in Figure 6. 6e.

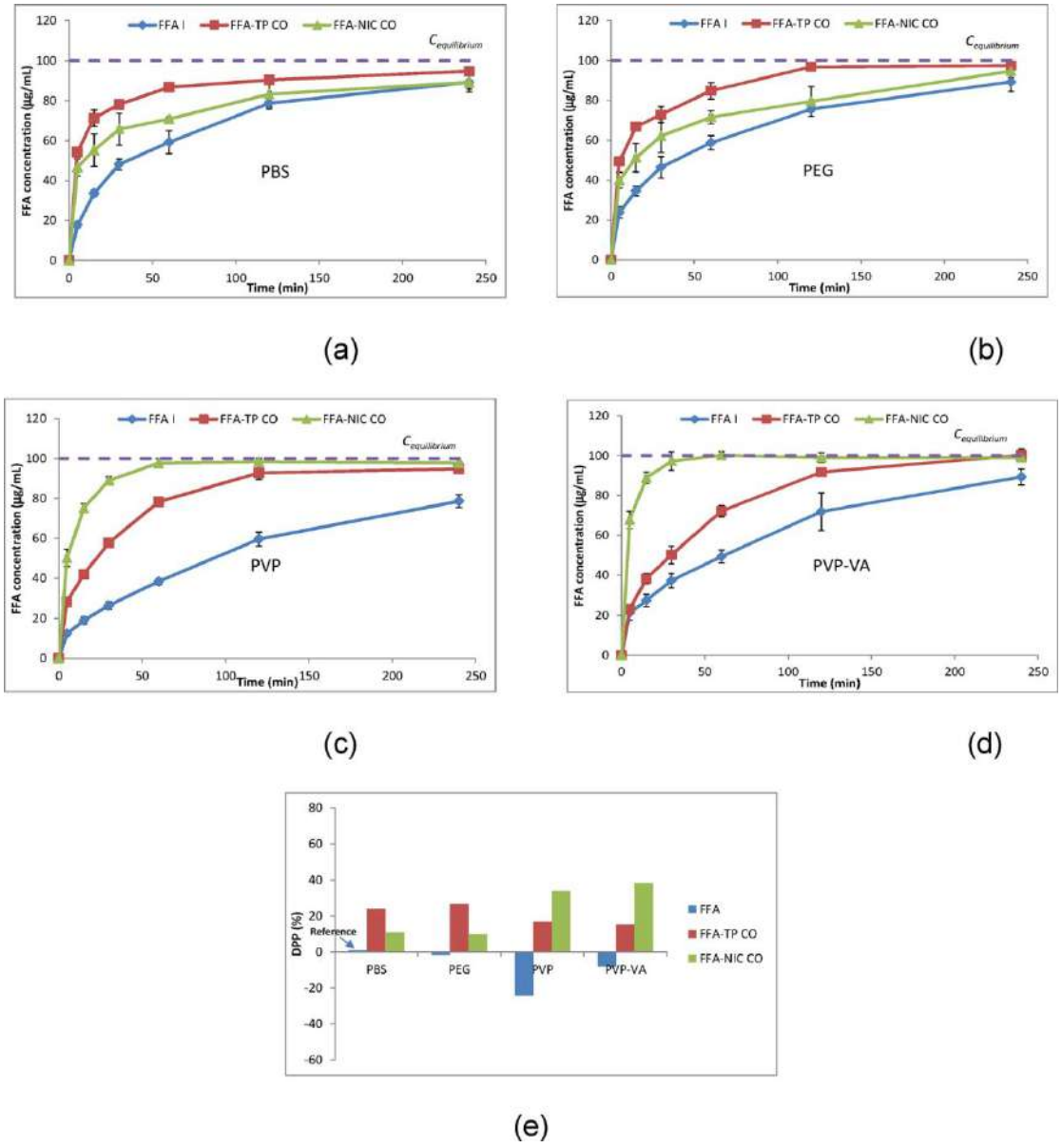

Figure 6. 6 Powder dissolution profiles in the absence or presence of a polymer under sink conditions: (a) PBS; (b) PBS with predissolved PEG; (c) PBS with predissolved PVP; (d) PBS with predissolved PVP-VA; (e) DPP comparison; The DPP of FFA in PBS as reference.

Figure 6. 7 shows the dissolution profiles of FFA I, FFA-TP CO, and FFA-NIC CO in the absence and presence of a polymer under non-sink conditions. Therefore, C_{eq} was the FFA I solubility of 373.3µg/mL measured in this study in Table 6. 2. T_{eq} and C_{max} values of each test are shown in Table 6. 3 and Table 6. 4. In the presence of a polymer, FFA I solids dissolved slower (Table 6. 3), in particular, the predissolved PVP lead to

38% reduction of AUC in Figure 6. 7e. There was no supersaturation generated from FFA I dissolution in PBS in the absence or presence of PEG, PVP or PVP-VA (Table 6. 4). FFA-TP COs show an advantage of improved dissolution relative to FFA I solids both in the absence or presence of a predissolved polymer. Predissolved PVP can modestly increase the DPP of FFA-TP COs, to 40% from 30% in pure PBS, while predissolved PVP-VA can slightly decrease its DPP to 24%. A significant increase of DPP of FFA-TP COs, to 56%, was observed in the predissolved PEG. Predissolved PEG in PBS can increase the dissolution rate of FFA-TP CO, showing a reduced T_{eq} in contrast to the slow FFA-TP CO dissolution in the presence of PVP or PVP-VA in PBS (Table 6. 3) There was no dissolution advantage observed for FFA-NIC COs in PBS alone or in the presence of predissolved PEG. However, in the presence of PVP in the solution, the advantage of FFA-NIC COs in dissolution performance was apparent, with a 64% increase of AUC (Figure 6. 7e), 50% higher peak solubility (Table 6. 4), and faster dissolution rate (Table 6. 3). Similarly, in the presence of PVP-VA in solution, the DPP of FFA-NIC COs was increased by 60% and the maximum FFA concentration was 1.6 times of its solubility.

Table 6. 3 T_{eq} values of powder dissolution under non-sink conditions.

Crystal	T_{eq} (min)			
	PBS	PBS with pre-dissolved PEG	PBS with pre-dissolved PVP	PBS with pre-dissolved PVP-VA
FFA I	166	196	>240	186
FFA-TP CO	50	10	62	87
FFA-NIC CO	223	196	23	22

Table 6. 4 C_{max} values of powder dissolution under non-sink conditions.

Crystal	C_{max} (μg/mL)			
	PBS	PBS with pre-dissolved PEG	PBS with pre-dissolved PVP	PBS with pre-dissolved PVP-VA

FFA I	415.3±6.0	397.8±8.40	283.3±44.8	415.4±32.8
FFA-TP CO	497.5±20.7	527.1±23.3	538.8±32.9	539.4±1.6
FFA-NIC CO	383.6±34.1	397.3±20.7	609.4±14.0	629±10.1

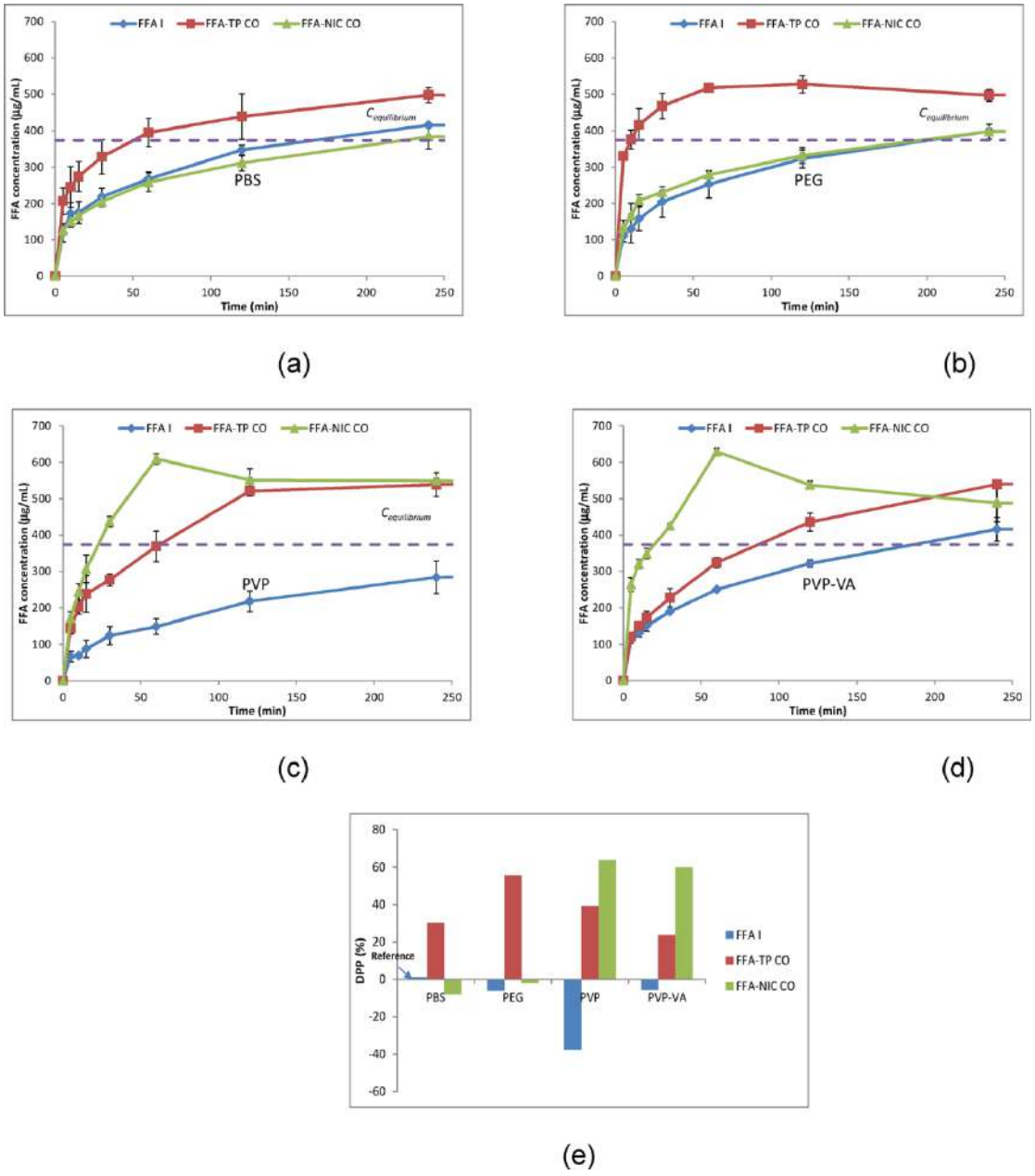

Figure 6. 7. Powder dissolution profiles in the absence or presence of a polymer under non-sink conditions: (a) PBS; (b) PBS with predissolved PEG; (c) PBS with predissolved PVP; (d) PBS with predissolved PVP-VA; (e) DPP comparison.

The XRPD results of the solid residues collected after the FFA I dissolution experiments were the same as for the starting materials, shown in Figure 6. 8a,

indicating that there was no phase transformation for FFA I in solution. The solid residues from FFA-NIC CO experiments in the presence or absence of a predissolved polymer gave XRPD patterns (Figure 6. 8c) that matched the characteristic features of FFA III [226], indicating that FFA III crystals precipitated during dissolution. Interestingly, in the presence of PVP or PVP-VA, the solid residues after the FFA-TP CO dissolution tests were their starting materials, FFA-TP COs, as shown in Figure 6. 8b. In contrast, the solid residues after FFA-TP CO dissolution tests in PBS or in the presence of predissolved PEG were the mixtures of FFA-TP CO and FFA III solids. The DSC and FTIR results of the solid residues are shown in Figure A3. 8 and Figure A3. 9 in the appendixes.

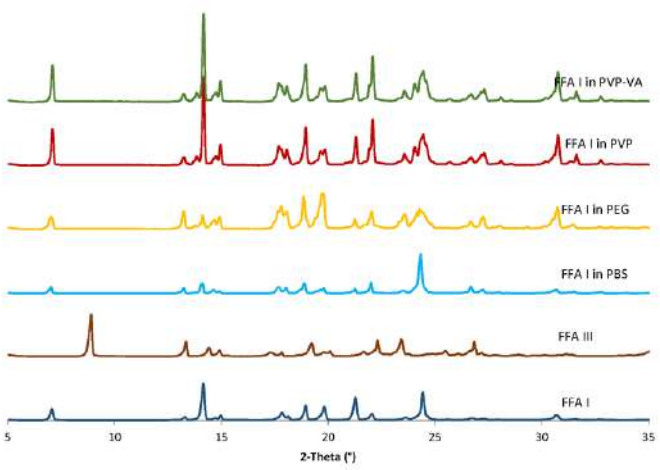

(a)

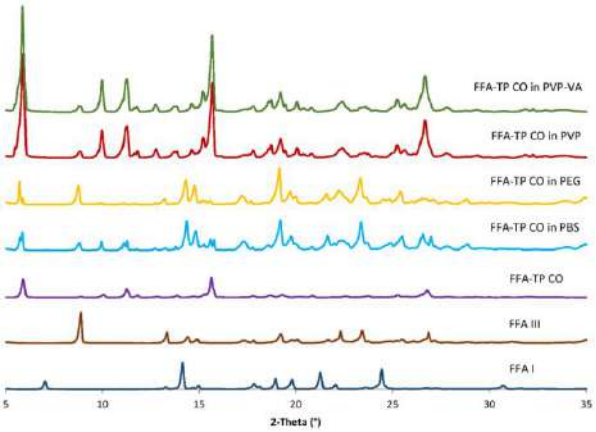

(b)

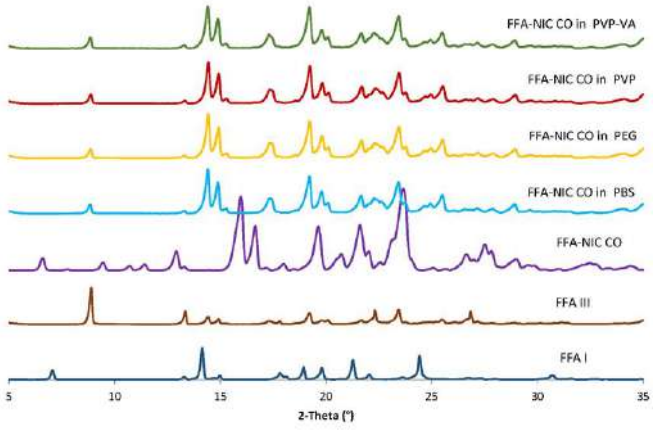

(c)

Figure 6. 8 XRPD test results of solid residues after dissolution tests under non-sink conditions: (a) FFA I; (b) FFA-TP CO (c) FFA-NIC CO

6.4 Discussion

It is well-known that the dissolution mechanism of cocrystals of poorly water-soluble drugs is complex, in which both dissolution of cocrystals and the precipitation of the parent drug can occur simultaneously depending on the properties of the parent drug and coformer and the experimental conditions [145]. In this study, through rational selection of a coformer as well as the dissolution medium in the presence of a polymeric additive, we aimed to provide mechanistic insights into the intrinsic relationship among dissolution, supersaturation and precipitation for pharmaceutical cocrystals.

Based on the measured transition concentrations of the parent drug FFA I and coformers of NIC and TP, it was shown that FFA-NIC CO increased the FFA solubility by 7.83 folds, while the increase was 2.25 folds for FFA-TP CO. Discrepancies between predicted and observed solubility advantages were significant in the bulk experiments. In the powder dissolution experiments FFA-TP CO partially revealed its solubility advantage in PBS. Under sink conditions (Figure 6. 6a) it showed 24% increase of AUC and under non-sink conditions (Figure 6. 7a) achieved a maximum FFA concentration of 497.5μg/mL, which was just 1.33 folds of its parent drug solubility. Despite having a higher solubility, FFA-NIC CO dissolved slower than FFA-TP CO in PBS under either sink or non-sink conditions (Figure 6. 6a and Figure 6. 7a). However, when PVP or PVP-VA was predissolved in the dissolution medium, the expected improvements in dissolution rate and apparent FFA concentration were clearly revealed in the bulk dissolution experiments of FFA-NIC CO shown in Figure 6. 6c, d and Figure 6. 7c, d. In contrast, under non-sink conditions the dissolution rate of FFA-TP CO decreased with slightly higher C_{max} in the presence of PVP or PVP-VA relative to dissolution in PBS without a polymer.

Based on the crystal structure illustrated in Figure 6. 1 it is shown that the hydrogen bonding between the FFA and NIC molecules creates a layer structure of the crystal lattice where the NIC molecules form channels among the FFA molecules. Such configuration in the crystal lattice allows complete layers of molecules to be easily removed from the surface by the solvent medium [312]. Therefore, the etching surface shown in Figure 6. 3l of the FFA-NIC CO (01−1) face etched by PBS was almost same

as the initial surface Figure 6. 3k. Due to rapid removal of the hydrophilic NIC molecules from the surface during dissolution, a local supersaturation of FFA near the dissolving surface of FFA-NIC CO was generated, leading to precipitation of the stable form FFA solids on the cocrystal particle, indicating changes in the roughness of the etching surface (Figure A3. 6 in the appendixes) observed by AFM. Consequently, this resulted in reduction of the dissolution rate of FFA-NIC CO. Therefore, the dissolution profile of FFA-NIC CO was like FFA I, which was observed in the bulk powder dissolution in Figure 6. 7a. It has been reported that FFA has up to nine different crystal forms, among which FFA I (white color) and FFA III (yellow color) are the most commonly encountered [226]. Below a temperature of 42 °C FFA III is the most stable form and has a lower solubility than its metastable form of FFA I, although the solubility difference between the two forms is very small with less than 1μg/mL [313]. Precipitation of the solid FFA III during dissolution under non-sink conditions shown in Figure 6. 8c demonstrated that the supersaturation was first generated by the FFA-NIC CO dissolution and then followed by precipitation of the stable form FFA III. Furthermore, a nonlinear relationship of the concentration vs time data acquired for the FFA-NIC CO (01−1) face in Figure 6. 4b9 also concluded precipitation of FFA solids on the dissolving crystal surface. In contrast, no supersaturation was generated by dissolution of FFA I crystals, confirmed by the XRPD results in Figure 6. 8a, where the solid residues collected after the FFA I dissolution tests were the same as the starting materials.

According to the FFA-TP CO structure shown in Figure 6. 1, an extended chain structure formed by a supramolecular ladder network involving both FFA and TP molecules with a strong hydrogen bond and interactions of C−H···π and π···π implies that the stronger crystal lattice of FFA-TP COs hinders surface dissolution and hence impacts the overall solubility. However, each surface of a FFA-TP CO becomes more hydrophilic due to inclusion of TP molecules in the crystal lattice in comparison with those of FFA I shown in Figure 6. 1, leading to an increased interaction force between the faces of FFA-TP COs and aqueous solvent molecules. Therefore, FFA-TP CO has a limited ability to improve the FFA solubility by 2.25 folds in Table 6. 2. Similarly, the parent drug FFA I, the dissolution mechanism of FFA-TP COs appears to be controlled by defect locations on the crystal surface and the underlying crystal lattice. Because the

molecules at defect sites have higher mobility to be detached from the surface, a regular etching pattern can be formed during etching dissolution, which was observed in the AFM etching images of both FFA I and FFA-TP CO faces shown in Figure 6. 3b and Figure 6. 3g. Formation of the etching pattern on the crystal surface is determined by the crystal interaction network together with the interactions between solvent and crystal surface [314]. On the (100) face of FFA I, there are two nonperpendicular crystallographic axes: the b-axis and c-axis, in which the COOH or CF3 (see bottom) group (Figure 6. 1) is exposed out of the surface. Each molecule is surrounded by six neighbors, each attracted through π–π stacking inside the surface, resulting in nondirectional force along either the b-axis or c-axis. Therefore, the pits on the (100) face of FFA I were circular shape without specific preference of directions shown in Figure 6. 3b. Presumably, the size or strain of individual defects on the surface of FFA I was different before dissolution, leading to a wide size distribution of the pits. However, the situation is different for FFA-TP CO dissolution. When FFA-TP CO dissolves, both of FFA and TP molecules detach from the FFA-TP CO lattice from the defect sites on the surface. The different etching pattern in Figure 6. 3g in comparison with that on the FFA I (100) face in Figure 6. 3b reflects the more anisotropic nature of the interactions in FFA-TP CO, with ditches roughly parallel to the strong hydrogen bonds. According to the single crystal dissolution experiments, linear dissolution rates were obtained for both the FFA-TP (001) and (100) faces, indicating that no solid form conversion occurred during dissolution (Figure 6. 4b5) Under non-sink conditions, the precipitation of FFA III solids was observed after 50 min (Figure 6. 7a), when the FFA concentration in solution was above its solubility. Therefore, a bulk precipitation mechanism is proposed for the FFA-TP CO dissolution, where the dissolved parent drug precipitates as individual crystals from the bulk solution, in contrast to a surface precipitation mechanism for the FFA-NIC CO dissolution, where the parent drug precipitates directly onto the surface of the dissolving cocrystals as a coating layer. The strong interaction between FFA and TP, along with the smaller difference in hydrophobicity between the coformers in FFA-TP CO relative to FFA-NIC CO, suggests that the coformers are more likely to remain closely associated in the case of FFA-TP CO. This would then lead to a smaller local supersaturation of FFA near the dissolving FFA-TP CO surface, thereby explaining the lack of surface precipitation.

When a polymer of PEG, PVP, or PVP-VA was predissolved in the dissolution medium, dissolution profiles of FFA-NIC CO or FFA-TP CO changed to significantly different extents under either sink or non-sink conditions. In this study, the used polymer concentration of 200μg/mL was so low that the solution viscosity remained the same as that of the PBS dissolution medium alone. Furthermore, the predissolved polymer had no effect on the solubility of FFA I (Table 6. 2). Therefore, the effects of polymeric additives on the dissolution of FFA cocrystals are attributed to surface adsorption of the polymers through specific interactions with the crystal surface, in particular, hydrogen bonding [192, 200, 314-319]. Among the polymers used in this study, PEG, containing a high percentage of hydrogen acceptors in the backbone, is the most hydrophilic, while PVP-VA, containing 40% acetate side chains in comparison to PVP, is the most hydrophobic [183].

Based on the dissolution experiment of the single FFA I crystal, the FFA I (100) face is more hydrophobic because it has a slower face dissolution rate in Figure 6. 4b1. The hydrophilic polymer of PEG with its rigid backbone chains should not be easily absorbed on the crystal surface. Therefore, that there was no change of the etching patterns of FFA I (100) face in PBS in the presence of predissolved PEG in Figure 6. 3c. Bigger and steeper pits observed were most likely caused by an enhanced diffusion rate of FFA molecules from the crystal surface attracted by PEG in solution due to less hydrophilic environment generated than water around the surface, indicating a slightly increased surface dissolution rate in the single crystal dissolution measurement in Figure 6. 5. PVP and PVP-VA have oxygen molecules at the side chain positions, therefore, there should be no strong steric repulsion for them to form hydrogen bonds with the COOH groups of FFA I on the crystal surface. Once the polymers were adsorbed onto the surface, they prevented the dissolution medium contacting the crystal surface to retard the etching locally, leading smaller and less deep pits in Figure 6. 3d and Figure 6. 3e. A lower density of the pits with irregular etching patterns in PBS in the presence PVP-VA (Figure 6. 3e) indicated that PVP-VA had more chance to be adsorbed on the FFA I crystal surface due to more oxygen molecules at the side chains in comparison with PVP.

The hydrophobic nature of the FFA-TP CO (001) face was likely to prevent PEG to be adsorbed on it; therefore, there was no change of the surface etching patterns in comparison with those in PBS alone in Figure 6. 3g, h. With increasing the nonpolarity of PVP and PVP-VA, both of the polymers had more opportunities to be adsorbed on the crystal surface, affecting the etching patterns of the FFA-TP (001) face in Figure 6. 3i,j and also causing a reduction of the face dissolution rates in the single crystal face dissolution experiments in Figure 6. 5 and decreased DPP values in the powder dissolution experiments in Figure 6. 6e and Figure 6. 7e. It has to be stressed that PVP or PVP-VA not only decreased the dissolution rates of FFA-TP CO but also prevented the precipitation of FFA III when the FFA concentration was above its solubility through intermolecular interaction in solution without increasing the solubility of FFA I [183], confirmed by the XRPD results of the solid residues where FFA-TP COs were the only solid phase in Figure 6. 8b. Consequently, an increased C_{max} in Table 6. 4 was generated by the FFA-TP CO dissolution.

In the presence of PEG in PBS, the FFA-NIC (01−1) face dissolution rate increased and its (100) face dissolution rate reduced in Figure 6. 4b10, therefore there was no change of the overall dissolution performance of FFA-NIC CO in the bulk dissolution experiments in Figure 6. 6e and Figure 6. 7e. In contrast, both PVP and PVP-VA were easily adsorbed on the FFA-NIC CO surface to slow down the crystal dissolution rate. Consequently, precipitation rate of the stable form FFA III solids on the surface of the dissolving cocrystals was reduced, showing a similar roughness of the etching FFA-NIC CO (01−1) in the predissolved PVP or PVP-VA as the original one prior to the etching experiment. Therefore, the advantages of the improved solubility and dissolution rates of FFA-NIC CO were observed in the single crystal dissolution experiments in Figure 6. 4b11, b12 and bulk dissolution experiments in Figure 6. 6e and Figure 6. 7e. It is worth re-emphasizing that the precipitation of the stable form FFA III was only partially inhibited by the predissolved PVP or PVP-VA in solution, supported by the evidence of the nonlinear face dissolution rates in Figure 6. 4 b11, b12 and XRPD results of solid residues after non-sink powder experiments in Figure 6. 8c. Except the surface roughness, no change of the appearance of the FFA-NIC CO (01−1) face after etching dissolution shown in Figure 6. 3l-o, another evidence to support the surface layer removal dissolution mechanisms of FFA-NIC CO. In order to maximize the advantages

of FFA-NIC CO, an increasing polymer concentration or new approaches have to be developed to completely inhibit the FFA precipitation, which is part of ongoing research in our group.

6.5 Chapter Conclusion

Understanding the dissolution mechanisms of pharmaceutical cocrystals can lead to strategies for improving cocrystal design and its optimum product development. In this study, effects of the three polymers, PEG, PVP, and PVP-VA, on the dissolution behavior of the cocrystals of FFA-TP CO and FFA-NIC CO were investigated at multiple length scales. It has been found that the dissolution mechanisms of FFA-TP CO are controlled by the defect sites of the crystal surface and by precipitation of the parent drug as individual crystals in the bulk fluid. In contrast, the dissolution mechanisms of FFA-NIC CO are controlled by the surface layer removal and by a surface precipitation mechanism, where the parent drug precipitates directly onto the surface of the dissolving cocrystals as a coating layer. Through controlling the dissolution environment by pre-dissolving a polymer, PVP or PVP-VA, which can interact with the crystal surface to alter its dissolution properties, the advantages of the improved solubility and dissolution rates of the FFA-TP cocrystal and FFA-NIC cocrystal can be demonstrated.

.

Chapter 7 Investigating Permeation Behavior of Flufenamic Acid Cocrystals Using a Dissolution and Permeation System

7.1 Chapter Overview

In this work we systematically, for the first time, examined the key processes occurred during cocrystal dissolution in the absence and presence of different concentrations of a polymer, i.e., the kinetics of drug supersaturation and subsequent drug permeation by using side-by-side cell. Cocrystals of FFA-NIC CO and FFA-TP CO along with two polymers of PVP and PVP-VA were selected. The molecular structures FFA cocrystals and the monomer units of the polymers are shown in Table 7. 1. To gain insight into the mechanism of the supersaturated solution and subsequent permeation behavior of the parent drug, the atomic-level information of molecular interactions among FFA, coformers and polymers was studied by one-dimensional proton nuclear magnetic resonance (^{1}H NMR) spectroscopy. Solution ^{1}H NMR is a powerful tool for investigating the molecular state of drugs to examine their hydrogen bonding interactions and aggregation properties, in which chemical shifts in ^{1}H NMR spectra reflect differences in the chemical environment of molecules and peak widths reflect molecular mobility [161, 216, 320-327]. ^{1}H NMR studies were conducted in singular, binary and ternary components' solutions of FFA, coformer and polymer to establish the possibility of interactions of drug/coformer, drug/polymer and coformer/polymer in low polarity solvent deuterated chloroform ($CDCl_3$).

Table 7. 1 Molecular structures of FFA cocrystals and monomer units of polymers

FFA I	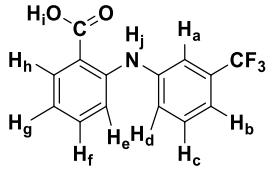
NIC	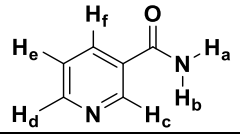
TP	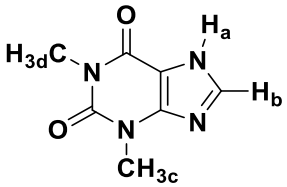
FFA-NIC CO	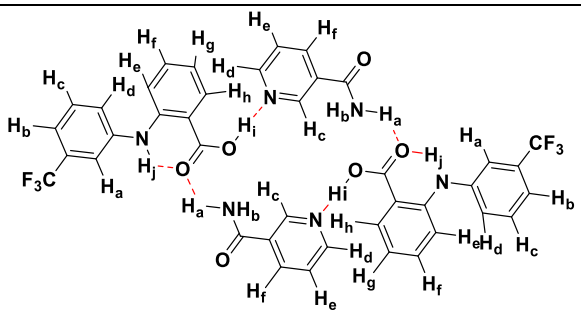
FFA-TP CO	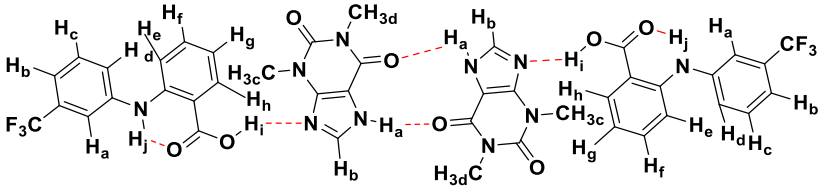
PVP	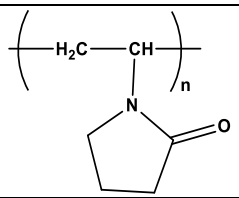
PVP-VA	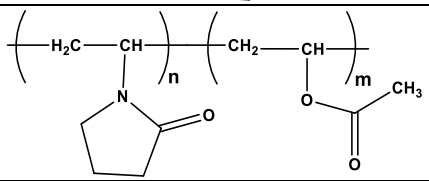

7.2 Materials and Methods

7.2.1 Materials

FFA I, NIC, TP, PVP, PVP-VA, methanol, ethanol, acetonitrile, KH_2PO_4, NaOH, $CDCl_3$ and double distilled water were used in this study. Detailed information of these materials can be found in Chapter 3.

7.2.2 Methods

7.2.2.1 0.01M pH 4.5 Phosphate Buffer Solution (PBS)

pH 4.5 PBS (0.01M) was used as a dissolution medium in this study, the detailed preparation method can be found in chapter 3.

7.2.2.2 Powder FFA Cocrystals Preparation

Cocrystals of FFA-NIC CO and FFA-TP CO were used in this chapter, the detailed method can be found in chapter 3.

7.2.2.3 Apparent Equilibrium Solubility of FFA I, NIC and TP in Solution with the Absence and Presence of a Pre-dissolved Polymer

The apparent equilibrium solubility of individual components of FFA I, NIC and TP was determined in 0.01M pH 4.5 PBS with or without different concentrations of a pre-dissolved polymer (i.e. PVP or PVP-VA) in a shaking water bath at 150RPM shaking rate and 37±0.5°C for 24h. The concentrations of a polymer were 200μg/mL, 500μg /mL, 1000μg/mL, 2000μg/mL, 4000μg/mL, 8000μg/mL, 12000μg/mL and 16000μg/mL, respectively.

To investigate the effect of a combined coformer and polymer on the FFA I solubility, apparent equilibrium solubility of FFA I at different concentrations of a polymer under a constant coformer concentration (47.8μg/mL for NIC or 71.1μg/mL of TP) was also determined. A coformer concentration selected in the experiments was based on the flux rate experiments where 1.43mg (1mg FFA and 0.43mg NIC) of FFA-NIC CO and 1.64mg (1mg FFA and 0.64mg TP) of FFA-TP CO were used in 9mL solution, leading

to 47.8μg/mL of NIC and 71.1μg/mL of TP in the donor compartment under the assumption of completely dissolving of the FFA cocrystals.

The detailed method for solubility testing can be found in chapter 3.

7.2.2.4 Dissolution and Permeation Measurements

The dissolution and permeation properties of FFA I and FFA cocrystals were determined by D/P system. One milligram of FFA I or cocrystal powders with equivalent 1mg of FFA I were used. All FFA I and FFA cocrystal crystalline materials used in the experiments were slightly grounded by a mortar and pestle and sieved by a 60mesh sieve to control the particle size below 250μm. The concentrations of PVP or PVP-VA were 200μg/mL, 4000μg/mL, and 16000μg/mL, respectively. Samples of 0.5mL were withdrawn from the donor compartment at the predefined sampling points of 5, 10, 15, 30, 60, 120 and 240mins and 0.5mL of the sample was taken from the acceptor cell at 30, 60, 120 and 240mins. The detailed method can be found in chapter 3.

7.2.2.5 NMR Measurement

^{1}H NMR experiments were used to probe interactions among drug, coformer and polymer in solution. Details of the measured samples are shown in Table A4. 1 in the appendix, including the singular component solutions of FFA I, NIC, TP, PVP and PVP-VA, the binary component solutions of FFA/NIC, FFA/TP, FFA/PVP, FFA/PVP-VA, NIC/PVP, NIC/PVP-VA, TP/PVP and TP/PVP-VA, and ternary component solutions of FFA/NIC/PVP, FFA/NIC/PVP-VA, FFA/TP/PVP and FFA/TP/PVP-VA. Three different concentrations of FFA solutions were prepared, including 500μg/mL, 1000μg/mL and 5000μg/mL. In order to mimic a cocrystal system, an equal molar concentration of a coformer as that of FFA was prepared in solution, i.e. 215μg/mL of NIC or 320μg/mL of TP in 500μg/mL of FFA solution, 430μg/mL of NIC or 640μg/mL of TP in 1000μg/mL of FFA solution, and 2150μg/mL of NIC or 3200μ/mL of TP in 5000μg/mL of FFA solution. Two different concentrations of a pre-dissolved polymer of PVP or PVP-VA, 200μg/mL and 5000μg/mL, were prepared

in solution to investigate its concentration dependent interactions with FFA and/or a coformer of NIC or TP. The details about the NMR setting can be found in chapter 3.

7.2.2.6 Analytical Techniques

Automatic HPLC was used to determine the solubility, dissolution and permeation property of FFA I, FFA cocrystals. Detailed information can be found in chapter 3.

7.3 Results

7.3.1 Effect of a Pre-dissolved Polymer, Coformer and Combination of a Polymer and Coformer on the Equilibrium Solubility of FFA I

Figure 7. 1 shows the variations of the FFA concentrations in 0.01M pH 4.5 PBS in the absence and presence of different concentrations of a pre-dissolved polymer of PVP or PVP-VA with or without a fixed concentration of a coformer of NIC or TP at equilibrium after 24h. The equilibrium solubility of FFA I at 37°C measured was 9.0 ±0.7μg/mL. It was observed that PVP had an insignificant solubilization effect on FFA molecules in solution. The solubility of FFA I slightly increased with a pre-dissolved PVP at a concentration of 500μg/mL, reached the maximum of 14.88±0.98μg/mL at the PVP concentration of 2000μg/mL and then keeps constant with increasing the PVP concentration. FFA I solubility started to increase when the pre-dissolved PVP-VA concentration was above 1000μg/mL and then kept increasing significantly with increasing the PVP-VA concentration.

With a pre-dissolved NIC concentration of 47.8μg/mL, the equilibrium solubility of FFA I was the same as that in the pure 0.01M pH 4.5 PBS, while as the equilibrium solubility of FFA I slightly increased to 10.24±0.71μg/mL with a pre-dissolved TP concentration of 71.1μg/mL. The equilibrium solubility of FFA I at different concentrations of PVP solutions was almost the same as those without the pre-dissolved NIC, indicating that PVP was the dominating factor to affect the solubility of FFA I. In the presence of 71.1μg/mL of pre-dissolved TP in solution, a slight change of the FFA equilibrium solubility curve was observed at different PVP concentrations. At a lower PVP concentration up to 500μg/mL, the solubility of FFA I was constant as that in the pre-dissolved TP in the absence of PVP. At the PVP concentration up to 4000μg/mL, the equilibrium solubility of FFA I was the same as that without the pre-dissolved TP.

In contrast, the solubilization ability of PVP-VA on the FFA I equilibrium solubility has been strengthened significantly due to the pre-dissolved coformer of NIC or TP in solution, indicating that the solubility of FFA I significantly increased even at a very low PVP-VA concertation of 200μg/mL. In comparison with NIC, TP was more

capable to enhance the solubilization ability of PVP-VA on FFA in solution shown in Figure 7. 1.

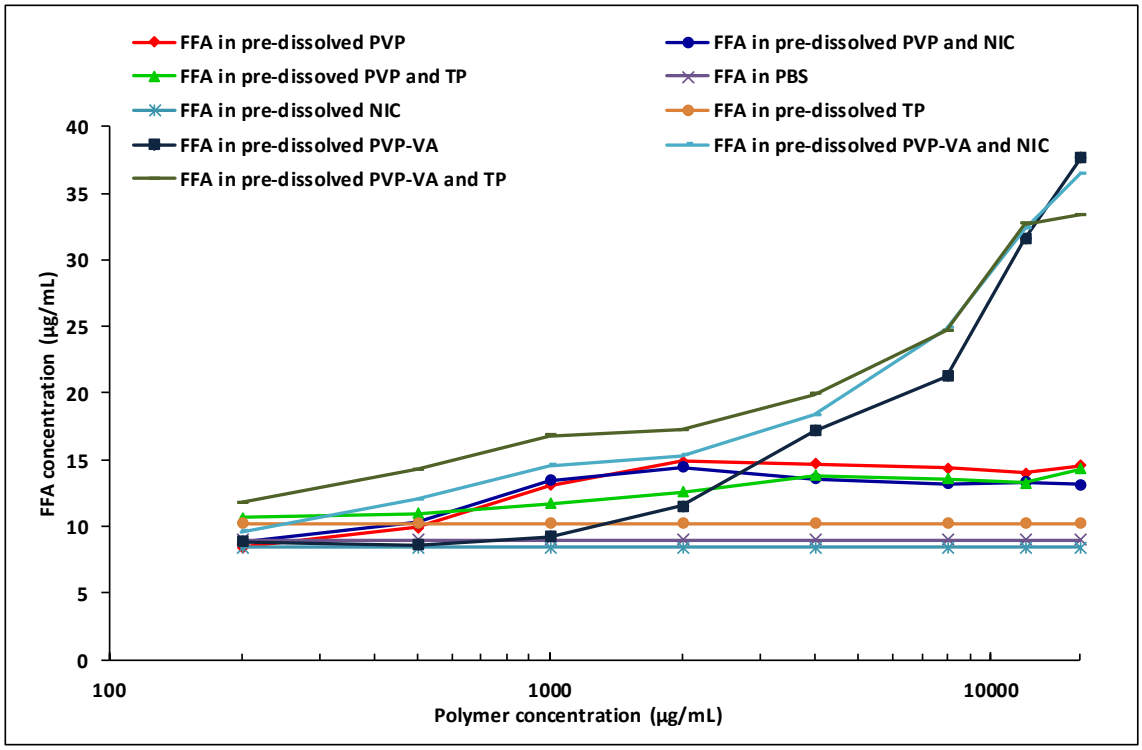

Figure 7. 1 Apparent equilibrium solubility of FFA I at different concentrations of a pre-dissolved polymer with or without a coformer of NIC or TP

7.3.2 Effect of a Polymer on FFA Cocrystal Dissolution and Permeation

The molecular weight cut off pore size of the dialysis membrane used in the study was 6-8 KDa. Thus, FFA, which has a MW of 281, can cross the membrane into the acceptor cell while the polymers cannot, i.e. PVP (MW 40,000) and PVP-VA (MW 51,000). Therefore, the membrane can separate drug molecules associated with polymers before they diffuse into the acceptor cell.

7.3.2.1 Pure PBS

Figure 7. 2 shows the dissolution and permeation profiles of FFA I and FFA cocrystals of FFA-NIC COs and FFA-TP COs in 0.01M pH4.5 PBS without polymers in the D/P system. There was no significant difference in the dissolution profiles of the solid powders of FFA I and FFA-TP COs in the donor cell, where FFA concentration reached its solubility around 60min and then was kept constant afterwards. FFA-NIC COs

showed a slightly different dissolution profile, where the FFA concentration quickly reached its maximum at 5min and after that the FFA concentration started to decline and reach its minimum at 120min. The quantitative comparison of DPPs in Figure 7. 5(a), based on our previous publication [4], indicated that FFA-TP CO has a comparable DPP with FFA I while FFA-NIC CO is the lowest DPP. The FFA concentration profiles of the FFA I and FFA-TP COs in the acceptor cell were also the same, showing a linear increase with time in Figure 7. 2(b). The FFA concentration in the FFA-NIC COs acceptor cell showed a reduced flux rate after 60min. Quantitative comparison of the mass flux rates of the systems in Figure 7. 5(b) shows that the FFA mass flux rate of a formulation system is proportional to its DDP.

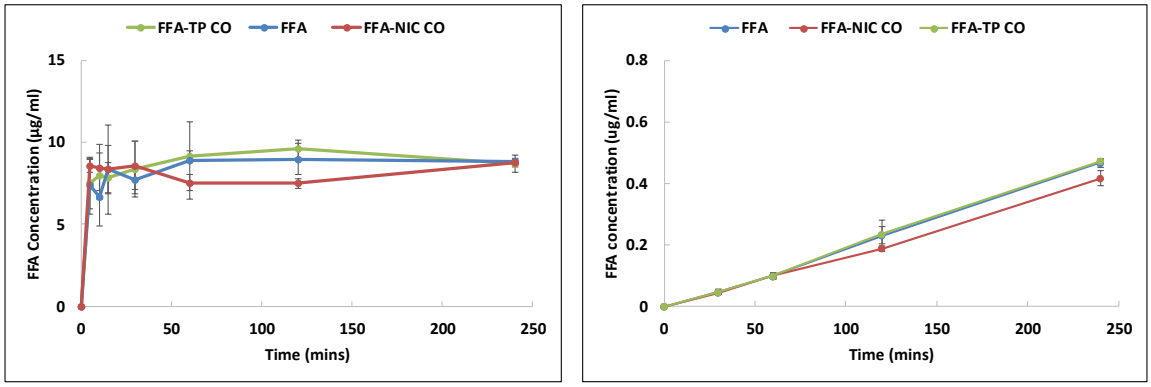

(a) (b)

Figure 7. 2 Dissolution and permeation profiles of FFA I and FFA cocrystals in PBS in the D/P system: (a) dissolution; (b) permeation

7.3.2.2 PBS in the Presence of a Pre-dissolved Polymer of PVP or PVP-VA

Figure 7. 3 shows the effect of a pre-dissolved PVP on the dissolution of FFA I and FFA cocrystals in the donor cell and its corresponding permeation profiles in the acceptor cell. It was found that both FFA-NIC COs and FFA-TP COs showed the enhanced dissolution profiles in comparison with the parent drug of FFA I when PVP was added into the dissolution media. The dissolution performances of the FFA COs were dependent on the PVP concentration. In the dissolution media with a low PVP concentration of 200µg/mL, a supersaturated state of FFA in solution was observed by dissolving either FFA-TP COs or FFA-NIC COs, where the maximal FFA concentration of 16.7µg/mL was achieved by FFA-TP COs after 5min and 12.2µg/mL

of FFA concentration was obtained by FFA-NIC COs after 15min. And then the FFA concentration was reduced and stabilized approximately to its parent drug solubility for both FFA cocrystal systems after 60min. The permeated amount of FFA molecules was enhanced by PVP for FFA-TP COs by 1.23-fold or for FFA-NIC COs by 1.17-fold shown in Figure 7. 5(b). In contrast, the DPP of FFA I in PBS with PVP was reduced by 15.4% compared with the pure dissolution medium in Figure 7. 5(a), indicating that the pre-dissolved PVP in solution can slow down the drug dissolution and the permeated amount of FFA molecules was reduced by PVP for FFA I by 0.90-fold in Figure 7. 5(b).

At 4000 μg/mL of PVP concentration, the maximum FFA concentration in the FFA-TP COs donor cell can reach 40μg/mL at 15min, which is approximately 4.5-fold of the solubility of FFA I, while as it was 23.6μg/mL at 15min for FFA-NIC COs, indicating FFA-TP COs had a better dissolution performance than FFA-NIC COs. In the FFA-NIC CO donor cell the FFA concentration quickly decreased to a constant of 19.5 μg/mL at 30min. In contrast, the FFA concentration in the FFA-TP CO donor cell decreased slowly from its maximum and was stabilized at 28.8μg/mL after 60min. The FFA-TP CO's DPP was 228% higher than the parent drug of FFA I and it was 128% higher for FFA-NIC COs in Figure 7. 5(a). Accordingly, the permeated amount of FFA molecules increased significantly by FFA-TP COs with 1.69-fold and FFA-NIC COs with 1.27-fold in Figure 7. 5(b).

Increasing the PVP concentration to 16000μg/mL in solution, both of FFA-TP CO and FFA-NIC CO showed a reduced dissolution performance shown in Figure 7. 3(c5) and Figure 7. 5(a), in which the maximal FFA concentration in the FFA-TP CO donor cell was 27.5μg/mL at 15min and in the FFA-NIC CO donor cell the maximal FFA concentration was 19.7μg/mL. Unexpectedly it was observed that the permeated amount FFA molecules was reduced significantly for the FFA cocrystals in Figure 7. 3(c6) and the flux rate of the FFA-TP COs was 0.62-fold of the FFA I in the pure PBS and it was 0.45-fold for FFA-NIC COs in Figure 7. 5(b). At this polymer concentration, the dissolution rate of FFA I became significantly slow in Figure 7. 3(c5), showing 9% reduction of DPP in Figure 7. 5(a) and 0.34-fold of the flux rate in comparison with FFA I in the pure PBS in Figure 7. 5(b).

The dissolution and permeation profiles of FFA I and FFA cocrystals in PBS in the presence of the pre-dissolved PVP-VA in the donor cell are shown in Figure 7. 4. Increasing a pre-dissolved PVP-VA concentration in the donor cell, the dissolution performance of FFA cocrystals can be enhanced significantly. At a low PVP-VA concentration of 200μg/mL, a moderate increase of DPP was observed, i.e. 33.8% increase by FFA-NIC COs and 42.6% increase by FFA-TP COs in Figure 7. 5(a). At a high PVP-VA concentration of 16000μg/mL, the DPP can be increased to 460.5% by FFA-NIC COs and 409.4% by FFA-TP COs in Figure 7. 5(a) in comparison with FFA I in pure PBS. However, the permeated amount of FFA is not proportional to the increased DPPs shown in Figure 7. 5(a) and Figure 7. 5(b). The FFA flux rate of FFA I and FFA cocrystals reduced with increasing the concentration of a pre-dissolved PVP-VA. The FFA flux rates of FFA-NIC COs and FFA-TP COs at the pre-dissolved PVP-VA concentration of 200μg/mL or 4000μg/mL are higher than that of FFA I in the pure PBS shown in Figure 7. 5(b). At the highest PVP concentration of 16000μg/mL the flux rate of FFA-NIC COs or FFA-TP COs was lower than FFA I in the pure PBS.

Pre-dissolved PVP concentration	Dissolution profile	Permeation profile
200μg/mL	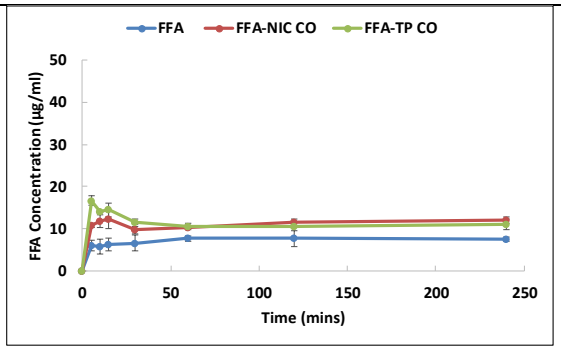 (c1)	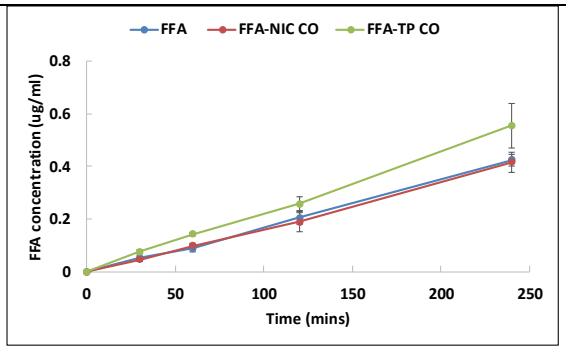 (c2)
4000μg/mL	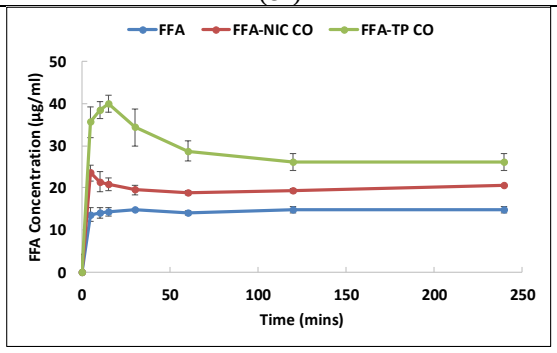 (c3)	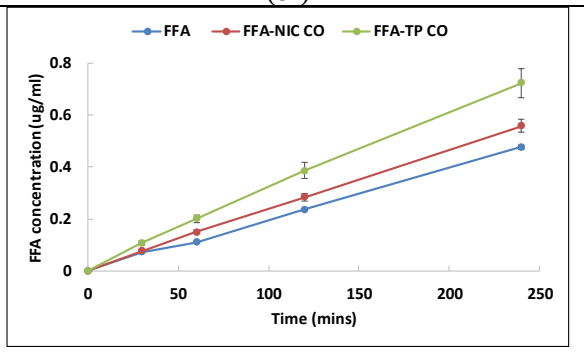 (c4)

16000μg/mL	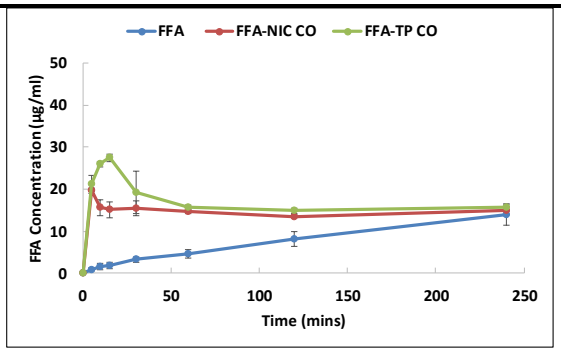 (c5)	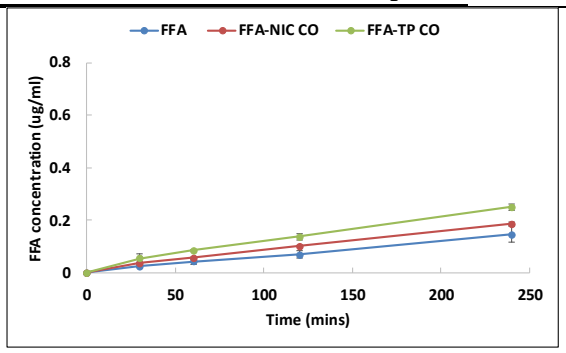 (c6)

Figure 7. 3 Dissolution and permeation profiles of FFA I and FFA cocrystals in PBS in the presence of a pre-dissolved PVP in the dissolution/permeation (D/P) system; The time for dissolution and permeability tests was 4h.

Pre-dissolved PVP-VA concentration	Dissolution profile	Permeation profile
200μg/mL	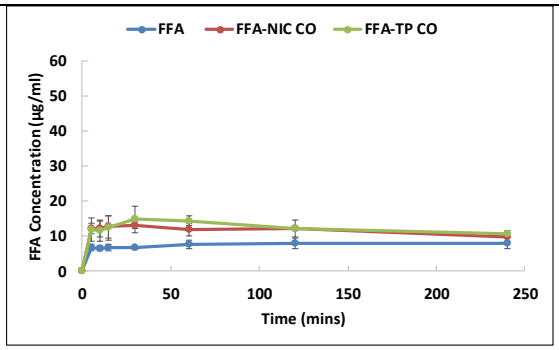 c1	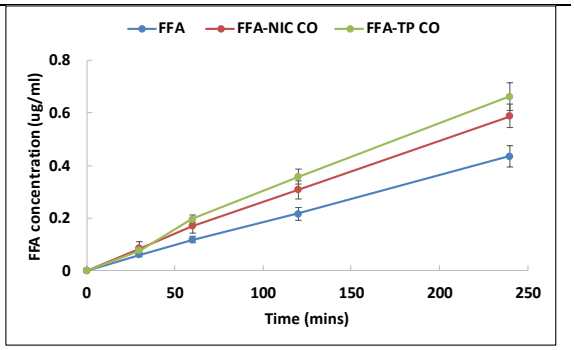 c2
4000μg/mL	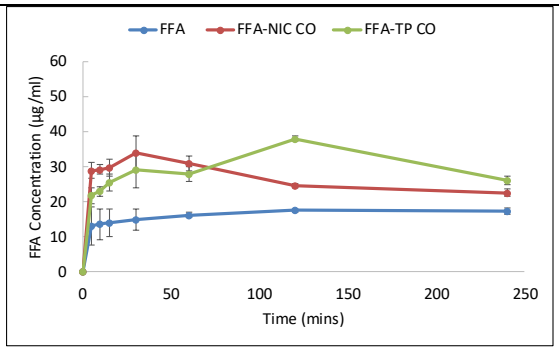 c3	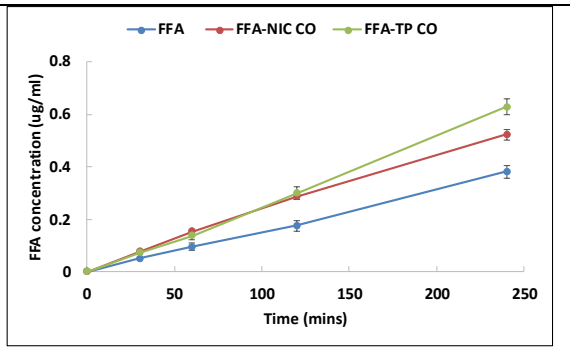 c4

16000μg/mL

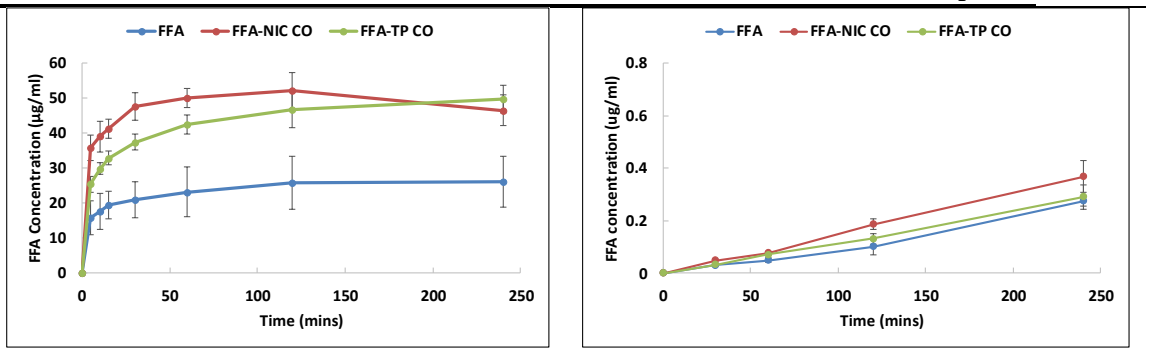

c5 c6

Figure 7. 4 Dissolution and permeation profiles of FFA I and FFA cocrystals in PBS in the presence of a pre-dissolved PVP-VA in the dissolution/permeation (D/P) system; The time for dissolution and permeability tests was 4h.

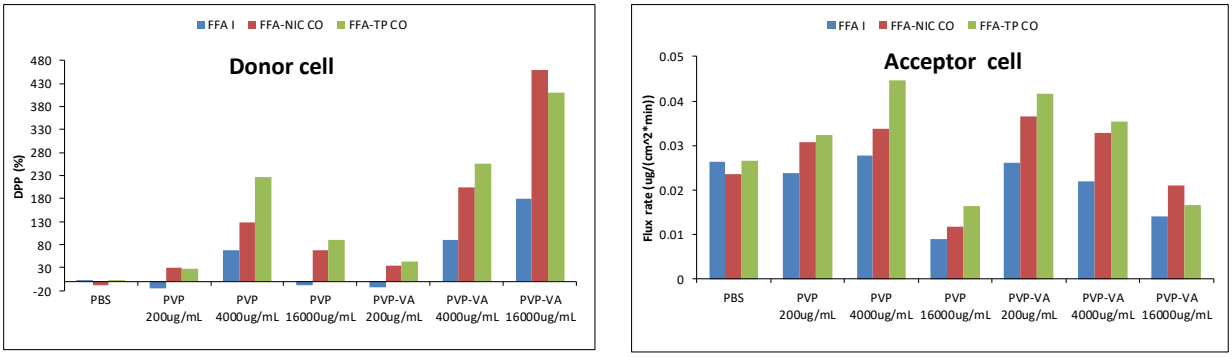

(a) (b)

Figure 7. 5 Comparison of dissolution and permeation profiles of FFA I and FFA cocrystals in the absence and presence of a pre-dissolved polymer: (a) The DPP results of FFA I, FFA-NIC CO and FFA-TP CO in donor cell and (b) the flux rate of FFA I, FFA-NIC CO and FFA-TP CO in the acceptor cell. The time for dissolution and permeability tests was 4h.

7.3.3 NMR Analysis

^{1}H NMR experiments in Table A4. 1were conducted to investigate the interactions among FFA, coformers and polymers in solution. Assignments of the ^{1}H chemical shifts of FFA, NIC, TP, PVP and PVP-VA were based on the previous work [325, 328-332]. In this work, we focused on examining the characteristic chemical shifts of the protons in each of the molecules of FFA, TP, and NIC affected by their hydrogen bonding interactions and self-aggregation properties in solution in the absence and presence of a polymer of PVP or PVP-VA: i) the chemical shifts of the singlet peak of H_j and two doublet peaks of H_h of FFA; ii) the chemical shifts of H_a, H_b and H_c of NIC; iii) the

chemical shifts of H_a, H_b, H_c and H_d of TP. The proton details of each molecule can be found in Table 7. 1. The full ^{1}H NMR spectra of the experiments can be found in Figure A4. 1 in Appendix.

7.3.3.1 ^{1}H NMR Analysis of a Singular Component

Figure 7. 6(a) shows the ^{1}H NMR chemical shifts of H_j and H_h of FFA at different drug concentrations in $CDCl_3$, suggesting that the proton chemical shifts were concentration dependent. It is well known that there exists an intramolecular hydrogen bond between the NH_j group and the C=O of the carboxylic acid of FFA, the chemical shift of H_j is impacted by the molecule conformations in solution associated to the dimer formation [329]. Increasing FFA concentration, the self-association of FFA occurs through inter carboxylic acid hydrogen bonding of two FFA molecules, causing a downfield change of the chemical shift of H_h from 8.049ppm at a lower FFA concentration of 500μg/mL to 8.061ppm at 1000μg/mL, and to 8.082ppm at 5000μg/mL, due to proton deshielding by the hydrogen bonds which lengthens the O-H bond and subsequently reduces the valence electro density around the proton of H_h. The intermolecular association of the dimer formation of FFAs was induced with increasing FFA concentrations can strengthen the intramolecular interaction N-H_j···O=C [329], showing an upfield change of the chemical shift of H_j from 9.463ppm at a lower FFA concentration of 500μg/mL to 9.443ppm at 1000μg/mL, and to 9.410ppm at 5000μg/mL . The self-association of NIC in solution occurs through inter-amide hydrogen bonding and does not occur through stacking of the pyridine rings [333]. It has been shown that with an increased NIC concentration, downfield chemical shifts of H_a and H_b ($\Delta\delta$=0.021 at 430μg/mL and $\Delta\delta$=0.134 at 2150μg/mL for H_a; $\Delta\delta$=0.005 at 430μg/mL and $\Delta\delta$=0.041 at 2150μg/mL for H_b) were observed in comparison with H_c whose chemical shift was almost constant ($\Delta\delta$=0.001 at 430μg/mL and $\Delta\delta$=0.005 at 2150μg/mL) in Figure 7. 6(b). In $CDCl_3$, TP self-association occurs through the asymmetric dimer involving hydrogen bonding of H_b···O of C-CO-N-CH_d and C=N···H_aN-C [334], showing that all of ^{1}H chemical shifts of H_a and H_b moved to a lower field as the concentration increased ($\Delta\delta$=0.228 at 640μg/mL and $\Delta\delta$=1.034 at 3200μg/mL for H_a; $\Delta\delta$=0.007 at 640μg/mL and $\Delta\delta$=0.039 at 3200μg/mL for H_b) while as ^{1}H chemical shifts of H_c and H_d were slightly downfield

changes ($\Delta\delta$=0.003 of H_c and $\Delta\delta$=0.005 of H_d at 640μg/mL and $\Delta\delta$=0.013 of H_c and $\Delta\delta$=0.020 of H_d at 3200μg/mL), shown in Figure 7. 6(c).

(a) FFA	$\Delta\delta = \delta_{high\ FFA\ concentration} - \delta_{500\mu g/mL\ FFA}$ 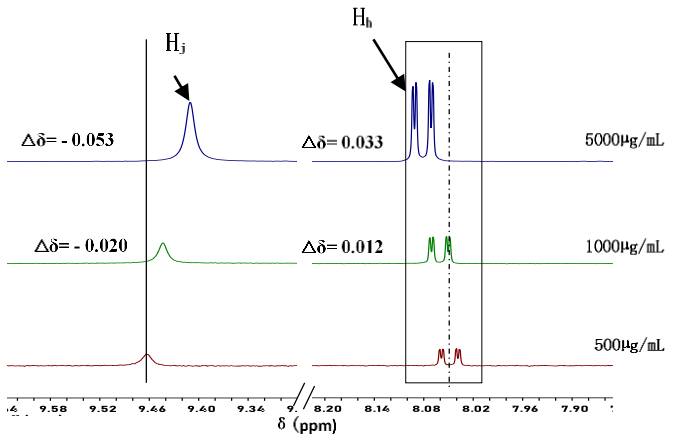
(b) NIC	$\Delta\delta = \delta_{high\ NIC\ concentration} - \delta_{215\mu g/mL\ NIC}$ 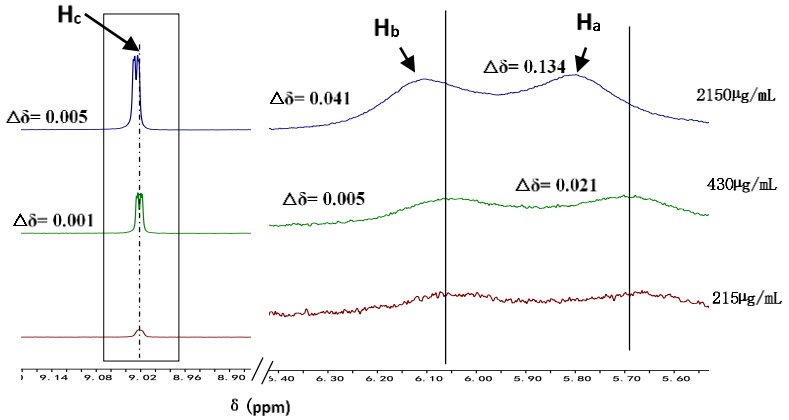

(c) TP

$$\Delta\delta = \delta_{high\ TP\ concentration} - \delta_{320\mu g/mL\ TP}$$

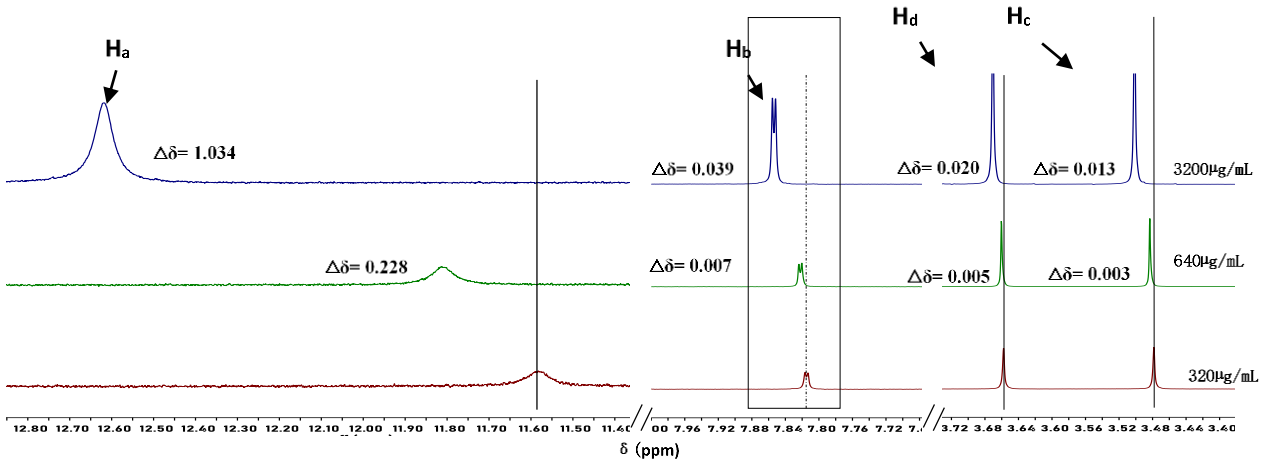

Figure 7. 6 ^{1}H NMR spectra of a singular component at difference concentrations in $CDCl_3$

7.3.3.2 ^{1}H NMR Analysis of Binary Components

For clarity, here we only analyzed one set of experiments, i.e. FFA at 1000μg/mL, NIC at 430μg/mL or TP at 640μg/mL in the presence of two different concentrations of a polymer (PVP or PVP-VA), as an example to discuss the properties of the drug self-association and its interaction with the polymer in solution.

Figure 7. 7 shows chemical shifts of individual components of FFA, NIC and TP in the presence of two different concentrations of a polymer of PVP or PVP-VA in $CDCl_3$.

At a low polymer (either PVP or PVP-VA) concentration of 200μg/mL, the chemical shift of H_h of FFA changed to downfield, indicating a hydrogen bonding interaction between O-H of the carboxylic acid function group of FFA with the carbonyl O group of PVP or PVP-VA. Although O=C of the carboxylic acid function group of FFA is not involved into the interaction with the polymer, the long backbone chains of polymers can affect the confirmation of the FFA molecules to disturb the intramolecular interaction of N-H_j···O=C, indicating a downfield chemical shift of H_j of FFA in the presence of a polymer in solution in Figure 7. 7(a). Increasing the polymer concentration to 5000μg/mL in solution, the chemical shifts of H_j and H_h peaks moved to opposite directions, i.e., an upfield (shielding) shift for H_h, and a downfield shift for H_j, suggesting a different interacting mechanism between the FFA and the polymer at the high concentration. The upfield shift of H_h peak was probably associated with the transition of a solution environment from hydrophilic to hydrophobic with increasing a polymer concentration, leading to hydrophobic interaction between FFA and polymer molecules [217, 332]. Obviously, the hydrophobic interaction affects the conformation of FFA molecules in solution, resulting in the change of the intramolecular interaction N-H_j···O=C where the downfield shift of H_j peak was observed. Furthermore, broader ^{1}H NMR peaks of FFA in PVP solution were observed in comparison with those in PVP-VA solution, demonstrating that PVP can significantly suppress the mobility of FFA molecules in solution.

The chemical shifts of NIC in Figure 7. 7(b) were not affected by PVP or PVP-VA at a lower concentration of 200μg/mL, implying that there was no or weak interaction between NIC and PVP or PVP-VA. In 5000μg/mL of PVP or PVP-VA solution, the

hydrogen bonding interactions between NIC and a polymer were formed, observing the downfield shifts of ^{1}H NMR peaks of NIC.

^{1}H NMR spectra of TP are complex, which can be affected by interactions of solute-solvent, solute-solute and solute-polymer. In $CDCl_3$, dimerization of TP molecules is found to be the dominating factor affecting the ^{1}H chemical shifts of TP [334]. Because TPs are good proton donors, PVP or PVP-VA can disrupt TP dimers in solution, indicating downfield shifts of ^{1}H NMR peaks of TP at a low polymer concentration of 200μg/mL shown in Figure 7. 7(c). At a high polymer concentration, upfield (shielding) shifts for H_b, H_d and H_c of TP were observed.

In the solid state of 1:1 FFA-NIC COs, hydrogen bonds are formed by two FFA and two NIC molecules, where H_i of carboxyl acid of the FFA and aromatic N of the first NIC form a hydrogen bond and the amide H_a or H_b of the second NIC forms a hydrogen bond with the carbonyl O atom of the acid of same FFA [234]. It seems that same interactions of FFA and NIC are formed in $CDCl_3$, indicating the deshielding of chemical shifts of the H_h of FFA and H_c, H_a and H_b of NIC to downfield when equal molar FFA and NIC dissolved in $CDCl_3$ in Figure 7. 8(a). Due to formation of a hydrogen bond of the carbonyl O atom of the acid of FFA with one NIC, the intramolecular N-H_j···O=C was disrupted, resulting to the downfield movement of the chemical shift of H_j of FFA.

It is suggested that a dimer of FFA and TP can be formed through H_i of carboxyl acid of FFA with N of C-N=CH_b of TP [295], therefore, there is a significant chemical shift of H_h of FFA to downfield shown in Figure 7. 8(b). Because the C=O atom of the acid of the same FFA has not been involved in the intermolecular interaction with TP, the intramolecular N-H_j···O=C of FFA is not disrupted, showing a constant chemical shift of H_j without or with TP in $CDCl_3$.

(a) FFA	$\Delta\delta = \delta_{FFA\ in\ polymer} - \delta_{FFA\ in\ CDCl3}$ 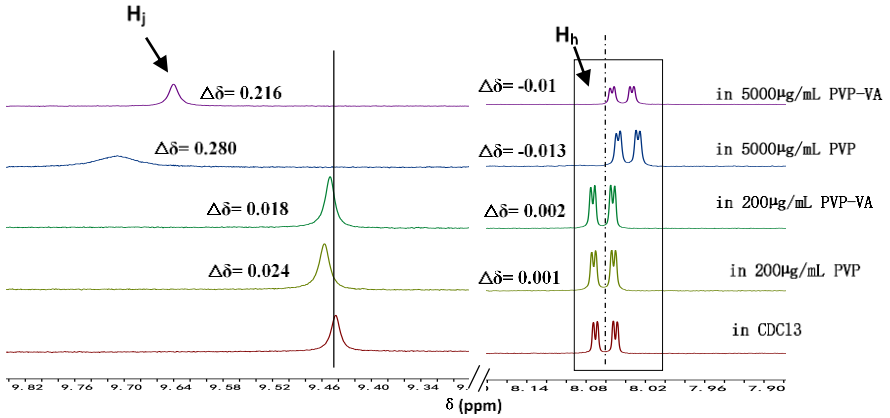
(b) NIC	$\Delta\delta = \delta_{NIC\ in\ polymer} - \delta_{NIC\ in\ CDCl3}$ 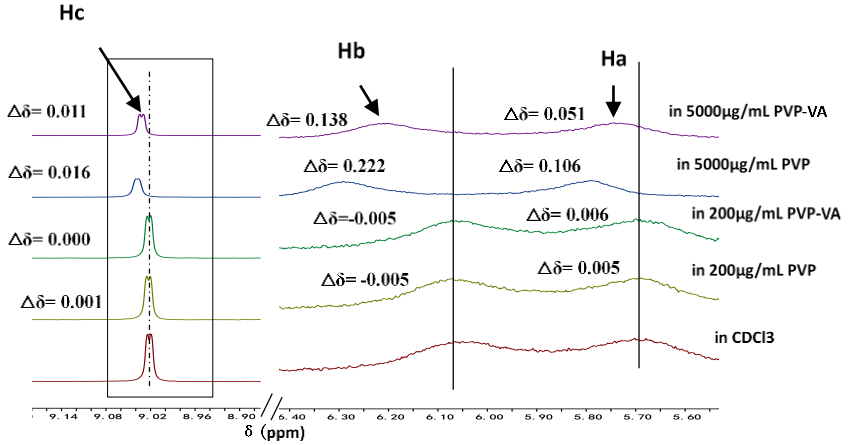

(c) TP

$$\Delta\delta = \delta_{TP\ in\ polymer} - \delta_{TP\ in\ CDCl3}$$

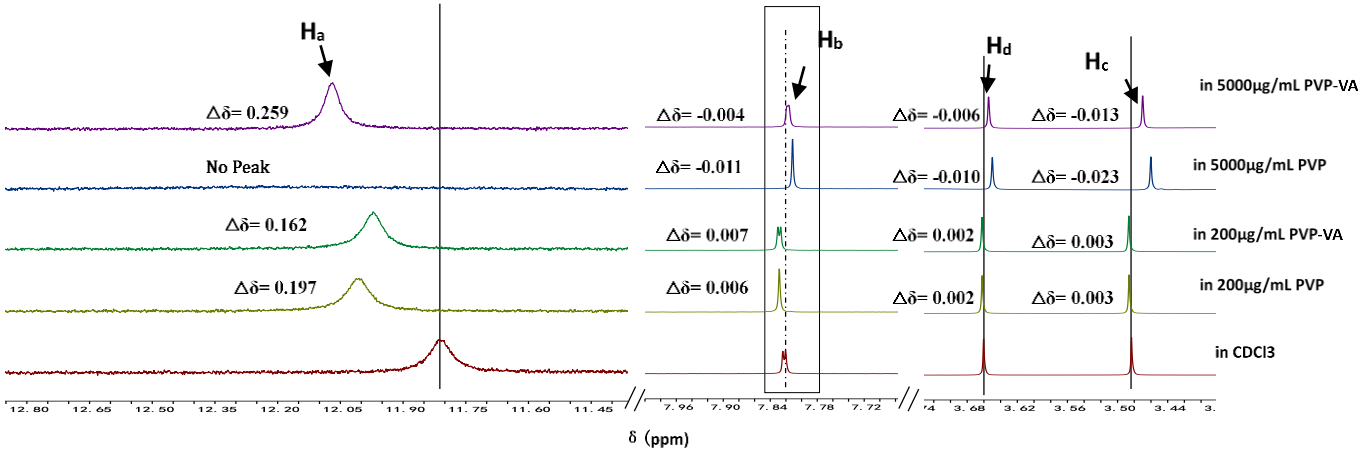

Figure 7. 7 ^{1}H NMR spectra of FFA, NIC and TP at two difference concentrations of a polymer in $CDCl_3$

(a) 1:1 molar ratio of FFA and NIC	FFA	$\Delta\delta = \delta_{FFA-NIC} - \delta_{FFA}$ 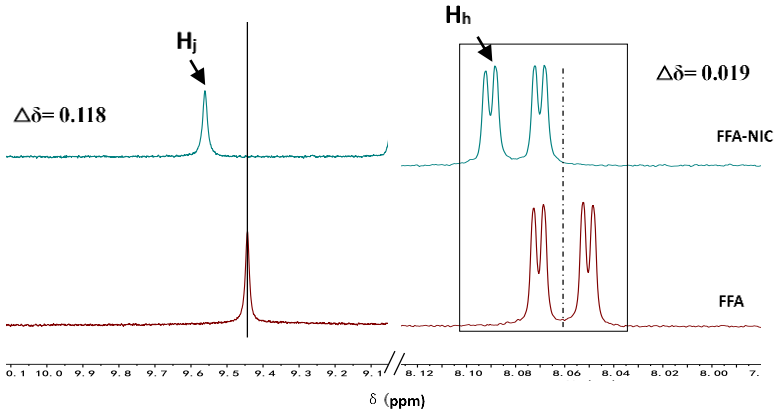
	NIC	$\Delta\delta = \delta_{FFA-NIC} - \delta_{NIC}$ 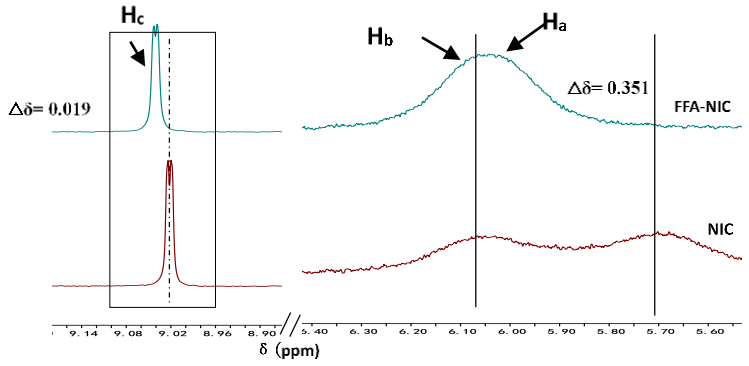
(b) 1:1 molar ratio of	FFA	$\Delta\delta = \delta_{FFA-TP} - \delta_{FFA}$

FFA and TP		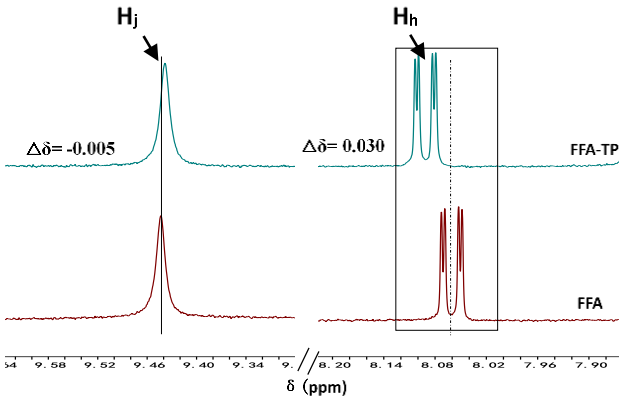
	TP	$\Delta\delta = \delta_{FFA-TP} - \delta_{TP}$ 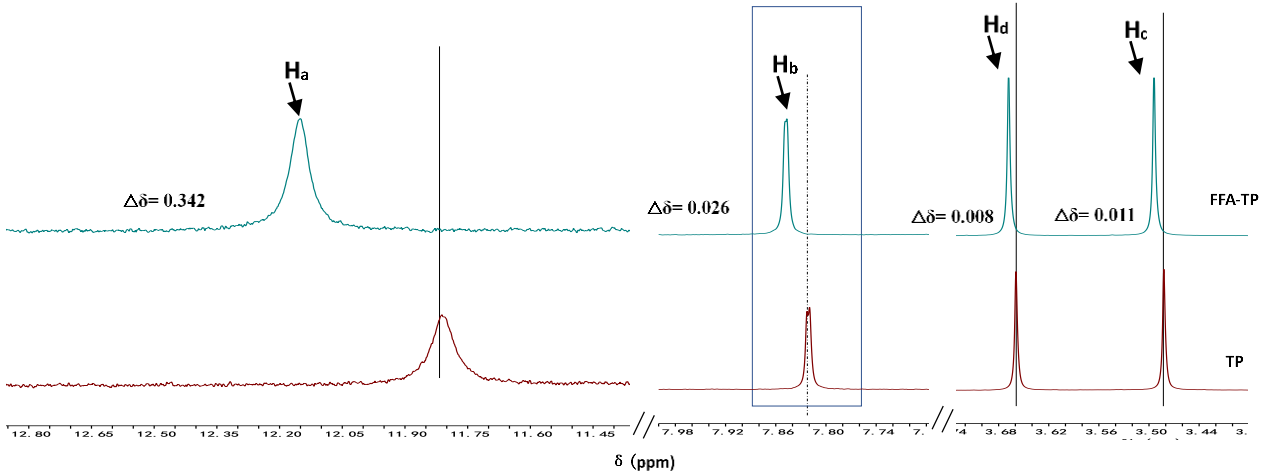

Figure 7. 8 ^{1}H NMR spectra of mixture of FFA and a coformer of NIC or TP in $CDCl_3$

7.3.3.3 ^{1}H NMR Analysis of Ternary Components

Similar to the above, we only discussed experimental results of the mixtures of FFA at a concentration of 1000μg/mL with its equal molar concentration of a coformer of NIC or TP in different concentrations of a polymer in $CDCl_3$ shown in Figure 7. 9.

At a low PVP concentration of 200μg/mL in $CDCl_3$, characteristic chemical shifts of the H_h and H_j of FFA moved to upfield, suggesting that some of hydrogen bonds between FFA and NIC have been disrupted due to the interactions of FFA and PVP shown in Figure 7. 9(a). In contrast, at the same PVP-VA concentration of 200μg/mL in $CDCl_3$, characteristic chemical shifts of the H_h and H_j of FFA were almost constant as those without the polymer, indicating that the interaction between FFA-NIC was a dominating force shown in Figure 7. 9(b). At a higher PVP or PVP-VA concentration of 5000μg/mL, chemical shifts of H_j and H_h peaks moved to opposite directions in Figure 7. 9(a)-(b), indicating the hydrophobic interaction between FFA and the polymer became the dominating force suppressing the hydrogen bonding among FFA, NIC and the polymer.

For a mixture of FFA and TP in $CDCl_3$ in the presence of a lower concentration of PVP or PVP-VA of 200μg/mL in Figure 7. 9(c)-(d), the chemical shift of H_h of FFA slightly moved to upfield while as the chemical shift of H_j of FFA slightly downfield shifts, indicating that hydrogen bonds between FFA and TP were disturbed by the polymer. At a higher PVP or PVP-VA concentration of 5000μg/mL, chemical shifts of H_j and H_h peaks moved to opposite directions in Figure 7. 9(c)-(d) similar as those of a mixture of FFA and NIC, showing the dominating hydrophobic interaction between FFA and the polymer.

1:1 molar ratio of FFA and NIC	(a) PVP	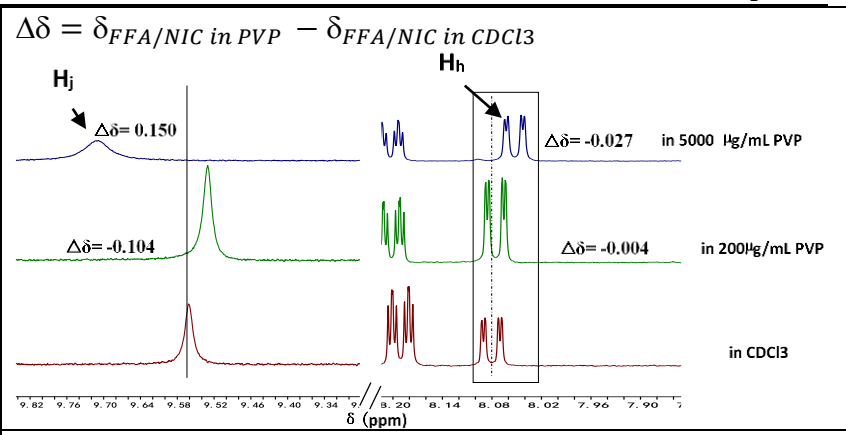
	(b) PVP-VA	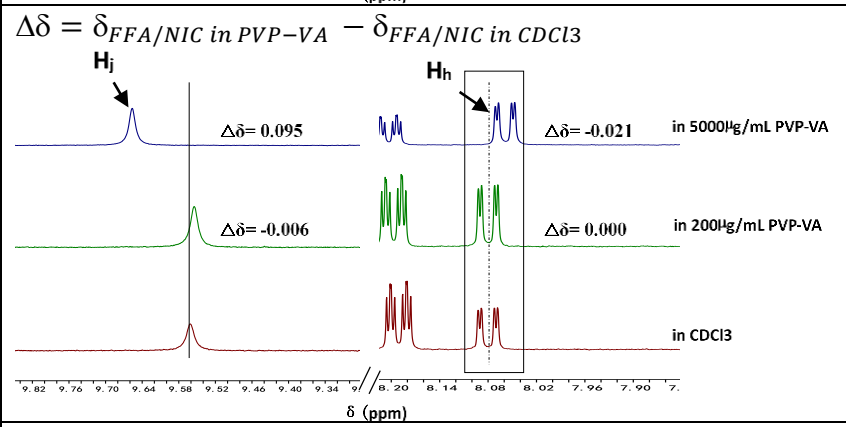
1:1 molar ratio of FFA and TP	(c) PVP	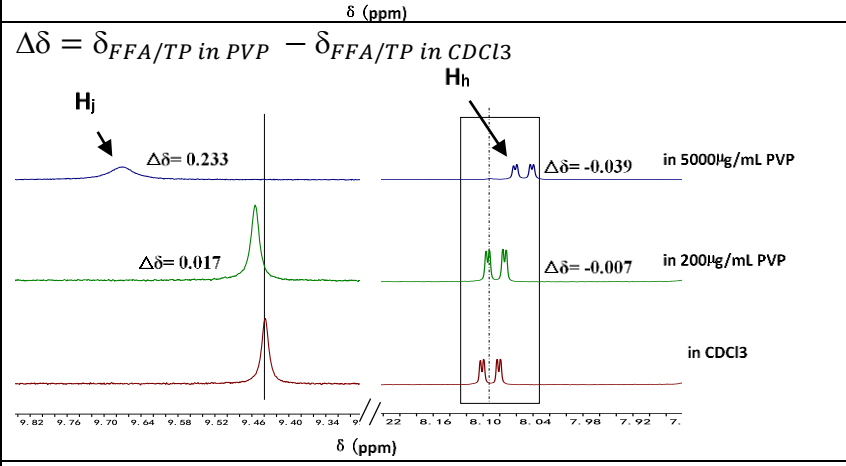
	(d) PVP-VA	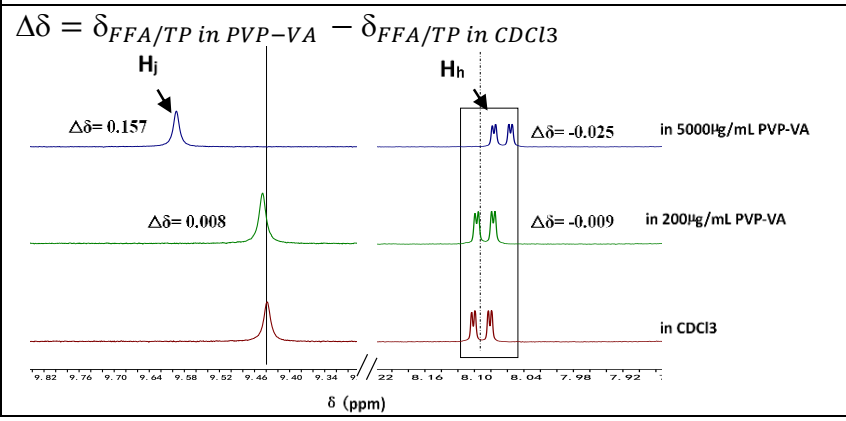

Figure 7. 9 ^{1}H NMR spectra of FFA in an equal molar mixture of FFA and NIC or TP at difference concentrations of a polymer in $CDCl_3$

7.4 Discussion

In this study, we have demonstrated that the supersaturated drug concentration generated by the cocrystal dissolution can be maintained through inclusion of a polymeric excipient in formulations, showing the improved dissolution performance of FFA-NIC COs or FFA-TP COs by a pre-dissolved polymer of PVP or PVP-VA in the donor cell in Figure 7. 5(a) [10, 183, 335]. In the presence of pre-dissolved PVP or PVP-VA in solution, the DPP of a FFA cocrystal system was much higher than that in solution without a pre-dissolved polymer in Figure 7. 5(a) and it was also proportional to the polymer concentration. However, an elevated drug concentration in the donor cell did not always improve the flux rate of FFA to the acceptor cell shown in Figure 7. 5(b). This erratic drug permeation could lead to poor drug bioavailability, which was crucially related to the amount of drug molecules going through the GI membrane. Therefore, it is critical importance to explore the interplay of the solubility and permeability in a cocrystal based formulation, similar to many other solubility enabling formulations, such as surfactants, cyclodextrins, cosolvents, or solid dispersions, where an enhanced drug solubility may lead to decrease, remain unchanged and even increase the drug permeability [25, 336-338]. The mechanism of the effects of a polymer on the dissolution behavior of cocrystals has been explored in our recent publication [335], indicating that a pre-dissolved polymer can interact with the crystal surface to alter the cocrystal dissolution properties for inhibition of the drug precipitation in solution. The discussion here was focused on the mechanistic understanding of the interactions among FFA, a coformer of NIC or TP and a polymer of PVP or PVP-VA in the solution which affect the maintaining of the supersaturated FFA concentration and subsequent permeation to the acceptor cell.

Both PVP and PVP-VA are water soluble polymers, however, due to differences in their molecular structures in Table 7. 1, intermolecular interactions of polymer/FFA and polymer/coformer are different, which not only affect FFA nucleation and growth kinetics in solution [183] but also the permeation properties of FFA shown in Figure 7. 5(b). Interestingly, for a given FFA cocrystal formulation of FFA-NIC CO or FFA-TP CO at the same polymer concentration, the DPP of the formulation in the presence of the PVP-VA was always higher than that of the same formulation in the presence of PVP. However, the permeation property was not the case, i.e., the flux rate of the

formulation in the presence of the PVP-VA could be higher or lower than that of the same formulation in the presence of the PVP, depending on the polymer concentration. Furthermore, in the presence of PVP-VA, the FFA flux rate across the membrane for a given formulation is in inverse to its DPP while as it is proportional to its DPP in the presence of PVP except 16000μg/mL PVP. Therefore, a wrong conclusion could be drawn if only the DPP of a cocrystal formulation is considered.

Based on the solubility results in Figure 7. 1, it was suggested that PVP acted as a stabilizing agent in the formulation because the equilibrium solubility of FFA did not increase significantly over the whole range of the concentrations studied. The hydrogen bonding interaction of FFA and PVP molecules should be a dominant force at a low PVP concentration (below 4000μg/mL), confirmed by the solution ^{1}H NMR spectra of FFA showing the downfield chemical shifts of H_h of FFA in Figure 7. 7(a). Maintaining the supersaturated FFA concentration should be achieved through inhibiting FFA nucleation by PVP in Figure 7. 3(c1, c3) [183], leading to the increased FFA flux rate from the donor cell to the acceptor cell in Figure 7. 3(c2, c4). The flux rate was determined by the degree of supersaturation (ratio of dissolved amount of unchanged API to its thermodynamic solubility), which was the driving force for transporting the drug substance across the membrane [337]. The FFA flux rate achieved by the FFA-TP COs is higher than that of FFA-NIC COs because FFA-TP COs can generate a higher FFA supersaturation due to the bulk precipitation dissolution mechanism [335]. When the PVP concentration was above 4000μg/mL, the interaction force between FFA and PVP has changed into hydrophobic interactions dominantly due to confined spaces between FFA and PVP molecules, showing the upfield chemical shifts of H_h of FFA in Figure 7. 7(a). It has to stress that micellization of PVP did not occur due to its rigorous backbone structure and there was no significant change of the equilibrium solubility of FFA in Figure 7. 1. Consequently, the FFA mobility in solution was reduced at a higher PVP concentration, illustrated by a broaden peak of H_j of FFA in Figure 7. 7(a), resulting in stabilizing the FFA supersaturated solution in Figure 7. 3 (c3). Reduced FFA flux rate at a PVP concentration of 16000μg/mL in Figure 7. 5(b) was caused by the combined factors of reduced dissolution performance of the cocrystals in Figure 7. 3(c5) and reduced solute activity coefficient [339]. Although the interaction of FFA and PVP was disturbed due to the interactions of a coformer and the polymer shown in the

^{1}H NMR analysis of binary components in Figure 7. 7 and ^{1}H NMR analysis of ternary components in Figure 7. 9, the role of PVP as a stabilizing agent in the formulation did not change, supported by the evidence of a minor change of the FFA solubility curves with or without pre-dissolved coformer in Figure 7. 1. Therefore, the FFA flux rate to the acceptor cell depends solely on the DPP of a cocrystal formulation, where the maximal FFA flux rate was obtained by the FFA-TP CO formulation in the presence of 4000μg/mL of PVP.

Based on the FFA solubility curve in Figure 7. 1, PVP-VA showed a transitional role in a cocrystal formulation, depending on its concentration. At a lower PVP-VA concentration up to 1000μg/mL without a pre-dissolved coformer of NIC or TP, it should be treated as a stabilizing agent in the formulation because the equilibrium solubility of FFA did not increase in Figure 7. 1. The downfield chemical shifts of H_h of FFA in Figure 7. 7(a) indicated the formation of the hydrogen bonding interactions of FFA and PVP-VA in solution. Compared with PVP, PVP-VA is more hydrophobic and flexible due to the addition of hydrophobic monomer vinyl acetate (VA), leading to micellization at a higher concentration [340]. The critical micelle concentration (CMC) of PVP-VA was found to be 1000μg/mL in absence of coformer in this study. Therefore, above 1000μg/mL of PVP-VA concentration, the FFA solubility increases significantly with an elevated PVP-VA concentration. On the basis of the solution ^{1}H NMR spectra of FFA, showing the upfield chemical shifts of H_h of FFA in a higher PVP-VA solution in Figure 7. 7(a), it was concluded that encapsulation of FFA in PVP-VA micelles took place. The role of PVP-VA has changed to be a solubilization agent in the cocrystal formulation. In the presence of a coformer of NIC or TP in solution, a significant increase in the solubilization capacity of PVP-VA was observed in Figure 7. 1. It was likely the consequence of the association of PVP-VA and a coformer in Figure 7. 7(b)-(c) to provide an expanded region the inner core for drug solubilization [341]. The CMC of PVP-VA was reduced significantly to be around 200μg/mL, where the equilibrium solubility of FFA started to increase in Figure 7. 1. Therefore PVP-VA became a solubilization agent in the cocrystal formulations regardless its concentration. Due to increased FFA equilibrium solubility, DPPs of the FFA cocrystal formulations are proportional to the PVP-VA concentration in Figure 7. 5(a). From a thermodynamic perspective, the elevated solution concentrations obtained by PVP-VA are

fundamentally different from supersaturation solutions generated in the presence of the stabilizing agent of PVP in the formulation. Solubilizing additives increase concentration by increasing the equilibrium solubility rather than increasing chemical potential, showing a reduction in FFA flux rate across the membrane with an increased PVP-VA concentration in Figure 7. 5(b) which is consistent with many other enabling formulation studies [25, 336-338]. The maximal FFA flux rate was obtained from the FFA-TP CO formulation in the presence of the lowest PVP-VA concentration of 200μg/mL.

In conclusion, the permeation preformation of a FFA cocrystal formulation is determined by the combination of several factors together, including the type of a polymer, the polymer concentration and coformer. In particular, the interaction between a polymeric excipient with the coformer could play a key role for the improved absorption of APIs studied.

7.5 Chapter Conclusion

In this work, we examined the dissolution and permeation performances of two cocrystals of FFA-NIC COs and FFA-TP COs in the presence of two polymers of PVP and PVP-VA in solution using a dissolution/permeation (D/P) system. The study showed that the type of a polymer, its concentration and the interaction of the polymer with a coformer in solution had significantly effects on the dissolution and permeation performances of FFA cocrystals. It was found that the role of PVP as a stabilizing agency the formulations has not been altered in spite of the interactions with the coformer of NIC or TP in solution, indicating the FFA flux rate from the donor cell to the acceptor cell depends solely on the DPP of a cocrystal formulation. Through selection of an appropriate PVP concentration in solution, the maximal FFA flux rate can be obtained for a given FFA cocrystal formulation. The situation is complicated in a cocrystal formulation in the presence of PVP-VA. The role of PVP-VA in the formulation can be changed due to the association of PVP-VA and a coformer, particularly a transition from a stabilizing agent to a solubilization agent at a very low polymer concentration. Therefore, it is found that in the presence of PVP-VA the FFA flux rate across the membrane in a given formulation is in inverse to its DPP. The maximal FFA flux rate can only be obtained in a cocrystal formulation in the presence

of a very low concentration of PVP-VA. Solution ^{1}H NMR is approved to be a powerful tool in which the atomic-level information of molecular interactions among FFA, coformers and polymers have been revealed. In conclusion, in order to design an optimal cocrystal formulation, we need to explore scientific approaches through mechanistic understanding of the molecular state of drug molecules among API, coformer and plyometric excipients to determine the optimal solubility-permeability balance thereby maximizing the oral drug product performance.

.

Chapter 8 Conclusions and Future works

Conclusions

This dissertation has focused on investigating the dissolution and permeation properties of two cocrystals of FFA-NIC CO and FFA-TP CO in order to design an effective cocrystal formulation. The specific goals of the study were to (1) develop a strategy for selecting desirable polymers to prevent the recrystallization of FFA in supersaturated cocrystals solution; (2) reveal the dissolution mechanism of FFA I and FFA cocrystals and explore how the polymers alter the dissolution pattern of FFA cocrystals and (3) evaluate the underlying relationship between supersaturated state and permeation property of cocrystals during dissolution in presence of pre-dissolved polymers.

The influence of the three polymers PEG, PVP, and PVP-VA on the FFA crystallization in three different supersaturated solutions of the pure FFA and two cocrystals of FFA-NIC CO and FFA-TP CO has been investigated by measuring nucleation induction times and desupersaturation rates in the presence and absence of seed crystals. It was found that the ability of these three polymers on inhibiting the crystallization of FFA is different. Furthermore, it was found that the competition of intermolecular hydrogen bonding among drug/coformer, drug/polymer, and coformer/polymer was a key factor responsible for maintaining the supersaturation through nucleation inhibition and crystal growth modification in a cocrystal solution. Supersaturated cocrystal solutions with predissolved PEG demonstrated the effectiveness at stabilizing supersaturated solution compared to pure FFA in the presence of the same polymer. In contrast, the two cocrystal solutions in the presence of PVP or PVP-VA did not perform as well as pure FFA with the same predissolved polymer. This study suggested that the selection of a polymeric excipient in a cocrystal formulation should not be solely dependent on the interplay of the parent drug and polymer without considering the coformer effects.

Effects of the three polymers, PEG, PVP, and PVP-VA, on the dissolution behavior of cocrystals of FFA-TP CO and FFA-NIC CO were investigated at multiple length scales. At the molecular level, the interactions of a crystal surface with a polymer by observing etching pattern changes using AFM. At the macroscopic scale, dissolution rates of particular faces of a single crystal were determined by measurement of the physical

retreated velocities of the faces using OLM. In the bulk experiments, the FFA concentration in a dissolution medium in the absence or presence of a polymer was measured under both sink and non-sink conditions. It has been found that the dissolution mechanisms of FFA-TP CO are controlled by the defect sites of the crystal surface and by precipitation of the parent drug as individual crystals in the bulk fluid. In contrast, the dissolution mechanisms of FFA-NIC CO are controlled by the surface layer removal and by a surface precipitation mechanism, where the parent drug precipitates directly onto the surface of the dissolving cocrystals as a coating layer. Through controlling the dissolution environment by pre-dissolving the polymer, PVP or PVP-VA, which can interact with the crystal surface to alter its dissolution properties, the advantages of the improved solubility and dissolution rates of the FFA-TP CO and FFA-NIC CO can be demonstrated.

The dissolution and permeation performances of the FFA-NIC CO and FFA-TP CO in the presence of two polymers of PVP and PVP-VA were systematically examined using a dissolution/permeation (D/P) system separated. The study showed that the type and concentration of a polymer and its interaction with a coformer in solution had significant effects on the dissolution and permeation performances of FFA cocrystals. The role of PVP as a stabilizing agent in the formulations was not altered in spite of its interaction with the coformer of NIC or TP in solution, indicating that the FFA flux rate into the acceptor cell was proportional to the dissolution performance parameter (DPP) of a cocrystal formulation. In presence of PVP-VA, the situation was complex for FFA cocrystal. The role of PVP-VA seemed to be changed due to its association with a coformer, i.e., PVP-VA transited from a stabilizing agent to a solubilization agent at a very low polymer concentration. An inverse relationship of the FFA flux rate and its DDP of FFA cocrystals was found in the presence of PVP-VA. The maximal FFA flux rate can only be achieved at a very low concentration of PVP-VA. Finally, the interactions among FFA, coformers and polymers were analyzed at atomic level to gain insight into the mechanism of the supersaturated solution and subsequent permeation behavior of the parent drug by ^{1}H NMR spectroscopy.

Future Works

The future directions can focus on carrying on more fundamental researches on selecting suitable polymers in cocrystal formulation system, scale up, animals test and finally commercial cocrystal products.

Cocrystals have been demonstrated that can improve the solubility, increase the dissolution rate and create a supersaturated state of poorly water solution drugs. But the advantages of cocrystals are reduced because of the recrystallization of stable form in a supersaturated solution. This problem is one of the challenges for developing cocrystals formulation. Although the pre-dissolved polymers can inhibit the recrystallization of API, the mechanism under the effect of polymers on cocrystals has not been fully revealed. More efforts should be made to design a model for predicting the effect of polymers.

The other challenge of cocrystals is to find an effective method to scale up the cocrystal synthesis. Generally, stirred tanks is a convenient option for scale up crystals, but it is not suitable for cocrystals because the harsh requirement of the solubility of cocrystal components. Mechanochemical methods of solid-state grinding is difficult to produce pure cocrystals. Therefore, it is important to find a way to scale up the cocrystal.

So far, animal studies on cocrystals' bioavailability is rare. Only few studies were carried on for exploring the pharmacokinetic properties of cocrystals and found out that not all pharmaceutical cocrystals can improve the pharmacokinetics compared to the pure drugs. Hence, in vivo studies need to be applied to study the bioavailability of cocrystals.

REFERENCES

1. Savjani, K.T., A.K. Gajjar, and J.K. Savjani, *Drug solubility: importance and enhancement techniques.* ISRN pharmaceutics, 2012. **2012**.
2. Qiao, N., et al., *Pharmaceutical cocrystals: an overview.* International journal of pharmaceutics, 2011. **419**(1): p. 1-11.
3. Junyaprasert, V.B. and B. Morakul, *Nanocrystals for enhancement of oral bioavailability of poorly water-soluble drugs.* asian journal of pharmaceutical sciences, 2015. **10**(1): p. 13-23.
4. Neduri, K., V.K. Bontha, and S.K. Vemula, *Different techniques to enhance the dissolution rate of lovastatin: formulation and evaluation.* Asian journal of pharmaceutical and clinical research, 2013. **6**(1): p. 56-60.
5. Chaumeil, J., *Micronization: a method of improving the bioavailability of poorly soluble drugs.* Methods and Findings in Experimental and Clinical Pharmacology, 1998. **20**(3): p. 211-216.
6. Serajuddin, A., *Solid dispersion of poorly water‐soluble drugs: Early promises, subsequent problems, and recent breakthroughs.* Journal of pharmaceutical sciences, 1999. **88**(10): p. 1058-1066.
7. Gao, N., et al., *Application of hot melt extrusion to enhance the dissolution and oral bioavailability of oleanolic acid.* asian journal of pharmaceutical sciences, 2017. **12**(1): p. 66-72.
8. Merisko-Liversidge, E.M. and G.G. Liversidge, *Drug nanoparticles: formulating poorly water-soluble compounds.* Toxicologic pathology, 2008. **36**(1): p. 43-48.
9. Li, M., et al., *Investigation of the effect of hydroxypropyl methylcellulose on the phase transformation and release profiles of carbamazepine-nicotinamide cocrystal.* Pharmaceutical research, 2014. **31**(9): p. 2312-2325.
10. Qiu, S., et al., *Role of polymers in solution and tablet-based carbamazepine cocrystal formulations.* CrystEngComm, 2016. **18**(15): p. 2664-2678.
11. McNamara, D.P., et al., *Use of a glutaric acid cocrystal to improve oral bioavailability of a low solubility API.* Pharmaceutical research, 2006. **23**(8): p. 1888-1897.
12. Variankaval, N., et al., *Preparation and solid-state characterization of nonstoichiometric cocrystals of a phosphodiesterase-IV inhibitor and L-tartaric acid.* Crystal growth & design, 2006. **6**(3): p. 690-700.
13. Blagden, N., et al., *Current directions in co-crystal growth.* New Journal of Chemistry, 2008. **32**(10): p. 1659-1672.
14. Blagden, N., S. Coles, and D. Berry, *Pharmaceutical co-crystals–are we there yet?* CrystEngComm, 2014. **16**(26): p. 5753-5761.
15. Duggirala, N.K., et al., *Pharmaceutical cocrystals: along the path to improved medicines.* Chem Commun (Camb), 2016. **52**(4): p. 640-55.

16. Almeida e Sousa, L., et al., *Supersaturation potential of salt, co-crystal, and amorphous forms of a model weak base.* Crystal Growth & Design, 2016. **16**(2): p. 737-748.

17. Yoshimura, M., et al., *Impact of the Dissolution Profile of the Cilostazol Cocrystal with Supersaturation on the Oral Bioavailability.* Crystal Growth & Design, 2017. **17**(2): p. 550-557.

18. Yamashita, H. and C.C. Sun, *Harvesting potential dissolution advantages of soluble cocrystals by depressing precipitation using the common coformer effect.* Cryst. Growth Des., 2016. **16**(12): p. 6719-6721.

19. Cherukuvada, S., N.J. Babu, and A. Nangia, *Nitrofurantoin–p-aminobenzoic acid cocrystal: Hydration stability and dissolution rate studies.* Journal of pharmaceutical sciences, 2011. **100**(8): p. 3233-3244.

20. Remenar, J.F., et al., *Celecoxib: nicotinamide dissociation: using excipients to capture the cocrystal's potential.* Molecular pharmaceutics, 2007. **4**(3): p. 386-400.

21. Terebetski, J.L. and B. Michniak-Kohn, *Combining ibuprofen sodium with cellulosic polymers: A deep dive into mechanisms of prolonged supersaturation.* International journal of pharmaceutics, 2014. **475**(1): p. 536-546.

22. Curatolo, W., J.A. Nightingale, and S.M. Herbig, *Utility of hydroxypropylmethylcellulose acetate succinate (HPMCAS) for initiation and maintenance of drug supersaturation in the GI milieu.* Pharmaceutical research, 2009. **26**(6): p. 1419-1431.

23. Xu, S. and W.-G. Dai, *Drug precipitation inhibitors in supersaturable formulations.* International Journal of Pharmaceutics, 2013. **453**(1): p. 36-43.

24. Warren, D.B., et al., *Using polymeric precipitation inhibitors to improve the absorption of poorly water-soluble drugs: A mechanistic basis for utility.* Journal of Drug Targeting, 2010. **18**(10): p. 704-731.

25. Beig, A., et al., *Head-To-Head Comparison of Different Solubility-Enabling Formulations of Etoposide and Their Consequent Solubility–Permeability Interplay.* Journal of Pharmaceutical Sciences, 2015. **104**(9): p. 2941-2947.

26. Dahan, A., et al., *The Solubility–Permeability Interplay in Using Cyclodextrins as Pharmaceutical Solubilizers: Mechanistic Modeling and Application to Progesterone.* Journal of Pharmaceutical Sciences, 2010. **99**(6): p. 2739-2749.

27. Miller, J.M., et al., *The solubility–permeability interplay: mechanistic modeling and predictive application of the impact of micellar solubilization on intestinal permeation.* Molecular pharmaceutics, 2011. **8**(5): p. 1848-1856.

28. Sanphui, P., et al., *Cocrystals of Hydrochlorothiazide: Solubility and Diffusion/Permeability Enhancements through Drug–Coformer Interactions.* Molecular Pharmaceutics, 2015. **12**(5): p. 1615-1622.

29. Yan, Y., J.-M. Chen, and T.-B. Lu, *Simultaneously enhancing the solubility and permeability of acyclovir by crystal engineering approach.* CrystEngComm, 2013. **15**(33): p. 6457-6460.

30. Ferretti, V., et al., *Indomethacin Co-Crystals and Their Parent Mixtures: Does the Intestinal Barrier Recognize Them Differently?* Molecular Pharmaceutics, 2015. **12**(5): p. 1501-1511.

31. Thiel-Demby, V.E., et al., *Biopharmaceutics classification system: validation and learnings of an in vitro permeability assay.* Molecular pharmaceutics, 2008. **6**(1): p. 11-18.

32. Food and D. Administration, *Guidance for industry: Waiver of in vivo bioavailability and bioequivalence studies for immediate-release solid oral dosage forms based on a biopharmaceutics classification system.* Food and Drug Administration, Rockville, MD, 2000.

33. Kalepu, S., M. Manthina, and V. Padavala, *Oral lipid-based drug delivery systems–an overview.* Acta Pharmaceutica Sinica B, 2013. **3**(6): p. 361-372.

34. Smith, A.J., et al., *Cocrystals of quercetin with improved solubility and oral bioavailability.* Molecular pharmaceutics, 2011. **8**(5): p. 1867-1876.

35. Jung, J.-Y., et al., *Enhanced solubility and dissolution rate of itraconazole by a solid dispersion technique.* International journal of pharmaceutics, 1999. **187**(2): p. 209-218.

36. Kang, J., et al., *Cyclodextrin complexation: influence on the solubility, stability, and cytotoxicity of camptothecin, an antineoplastic agent.* European Journal of Pharmaceutical Sciences, 2002. **15**(2): p. 163-170.

37. Blagden, N., et al., *Crystal engineering of active pharmaceutical ingredients to improve solubility and dissolution rates.* Advanced drug delivery reviews, 2007. **59**(7): p. 617-630.

38. Atkinson, R.M., et al., *The Effect of Griseofulvin Particle Size on Blood Levels in Man.* Antibiotics & Chemotherapy, 1962. **12**(4): p. 232-8.

39. Reverchon, E., et al., *Solubility and micronization of griseofulvin in supercritical CHF3.* Industrial & engineering chemistry research, 1995. **34**(11): p. 4087-4091.

40. Türk, M., et al., *Micronization of pharmaceutical substances by the rapid expansion of supercritical solutions (RESS): a promising method to improve bioavailability of poorly soluble pharmaceutical agents.* The Journal of supercritical fluids, 2002. **22**(1): p. 75-84.

41. Reverchon, E., et al., *Griseofulvin micronization and dissolution rate improvement by supercritical assisted atomization.* Journal of pharmacy and pharmacology, 2004. **56**(11): p. 1379-1387.

42. Smirnova, I., et al., *Comparison of different methods for enhancing the dissolution rate of poorly soluble drugs: case of griseofulvin.* Engineering in life sciences, 2005. **5**(3): p. 277-280.

43. Carr, A.G., R. Mammucari, and N.R. Foster, *Solubility and micronization of griseofulvin in subcritical water.* Industrial & Engineering Chemistry Research, 2010. **49**(7): p. 3403-3410.

44. Simon, J.A., *Micronized progesterone: vaginal and oral uses.* Clinical obstetrics and gynecology, 1995. **38**(4): p. 902-914.

45. Fitzpatrick, L.A. and A. Good, *Micronized progesterone: clinical indications and comparison with current treatments.* Fertility and sterility, 1999. **72**(3): p. 389-397.

46. Hargrove, J.T., W.S. Maxson, and A. Colston Wentz, *Absorption of oral progesterone is influenced by vehicle and particle size.* American Journal of Obstetrics and Gynecology, 1989. **161**(4): p. 948-951.

47. Huang, Z., et al., *Solubility of progesterone in supercritical carbon dioxide and its micronization through RESS.* Powder Technology, 2014. **258**: p. 66-77.

48. Liversidge, G.G. and K.C. Cundy, *Particle size reduction for improvement of oral bioavailability of hydrophobic drugs: I. Absolute oral bioavailability of nanocrystalline danazol in beagle dogs.* International Journal of Pharmaceutics, 1995. **125**(1): p. 91-97.

49. Jounela, A.J., P.J. Pentikäinen, and A. Sothmann, *Effect of particle size on the bioavailability of digoxin.* European Journal of Clinical Pharmacology, 1975. **8**(5): p. 365-370.

50. Serajuddin, A.T.M., *Solid dispersion of poorly water‐soluble drugs: Early promises, subsequent problems, and recent breakthroughs.* Journal of Pharmaceutical Sciences, 1999. **88**(10): p. 1058-1066.

51. Serajuddin, A.T., *Salt formation to improve drug solubility.* Advanced drug delivery reviews, 2007. **59**(7): p. 603-616.

52. Childs, S.L., G.P. Stahly, and A. Park, *The Salt−Cocrystal Continuum: The Influence of Crystal Structure on Ionization State.* Molecular Pharmaceutics, 2007. **4**(3): p. 323-338.

53. Nelson, E., *Solution rate of theophylline salts and effects from oral administration.* Journal of Pharmaceutical Sciences, 1957. **46**(10): p. 607-614.

54. Nelson, E., *Comparative dissolution rates of weak acids and their sodium salts.* Journal of Pharmaceutical Sciences, 1958. **47**(4): p. 297-299.

55. Furesz, S., *Blood levels following oral administration of different preparations of novobiocin.* Antibiotics & chemotherapy (Northfield, Ill.), 1958. **8**(9): p. 446-449.

56. Nelson, E., et al., *Influence of the absorption rate of tolbutamide on the rate of decline of blood sugar levels in normal humans.* Journal of pharmaceutical sciences, 1962. **51**(6): p. 509-514.

57. Guzmán, H.R., et al., *Combined Use of Crystalline Salt Forms and Precipitation Inhibitors to Improve Oral Absorption of Celecoxib from Solid Oral Formulations.* Journal of Pharmaceutical Sciences, 2007. **96**(10): p. 2686-2702.

58. Gupta, P., V.K. Kakumanu, and A.K. Bansal, *Stability and solubility of celecoxib-PVP amorphous dispersions: a molecular perspective.* Pharmaceutical research, 2004. **21**(10): p. 1762-1769.

59. Abdul-Fattah, A.M. and H.N. Bhargava, *Preparation and in vitro evaluation of solid dispersions of halofantrine.* International Journal of Pharmaceutics, 2002. **235**(1): p. 17-33.

60. Sinha, S., et al., *Solid dispersion as an approach for bioavailability enhancement of poorly water-soluble drug ritonavir.* Aaps Pharmscitech, 2010. **11**(2): p. 518-527.

61. Mayersohn, M. and M. Gibaldi, *New method of solid‐state dispersion for increasing dissolution rates.* Journal of pharmaceutical sciences, 1966. **55**(11): p. 1323-1324.

62. Simonelli, A., S. Mehta, and W. Higuchi, *Dissolution rates of high energy polyvinylpyrrolidone (PVP) - sulfathiazole coprecipitates.* Journal of pharmaceutical sciences, 1969. **58**(5): p. 538-549.

63. Chiou, W.L. and S. Riegelman, *Oral absorption of griseofulvin in dogs: increased absorption viasolid dispersion in polyethylene glycol 6000.* Journal of pharmaceutical sciences, 1970. **59**(7): p. 937-942.

64. Loftsson, T. and M.E. Brewster, *Pharmaceutical applications of cyclodextrins. 1. Drug solubilization and stabilization.* Journal of pharmaceutical sciences, 1996. **85**(10): p. 1017-1025.

65. Rajewski, R.A. and V.J. Stella, *Pharmaceutical applications of cyclodextrins. 2. In vivo drug delivery.* Journal of pharmaceutical sciences, 1996. **85**(11): p. 1142-1169.

66. Szejtli, J., *Cyclodextrins and Their Inclusion Complexes, Akademiai Kiado, Budapest, 1982; Search PubMed; J. Szejtli, Cyclodextrin Technology*. 1988, Kluwer Academic Publishers, Budapest.

67. Gould, S. and R.C. Scott, *2-Hydroxypropyl-β-cyclodextrin (HP-β-CD): a toxicology review.* Food and Chemical Toxicology, 2005. **43**(10): p. 1451-1459.

68. BREWSTER, M.E., et al., *The use of solubilizing excipients and approaches to generate toxicology vehicles for contemporary drug pipelines*, in *Solvent systems and their selection in pharmaceutics and biopharmaceutics*. 2007, Springer. p. 221-256.

69. Ammar, H., S. El-Nahhas, and R. Khalil, *Cyclodextrins in acetazolamide eye drop formulations.* Die Pharmazie, 1998. **53**(8): p. 559-562.

70. Brewster, M.E., et al., *Development of aqueous parenteral formulations for carbamazepine through the use of modified cyclodextrins.* Journal of pharmaceutical sciences, 1991. **80**(4): p. 380-383.

71. Ran, Y., et al., *Solubilization of cyclosporin A.* Aaps Pharmscitech, 2001. **2**(1): p. 23-26.

72. Almeida, H.M. and H.M.C. Marques, *Physicochemical characterization of finasteride: PEG 6000 and finasteride: Kollidon K25 solid dispersions, and finasteride: β-cyclodextrin inclusion complexes.* Journal of Inclusion Phenomena and Macrocyclic Chemistry, 2011. **70**(3-4): p. 397-406.

73. Moyano, J., et al., *Study of the dissolution characteristics of oxazepam via complexation with β-cyclodextrin.* International Journal of Pharmaceutics, 1995. **114**(1): p. 95-102.

74. Trapani, G., et al., *Inclusion complexation of propofol with 2-hydroxypropyl-β-cyclodextrin. Physicochemical, nuclear magnetic resonance spectroscopic studies, and anesthetic properties in rat.* Journal of pharmaceutical sciences, 1998. **87**(4): p. 514-518.

75. Tønnesen, H.H., M. Másson, and T. Loftsson, *Studies of curcumin and curcuminoids. XXVII. Cyclodextrin complexation: solubility, chemical and photochemical stability.* International Journal of Pharmaceutics, 2002. **244**(1): p. 127-135.

76. Brewster, M.E. and T. Loftsson, *Cyclodextrins as pharmaceutical solubilizers.* Advanced drug delivery reviews, 2007. **59**(7): p. 645-666.

77. Stahly, G.P., *A survey of cocrystals reported prior to 2000.* Crystal Growth & Design, 2009. **9**(10): p. 4212-4229.

78. Wöhler, F., *Untersuchungen über das Chinon.* European Journal of Organic Chemistry, 1844. **51**(2): p. 145-163.

79. Schultheiss, N. and A. Newman, *Pharmaceutical Cocrystals and Their Physicochemical Properties.* Crystal Growth & Design, 2009. **9**(6): p. 2950-2967.

80. Shan, N. and M.J. Zaworotko, *The role of cocrystals in pharmaceutical science.* Drug discovery today, 2008. **13**(9): p. 440-446.

81. Jones, W., W.S. Motherwell, and A.V. Trask, *Pharmaceutical cocrystals: an emerging approach to physical property enhancement.* MRS bulletin, 2006. **31**(11): p. 875-879.

82. Ito, K. and K. Sekiguchi, *Studies on the molecular compounds of organic medicinals. II. Application of the solubility product principle and consideration by the phase rule to the solubility phenomena of the molecular compound of sulfanilamide and sulfathiazole.* Chemical and Pharmaceutical Bulletin, 1966. **14**(3): p. 255-262.

83. Perumalla, S.R. and C.C. Sun, *Design and Preparation of a 4:1 Lamivudine–Oxalic Acid CAB Cocrystal for Improving the Lamivudine Purification Process.* Crystal Growth & Design, 2014. **14**(8): p. 3990-3995.

84. Stanton, M.K. and A. Bak, *Physicochemical Properties of Pharmaceutical Co-Crystals: A Case Study of Ten AMG 517 Co-Crystals.* Crystal Growth & Design, 2008. **8**(10): p. 3856-3862.

85. Wenger, M. and J. Bernstein, *An Alternate Crystal Form of Gabapentin: A Cocrystal with Oxalic Acid.* Crystal Growth & Design, 2008. **8**(5): p. 1595-1598.

86. Childs, S.L. and K.I. Hardcastle, *Cocrystals of piroxicam with carboxylic acids.* Crystal Growth & Design, 2007. **7**(7): p. 1291-1304.

87. Basavoju, S., D. Boström, and S.P. Velaga, *Pharmaceutical cocrystal and salts of norfloxacin.* Crystal growth & design, 2006. **6**(12): p. 2699-2708.

88. Karagianni, A., M. Malamatari, and K. Kachrimanis, *Pharmaceutical Cocrystals: New Solid Phase Modification Approaches for the Formulation of APIs.* Pharmaceutics, 2018. **10**(1): p. 18.

89. Desiraju, G.R., *Crystal engineering. From molecules to materials.* Journal of molecular structure, 2003. **656**(1): p. 5-15.

90. Rodríguez-Spong, B., et al., *General principles of pharmaceutical solid polymorphism: a supramolecular perspective.* Advanced drug delivery reviews, 2004. **56**(3): p. 241-274.

91. Desiraju, G.R., *Hydrogen bridges in crystal engineering: interactions without borders.* Accounts of chemical research, 2002. **35**(7): p. 565-573.

92. Etter, M.C. and G.M. Frankenbach, *Hydrogen-bond directed cocrystallization as a tool for designing acentric organic solids.* Chemistry of Materials, 1989. **1**(1): p. 10-12.

93. Etter, M.C., *Hydrogen bonds as design elements in organic chemistry.* The Journal of Physical Chemistry, 1991. **95**(12): p. 4601-4610.

94. Donohue, J., *The hydrogen bond in organic crystals.* The Journal of Physical Chemistry, 1952. **56**(4): p. 502-510.

95. Etter, M.C., *Encoding and decoding hydrogen-bond patterns of organic compounds.* Accounts of Chemical Research, 1990. **23**(4): p. 120-126.

96. Etter, M.C., *Aggregate structures of carboxylic acids and amides.* Israel Journal of Chemistry, 1985. **25**(3-4): p. 312-319.

97. Leiserowitz, L., *Molecular packing modes. Carboxylic acids.* Acta Crystallographica Section B: Structural Crystallography and Crystal Chemistry, 1976. **32**(3): p. 775-802.

98. Leiserowitz, L. and G. Schmidt, *Molecular packing modes. Part III. Primary amides.* Journal of the Chemical Society A: Inorganic, Physical, Theoretical, 1969: p. 2372-2382.

99. Miroshnyk, I., S. Mirza, and N. Sandler, *Pharmaceutical co-crystals–an opportunity for drug product enhancement.* Expert opinion on drug delivery, 2009. **6**(4): p. 333-341.

100. Desiraju, G.R., *Supramolecular synthons in crystal engineering—a new organic synthesis.* Angewandte Chemie International Edition, 1995. **34**(21): p. 2311-2327.

101. Stahly, G.P., *Diversity in single-and multiple-component crystals. The search for and prevalence of polymorphs and cocrystals.* Crystal Growth & Design, 2007. **7**(6): p. 1007-1026.

102. He, G., et al., *Screening for cocrystallization tendency: the role of intermolecular interactions.* The Journal of Physical Chemistry B, 2008. **112**(32): p. 9890-9895.

103. Orpen, A.G., *Applications of the Cambridge Structural Database to molecular inorganic chemistry.* Acta Crystallographica Section B: Structural Science, 2002. **58**(3): p. 398-406.

104. Zhang, G.G., et al., *Efficient co-crystal screening using solution-mediated phase transformation.* Journal of pharmaceutical sciences, 2007. **96**(5): p. 990-995.

105. Childs, S.L., et al., *Screening strategies based on solubility and solution composition generate pharmaceutically acceptable cocrystals of carbamazepine.* CrystEngComm, 2008. **10**(7): p. 856-864.

106. Trask, A.V. and W. Jones, *Crystal engineering of organic cocrystals by the solid-state grinding approach.* Organic solid state reactions, 2005: p. 131-131.

107. Etter, M.C., S.M. Reutzel, and C.G. Choo, *Self-organization of adenine and thymine in the solid state.* Journal of the American Chemical Society, 1993. **115**(10): p. 4411-4412.

108. Caira, M.R., L.R. Nassimbeni, and A.F. Wildervanck, *Selective formation of hydrogen bonded cocrystals between a sulfonamide and aromatic carboxylic acids in the solid state.* Journal of the Chemical Society, Perkin Transactions 2, 1995(12): p. 2213-2216.

109. Kuroda, R., Y. Imai, and N. Tajima, *Generation of a co-crystal phase with novel coloristic properties via solid state grinding procedures.* Chemical Communications, 2002(23): p. 2848-2849.

110. Friščić, T., et al., *Screening for inclusion compounds and systematic construction of three-component solids by liquid-assisted grinding.* Angewandte Chemie, 2006. **118**(45): p. 7708-7712.

111. Pal, S., et al., *Thermal studies of furosemide–caffeine binary system that forms a cocrystal.* Journal of Thermal Analysis and Calorimetry, 2014. **115**(3): p. 2261-2268.

112. Berry, D.J., et al., *Applying hot-stage microscopy to co-crystal screening: a study of nicotinamide with seven active pharmaceutical ingredients.* Crystal Growth and Design, 2008. **8**(5): p. 1697-1712.

113. Etter, M.C., G.M. Frankenbach, and D.A. Adsmond, *Using hydrogen bonds to design acentric organic materials for nonlinear optical users.* Molecular Crystals and Liquid Crystals, 1990. **187**(1): p. 25-39.

114. Karki, S., et al., *Screening for pharmaceutical cocrystal hydrates via neat and liquid-assisted grinding.* Molecular pharmaceutics, 2007. **4**(3): p. 347-354.

115. Jung, S., I. Choi, and I.W. Kim, *Liquid-assisted grinding to prepare a cocrystal of adefovir dipivoxil thermodynamically less stable than its neat phase.* Crystals, 2015. **5**(4): p. 583-591.

116. Rahman, Z., et al., *Physico-mechanical and stability evaluation of carbamazepine cocrystal with nicotinamide.* AAPS PharmSciTech, 2011. **12**(2): p. 693-704.

117. Picknett, T.M. and S. Brenner, *X-Ray Crystallography*, in *Encyclopedia of Genetics*. 2001, Academic Press: New York. p. 2154.

118. Pan, Q., et al., *Comparative crystal structure determination of griseofulvin: Powder X-ray diffraction versus single-crystal X-ray diffraction.* Chinese Science Bulletin, 2012. **57**(30): p. 3867-3871.

119. Elbagerma, M., et al., *Characterization of new cocrystals by Raman spectroscopy, powder X-ray diffraction, differential scanning calorimetry, and transmission Raman spectroscopy.* Crystal Growth & Design, 2010. **10**(5): p. 2360-2371.

120. Schultheiss, N. and A. Newman, *Pharmaceutical cocrystals and their physicochemical properties.* Crystal growth and design, 2009. **9**(6): p. 2950-2967.

121. Vogt, F.G., et al., *Solid-state NMR analysis of organic cocrystals and complexes.* Crystal Growth and Design, 2008. **9**(2): p. 921-937.

122. Byrn, S.R., G. Zografi, and X.S. Chen, *Solid-State Properties of Pharmaceutical Materials*. 2017: John Wiley & Sons.

123. Buanz, A.B., G.N. Parkinson, and S. Gaisford, *Characterization of carbamazepine-nicatinamide cocrystal polymorphs with rapid heating DSC and XRPD.* Crystal Growth & Design, 2011. **11**(4): p. 1177-1181.

124. Good, D.J. and N.r. Rodríguez-Hornedo, *Solubility advantage of pharmaceutical cocrystals.* Crystal Growth and Design, 2009. **9**(5): p. 2252-2264.

125. Spong, B.R., *Enhancing the pharmaceutical behavior of poorly soluble drugs through the formation of cocrystals and mesophases*. 2005.

126. Trask, A.V., W.S. Motherwell, and W. Jones, *Pharmaceutical cocrystallization: engineering a remedy for caffeine hydration.* Crystal Growth & Design, 2005. **5**(3): p. 1013-1021.

127. Trask, A.V., W.D.S. Motherwell, and W. Jones, *Physical stability enhancement of theophylline via cocrystallization.* International Journal of Pharmaceutics, 2006. **320**(1): p. 114-123.

128. Basavoju, S., D. Boström, and S.P. Velaga, *Indomethacin–Saccharin Cocrystal: Design, Synthesis and Preliminary Pharmaceutical Characterization.* Pharmaceutical Research, 2008. **25**(3): p. 530-541.

129. Krantz, J.C., et al., *Sodium theophylline glycinate.* Journal of Pharmaceutical Sciences, 1947. **36**(8): p. 248-250.

130. Naito, T., H. Shirai, and N. Oda, *Molecular Compounds of Sulfa Drugs.* YAKUGAKU ZASSHI, 1953. **73**(7): p. 663-665.

131. Aakeröy, C.B., S. Forbes, and J. Desper, *Using Cocrystals To Systematically Modulate Aqueous Solubility and Melting Behavior of an Anticancer Drug.* Journal of the American Chemical Society, 2009. **131**(47): p. 17048-17049.

132. Remenar, J.F., et al., *Crystal engineering of novel cocrystals of a triazole drug with 1, 4-dicarboxylic acids.* Journal of the American Chemical Society, 2003. **125**(28): p. 8456-8457.

133. Chen, Y., et al., *Improving the Solubility and Bioavailability of Apixaban via Apixaban–Oxalic Acid Cocrystal.* Crystal Growth & Design, 2016. **16**(5): p. 2923-2930.

134. Childs, S.L., P. Kandi, and S.R. Lingireddy, *Formulation of a Danazol Cocrystal with Controlled Supersaturation Plays an Essential Role in Improving Bioavailability.* Molecular Pharmaceutics, 2013. **10**(8): p. 3112-3127.

135. Bak, A., et al., *The co-crystal approach to improve the exposure of a water-insoluble compound: AMG 517 sorbic acid co-crystal characterization and pharmacokinetics.* Journal of pharmaceutical sciences, 2008. **97**(9): p. 3942-3956.

136. Jung, M.S., et al., *Bioavailability of indomethacin-saccharin cocrystals.* Journal of Pharmacy and Pharmacology, 2010. **62**(11): p. 1560-1568.

137. Gao, Y., H. Zu, and J. Zhang, *Enhanced dissolution and stability of adefovir dipivoxil by cocrystal formation.* Journal of Pharmacy and Pharmacology, 2011. **63**(4): p. 483-490.

138. El-Gizawy, S.A., et al., *Aerosil as a novel co-crystal co-former for improving the dissolution rate of hydrochlorothiazide.* International journal of pharmaceutics, 2015. **478**(2): p. 773-778.

139. Childs, S.L., et al., *Crystal engineering approach to forming cocrystals of amine hydrochlorides with organic acids. Molecular complexes of fluoxetine hydrochloride with benzoic, succinic, and fumaric acids.* Journal of the American Chemical Society, 2004. **126**(41): p. 13335-13342.

140. Shiraki, K., et al., *Dissolution improvement and the mechanism of the improvement from cocrystallization of poorly water-soluble compounds.* Pharmaceutical research, 2008. **25**(11): p. 2581-2592.

141. Huang, N. and N. Rodríguez-Hornedo, *Engineering cocrystal solubility, stability, and pHmax by micellar solubilization.* Journal of pharmaceutical sciences, 2011. **100**(12): p. 5219-5234.

142. Lee, H.G., G.G. Zhang, and D. Flanagan, *Cocrystal intrinsic dissolution behavior using a rotating disk.* Journal of pharmaceutical sciences, 2011. **100**(5): p. 1736-1744.

143. Greco, K. and R. Bogner, *Solution-mediated phase transformation: Significance during dissolution and implications for bioavailability.* Journal of pharmaceutical sciences, 2012. **101**(9): p. 2996-3018.

144. Guo, M., et al., *Insight into Flufenamic Acid Cocrystal Dissolution in the Presence of a Polymer in Solution: from Single Crystal to Powder Dissolution.* Molecular pharmaceutics, 2017.

145. Qiao, N., et al., *In situ monitoring of carbamazepine–nicotinamide cocrystal intrinsic dissolution behavior.* European Journal of Pharmaceutics and Biopharmaceutics, 2013. **83**(3): p. 415-426.

146. Qiu, S. and M. Li, *Effects of coformers on phase transformation and release profiles of carbamazepine cocrystals in hydroxypropyl methylcellulose based matrix tablets.* International Journal of Pharmaceutics, 2015. **479**(1): p. 118-128.

147. Cao, F., et al., *Mechanistic Basis of Cocrystal Dissolution Advantage.* Journal of pharmaceutical sciences, 2018. **107**(1): p. 380-389.

148. Myerson, A.S. and R. Ginde, *Crystals, crystal growth, and nucleation*, in *Handbook of Industrial Crystallization (Second Edition)*. 2002, Elsevier. p. 33-65.

149. Callahan, C. and X.-W. Ni, *The Influence of hydrodynamic environment on the nucleation mechanism of a chiral crystallization*. 2014, Heriot-Watt University.

150. Khan, M., *Solid dispersions: Formulation, characterisation, permeability and genomic evaluation*. 2010, Aston University.

151. Hartman, P. and W.G. Perdok, *On the relations between structure and morphology of crystals. I.* Acta Crystallographica, 1955. **8**(1): p. 49-52.

152. Seddon, K.R. and M. Zaworotko, *Crystal engineering: the design and application of functional solids*. Vol. 539. 1999: Springer Science & Business Media.

153. Warren, D.B., et al., *Using polymeric precipitation inhibitors to improve the absorption of poorly water-soluble drugs: A mechanistic basis for utility.* Journal of drug targeting, 2010. **18**(10): p. 704-731.

154. Shi, N.-Q., J. Yao, and X.-L. Wang, *Effect of polymers and media type on extending the dissolution of amorphous pioglitazone and inhibiting the recrystallization from a supersaturated state.* Drug development and industrial pharmacy, 2014. **40**(8): p. 1112-1122.

155. Huang, N. and N. Rodríguez-Hornedo, *Effect of Micellar Solubilization on Cocrystal Solubility and Stability.* Crystal Growth & Design, 2010. **10**(5): p. 2050-2053.

156. DiNunzio, J.C., et al., *Amorphous compositions using concentration enhancing polymers for improved bioavailability of itraconazole.* Molecular pharmaceutics, 2008. **5**(6): p. 968-980.

157. Ilevbare, G.A., et al., *Understanding Polymer Properties Important for Crystal Growth Inhibition Impact of Chemically Diverse Polymers on Solution Crystal Growth of Ritonavir.* Crystal Growth & Design, 2012. **12**(6): p. 3133-3143.

158. Zimmermann, A., et al., *Adsorption of pharmaceutical excipients onto microcrystals of siramesine hydrochloride: effects on physicochemical properties.* European Journal of Pharmaceutics and Biopharmaceutics, 2009. **71**(1): p. 109-116.

159. Raghavan, S., et al., *Crystallization of hydrocortisone acetate: influence of polymers.* International journal of pharmaceutics, 2001. **212**(2): p. 213-221.

160. Kuminek, G., et al., *Cocrystals to facilitate delivery of poorly soluble compounds beyond-rule-of-5.* Advanced drug delivery reviews, 2016. **101**: p. 143-166.

161. Ueda, K., et al., *Inhibitory effect of hydroxypropyl methylcellulose acetate succinate on drug recrystallization from a supersaturated solution assessed using nuclear magnetic resonance measurements.* Molecular pharmaceutics, 2013. **10**(10): p. 3801-3811.

162. Ozaki, S., et al., *Inhibition of crystal nucleation and growth by water-soluble polymers and its impact on the supersaturation profiles of amorphous drugs.* Journal of pharmaceutical sciences, 2013. **102**(7): p. 2273-2281.

163. Ilevbare, G.A., et al., *Maintaining supersaturation in aqueous drug solutions: impact of different polymers on induction times.* Crystal Growth & Design, 2012. **13**(2): p. 740-751.

164. Trasi, N.S., et al., *Evaluating the influence of polymers on nucleation and growth in supersaturated solutions of acetaminophen.* CrystEngComm, 2015. **17**(6): p. 1242-1248.

165. Alonzo, D.E., et al., *Characterizing the impact of hydroxypropylmethyl cellulose on the growth and nucleation kinetics of felodipine from supersaturated solutions.* Crystal Growth & Design, 2012. **12**(3): p. 1538-1547.

166. Schram, C.J., S.P. Beaudoin, and L.S. Taylor, *Impact of polymer conformation on the crystal growth inhibition of a poorly water-soluble drug in aqueous solution.* Langmuir, 2014. **31**(1): p. 171-179.

167. Tian, F., et al., *The influence of various excipients on the conversion kinetics of carbamazepine polymorphs in aqueous suspension.* Journal of pharmacy and pharmacology, 2007. **59**(2): p. 193-201.

168. Pan, Z., A. Campbell, and P. Somasundaran, *Polyacrylic acid adsorption and conformation in concentrated alumina suspensions.* Colloids and Surfaces A: Physicochemical and Engineering Aspects, 2001. **191**(1-2): p. 71-78.

169. Ilevbare, G.A., et al., *Impact of Polymers on Crystal Growth Rate of Structurally Diverse Compounds from Aqueous Solution.* Molecular Pharmaceutics, 2013. **10**(6): p. 2381-2393.

170. Duro, R., et al., *Cellulose ethers-polysorbate 80 interactions. Implications on the stability of pyrantel pamoate suspensions.* Chem. Pharm. Bull, 1998. **46**: p. 1421-1427.

171. Rodríguez-hornedo, N. and D. Murphy, *Significance of controlling crystallization mechanisms and kinetics in pharmaceutical systems.* Journal of Pharmaceutical Sciences, 1999. **88**(7): p. 651-660.

172. Vandecruys, R., et al., *Use of a screening method to determine excipients which optimize the extent and stability of supersaturated drug solutions and application of this system to solid formulation design.* International journal of pharmaceutics, 2007. **342**(1-2): p. 168-175.

173. Ozaki, S., et al., *Inhibition of crystal nucleation and growth by water-soluble polymers and its impact on the supersaturation profiles of amorphous drugs.* Journal of pharmaceutical sciences, 2013. **102**(7): p. 2273-2281.

174. Alhalaweh, A., H.R.H. Ali, and S.P. Velaga, *Effects of Polymer and Surfactant on the Dissolution and Transformation Profiles of Cocrystals in Aqueous Media.* Crystal Growth & Design, 2014. **14**(2): p. 643-648.

175. Williams III, R.O., A.B. Watts, and D.A. Miller, *Formulating poorly water soluble drugs*. 2012: Springer.

176. Ozaki, S., et al., *Supersaturation–Nucleation Behavior of Poorly Soluble Drugs and its Impact on the Oral Absorption of Drugs in Thermodynamically High-Energy Forms.* Journal of Pharmaceutical Sciences, 2012. **101**(1): p. 214-222.

177. Schram, C.J., S.P. Beaudoin, and L.S. Taylor, *Polymer inhibition of crystal growth by surface poisoning.* Crystal Growth & Design, 2016. **16**(4): p. 2094-2103.

178. Vandecruys, R., et al., *Use of a screening method to determine excipients which optimize the extent and stability of supersaturated drug solutions and application of this system to solid formulation design.* International Journal of Pharmaceutics, 2007. **342**(1): p. 168-175.

179. Sun, D.D. and P.I. Lee, *Evolution of supersaturation of amorphous pharmaceuticals: the effect of rate of supersaturation generation.* Molecular pharmaceutics, 2013. **10**(11): p. 4330-4346.

180. Konno, H., et al., *Effect of polymer type on the dissolution profile of amorphous solid dispersions containing felodipine.* European Journal of Pharmaceutics and Biopharmaceutics, 2008. **70**(2): p. 493-499.

181. Bevernage, J., et al., *Drug precipitation–permeation interplay: Supersaturation in an absorptive environment.* European Journal of Pharmaceutics and Biopharmaceutics, 2012. **82**(2): p. 424-428.

182. Crowley, K.J. and G. Zografi, *The effect of low concentrations of molecularly dispersed poly (vinylpyrrolidone) on indomethacin crystallization from the amorphous state.* Pharmaceutical research, 2003. **20**(9): p. 1417-1422.

183. Guo, M., et al., *Investigating the influence of polymers on supersaturated flufenamic acid cocrystal solutions.* Molecular pharmaceutics, 2016. **13**(9): p. 3292-3307.

184. Brandel, C. and J.H. ter Horst, *Measuring induction times and crystal nucleation rates.* Faraday discussions, 2015. **179**: p. 199-214.

185. Skibsted, L.H., J. Risbo, and M.L. Andersen, *Chemical deterioration and physical instability of food and beverages*. 2010: Elsevier.

186. Deubener, J., R. Brückner, and M. Sternitzke, *Induction time analysis of nucleation and crystal growth in di-and metasilicate glasses.* Journal of non-crystalline solids, 1993. **163**(1): p. 1-12.

187. Chen, J., et al., *Impact of surfactants on the crystallization of aqueous suspensions of celecoxib amorphous solid dispersion spray dried particles.* Molecular pharmaceutics, 2015. **12**(2): p. 533-541.

188. Raina, S.A., et al., *Impact of polymers on the crystallization and phase transition kinetics of amorphous nifedipine during dissolution in aqueous media.* Molecular pharmaceutics, 2014. **11**(10): p. 3565-3576.

189. Guo, M., et al., *Insight into Flufenamic Acid Cocrystal Dissolution in the Presence of a Polymer in Solution: from Single Crystal to Powder Dissolution.* Mol Pharm, 2017. **14**(12): p. 4583-4596.

190. Pingali, K.C., et al., *AFM study of hydrophilicity on acetaminophen crystals.* International journal of pharmaceutics, 2012. **438**(1-2): p. 184-190.

191. Wen, H., et al., *How solvents affect acetaminophen etching pattern formation: Interaction between solvent and acetaminophen at the solid/liquid interface.* The Journal of Physical Chemistry B, 2004. **108**(7): p. 2270-2278.

192. Wen, H., K.R. Morris, and K. Park, *Synergic effects of polymeric additives on dissolution and crystallization of acetaminophen.* Pharmaceutical research, 2008. **25**(2): p. 349-358.

193. Li, T., K.R. Morris, and K. Park, *Influence of solvent and crystalline supramolecular structure on the formation of etching patterns on acetaminophen single crystals: A study with atomic force microscopy and computer simulation.* The Journal of Physical Chemistry B, 2000. **104**(9): p. 2019-2032.

194. Vasil'chenko, M., et al., *Topochemistry of the initial stages of the dissolution of single crystals of acetaminophen.* Journal of pharmaceutical sciences, 1996. **85**(9): p. 929-934.

195. Plomp, M., W. Van Enckevort, and E. Vlieg, *Etching and surface termination of K2Cr2O7 {0 0 1} faces observed using in situ atomic force microscopy.* Journal of crystal growth, 2000. **216**(1-4): p. 413-427.

196. Danesh, A., et al., *An in situ dissolution study of aspirin crystal planes (100) and (001) by atomic force microscopy.* Pharmaceutical research, 2001. **18**(3): p. 299-303.

197. Mersmann, A., C. Heyer, and A. Eble, *Activated nucleation.* Crystallization technology handbook, 2001. **2**.

198. Adobes-Vidal, M., et al., *Face-discriminating dissolution kinetics of furosemide single crystals: in situ three-dimensional multi-microscopy and modeling.* Crystal Growth & Design, 2016. **16**(8): p. 4421-4429.

199. Kramarenko, E.Y., et al., *Molecular dynamics simulation study of adsorption of polymer chains with variable degree of rigidity. I. Static properties.* The Journal of chemical physics, 1996. **104**(12): p. 4806-4813.

200. Wen, H., K.R. Morris, and K. Park, *Hydrogen bonding interactions between adsorbed polymer molecules and crystal surface of acetaminophen.* Journal of colloid and interface science, 2005. **290**(2): p. 325-335.

201. Prasad, K.V.R., et al., *Dissolution kinetics of paracetamol single crystals.* International Journal of Pharmaceutics, 2002. **238**(1): p. 29-41.

202. Perry, A.R., M. Peruffo, and P.R. Unwin, *Quantitative Plane-Resolved Crystal Growth and Dissolution Kinetics by Coupling In Situ Optical Microscopy and Diffusion Models: The Case of Salicylic Acid in Aqueous Solution.* Crystal Growth & Design, 2013. **13**(2): p. 614-622.

203. Raghavan, S., et al., *Dissolution kinetics of single crystals of α-lactose monohydrate.* Journal of pharmaceutical sciences, 2002. **91**(10): p. 2166-2174.

204. Higuchi, T., *Physical chemical analysis of percutaneous absorption process from creams and ointments.* J. Soc. Cosmet. Chem, 1960. **11**: p. 85-97.

205. Corrigan, O., M. Farvar, and W. Higuchi, *Drug membrane transport enhancement using high energy drug polyvinylpyrrolidone (PVP) co-precipitates.* International Journal of Pharmaceutics, 1980. **5**(3): p. 229-238.

206. Davis, A. and J. Hadgraft, *Effect of supersaturation on membrane transport: 1. Hydrocortisone acetate.* International journal of pharmaceutics, 1991. **76**(1-2): p. 1-8.

207. Pellett, M., A. Davis, and J. Hadgraft, *Effect of supersaturation on membrane transport: 2. Piroxicam.* International journal of pharmaceutics, 1994. **111**(1): p. 1-6.

208. Kumprakob, U., J. Kawakami, and I. Adachi, *Permeation enhancement of ketoprofen using a supersaturated system with antinucleant polymers.* Biological and Pharmaceutical Bulletin, 2005. **28**(9): p. 1684-1688.

209. Santos, P., et al., *Enhanced permeation of fentanyl from supersaturated solutions in a model membrane.* International journal of pharmaceutics, 2011. **407**(1-2): p. 72-77.

210. Frank, K.J., et al., *Amorphous solid dispersion enhances permeation of poorly soluble ABT-102: true supersaturation vs. apparent solubility enhancement.* International journal of pharmaceutics, 2012. **437**(1-2): p. 288-293.

211. Miller, J.M., et al., *A win–win solution in oral delivery of lipophilic drugs: supersaturation via amorphous solid dispersions increases apparent solubility without sacrifice of intestinal membrane permeability.* Molecular pharmaceutics, 2012. **9**(7): p. 2009-2016.

212. Raina, S.A., et al., *Impact of solubilizing additives on supersaturation and membrane transport of drugs.* Pharmaceutical research, 2015. **32**(10): p. 3350-3364.

213. Miller, J.M., et al., *The solubility-permeability interplay when using cosolvents for solubilization: revising the way we use solubility-enabling formulations.* Mol Pharm, 2012. **9**(3): p. 581-90.

214. Miller, J.M. and A. Dahan, *Predicting the solubility–permeability interplay when using cyclodextrins in solubility-enabling formulations: model validation.* International journal of pharmaceutics, 2012. **430**(1-2): p. 388-391.

215. Beig, A., J.M. Miller, and A. Dahan, *Accounting for the solubility–permeability interplay in oral formulation development for poor water solubility drugs: the effect of PEG-400 on carbamazepine absorption.* European Journal of Pharmaceutics and Biopharmaceutics, 2012. **81**(2): p. 386-391.

216. Ueda, K., et al., *Mechanistic Differences in Permeation Behavior of Supersaturated and Solubilized Solutions of Carbamazepine Revealed by Nuclear Magnetic Resonance Measurements.* Molecular Pharmaceutics, 2012. **9**(11): p. 3023-3033.

217. Otsuka, N., et al., *An Insight into Different Stabilization Mechanisms of Phenytoin Derivatives Supersaturation by HPMC and PVP*. Journal of Pharmaceutical Sciences, 2015. **104**(8): p. 2574-2582.

218. Wilkinson, J.H. and I.L. Finar, *6. A study of the properties of fluorine-substituted 5-aminoacridines and related compounds. Part II. 5-Amino-2-and -4-trifluoromethyl acridines.* Journal of the Chemical Society (Resumed), 1948(0): p. 32-35.

219. Winder, C.V., et al., *Anti-inflammatory and antipyretic properties of N-(α, α, α-Trifluoro-m-tolyl) anthranilic acid (CI-440; flufenamic acid).* Arthritis & Rheumatology, 1963. **6**(1): p. 36-47.

220. Flower, R., et al., *Effects of Anti-inflammatory Drugs on Prostaglandin Biosynthesis.* Nature New Biology, 1972. **238**: p. 104.

221. Domanska, U., A. Pobudkowska, and A. Pelczarska, *Solubility of sparingly soluble drug derivatives of anthranilic acid.* The Journal of Physical Chemistry B, 2011. **115**(11): p. 2547-2554.

222. Rajan, K., et al., *Flufenamic acid in rheumatoid arthritis.* Annals of the rheumatic diseases, 1967. **26**(1): p. 43.

223. Guinamard, R., C. Simard, and C. Del Negro, *Flufenamic acid as an ion channel modulator.* Pharmacology & therapeutics, 2013. **138**(2): p. 272-284.

224. Khansari, P.S. and R.F. Halliwell, *Evidence for neuroprotection by the fenamate NSAID, mefenamic acid.* Neurochemistry International, 2009. **55**(7): p. 683-688.

225. Lee, S.-H., et al., *Activating transcription factor 2 (ATF2) controls tolfenamic acid-induced ATF3 expression via MAP kinase pathways.* Oncogene, 2010. **29**(37): p. 5182-5192.

226. López-Mejías, V., J.W. Kampf, and A.J. Matzger, *Nonamorphism in Flufenamic Acid and a New Record for a Polymorphic Compound with Solved Structures.* Journal of the American Chemical Society, 2012. **134**(24): p. 9872-9875.

227. KRC, J.J., *Crystallographic properties of flufenamic*

acid, [N-(á,á,á trifluoro-m-tolyl) anthranilic acid]. Microscope 1977. **25**(1): p. 31-45.

228. Abignente, E. and P. de Caprariis, *Flufenamic Acid*, in *Analytical Profiles of Drug Substances*, K. Florey, Editor. 1982, Academic Press. p. 313-346.

229. Aitipamula, S., et al., *Cocrystallization with flufenamic acid: comparison of physicochemical properties of two pharmaceutical cocrystals.* CrystEngComm, 2014. **16**(26): p. 5793-5801.

230. Konno, T., *Physical and Chemical Changes of Medicinals in Mixtures with Adsorbents in the Solid State. IV.: Study on Reduced-Pressure Mixing for Practical Use of Amorphous Mixtures of Flufenamic Acid.* Chemical and Pharmaceutical Bulletin, 1990. **38**(7): p. 2003-2007.

231. ITAI, S., et al., *Influence of wetting factors on the dissolution behavior of flufenamic acid.* Chemical and Pharmaceutical Bulletin, 1985. **33**(12): p. 5464-5473.

232. Belhocine, Y., et al., *Inclusion Complex Formation of β-Cyclodextrin with the Nonsteroidal Anti-inflammatory Drug Flufenamic Acid: Computational Study.*

233. Peterson, S.A., et al., *Inhibiting transthyretin conformational changes that lead to amyloid fibril formation.* Proceedings of the National Academy of Sciences, 1998. **95**(22): p. 12956-12960.

234. Fábián, L., et al., *Cocrystals of fenamic acids with nicotinamide.* Crystal Growth & Design, 2011. **11**(8): p. 3522-3528.

235. Delaney, S.P. and T.M. Korter, *Terahertz Spectroscopy and Computational Investigation of the Flufenamic Acid/Nicotinamide Cocrystal.* The Journal of Physical Chemistry A, 2015. **119**(13): p. 3269-3276.

236. Nechipadappu, S.K., V. Tekuri, and D.R. Trivedi, *Pharmaceutical Co-Crystal of Flufenamic Acid: Synthesis and Characterization of Two Novel Drug-Drug Co-Crystal.* Journal of Pharmaceutical Sciences, 2017. **106**(5): p. 1384-1390.

237. Green, K.N., et al., *Nicotinamide restores cognition in Alzheimer's disease transgenic mice via a mechanism involving sirtuin inhibition and selective reduction of Thr231-phosphotau.* Journal of Neuroscience, 2008. **28**(45): p. 11500-11510.

238. Hino, T., J.L. Ford, and M.W. Powell, *Assessment of nicotinamide polymorphs by differential scanning calorimetry.* Thermochimica Acta, 2001. **374**(1): p. 85-92.

239. Li, J., S.A. Bourne, and M.R. Caira, *New polymorphs of isonicotinamide and nicotinamide.* Chemical Communications, 2011. **47**(5): p. 1530-1532.

240. Yano, Y., et al., *Anti-fibrotic effects of theophylline on lung fibroblasts.* Biochemical and Biophysical Research Communications, 2006. **341**(3): p. 684-690.

241. Saikia, B., et al., *Hydrogen bond synthons in the interplay of solubility and membrane permeability/diffusion in variable stoichiometry drug cocrystals.* Crystal Growth & Design, 2015. **15**(11): p. 5593-5603.

242. Markad, D. and S.K. Mandal, *An exploration into the amide–pseudo amide hydrogen bonding synthon between a new coformer with two primary amide groups and theophylline.* CrystEngComm, 2017. **19**(47): p. 7112-7124.

243. Sekhon, B.S., *Drug-drug co-crystals*. 2012, BioMed Central.

244. Aitipamula, S., P.S. Chow, and R.B. Tan, *Trimorphs of a pharmaceutical cocrystal involving two active pharmaceutical ingredients: potential relevance to combination drugs.* CrystEngComm, 2009. **11**(9): p. 1823-1827.

245. Neurohr, C., et al., *Naproxen–Nicotinamide Cocrystals: Racemic and Conglomerate Structures Generated by CO2 Antisolvent Crystallization.* Crystal Growth & Design, 2015. **15**(9): p. 4616-4626.

246. Remenar, J.F., et al., *Celecoxib:Nicotinamide Dissociation: Using Excipients To Capture the Cocrystal's Potential.* Molecular Pharmaceutics, 2007. **4**(3): p. 386-400.

247. Huang, Y., et al., *Baicalein–Nicotinamide Cocrystal with Enhanced Solubility, Dissolution, and Oral Bioavailability.* Journal of Pharmaceutical Sciences, 2014. **103**(8): p. 2330-2337.

248. Soares, F.L.F. and R.L. Carneiro, *Green Synthesis of Ibuprofen–Nicotinamide Cocrystals and In-Line Evaluation by Raman Spectroscopy.* Crystal Growth & Design, 2013. **13**(4): p. 1510-1517.

249. Zhao, L., et al., *From discovery to scale-up: [small alpha]-lipoic acid : nicotinamide co-crystals in a continuous oscillatory baffled crystalliser.* CrystEngComm, 2014. **16**(26): p. 5769-5780.

250. Sopyan, I., et al., *Simvastatin-nicotinamide co-crystal: design, preparation and preliminary characterization.* Tropical Journal of Pharmaceutical Research, 2017. **16**(2): p. 297-303.

251. Chow, S.F., et al., *Simultaneously Improving the Mechanical Properties, Dissolution Performance, and Hygroscopicity of Ibuprofen and Flurbiprofen by Cocrystallization with Nicotinamide.* Pharmaceutical Research, 2012. **29**(7): p. 1854-1865.

252. Berry, D.J., et al., *Applying Hot-Stage Microscopy to Co-Crystal Screening: A Study of Nicotinamide with Seven Active Pharmaceutical Ingredients.* Crystal Growth & Design, 2008. **8**(5): p. 1697-1712.

253. Wang, L., et al., *Pharmaceutical Cocrystals of Diflunisal with Nicotinamide or Isonicotinamide.* Organic Process Research & Development, 2013. **17**(11): p. 1413-1418.

254. Lin, H.-L., et al., *An Investigation of Indomethacin–Nicotinamide Cocrystal Formation Induced by Thermal Stress in the Solid or Liquid State.* Journal of Pharmaceutical Sciences, 2014. **103**(8): p. 2386-2395.

255. Pujari, T.A., *Cocrystals of nutraceuticals: Protocatechuic acid and quercetin.* 2009.

256. Chan, H.C.S., *Co-crystal screening of poorly water-soluble active pharmaceutical ingredients. Application of hot stage microscopy on curcumin-nicotinamide system and construction of ternary phase diagram of fenbufen-nicotinamide-water co-crystal system*. 2010, University of Bradford.

257. Chiodo, T., et al., *Multicomponent crystals comprising dasatinib and selected co-crystal formers*. 2016, Google Patents.

258. Haeria, A.N. and I. Ismail, *Characterization and Dissolution Test of Aspirin-Nicotinamide Cocrystal.* substance, 2015. **4**(5): p. 8-12.

259. Ueto, T., et al., *Polymorphs and a Hydrate of Furosemide–Nicotinamide 1:1 Cocrystal*. Crystal Growth & Design, 2012. **12**(1): p. 485-494.

260. Bevill, M.J., P.I. Vlahova, and J.P. Smit, *Polymorphic Cocrystals of Nutraceutical Compound p-Coumaric Acid with Nicotinamide: Characterization, Relative Solid-State Stability, and Conversion to Alternate Stoichiometries.* Crystal Growth & Design, 2014. **14**(3): p. 1438-1448.

261. Holland, J., D. Gooding, and A. Chorlton, *Rebamipide complexes and cocrystals*. 2016, Google Patents.

262. Gao, Y., et al., *Coformer selection based on degradation pathway of drugs: a case study of adefovir dipivoxil–saccharin and adefovir dipivoxil–nicotinamide cocrystals.* International journal of pharmaceutics, 2012. **438**(1-2): p. 327-335.

263. Renkoğlu, P., M. Çelebier, and B. Arıca-Yegin, *HPLC determination of olanzapine and carbamazepine in their nicotinamide cocrystals and investigation of the dissolution profiles of cocrystal tablet formulations.* Pharmaceutical development and technology, 2015. **20**(3): p. 380-384.

264. George, N., et al., *Co-crystals of propiconazole*. 2012, Google Patents.

265. Lu, J. and S. Rohani, *Preparation and characterization of theophylline− nicotinamide cocrystal.* Organic Process Research & Development, 2009. **13**(6): p. 1269-1275.

266. Vigilante, N.J. and M.A. Mehta, *A 13C solid-state NMR investigation of four cocrystals of caffeine and theophylline.* Acta Crystallographica Section C: Structural Chemistry, 2017. **73**(3): p. 234-243.

267. Mukaida, M., et al., *Stability Orders of Acetaminophen and Theophylline Co-crystals Determined by Co-crystal Former Exchange Reactions and Their Correlation With In Silico and Thermal Parameters.* Journal of pharmaceutical sciences, 2017. **106**(1): p. 258-263.

268. Goyal, P., D. Rani, and R. Chadha, *Crystal Engineering: A Remedy to Tailor the Biopharmaceutical Aspects of Glibenclamide.* Crystal Growth & Design, 2017.

269. Goud, N.R., R.A. Khan, and A. Nangia, *Modulating the solubility of sulfacetamide by means of cocrystals.* CrystEngComm, 2014. **16**(26): p. 5859-5869.

270. Surov, A.O., et al., *Pharmaceutical cocrystals of diflunisal and diclofenac with theophylline.* Molecular pharmaceutics, 2014. **11**(10): p. 3707-3715.

271. Leuner, C. and J. Dressman, *Improving drug solubility for oral delivery using solid dispersions.* European Journal of Pharmaceutics and Biopharmaceutics, 2000. **50**(1): p. 47-60.

272. Narang, A.S. and S.H. Boddu, *Excipient applications in formulation design and drug delivery*, in *Excipient Applications in Formulation Design and Drug Delivery*. 2015, Springer. p. 1-10.

273. Zhu, Q., M.T. Harris, and L.S. Taylor, *Modification of Crystallization Behavior in Drug/Polyethylene Glycol Solid Dispersions.* Molecular Pharmaceutics, 2012. **9**(3): p. 546-553.

274. Ma, X., J. Taw, and C.-M. Chiang, *Control of drug crystallization in transdermal matrix system.* International journal of pharmaceutics, 1996. **142**(1): p. 115-119.

275. Lindfors, L., et al., *Nucleation and crystal growth in supersaturated solutions of a model drug.* Journal of Colloid and Interface Science, 2008. **325**(2): p. 404-413.

276. Matsumoto, T. and G. Zografi, *Physical properties of solid molecular dispersions of indomethacin with poly (vinylpyrrolidone) and poly (vinylpyrrolidone-co-vinyl-acetate) in relation to indomethacin crystallization.* Pharmaceutical research, 1999. **16**(11): p. 1722-1728.

277. Van den Mooter, G., et al., *Physical stabilisation of amorphous ketoconazole in solid dispersions with polyvinylpyrrolidone K25.* European journal of pharmaceutical sciences, 2001. **12**(3): p. 261-269.

278. Taylor, L.S. and G. Zografi, *Spectroscopic characterization of interactions between PVP and indomethacin in amorphous molecular dispersions.* Pharmaceutical research, 1997. **14**(12): p. 1691-1698.

279. Mumper, R.J., et al., *Protective interactive noncondensing (PINC) polymers for enhanced plasmid distribution and expression in rat skeletal muscle.* Journal of Controlled Release, 1998. **52**(1): p. 191-203.

280. Chen, S., et al., *Preparation and Characterization of Solid Dispersions of Dipyridamole with a Carrier "Copolyvidonum Plasdone® S-630".* Drug development and industrial pharmacy, 2007. **33**(8): p. 888-899.

281. Kestur, U.S. and L.S. Taylor, *Role of polymer chemistry in influencing crystal growth rates from amorphous felodipine.* CrystEngComm, 2010. **12**(8): p. 2390-2397.

282. Kanaujia, P., et al., *Nanoparticle formation and growth during in vitro dissolution of ketoconazole solid dispersion.* Journal of pharmaceutical sciences, 2011. **100**(7): p. 2876-2885.

283. Shibata, Y., et al., *Effect of storage conditions on the recrystallization of drugs in solid dispersions with crospovidone.* Pharmaceutical development and technology, 2014. **19**(4): p. 468-474.

284. Rahman, M.M., et al., *Iron oxide nanoparticles*, in *Nanomaterials*. 2011, InTech.

285. Montenegro, R.V., *Crystallization, biomimetics and semiconducting polymers in confined systems.(German Title: Kristallisation, Biomimetik und halbleitende Polymere in räumlich begrenzten Systemen).* 2003.

286. Beig, A., et al., *Advantageous solubility-permeability interplay when using amorphous solid dispersion (ASD) formulation for the BCS class IV P-gp substrate rifaximin: simultaneous increase of both the solubility and the permeability.* The AAPS journal, 2017. **19**(3): p. 806-813.

287. Zeng, G., et al., *Nanomechanics of Amyloid Materials Studied by Atomic Force Microscopy*, in *Atomic Force Microscopy Investigations into Biology-From Cell to Protein*. 2012, InTech.

288. Fedors, R.F., *A method for estimating both the solubility parameters and molar volumes of liquids.* Polymer Engineering & Science, 1974. **14**(2): p. 147-154.

289. Stefanis, E. and C. Panayiotou, *Prediction of Hansen solubility parameters with a new group-contribution method.* International Journal of Thermophysics, 2008. **29**(2): p. 568-585.

290. Barton, A.F., *CRC Handbook of Solubility Parameters and Other Cohesion Parameters*. 1991: CRC Press.

291. Chen, Y., et al., *Drug–Polymer–Water Interaction and Its Implication for the Dissolution Performance of Amorphous Solid Dispersions.* Molecular Pharmaceutics, 2015. **12**(2): p. 576-589.

292. *DIFFUSION TESTING FUNDAMENTALS*. Available from: http://permegear.com/wp-content/uploads/2015/08/primer.pdf.

293. Jabeen, S., et al., *Raman and IR spectroscopic studies of fenamates – Conformational differences in polymorphs of flufenamic acid, mefenamic acid and tolfenamic acid.* Spectrochimica Acta Part A: Molecular and Biomolecular Spectroscopy, 2012. **96**: p. 972-985.

294. Ramalingam, S., et al., *FT-IR and FT-Raman vibrational spectra and molecular structure investigation of nicotinamide: A combined experimental and theoretical study*. Spectrochimica Acta Part A: Molecular and Biomolecular Spectroscopy, 2010. **75**(5): p. 1552-1558.

295. Aitipamula, S., et al., *Cocrystallization with flufenamic acid: comparison of physicochemical properties of two pharmaceutical cocrystals.* CrystEngComm, 2014. **16**(26): p. 5793-5801.

296. Yamashita, T., S. Ozaki, and I. Kushida, *Solvent shift method for anti-precipitant screening of poorly soluble drugs using biorelevant medium and dimethyl sulfoxide.* International Journal of Pharmaceutics, 2011. **419**(1–2): p. 170-174.

297. Alvarez, A.J., A. Singh, and A.S. Myerson, *Polymorph Screening: Comparing a Semi-Automated Approach with a High Throughput Method.* Crystal Growth & Design, 2009. **9**(9): p. 4181-4188.

298. Jabeen, S., et al., *Raman and IR spectroscopic studies of fenamates–Conformational differences in polymorphs of flufenamic acid, mefenamic acid and tolfenamic acid.* Spectrochimica Acta Part A: Molecular and Biomolecular Spectroscopy, 2012. **96**: p. 972-985.

299. Vekilov, P.G., *The two-step mechanism of nucleation of crystals in solution.* Nanoscale, 2010. **2**(11): p. 2346-2357.

300. Baranska, M. and H. Schulz, *Chapter 4 Determination of Alkaloids through Infrared and Raman Spectroscopy*, in *The Alkaloids: Chemistry and Biology*, A.C. Geoffrey, Editor. 2009, Academic Press. p. 217-255.

301. Van Eerdenbrugh, B. and L.S. Taylor, *An ab initiopolymer selection methodology to prevent crystallization in amorphous solid dispersions by application of crystal engineering principles.* CrystEngComm, 2011. **13**(20): p. 6171-6178.

302. Raina, S.A., et al., *Enhancements and limits in drug membrane transport using supersaturated solutions of poorly water soluble drugs.* Journal of pharmaceutical sciences, 2014. **103**(9): p. 2736-2748.

303. Indulkar, A.S., et al., *Exploiting the phenomenon of liquid–liquid phase separation for enhanced and sustained membrane transport of a poorly water-soluble drug.* Molecular pharmaceutics, 2016. **13**(6): p. 2059-2069.

304. Hendriksen, B.A., et al., *Crystallisation of paracetamol (acetaminophen) in the presence of structurally related substances.* Journal of Crystal Growth, 1998. **183**(4): p. 629-640.

305. Lou, B. and S.P. Velaga, *Polymorph control of felodipine form II in an attempted cocrystallization.* Crystal Growth and Design, 2009. **9**(3): p. 1254-1257.

306. Thomas, L.H., et al., *Paracetamol form II: an elusive polymorph through facile multicomponent crystallization routes.* Crystal Growth & Design, 2011. **11**(5): p. 1450-1452.

307. Yoreo, J.J.D. and P.G. Vekilov, *Principles of crystal nucleation and growth*. Vol. 54. 2003.

308. Ilevbare, G.A., et al., *Effect of Binary Additive Combinations on Solution Crystal Growth of the Poorly Water-Soluble Drug, Ritonavir.* Crystal Growth & Design, 2012. **12**(12): p. 6050-6060.

309. Good, D.J. and N. Rodríguez-Hornedo, *Solubility Advantage of Pharmaceutical Cocrystals.* Crystal Growth & Design, 2009. **9**(5): p. 2252-2264.

310. Delaney, S.P., T.M. Smith, and T.M. Korter, *Conformational origins of polymorphism in two forms of flufenamic acid.* Journal of Molecular Structure, 2014. **1078**: p. 83-89.

311. Li, M., N. Qiao, and K. Wang, *Influence of Sodium Lauryl Sulfate and Tween 80 on Carbamazepine–Nicotinamide Cocrystal Solubility and Dissolution Behavior*. Pharmaceutics, 2013. **5**(4): p. 508.

312. Putra, O.D., et al., *Solubility improvement of epalrestat by layered structure formation via cocrystallization.* CrystEngComm, 2017. **19**(19): p. 2614-2622.

313. Hu, Y., et al., *Crystallization Monitoring by Raman Spectroscopy: Simultaneous Measurement of Desupersaturation Profile and Polymorphic Form in Flufenamic Acid Systems.* Industrial & Engineering Chemistry Research, 2005. **44**(5): p. 1233-1240.

314. Wen, H., et al., *How Solvents Affect Acetaminophen Etching Pattern Formation: Interaction between Solvent and Acetaminophen at the Solid/Liquid Interface.* The Journal of Physical Chemistry B, 2004. **108**(7): p. 2270-2278.

315. Wen, H., et al., *Dissolution Study on Aspirin and α-Glycine Crystals.* The Journal of Physical Chemistry B, 2004. **108**(30): p. 11219-11227.

316. Li, T., K.R. Morris, and K. Park, *Influence of Tailor-Made Additives on Etching Patterns of Acetaminophen Single Crystals.* Pharmaceutical Research, 2001. **18**(3): p. 398-402.

317. Vasil'chenko, M.A., et al., *Topochemistry of the initial stages of the dissolution of single crystals of acetaminophen.* Journal of Pharmaceutical Sciences, 1996. **85**(9): p. 929-934.

318. Li, T., K.R. Morris, and K. Park, *Influence of Solvent and Crystalline Supramolecular Structure on the Formation of Etching Patterns on Acetaminophen Single Crystals: A Study with Atomic Force Microscopy and Computer Simulation.* The Journal of Physical Chemistry B, 2000. **104**(9): p. 2019-2032.

319. Bukovec, P., et al., *Influence of crystal habit on the dissolution of simvastatin single crystals*. 2015. Vol. 62. 2015.

320. Abu-Diak, O.A., D.S. Jones, and G.P. Andrews, *An Investigation into the Dissolution Properties of Celecoxib Melt Extrudates: Understanding the Role of Polymer Type and Concentration in Stabilizing Supersaturated Drug Concentrations.* Molecular Pharmaceutics, 2011. **8**(4): p. 1362-1371.

321. Maniruzzaman, M., et al., *Drug–polymer intermolecular interactions in hot-melt extruded solid dispersions.* International Journal of Pharmaceutics, 2013. **443**(1): p. 199-208.

322. Ueda, K., et al., *Equilibrium State at Supersaturated Drug Concentration Achieved by Hydroxypropyl Methylcellulose Acetate Succinate: Molecular Characterization Using 1H NMR Technique.* Molecular Pharmaceutics, 2015. **12**(4): p. 1096-1104.

323. Ueda, K., K. Higashi, and K. Moribe, *Direct NMR Monitoring of Phase Separation Behavior of Highly Supersaturated Nifedipine Solution Stabilized with Hypromellose Derivatives.* Molecular Pharmaceutics, 2017. **14**(7): p. 2314-2322.

324. Ueda, K., et al., *In situ molecular elucidation of drug supersaturation achieved by nano-sizing and amorphization of poorly water-soluble drug.* European Journal of Pharmaceutical Sciences, 2015. **77**: p. 79-89.

325. Roscigno, P., et al., *Complex Formation between Poly(vinylpyrrolidone) and Sodium Decyl Sulfate Studied through NMR.* Langmuir, 2003. **19**(23): p. 9638-9644.

326. Prasad, D., H. Chauhan, and E. Atef, *Role of Molecular Interactions for Synergistic Precipitation Inhibition of Poorly Soluble Drug in Supersaturated Drug–Polymer–Polymer Ternary Solution.* Molecular Pharmaceutics, 2016. **13**(3): p. 756-765.

327. Chen, Y., et al., *Sodium Lauryl Sulfate Competitively Interacts with HPMC-AS and Consequently Reduces Oral Bioavailability of Posaconazole/HPMC-AS*

Amorphous Solid Dispersion. Molecular Pharmaceutics, 2016. **13**(8): p. 2787-2795.

328. Singha, N.C. and D.N. Sathyanarayana, *1H and 13C NMR spectral studies of conformation of some N-(2-pyridinyl)-3-pyridinecarboxamides.* Journal of Molecular Structure, 1998. **449**(1): p. 91-98.

329. Munro, S.L.A. and D.J. Craik, *NMR conformational studies of fenamate non-steroidal anti-inflammatory drugs.* Magnetic Resonance in Chemistry, 1994. **32**(6): p. 335-342.

330. You, Z.Y., et al., *Synthesis of Deuterium Labeled Standards of 1-Benzylpiperazine, Fenetylline, Nicocodeine and Nicomorphine.* Journal of the Chinese Chemical Society, 2008. **55**(3): p. 663-667.

331. Ma, J.-h., et al., *Probing Paeonol−Pluronic Polymer Interactions by 1H NMR Spectroscopy.* The Journal of Physical Chemistry B, 2007. **111**(47): p. 13371-13378.

332. Ma, J.-h., et al., *Interaction of Urea with Pluronic Block Copolymers by 1H NMR Spectroscopy.* The Journal of Physical Chemistry B, 2007. **111**(19): p. 5155-5161.

333. Charman, W., et al., *Self-Association of Nicotinamide in Aqueous-Solution: N.M.R. Studies of Nicotinamide and the Mono- and Di-methyl-Substituted Amide Analogs.* Australian Journal of Chemistry, 1993. **46**(3): p. 377-385.

334. Bobrovs, R., L. Seton, and N. Dempster, *The reluctant polymorph: investigation into the effect of self-association on the solvent mediated phase transformation and nucleation of theophylline.* CrystEngComm, 2015. **17**(28): p. 5237-5251.

335. Guo, M., et al., *Insight into Flufenamic Acid Cocrystal Dissolution in the Presence of a Polymer in Solution: from Single Crystal to Powder Dissolution.* Molecular Pharmaceutics, 2017. **14**(12): p. 4583-4596.

336. Dahan, A., et al., *The solubility–permeability interplay and oral drug formulation design: Two heads are better than one.* Advanced Drug Delivery Reviews, 2016. **101**: p. 99-107.

337. Borbás, E., et al., *Investigation and Mathematical Description of the Real Driving Force of Passive Transport of Drug Molecules from Supersaturated Solutions.* Molecular Pharmaceutics, 2016. **13**(11): p. 3816-3826.

338. Dahan, A. and J.M. Miller, *The Solubility–Permeability Interplay and Its Implications in Formulation Design and Development for Poorly Soluble Drugs.* The AAPS Journal, 2012. **14**(2): p. 244-251.

339. Raina, S.A., et al., *Impact of Solubilizing Additives on Supersaturation and Membrane Transport of Drugs.* Pharmaceutical Research, 2015. **32**(10): p. 3350-3364.

340. Humpolíčková, J., et al., *Solvent Relaxation Study of pH-Dependent Hydration of Poly(oxyethylene) Shells in Polystyrene-block-poly(2-vinylpyridine)-block-poly(oxyethylene) Micelles in*

Aqueous Solutions. The Journal of Physical Chemistry A, 2005. **109**(48): p. 10803-10812.

341. Oliveira, C.P., et al., *The effect of water-soluble polymers, PEG and PVP, on the solubilization of griseofulvin in aqueous micellar solutions of Pluronic F127.* International Journal of Pharmaceutics, 2011. **421**(2): p. 252-257.

APPENDIXES

A1 Figures and Tables for Chapter 4

Table A1. 1 Summary of IR peak identities of FFA I, NIC, TP, FFA-NIC CO and FFA-TP CO

Sample	Peak position (cm^{-1})	Function group
FFA I	3318	-N-H stretching
	1651	-(C=O)- stretching
NIC	3353	-N-H stretching
	1592	Pyridine ring stretching
FFA-NIC CO	3395	-N-H stretching of NIC
	3324	-N-H stretching of FFA
	1660	-(C=O)- stretching of FFA
	1608	Pyridine ring stretching of NIC
TP	3119	-N-H stretching
	1660	-C=O stretching
	1561	-C=N stretching
FFA-TP CO	3280	-N-H stretching of FFA
	3068	-N-H stretching of TP
	1669	-(C=O)- stretching of TP
	1647	-(C=O)- stretching of FFA
	1558	-C=N stretching of TP

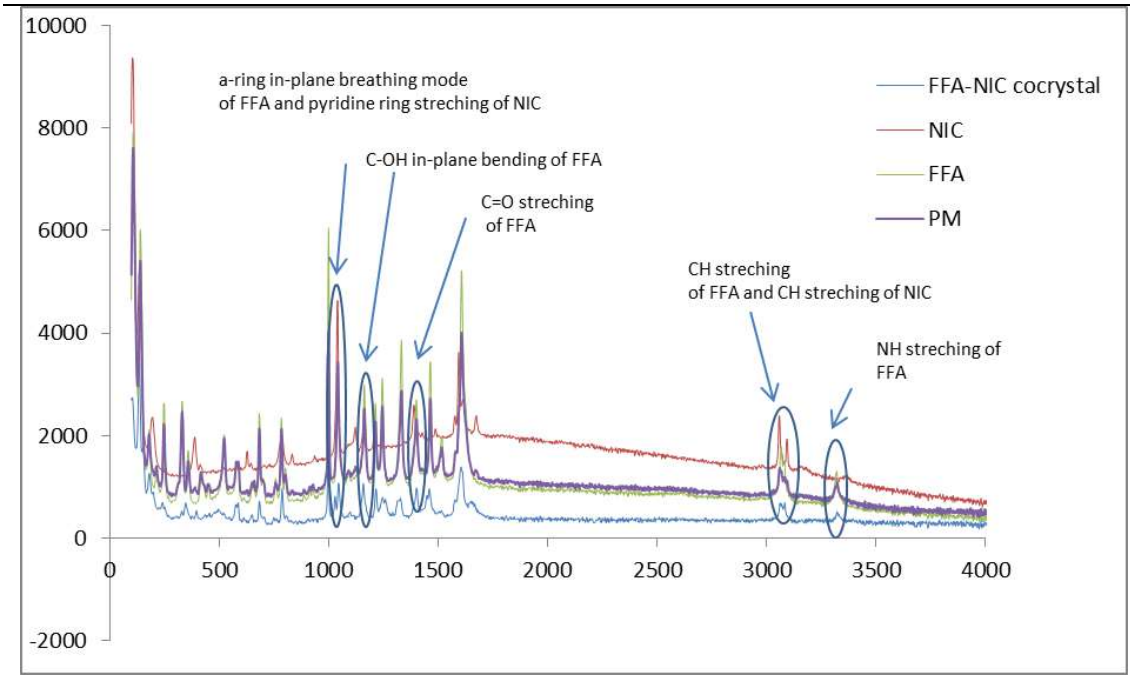

(a)

Figure A1. 1 Raman results of FFA I, NIC and FFA-NIC CO: (a) Raman spectra; (b) summary of Raman peak identities

Functional group	FFA peak (cm^{-1})	NIC peak (cm^{-1})	FFA-NIC CO peak (cm^{-1})
NH stretching	3319	---------	3321
CH stretching	3064	3056/3092	3060/3082
C=O stretching	-------	1669	-----
Benzene ring stretching coupled with in-plane NH deformation and CN stretching.	1515	----------	1513w
In-plane CH deformation coupling with benzene ring deformation	1402, 1462,	----------	1400,1458
C=O stretching	1397	----------	1402
CN and C=C stretching	1331	----------	1327
In-plane CH deformation, CN stretching combined with in-plane NH deformation	1244	----------	1246,1256 (double peak)
pyridine ring stretching	-------	1155	1158
in-plane C-OH bending	1162	---------	1158
Antisymmetric CF_3 structure	1085	----------	1158

In-plane CH blending	------	1121	1097
NH2 rock	--------	1092vw	1097vw
pyridine ring stretching	--------	1041	1029, 1043 (double peak)
out-of-plane CH bending	-------	832	----------
In-plane ring bending		784	794
Vibrations of CF_3	648, 756	---------	649,749

(b)

Figure A1. 2 Raman results of FFA I, TP and FFA-TP CO: (a) Raman spectra; (b) summary of Raman peak identities

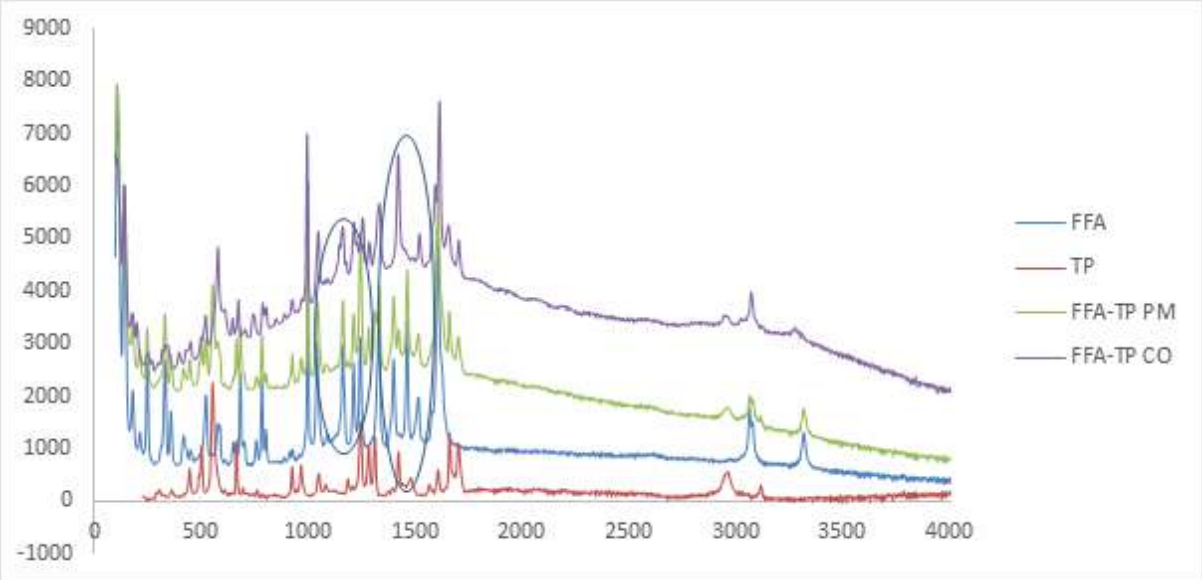

(a)

Functional group	FFA peak (cm^{-1})	TP peak (cm^{-1})	FFA-TP CO peak (cm^{-1})
NH stretching	3319	3122	3269, 3077
CH stretching	3064	---------	3077
C=O stretching	-------	1706, 1663	1710, 1661
C-C stretching	------	1611	1613
Benzene ring stretching coupled with in-plane NH deformation and CN stretching.	1515	----------	1520
In-plane CH deformation coupling with benzene ring deformation	1402, 1462,	1425	1425
C=O stretching	1397	----------	1423

		-	
CN and C=C stretching	1331	----------	1332
In-plane CH deformation, CN stretching combined with in-plane NH deformation	1244	1249	1258
in-plane C-OH bending	1162	---------	1161, 1165 double peaks
Antisymmetric CF_3 structure	1100	----------	1100
N-CH_3 stretching	--------	1090, 1054	1100, 1051
CH_3 rocking	--------	970	965
Imidazole in-plane ring deformation	-------	928	930
Pyrimidine In-plane ring deformation	-------	662	686
Vibrations of CF_3	648, 760	-------	651, 746
Pyrimidine breathing	-----	555	576

(b)

A2 Figures and Tables for Chapter 5

Table A2. 1 SP values of FFA, NIC, TP, and polymers

NIC		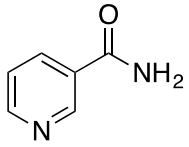	
Group	Fdi	Fpi^2	Ehi
=CH-(4)	800	0	0
=C- (1)	70	0	0
 (1)	290	592900	4500
$-NH_2$ (1)	280	-	8400
-N=(1)	164	1750329	1759
Sum	1604	2343229	14659
$Vm=M/\rho=122.13(g/mol)/1.4463(g/cm^3)=84.35\ (cm^3/mol)$ $\delta_d=\sum Fdi/\ Vm=1440/8435=19.01 MPa^{(1/2)}$ $\delta_p=18.14\ MPa^{(1/2)}$ $\delta_h=13.18 MPa^{(1/2)}$ $\delta=(\delta_d^2+\delta_p^2+\delta_h^2)^{(1/2)}=29.39\ MPa^{(1/2)}$			
TP		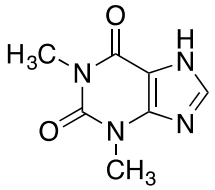	
Group	F_{di}	Fpi^2	Ehi
CH_3(2)	840	0	0
=CH (1)	200	0	0
=C-(2)	140	0	0
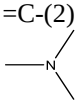 (2)	40	2560000	10000
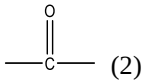 (2)	580	2371600	4000
-NH- (1)	160	44100	3100
=N-(1)	164	1750329	1759
sum	2124	6726029	18859
$Vm=M/\rho=180.164g/mol)/1.493(g/cm^3)=120.67\ (cm^3/mol)$ $\delta_d=\sum Fdi/\ Vm=17.6 MPa^{(1/2)}$ $\delta_p=21.49\ MPa^{(1/2)}$ $\delta_h=11.9 MPa^{(1/2)}$ $\delta=(\delta_d^2+\delta_p^2+\delta_h^2)^{(1/2)}=30.21\ MPa^{(1/2)}$			
PEG		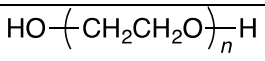	
Group	Fdi	Fpi^2	Ehi
$-CH_2-$(2)	540	0	0
-O- (1)	100	160000	3000
Sum	640	160000	3000

Vm=M/ρ=44(g/mol)/1.17(g/cm^3)=37.6(cm^3/mol)
δ_d=∑Fdi/ Vm=640/37.6=17MPa$^{(1/2)}$
δ_p=10.64MPa$^{(1/2)}$
δ_h=8.9MPa$^{(1/2)}$
$\delta=(\delta_d^2+\delta_p^2+\delta_h^2)^{(1/2)}$= 21.94MPa$^{(1/2)}$

PVP

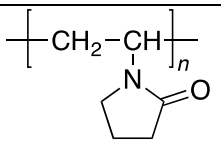

Group	Fdi	Fpi^2	Ehi
-CH_2-(4)	1080	0	0
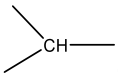 (1)	80	0	0
 (1)	20	640000	5000
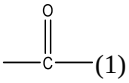 (1)	290	592900	2000
Sum	1470	1232900	7000

Vm=M/ρ=111(g/mol)/1.17(g/cm^3)=94.9(cm^3/mol)
δ_d =∑Fdi/ Vm=1470/94.9=15.5 MPa$^{(1/2)}$
δ_p=11.7 MPa$^{(1/2)}$
δ_h=8.6MPa$^{(1/2)}$
$\delta=(\delta_d^2+\delta_p^2+\delta_h^2)^{(1/2)}$= 21.24MPa$^{(1/2)}$

PVP-VA S-630

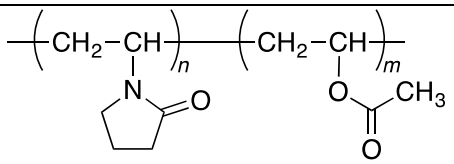

Group	Fdi	Fpi^2	Ehi
-CH3- (1)	420	0	0
-CH_2-(5)	1350	0	0
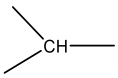 (2)	160	0	0
 (1)	20	640000	5000
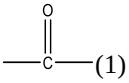 (1)	290	592900	2000
-coo-(1)	390	240100	7000
Sum	2630	1473000	14000

Vm=M/ρ=197(g/mol)/1.27(g/cm^3)=155.1 (cm^3/mol)
δ_d=∑Fdi/ Vm=2630/155.1= 17.0MPa$^{(1/2)}$
δ_p=7.8 MPa$^{(1/2)}$
δ_h=9.5MPa$^{(1/2)}$
$\delta=(\delta_d^2+\delta_p^2+\delta_h^2)^{(1/2)}$= 20.98MPa$^{(1/2)}$

Figure A2. 1 FTIR examining results of solid residuals after solubility test: (a) FFA; (b) FFA-NIC CO; (c) FFA-TP CO

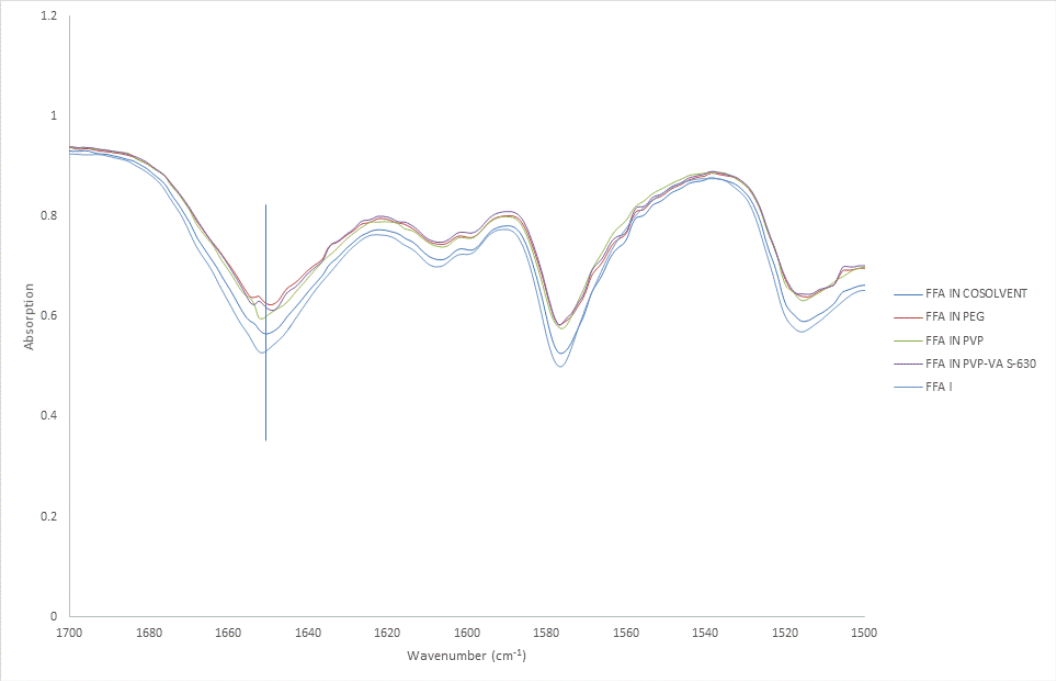

(a)

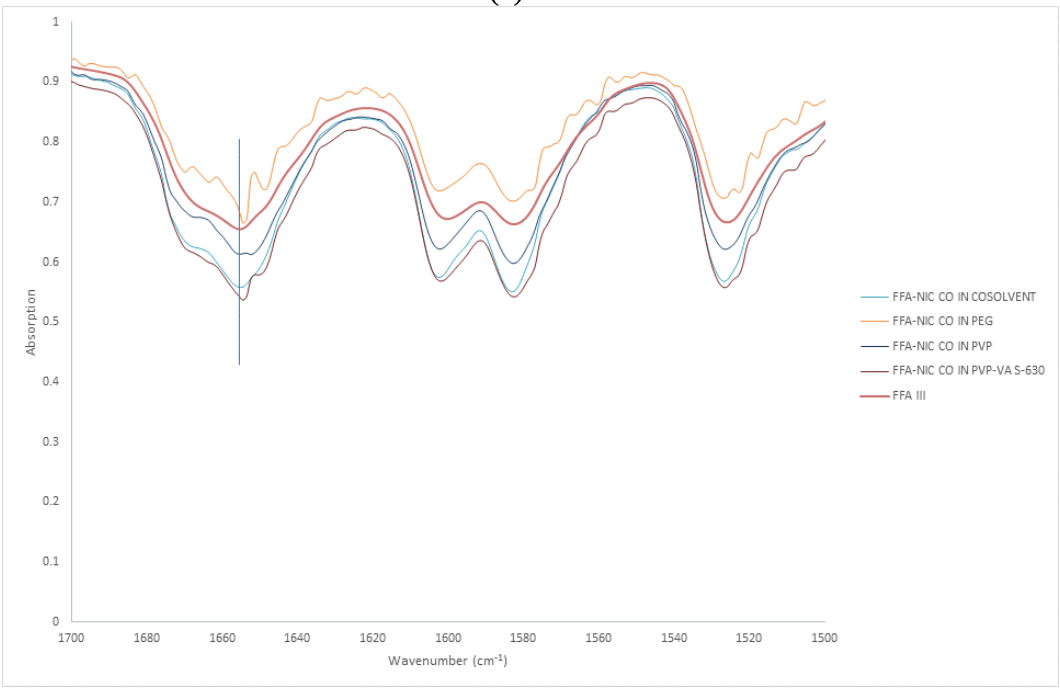

(b)

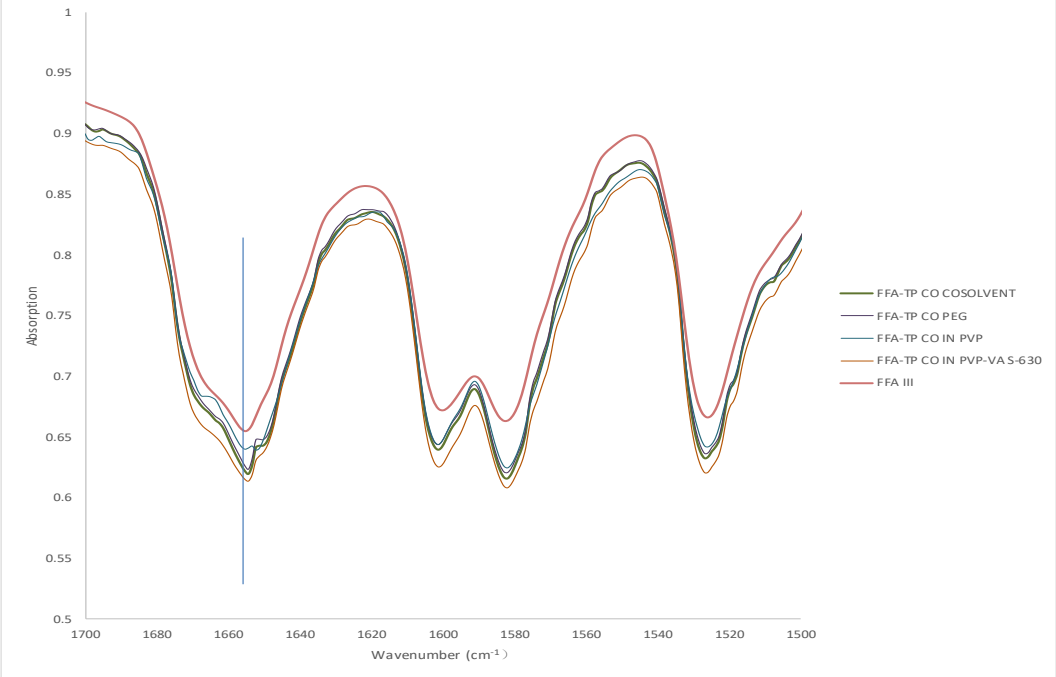
1
0.95
0.9
0.85
0.8
0.75
0.7
0.65
0.6
0.55
0.5
Absorption
1700
1680
1660
1640
1620
1600
1580
1560
1540
1520
1500
Wavenumber (cm-1)
FFA-TP CO COSOLVENT
FFA-TP CO PEG
FFA-TP CO IN PVP
FFA-TP CO IN PVP-VA S-630
FFA III

(c)

Figure A2. 2 Test results of solids collected after the seeded desupersaturation experiments (pictures): (a) DSC results: (b) images of solid residuals

	FFA solution	FFA-NIC CO solution	FFA-TP CO solution
cosolvent	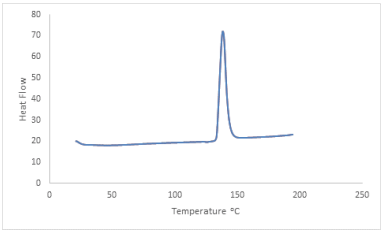	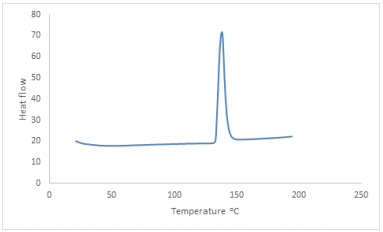	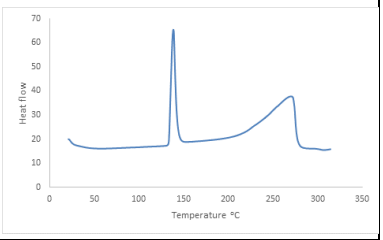
PEG	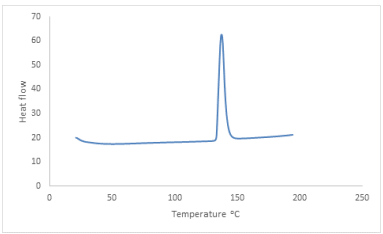	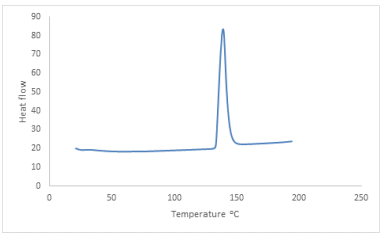	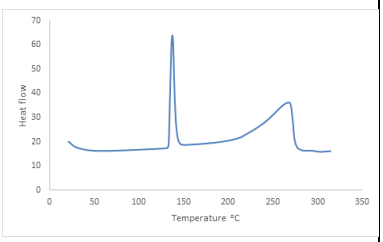
PVP	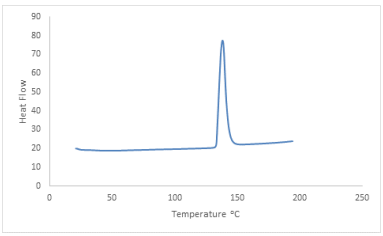	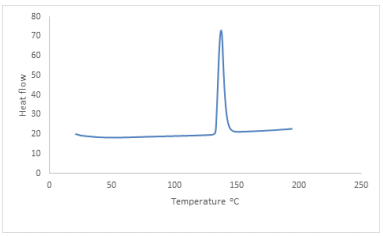	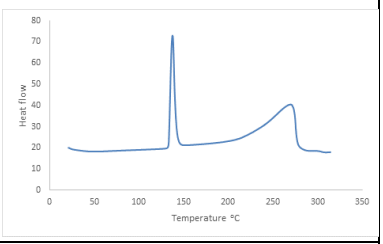
PVP-VA	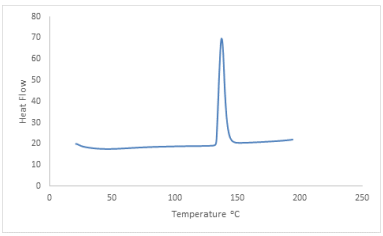	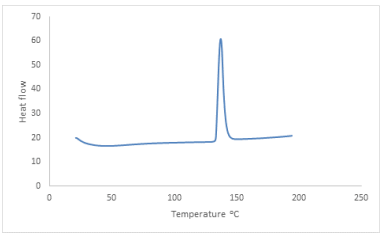	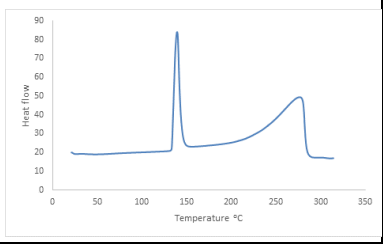

(a)

	Initial FFA I seeds		
			
	FFA	FFA-NIC CO	FFA-TP CO
Cosolvent	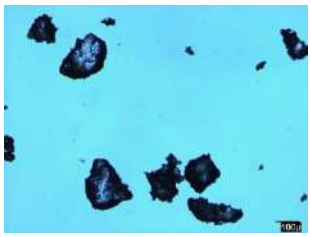	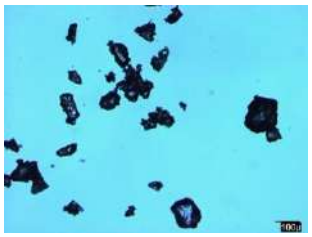	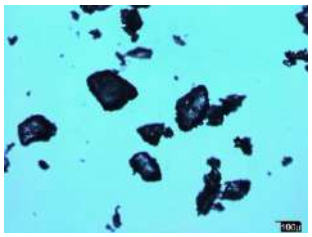
PEG	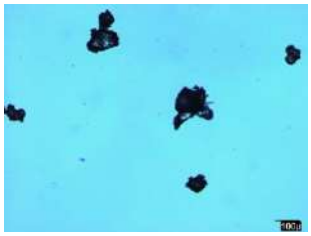	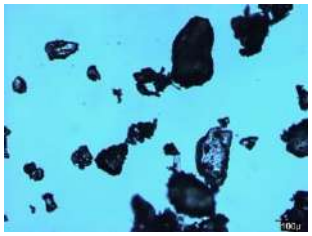	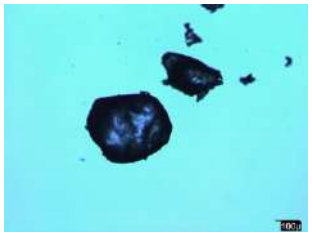
PVP	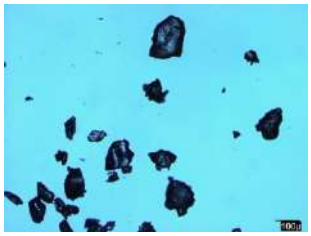	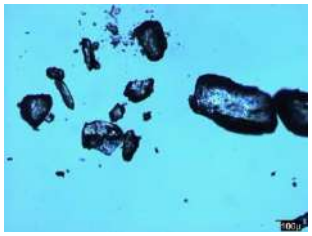	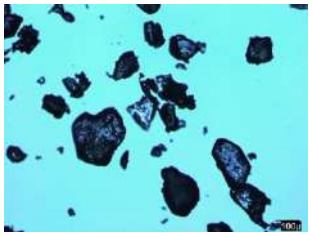
S-630	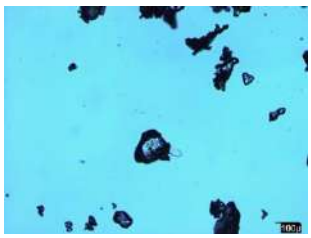	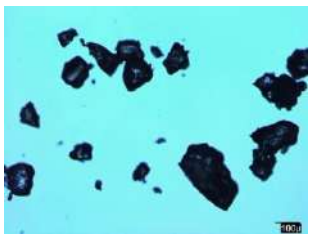	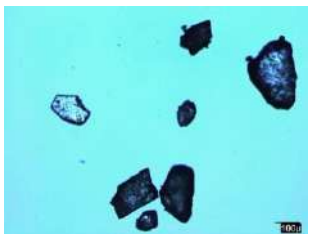

(b)

Figure A2. 3 Test results of solids collected after the unseeded desupersaturation experiments: (a) DSC results: (b) images of solid residuals

	FFA solution	FFA-NIC CO solution	FFA-TP CO solution
coso lvent	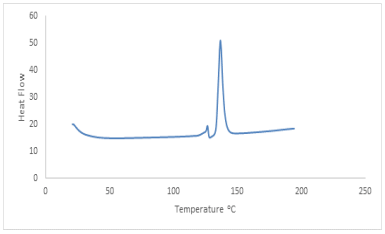	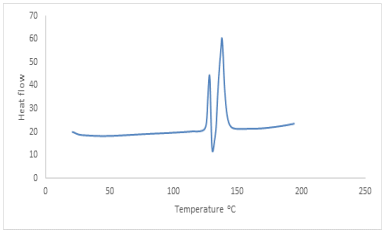	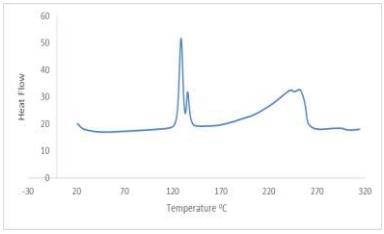
PEG	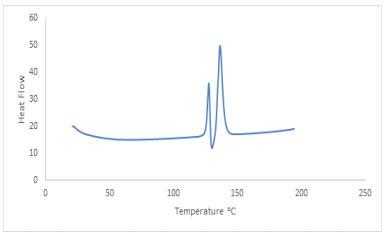	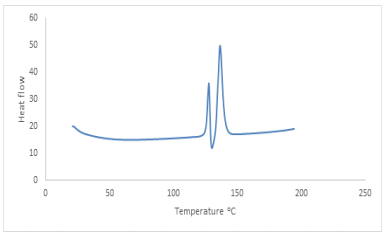	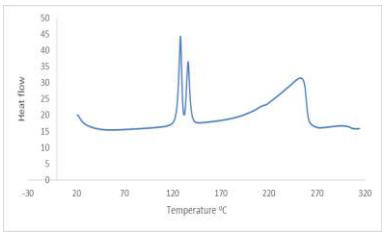
PVP	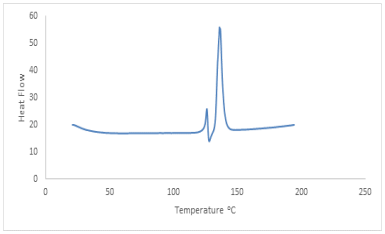	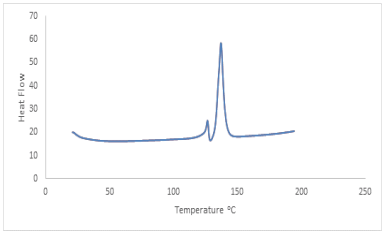	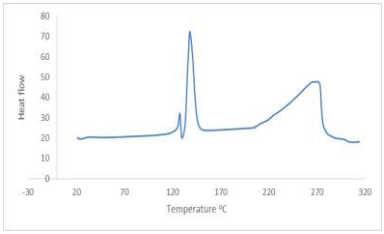
PVP -VA	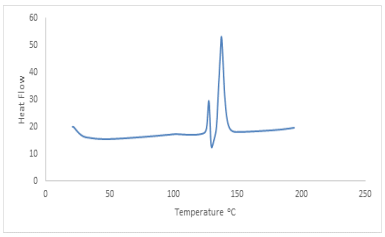	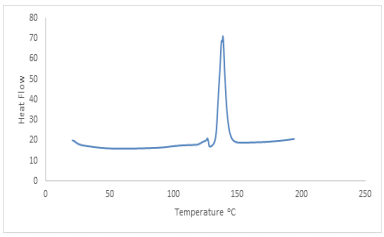	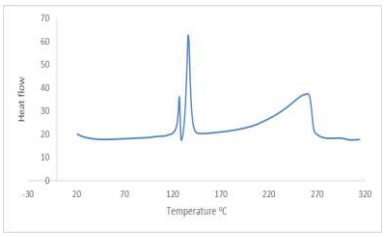

(a)

	FFA	FFA-NIC CO	FFA-TP CO
Cosolvent		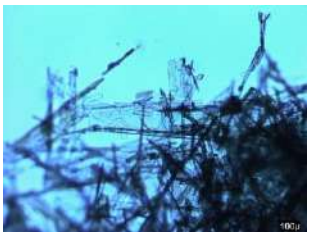	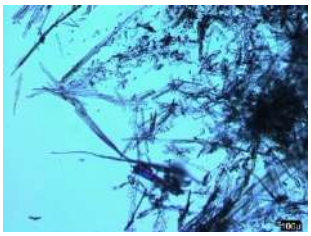
PEG	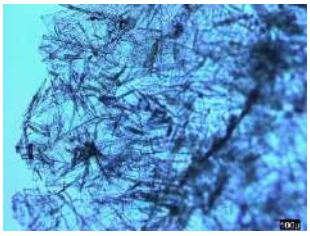	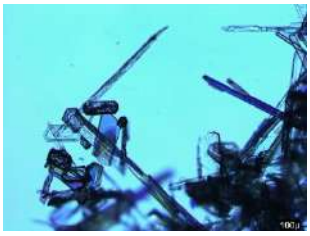	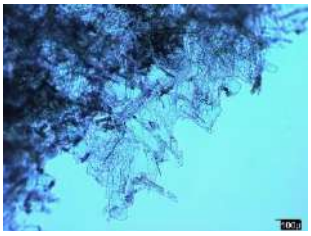
PVP	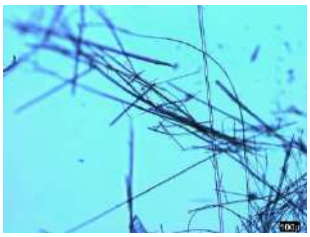	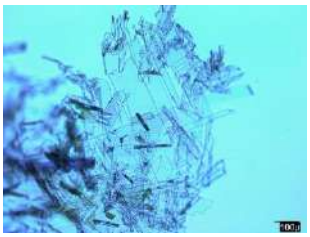	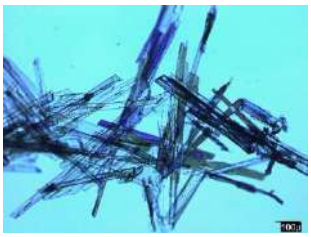
S-630		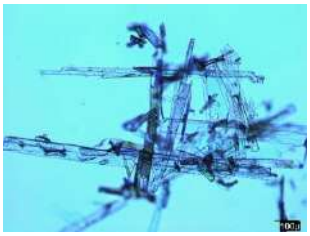	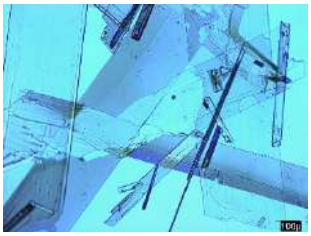

(b)

A3 Figures and Tables for Chapter 6

Table A3. 1 Crystal structure data and details of refinements

Parameter	FFA I	FFA-NIC CO	FFA-TP CO
Chemical formula	$C_{14}H_{10}F_3NO_2$	$C_{20}H_{16}F_3N_3O_3$	$C_{21}H_{18}F_3N_5O_4$
Formula weight	281.2	403.33	461.364
Crystal system	Monoclinic	Monoclinic	Triclinic
Space group	$P2_1/c$	$P2_1/c$	P-1
a(Å)	12.4157	5.1054	6.9931
b(Å)	7.7528	15.961	10.127
c(Å)	12.6469	22.119	15.112
α(°)	90	90	95.46
β(°)	94.688	90.471	96.7
γ(°)	90	90	101.17
V(Å^3)	1213.27	1802.36	1035.13
Z	4	4	2
2Θ range (°)	5-35	5-35	5-35
CCDC NO	FPAMCA18	EXAQAW	ZIQDUA

Figure A3. 1 Characterization of single crystals: (a) XRPD pattern; (b) IR spectra; (c) DSC thermographs

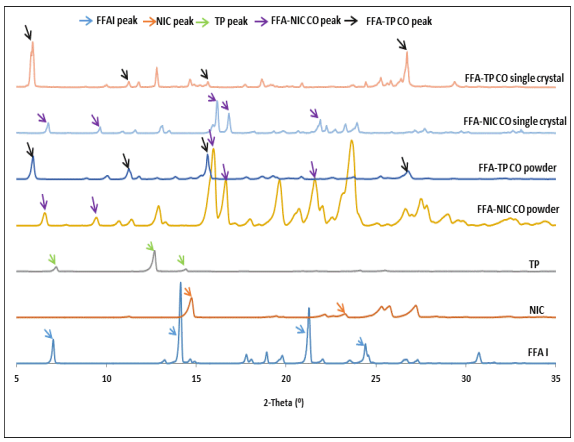

(a)

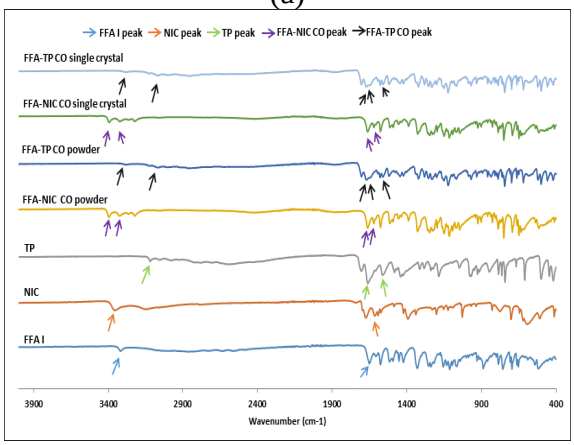

(b)

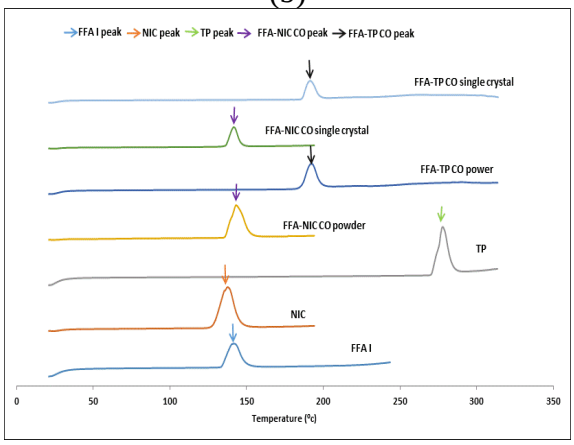

(c)

Figure A3. 2 Characterization of solid residues after FFA I equilibrium experiments in PBS in the absence or presence of 200 μg/mL polymer of PEG, PVP or PVP-VA: (a) XRPD patterns; (b) IR spectra; (c) DSC thermographs

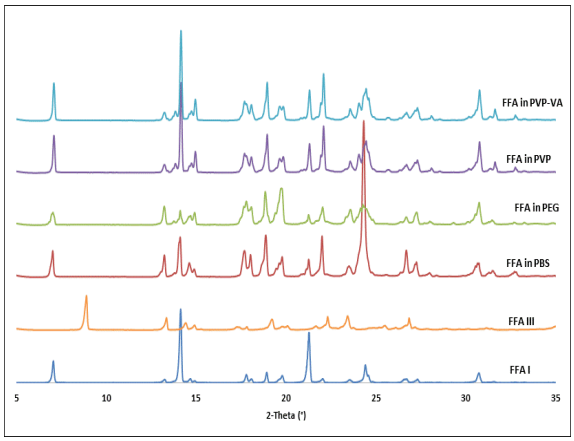

(a)

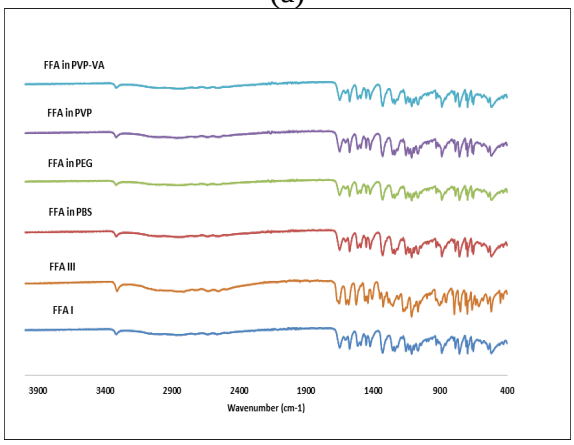

(b)

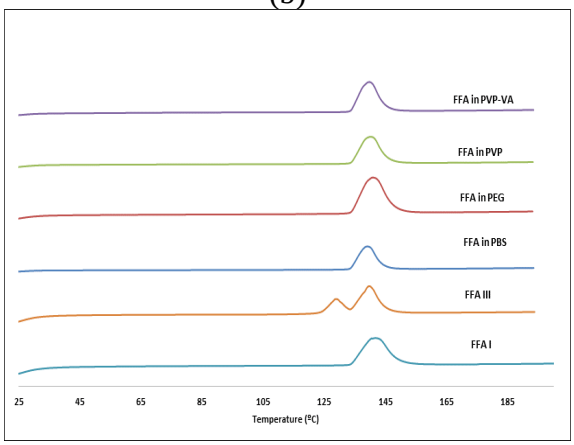

(c)

Figure A3. 3 Characterization of solid residues after the tests in TP solutions: (a) DSC thermographs; (b) IR results.

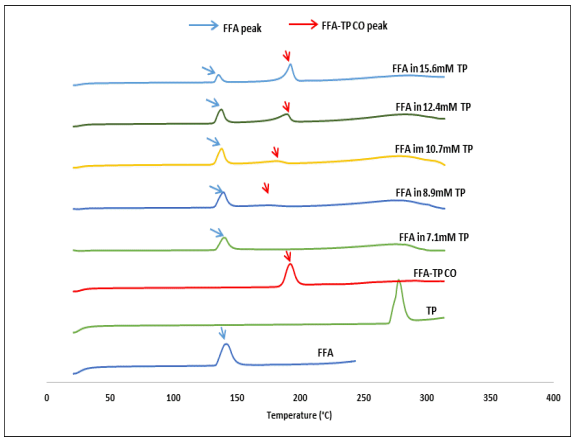

(a)

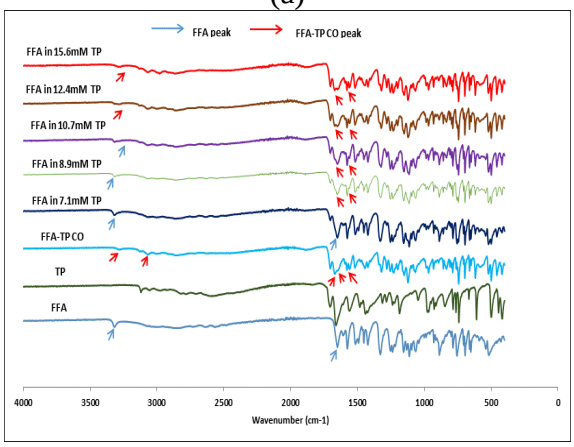

(b)

Figure A3. 4 Characterization of solid residues after the tests in NIC solutions: (a) DSC thermographs; (b) IR results

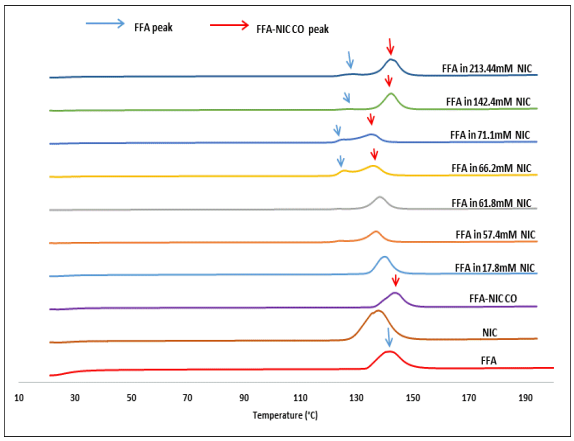

(a)

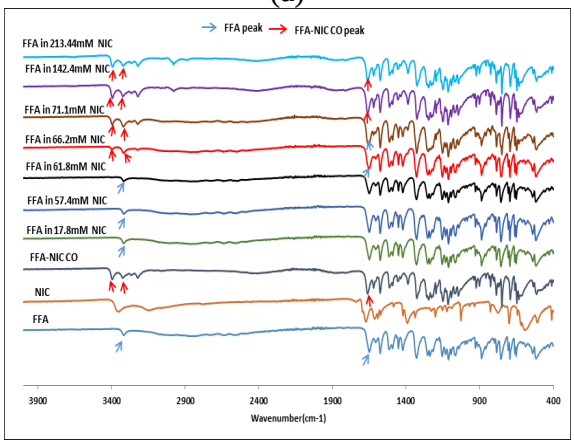

(b)

Figure A3. 5 AFM images

Crystal		Before dissolution	PBS	PEG	PVP	PVP-VA
FFA	80x80µm^2	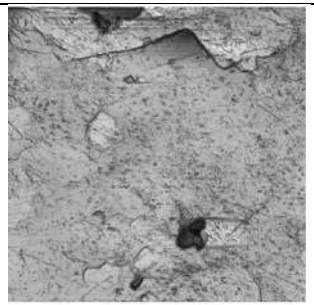	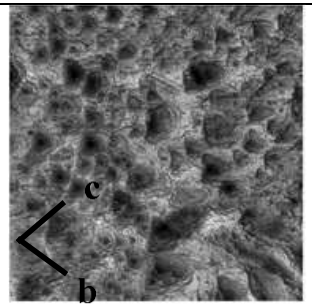	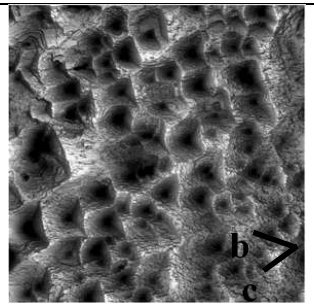	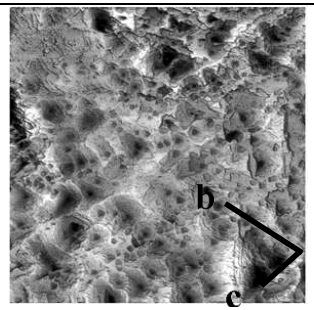	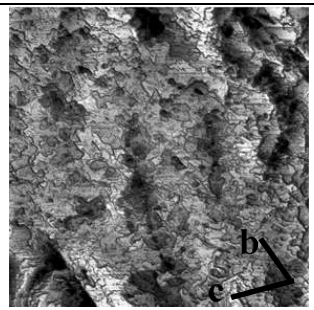
	20x20µm^2	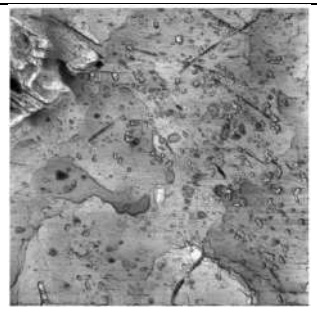	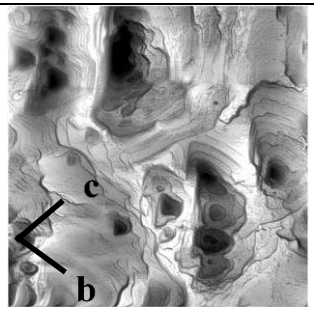	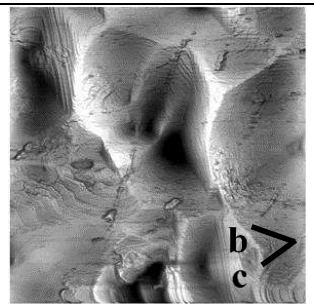	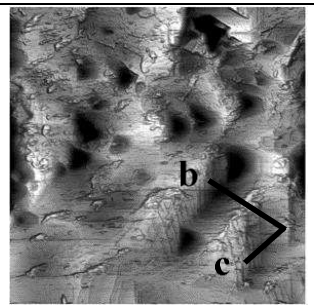	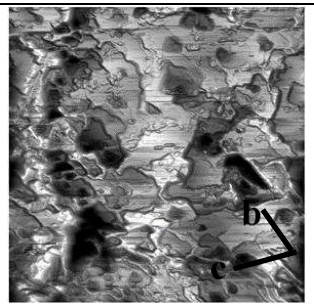
FFA-TP CO	80x80µm^2	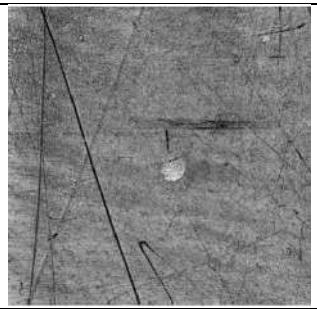	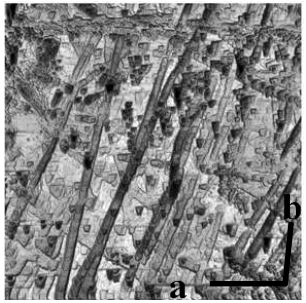	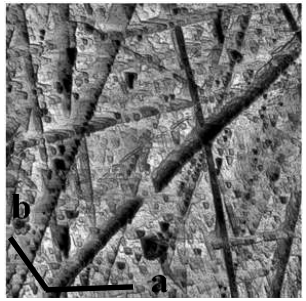	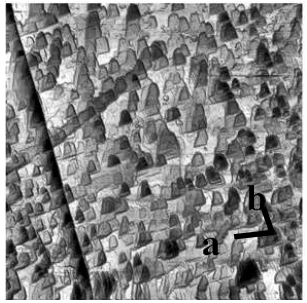	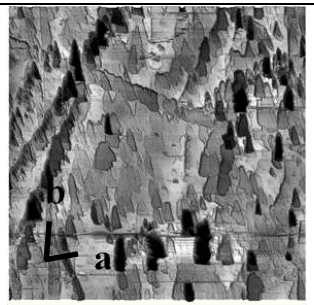

	20x20µm^2	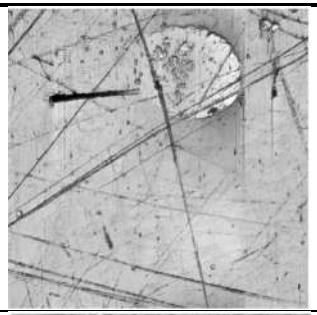	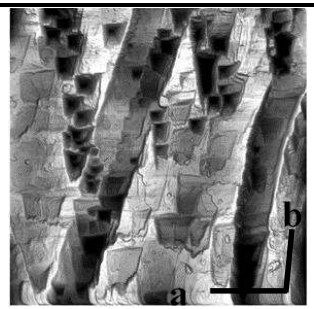	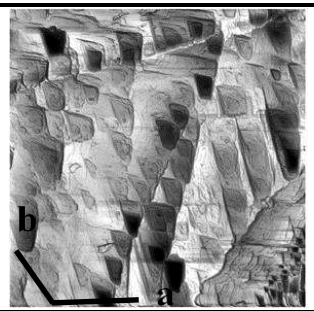	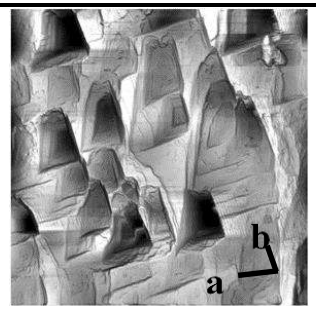	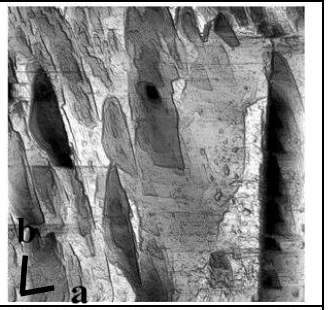
FFA-NIC CO	20x20µm^2	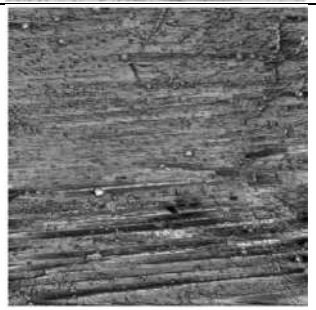	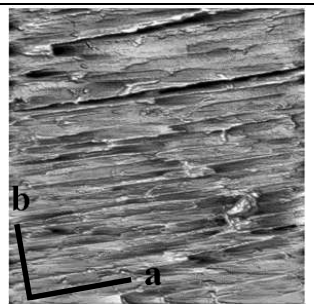		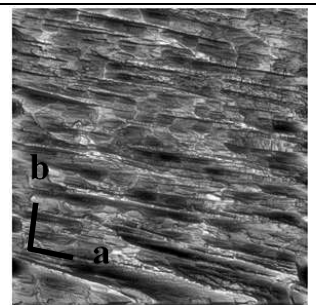	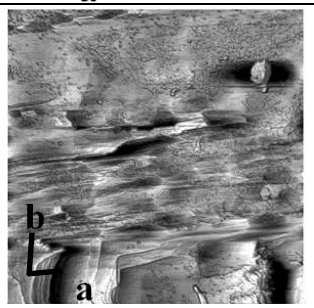
	10x10µm^2	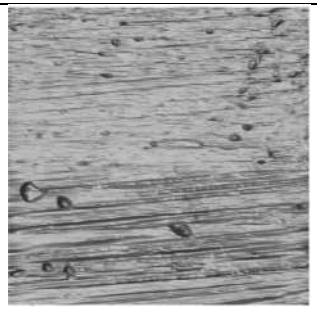	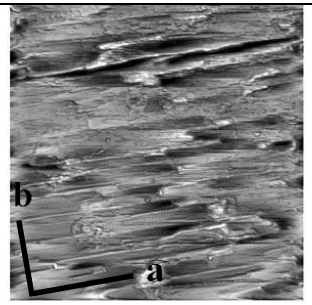	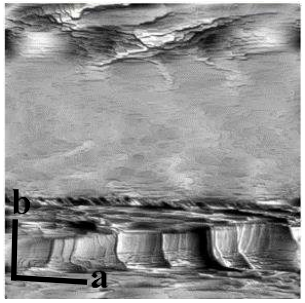	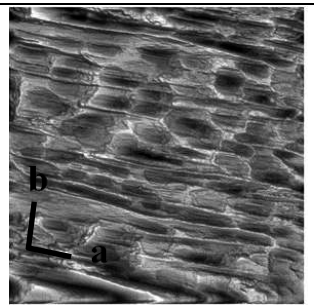	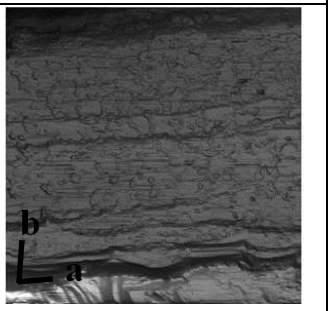

Figure A3. 6 Three-dimensional AFM images at a 40x40 μm^2 scan area

Crystal	Before Dissolution	PBS	PBS with Pre-dissolved PEG	PBS with Pre-dissolved PVP	PBS with Pre-dissolved PVP-VA
FFA	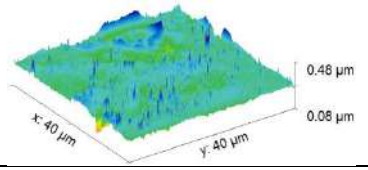	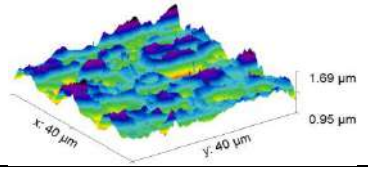	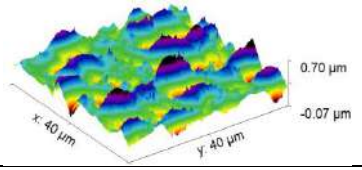	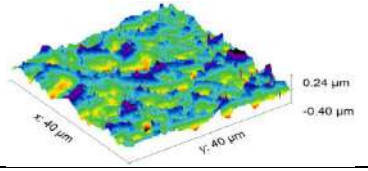	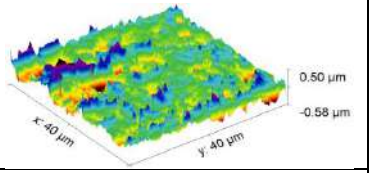
FFA-TP CO	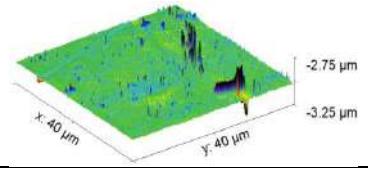	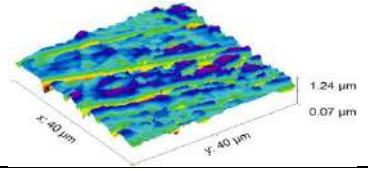	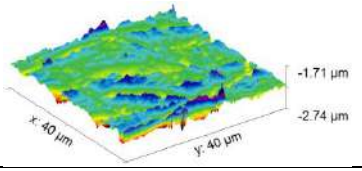	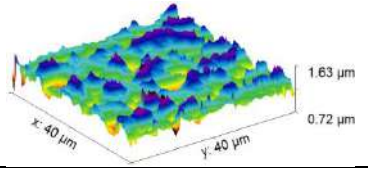	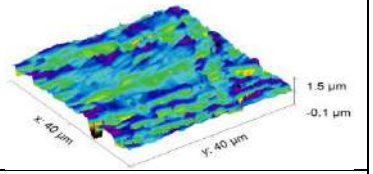
FFA-NIC CO	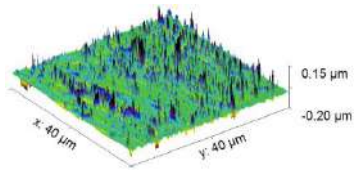	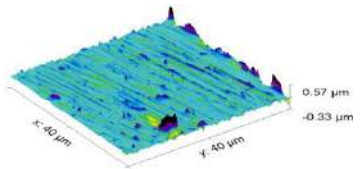	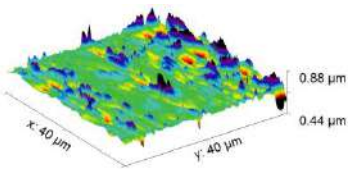	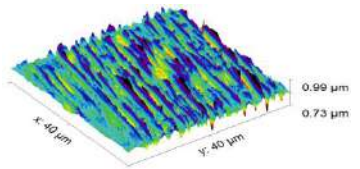	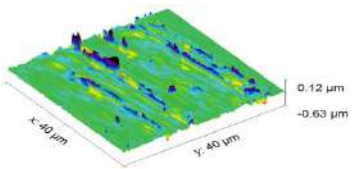

Figure A3. 7 OLM images

Crystal	Polymers	Face index	0h	2h	4h	6h
FFA	pH 6.8	100	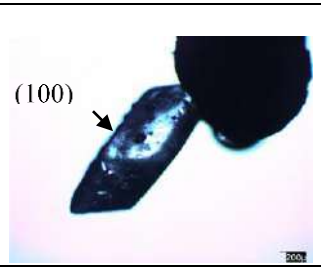	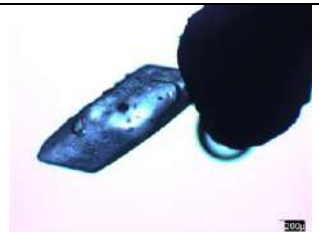	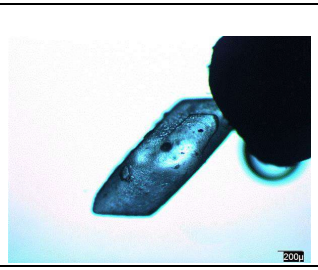	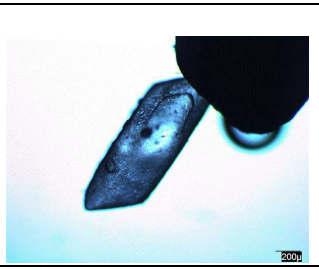
		0-11	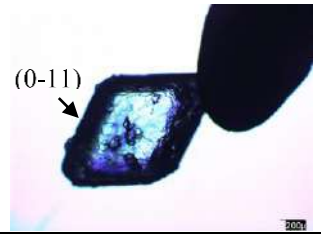	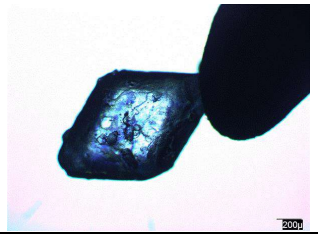	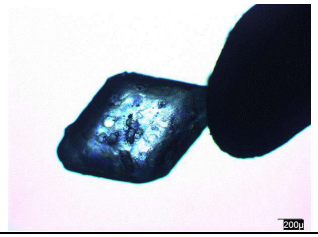	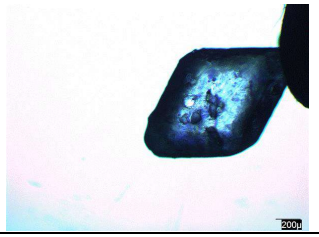
	PEG	100	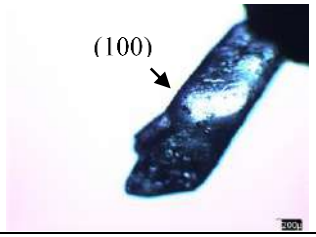	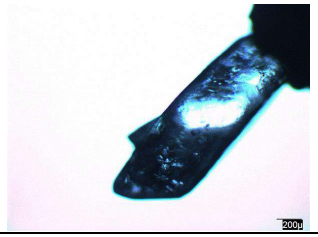	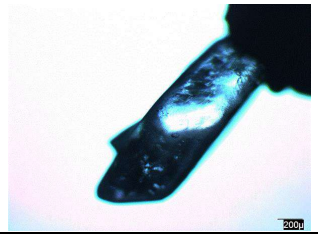	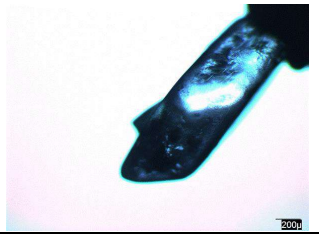

		0-11	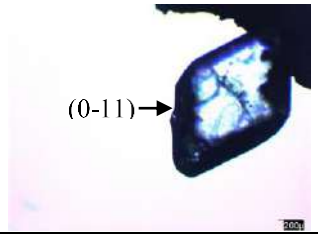	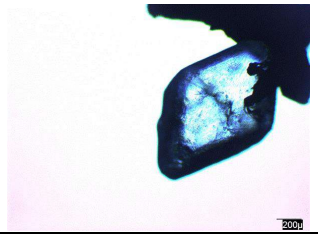	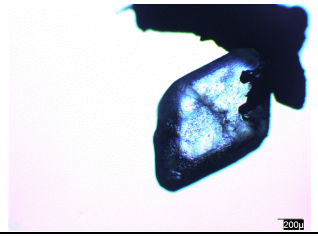	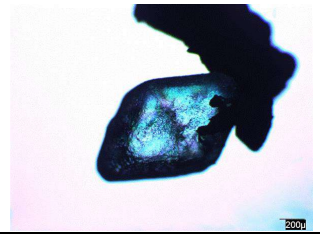
	PVP	100	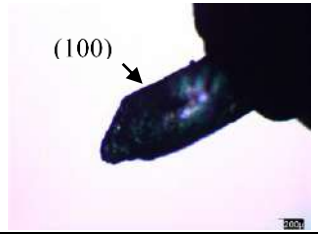	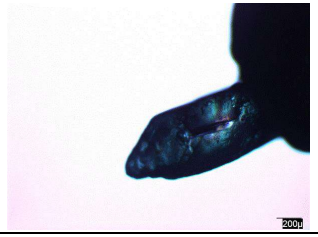	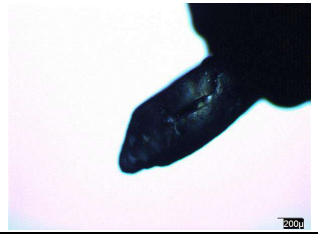	
		0-11	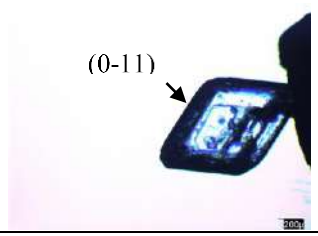	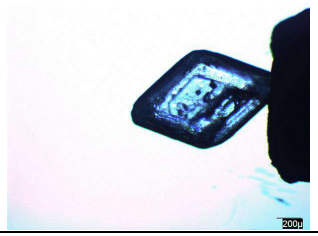	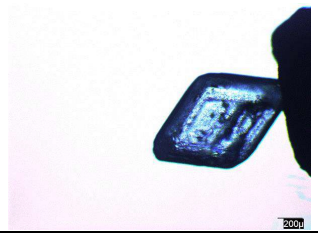	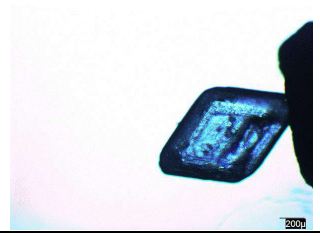
	PVP-VA	100	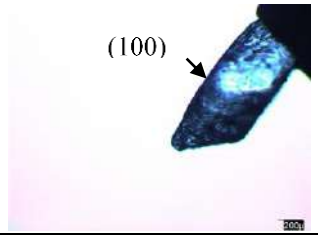	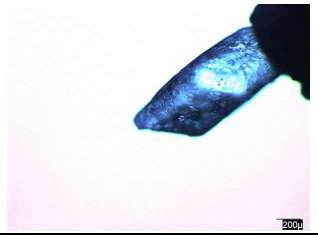		

		0-11	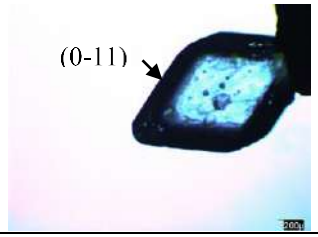	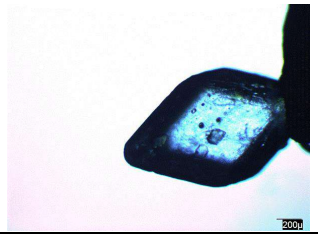	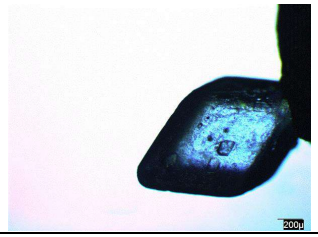	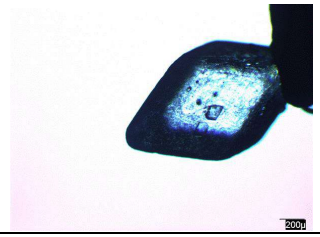
FFA-TPCO	pH 6.8	001	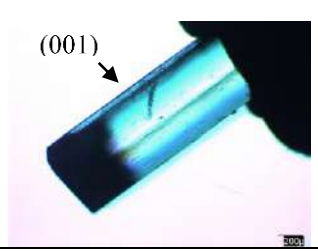	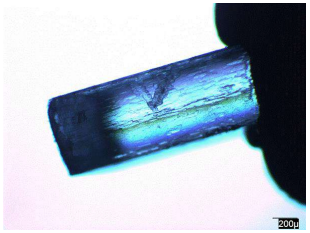	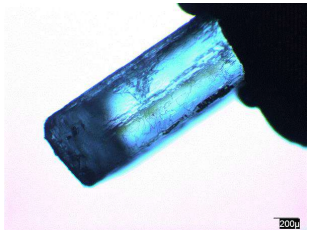	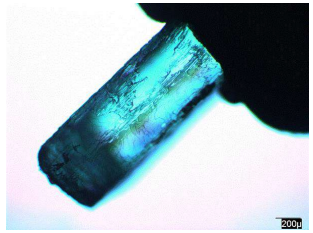
		100	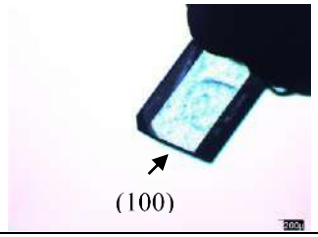	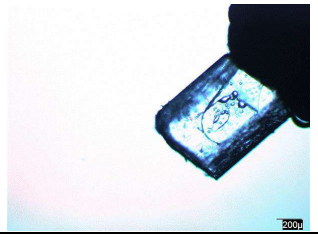	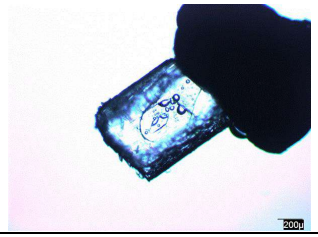	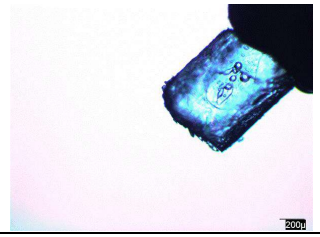
	PEG	001	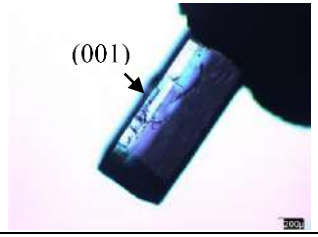	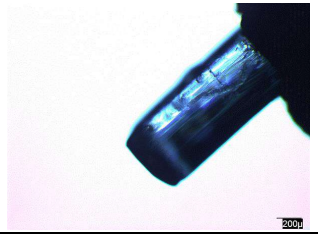	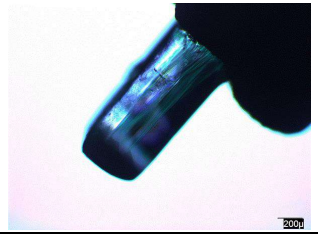	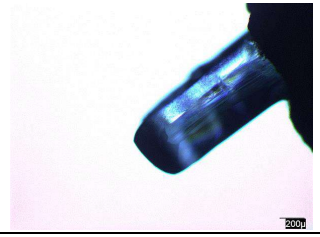

		100	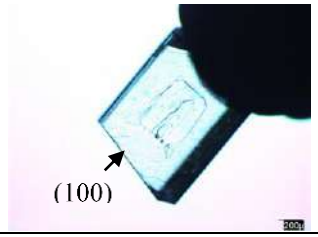	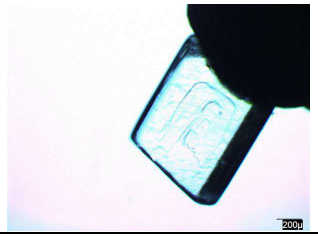	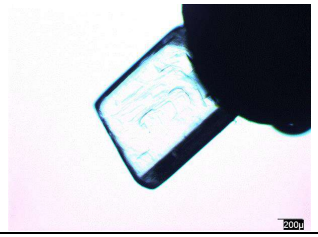	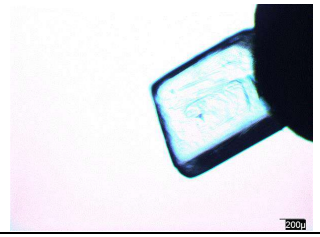
	PVP	001	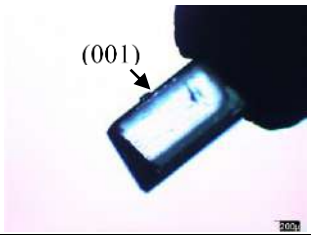	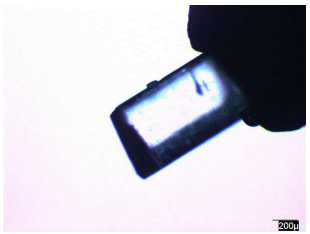	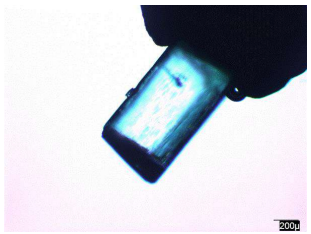	
		100	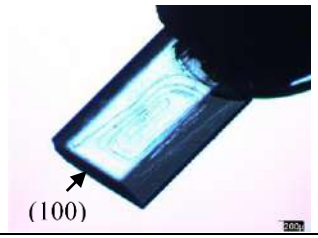	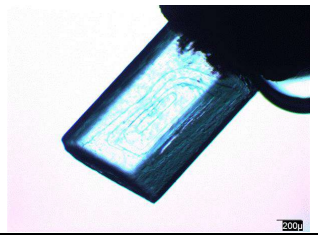	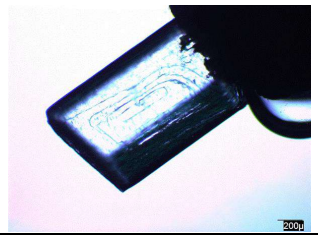	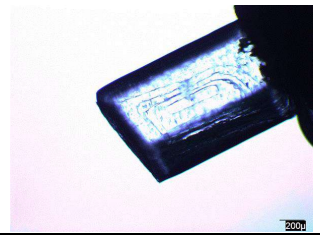
	PVP-VA	001	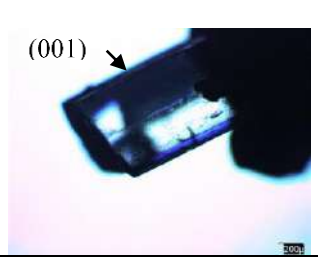	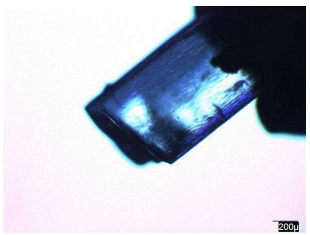	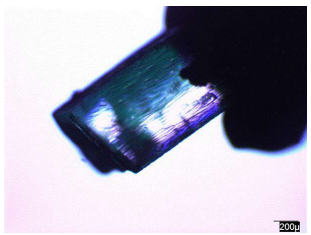	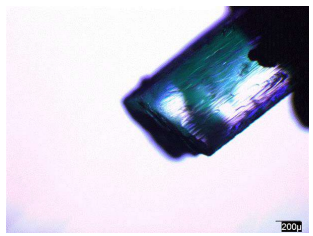

		100	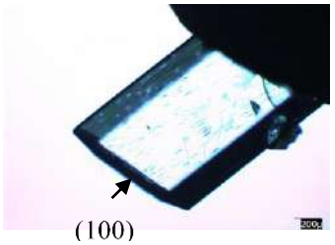	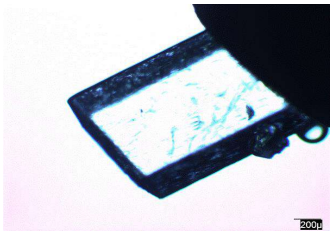	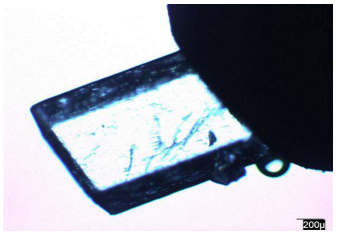	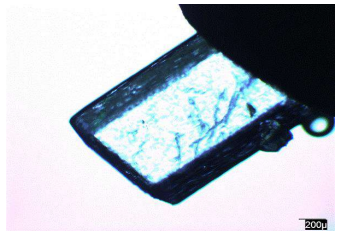
FFA-NICCO	pH 6.8	01-1 and 100	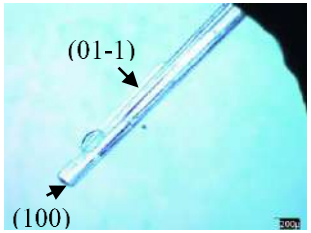	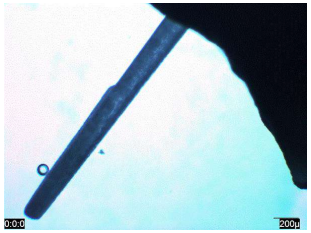	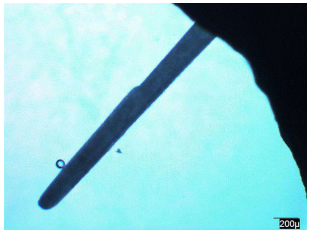	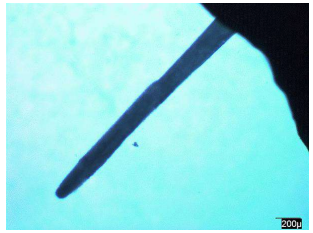
	PEG	01-1 and 100	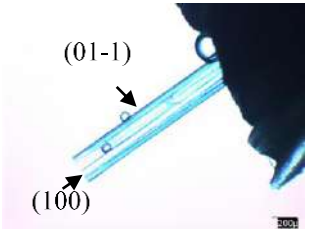	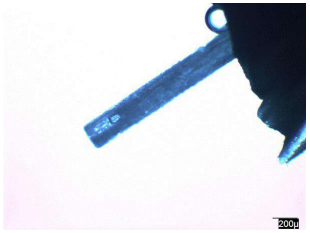		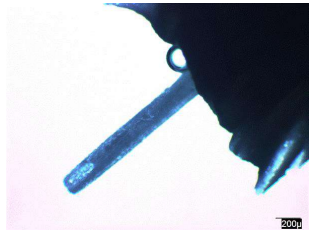
	PVP	01-1 and 100	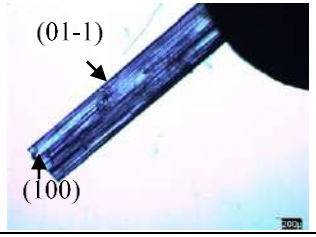	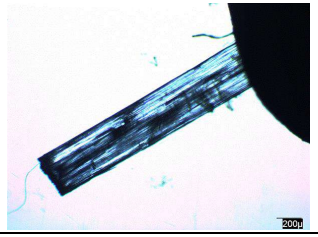	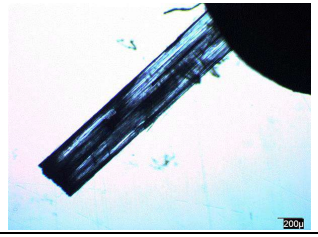	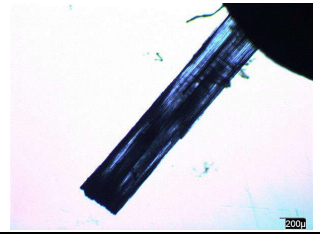

	PVP-VA	01-1 and 100	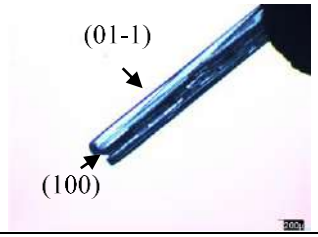	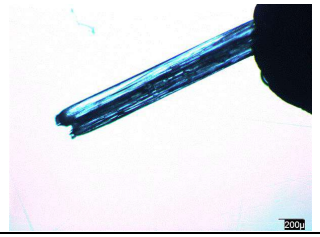	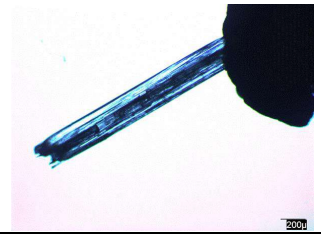	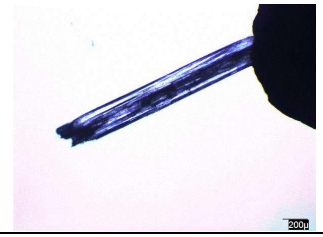

Figure A3. 8 DSC thermographs characterization of solid residues after un-sink condition dissolution: (a) FFA; (b) FFA-NIC CO; (C) FFA-TP CO.

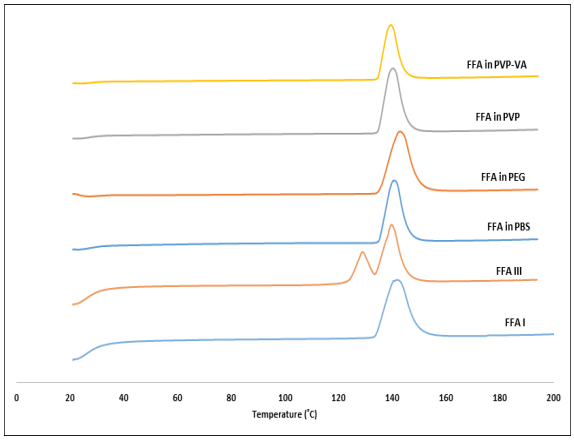

(a)

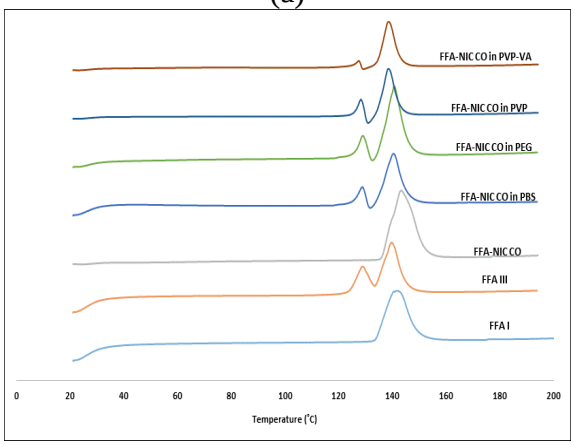

(b)

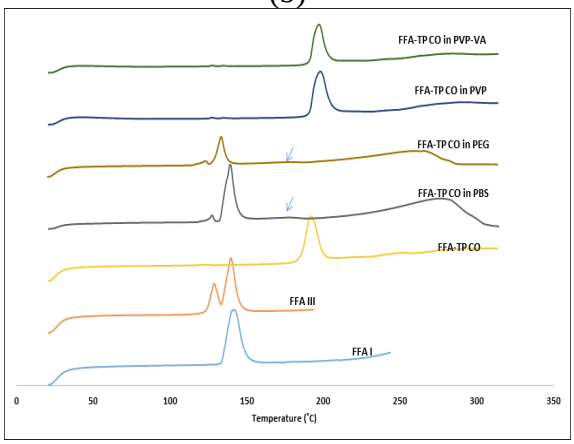

(c)

Figure A3. 9 IR results of solid residues after un-sink condition dissolution: (a) FFA; (b) FFA-NIC CO; (C) FFA-TP CO.

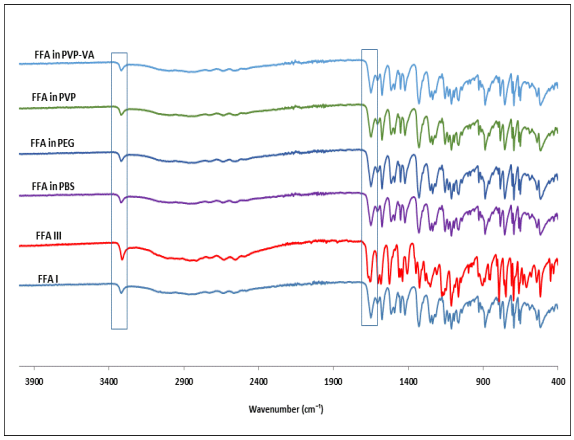

(a)

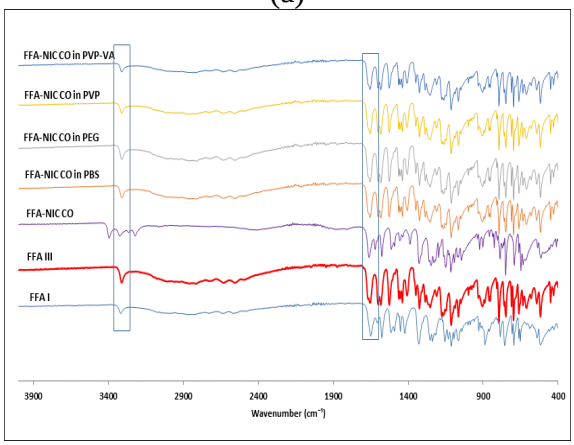

(b)

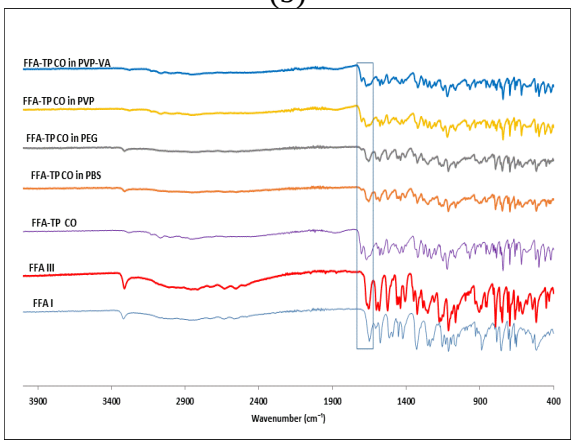

(c)

A4 Figures and Tables for Chapter 7

Table A4. 1 ^{1}H NMR samples

	Solute	concentration
Singular component	FFA	5000 μg/mL, 1000 μg/mL and 500 μg/mL.
	NIC	2150 μg/mL, 430 μg/mL and 215 μg/mL
	TP	3200 μ/mL, 640 μg/mL, and 320 μg/mL
	PVP	200 μg/mL and 5000 μg/mL
	PVP-VA	200 μg/mL and 5000 μg/mL
Binary components	FFA/NIC	(5000 μg/mL FFA, 2150 μg/mL NIC), (1000 μg/mL FFA, 430 μg/mL NIC) and (500 μg/mL FFA, 215 μg/mL NIC).
	FFA/TP	(5000 μg/mL FFA, 2150 μg/mL TP), (5000 μg/mL FFA, 430 μg/mL TP) and (5000 μg/mL FFA, 215 μg/mL TP)
	FFA/PVP	(5000 μg/mL FFA, 200 μg/mL PVP), (5000 μg/mL FFA, 5000 μg/mL PVP), (1000 μg/mL FFA, 200 μg/mL PVP), (1000 μg/mL FFA, 5000 μg/mL PVP), (500 μg/mL FFA, 200 μg/mL PVP), (500 μg/mL FFA, 5000 μg/mL PVP)
	FFA/PVP-VA	(5000 μg/mL FFA, 200 μg/mL PVP-VA), (5000 μg/mL FFA, 5000 μg/mL PVP-VA), (1000 μg/mL FFA, 200 μg/mL PVP-VA), (1000 μg/mL FFA, 5000 μg/mL PVP-VA), (500 μg/mL FFA, 200 μg/mL PVP-VA), (500 μg/mL FFA, 5000 μg/mL PVP-VA)
	NIC/PVP	(2150 μg/mL NIC, 200 μg/mL PVP), (2150 μg/mL NIC, 5000 μg/mL PVP), (430 μg/mL NIC, 200 μg/mL PVP), (430 μg/mL NIC, 5000 μg/mL PVP), (215 μg/mL NIC, 200 μg/mL PVP), (215 μg/mL NIC, 5000 μg/mL PVP)
	NIC/PVP-VA	(2150 μg/mL NIC, 200 μg/mL PVP-VA), (2150 μg/mL NIC, 5000 μg/mL PVP-VA), (430 μg/mL NIC, 200 μg/mL PVP-VA), (430 μg/mL NIC, 5000 μg/mL PVP-VA), (215 μg/mL NIC, 200 μg/mL PVP-VA), (215 μg/mL NIC, 5000 μg/mL PVP-VA)
	TP/PVP	(3200 μg/mL TP, 200 μg/mL PVP), (3200 μg/mL TP, 5000 μg/mL PVP), (640 μg/mL TP, 200 μg/mL PVP), (640 μg/mL TP, 5000 μg/mL PVP), (320 μg/mL TP, 200 μg/mL PVP), (320 μg/mL TP, 5000 μg/mL PVP)
	TP/PVP-VA	(3200 μg/mL TP, 200 μg/mL PVP0VA), (3200 μg/mL TP, 5000 μg/mL PVP-VA), (640 μg/mL TP, 200 μg/mL PVP-VA), (640 μg/mL TP, 5000 μg/mL PVP-VA), (320 μg/mL TP, 200 μg/mL PVP-VA), (320 μg/mL TP, 5000 μg/mL PVP-VA)
ternary components	FFA/NIC/PVP	(5000 μg/mL FFA, 2150 μg/mL NIC, 200 μg/mL PVP), (5000 μg/mL FFA, 2150 μg/mL NIC, 5000 μg/mL PVP), (1000 μg/mL

		FFA, 430 μg/mL NIC, 200 μg/mL PVP), (1000 μg/mL FFA, 430 μg/mL NIC, 5000 μg/mL PVP), (500 μg/mL FFA, 215 μg/mL NIC, 200 μg/mL PVP) and (500 μg/mL FFA, 215 μg/mL NIC, 5000 μg/mL PVP).
	FFA/NIC/PVP-VA	(5000 μg/mL FFA, 2150 μg/mL NIC, 200 μg/mL PVP-VA), (5000 μg/mL FFA, 2150 μg/mL NIC, 5000 μg/mL PVP-VA), (1000 μg/mL FFA, 430 μg/mL NIC, 200 μg/mL PVP-VA), (1000 μg/mL FFA, 430 μg/mL NIC, 5000 μg/mL PVP-VA), (500 μg/mL FFA, 215 μg/mL NIC, 200 μg/mL PVP-VA) and (500 μg/mL FFA, 215 μg/mL NIC, 5000 μg/mL PVP-VA).
	FFA/TP/PVP	(5000 μg/mL FFA, 3200 μg/mL TP, 200 μg/mL PVP), (5000 μg/mL FFA, 3200 μg/mL TP, 5000 μg/mL PVP), (1000 μg/mL FFA, 640 μg/mL TP, 200 μg/mL PVP), (1000 μg/mL FFA, 640 μg/mL TP, 5000 μg/mL PVP), (500 μg/mL FFA, 320 μg/mL TP, 200 μg/mL PVP) and (500 μg/mL FFA, 320 μg/mL TP, 5000 μg/mL PVP).
	FFA/TP/PVP-VA	(5000 μg/mL FFA, 3200 μg/mL TP, 200 μg/mL PVP-VA), (5000 μg/mL FFA, 3200 μg/mL TP, 5000 μg/mL PVP-VA), (1000 μg/mL FFA, 640 μg/mL TP, 200 μg/mL PVP-VA), (1000 μg/mL FFA, 640 μg/mL TP, 5000 μg/mL PVP-VA), (500 μg/mL FFA, 320 μg/mL TP, 200 μg/mL PVP-VA) and (500 μg/mL FFA, 320 μg/mL TP, 5000 μg/mL PVP-VA).

Figure A4. 1 The full ^{1}H NMR spectra of the experiments

	Solute	concentration
Singular component	FFA	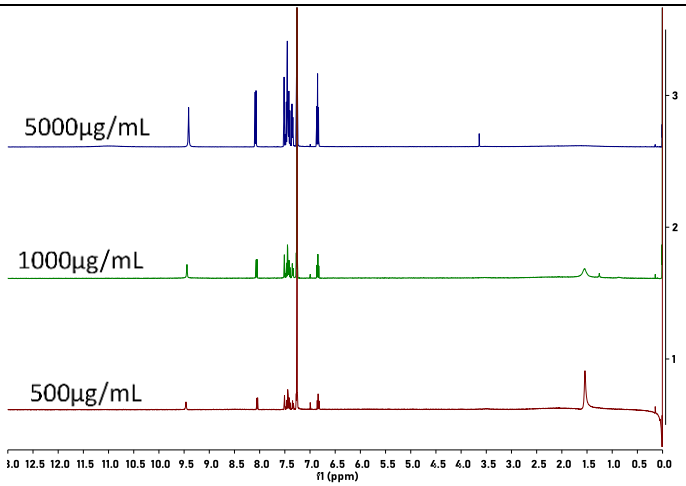

	NIC	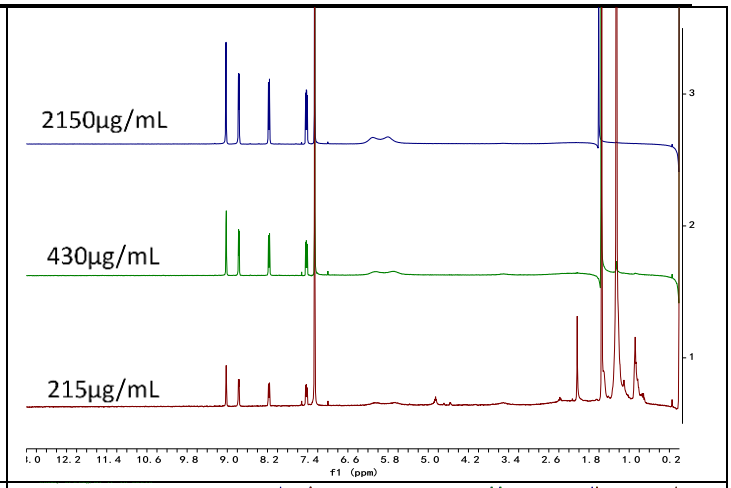 2150µg/mL 430µg/mL 215µg/mL f1 (ppm)
	TP	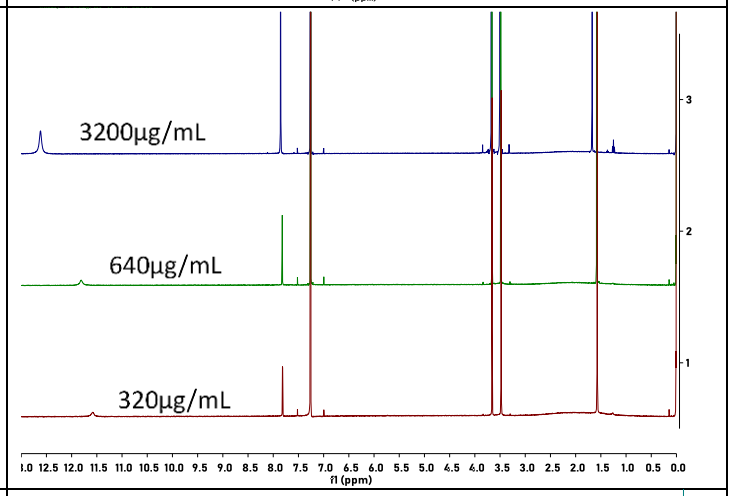 3200µg/mL 640µg/mL 320µg/mL f1 (ppm)
	PVP	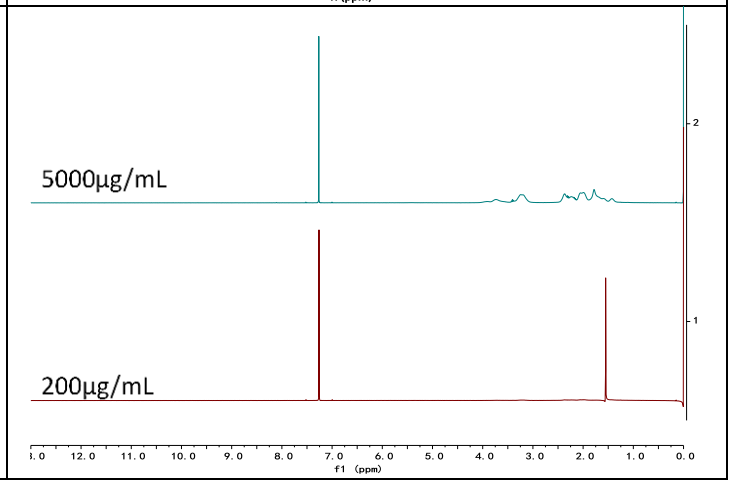 5000µg/mL 200µg/mL f1 (ppm)

	PVP-VA	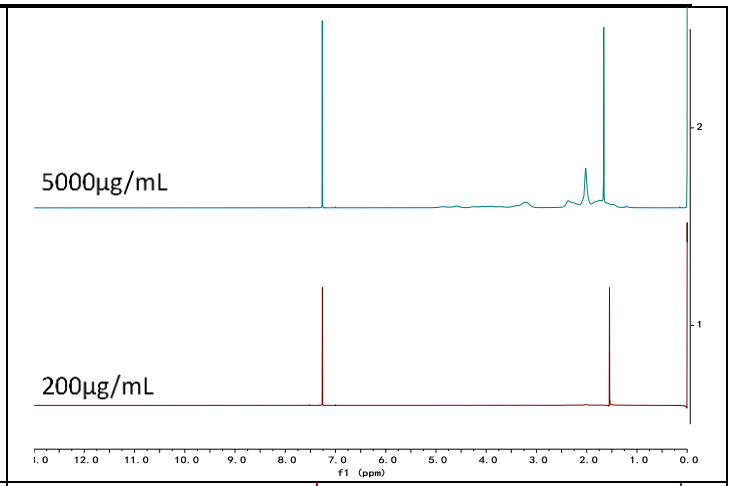
Binary components	FFA/NIC	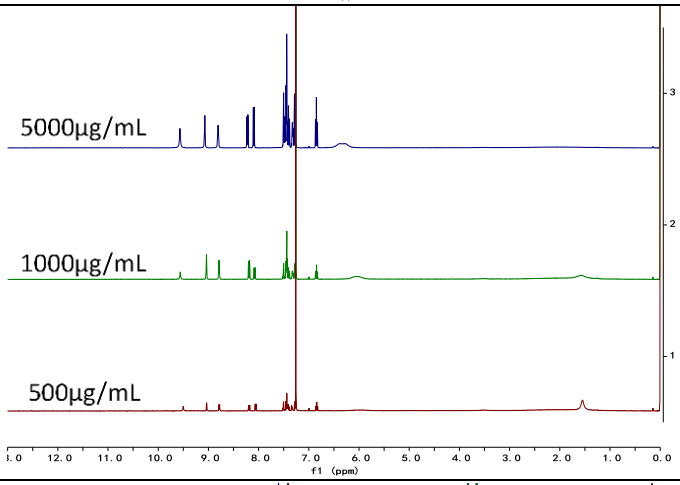
	FFA/TP	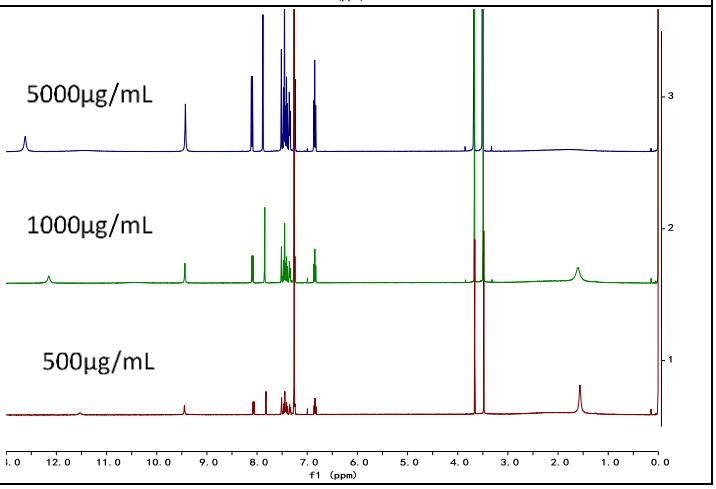

	FFA/ PVP	5000µg/mL FFA	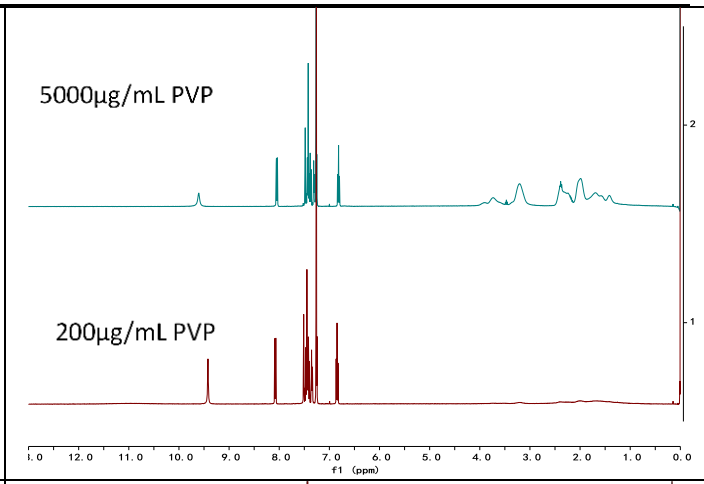
		1000µg/mL FFA	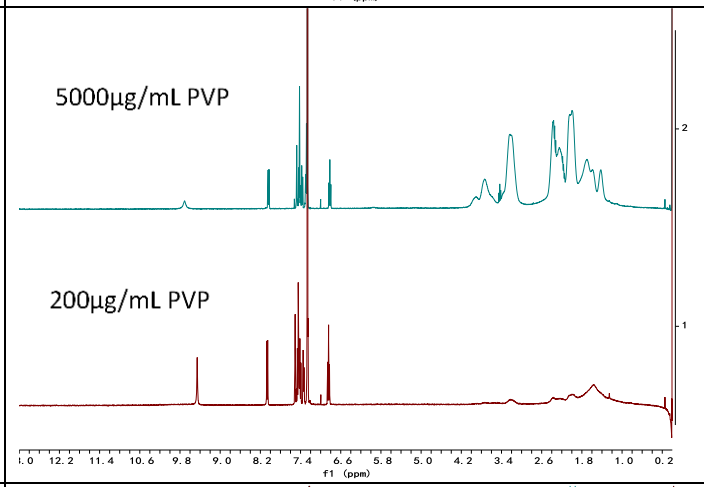
		500µg/mL FFA	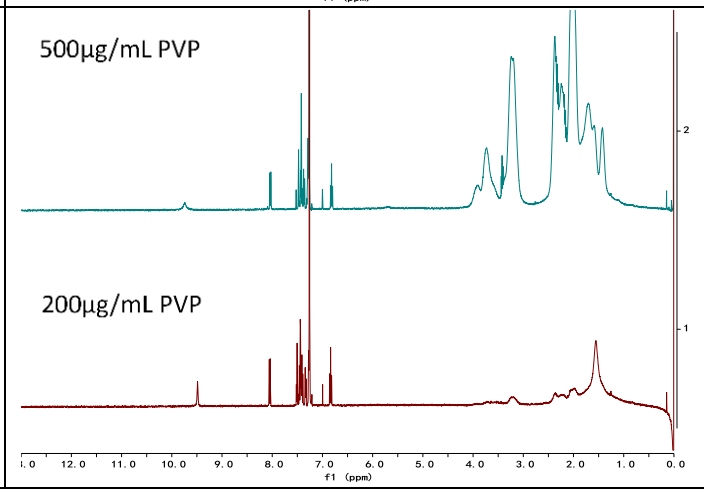

	FFA/ PVP -VA	5000µg/mL FFA	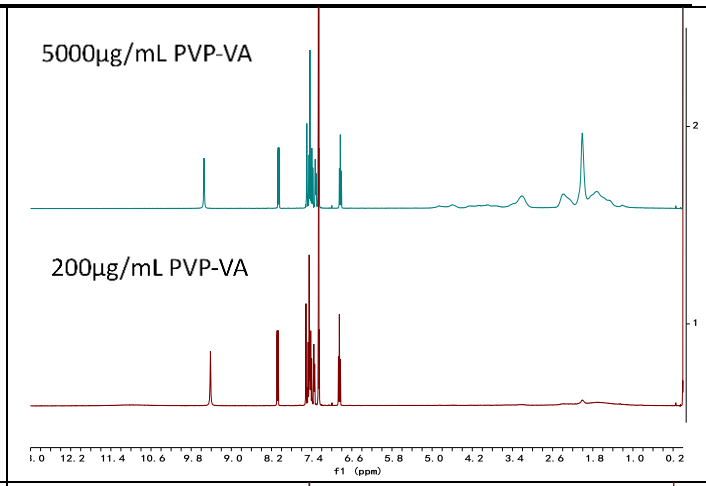
		1000µg/mL FFA	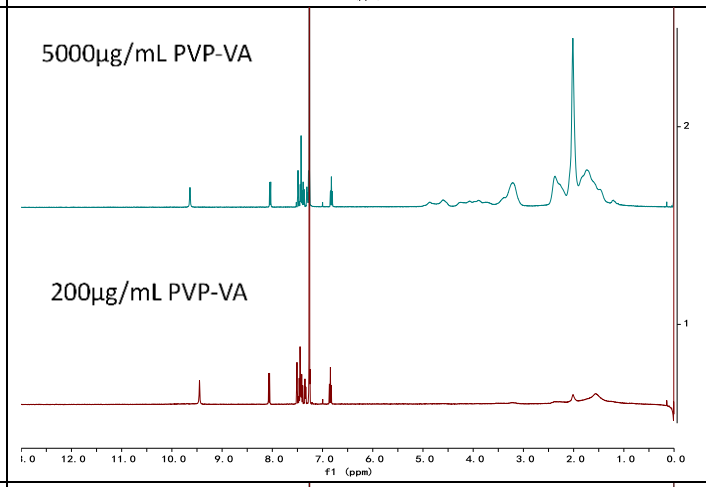
		500µg/mL FFA	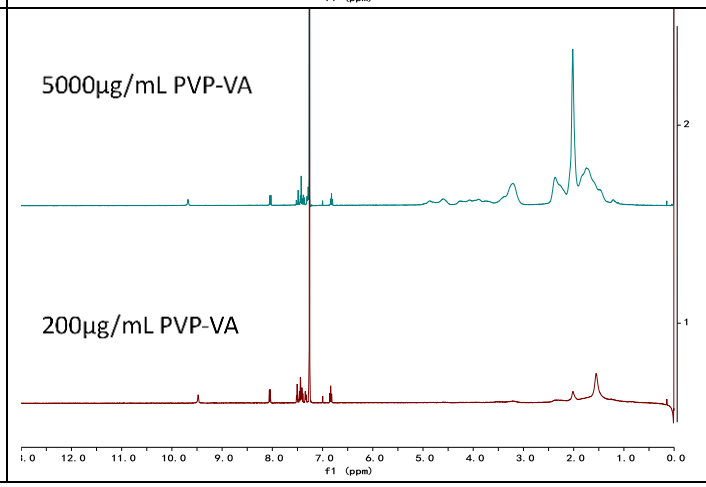

	NIC/ PVP	2150ug/mL NIC	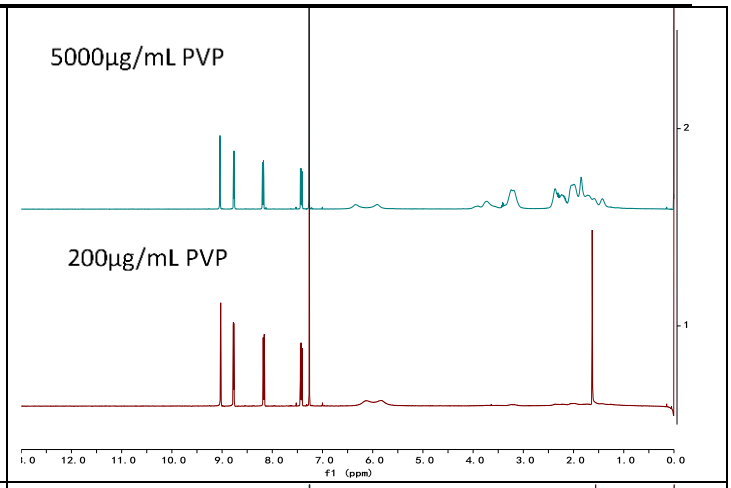
		430ug/mL NIC	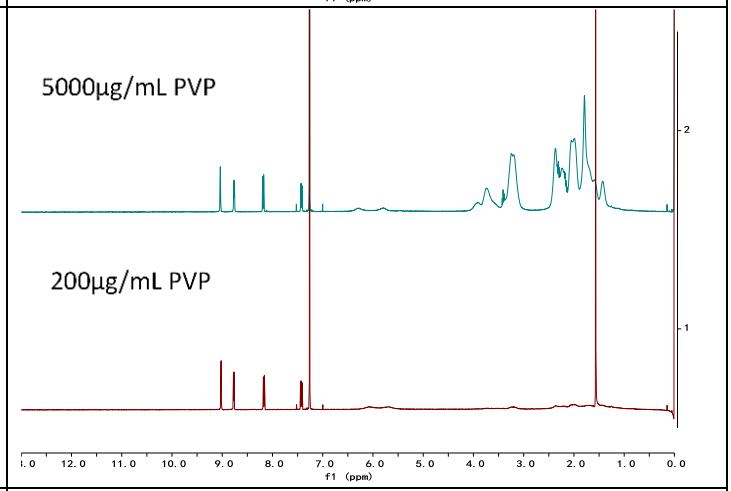
		215ug/mL NIC	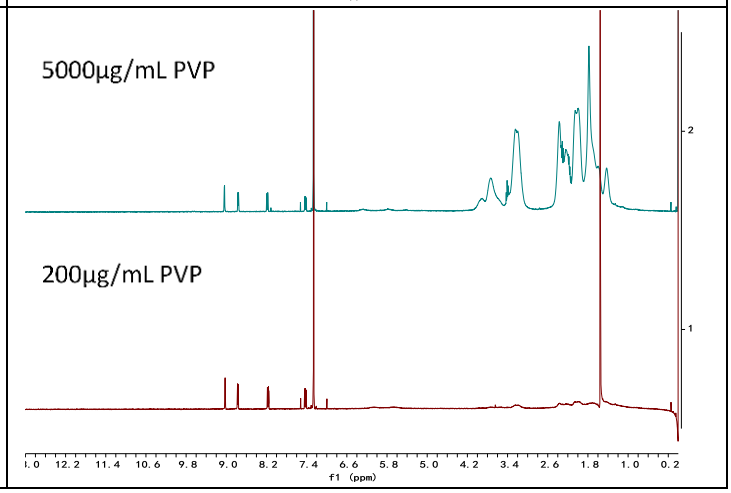

	NIC/ PVP -VA	2150ug/mL NIC	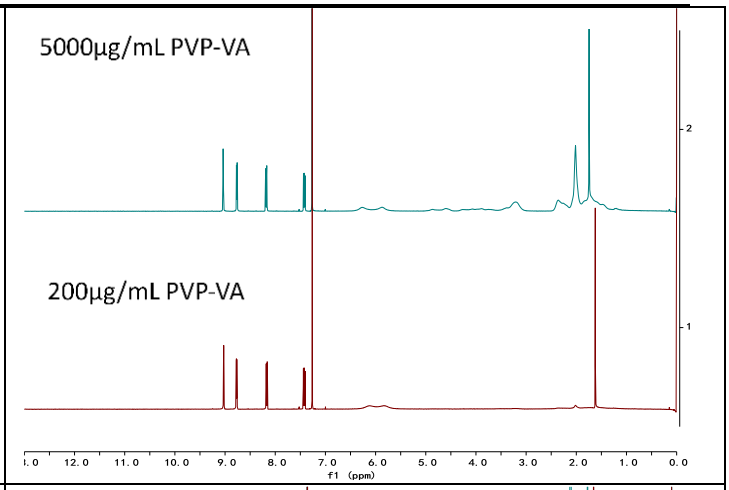
		430ug/mL NIC	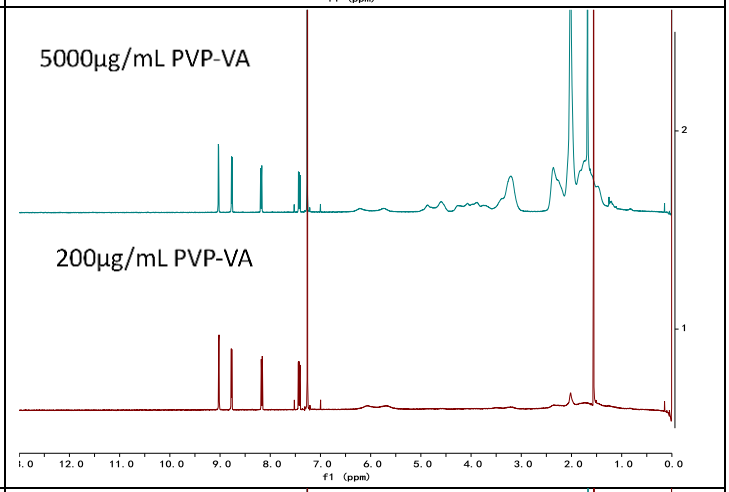
		215ug/mL NIC	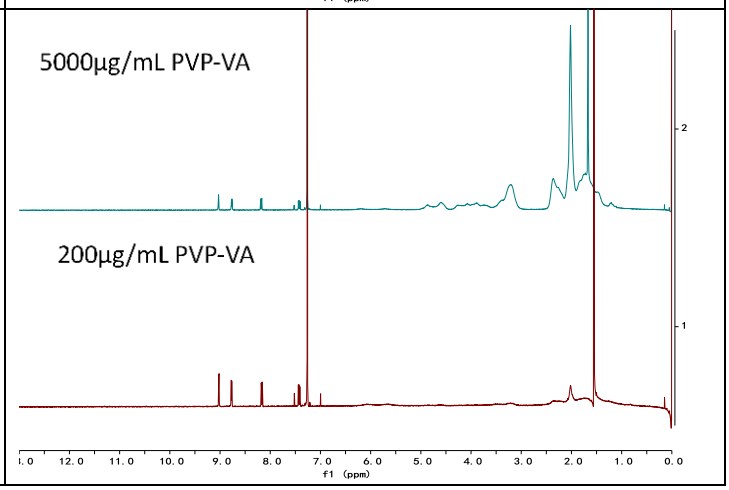

	TP/ PVP	3200ug/mL TP	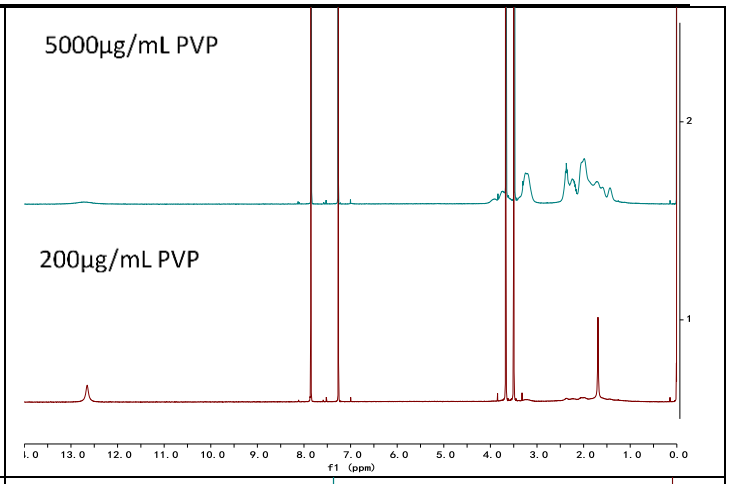
		640ug/mL TP	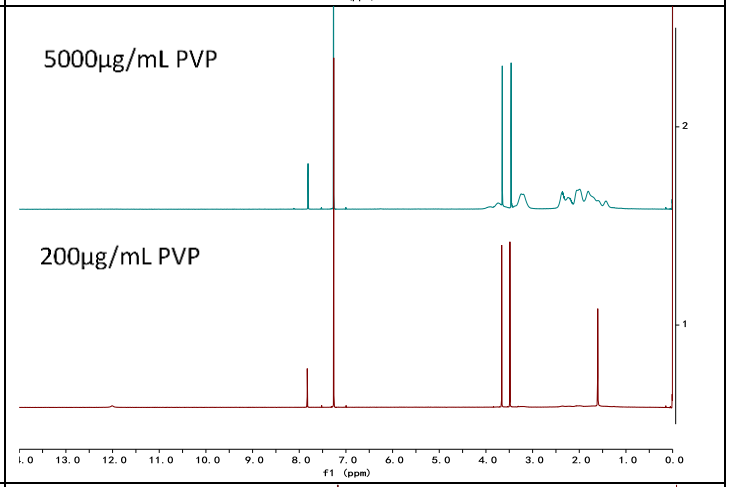
		320ug/mL TP	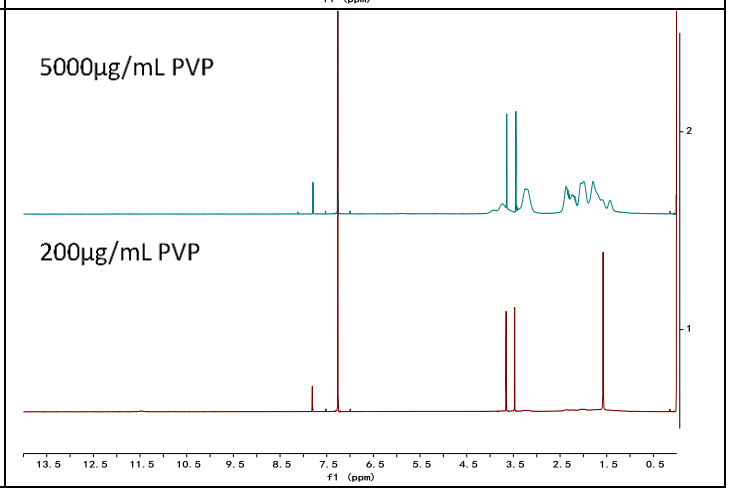

	TP/ PVP -VA	3200ug/mL TP	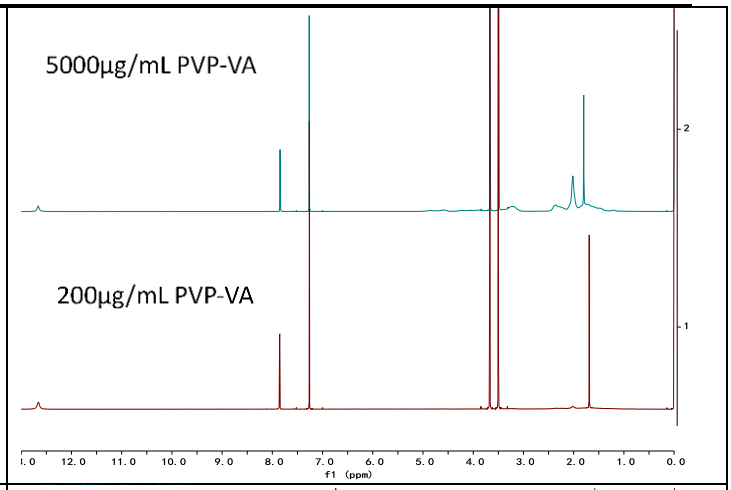
		640ug/mL TP	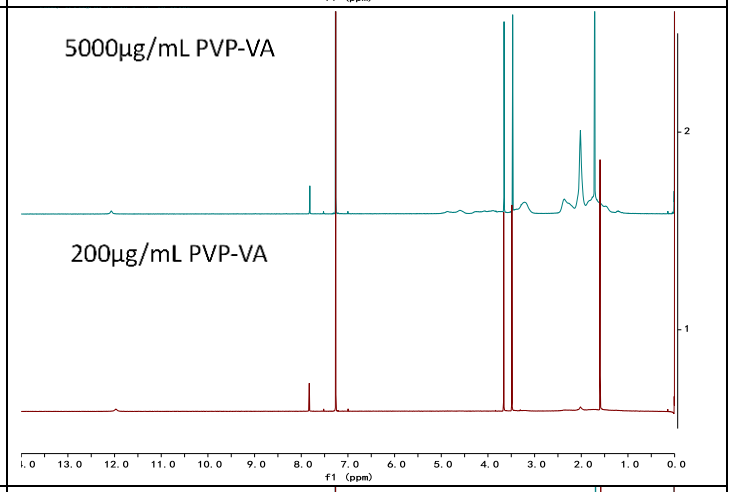
		320ug/mL TP	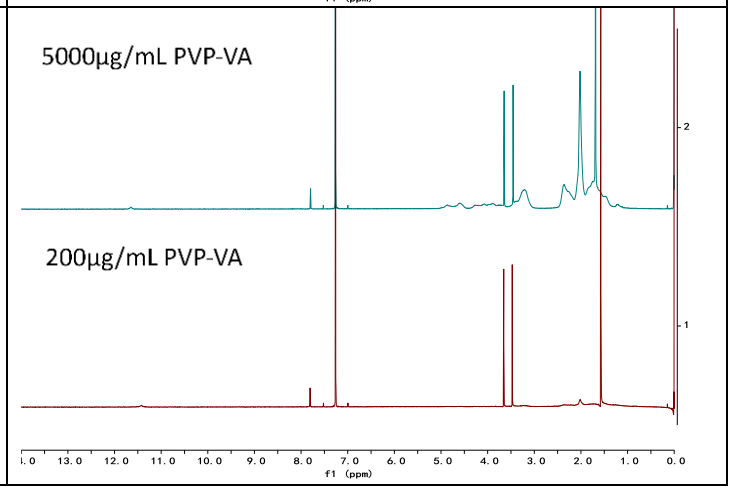

Ternary components	FFA/ NIC/ PVP	5000ug/mL FFA-NIC	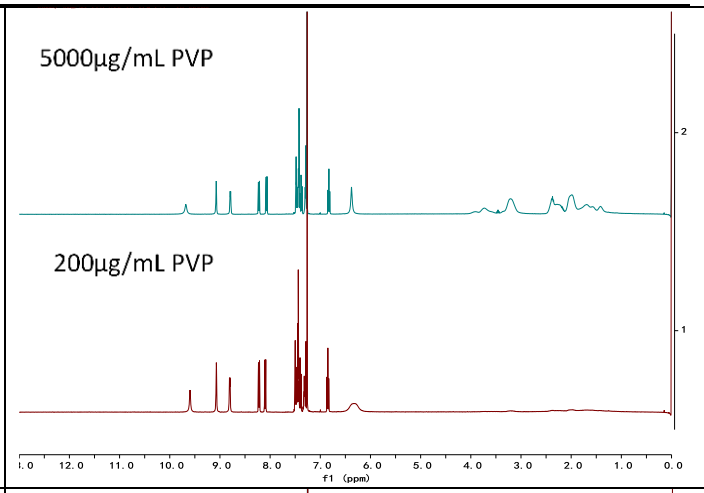
		1000ug/mL FFA-NIC	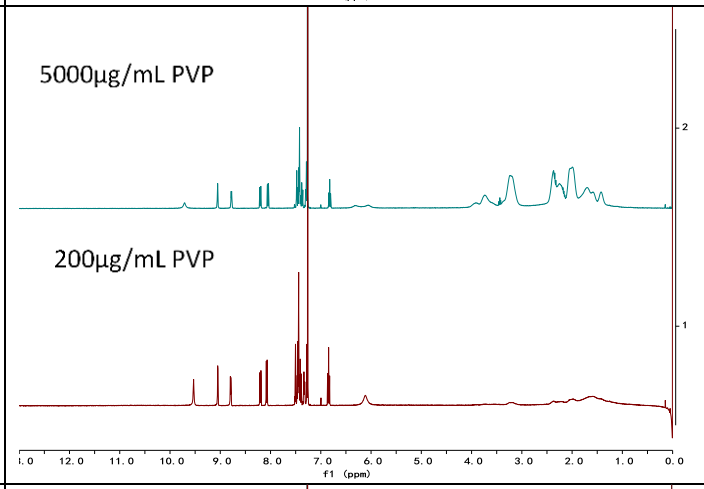
		500ug/mL FFA-NIC	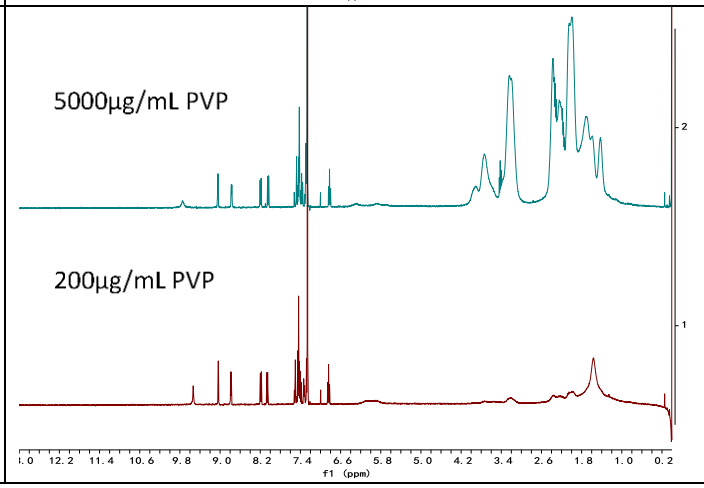

	FFA/ NIC/ PVP -VA	5000ug/mL FFA-NIC	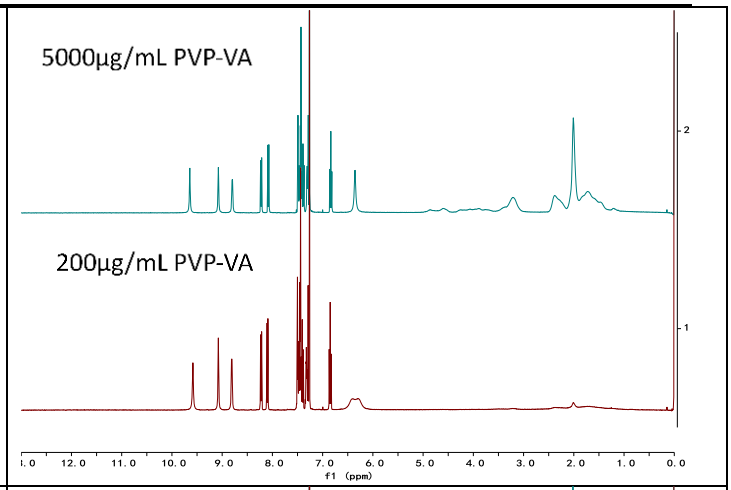
		1000ug/mL FFA-NIC	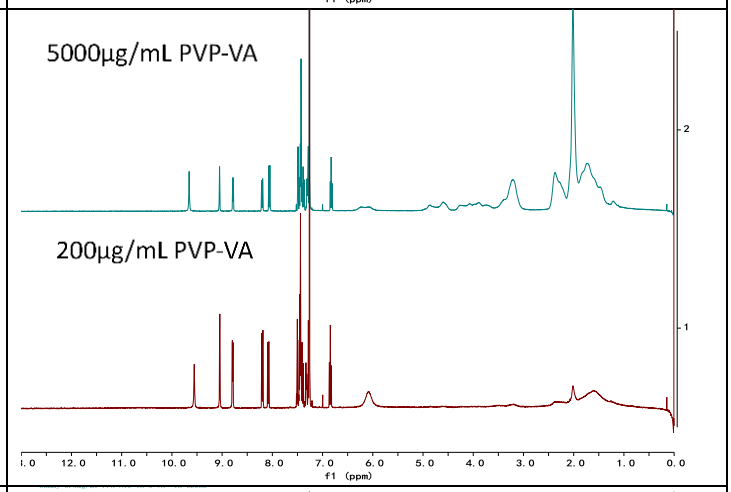
		500ug/mL FFA-NIC	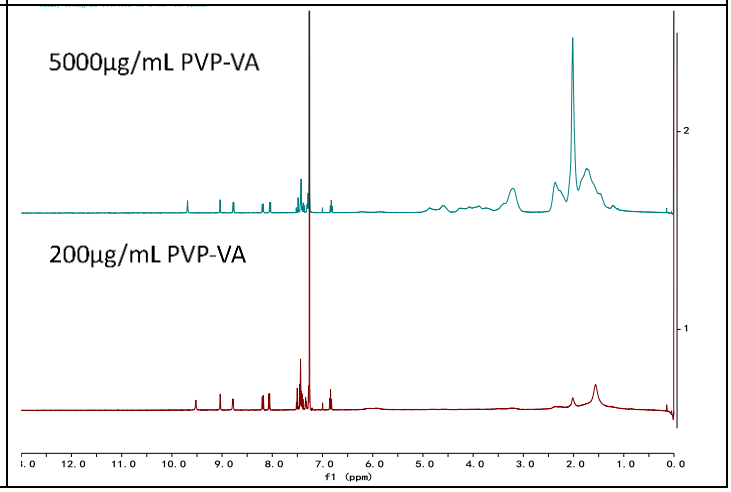

	FFA/ TP/ PVP	5000ug/mL FFA-TP	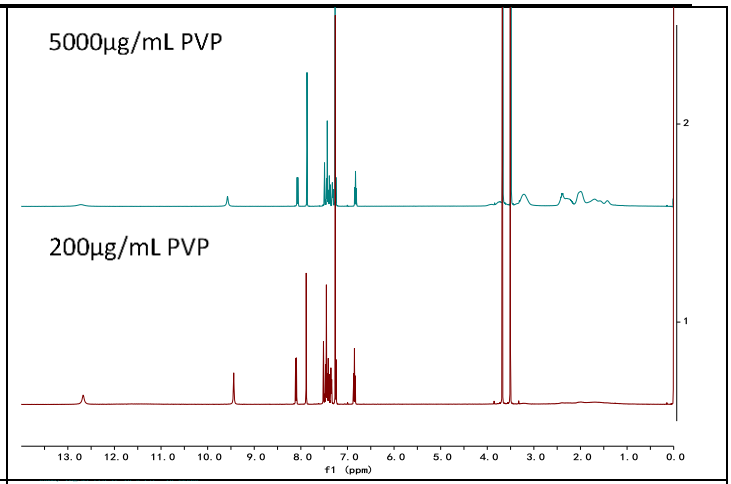
		1000ug/mL FFA-TP	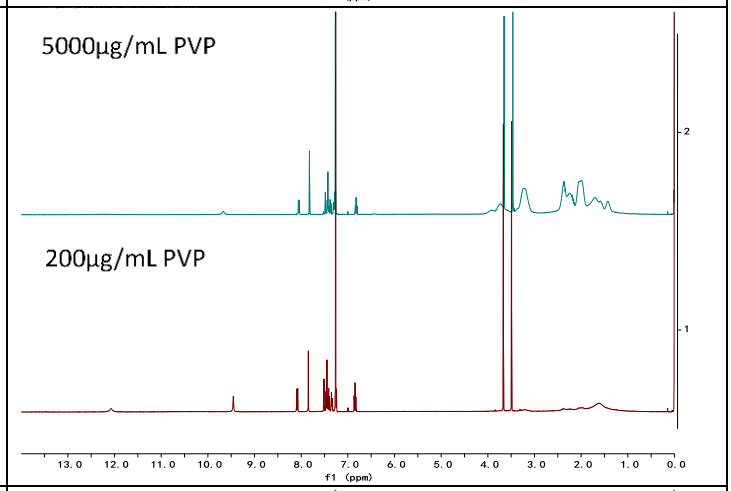
		500ug/mL FFA-TP	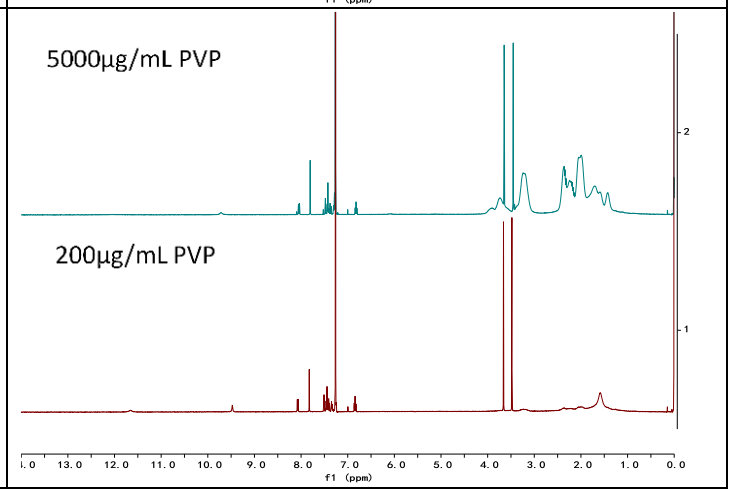

	FFA/ TP/ PVP -VA	5000ug/mL FFA-TP	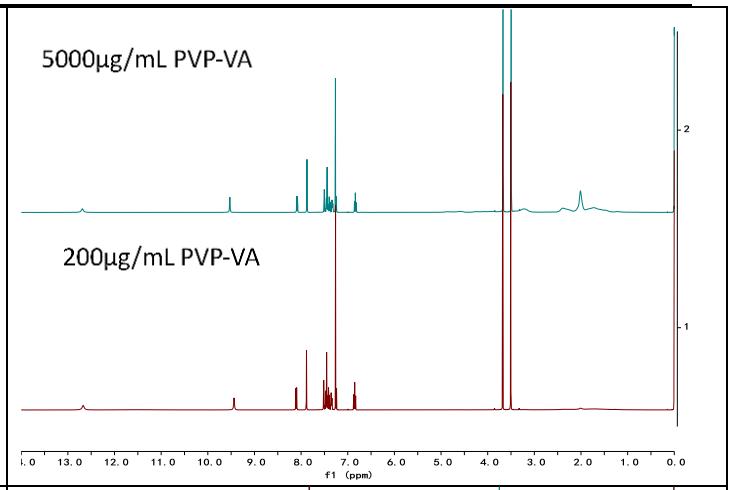
		1000ug/mL FFA-TP	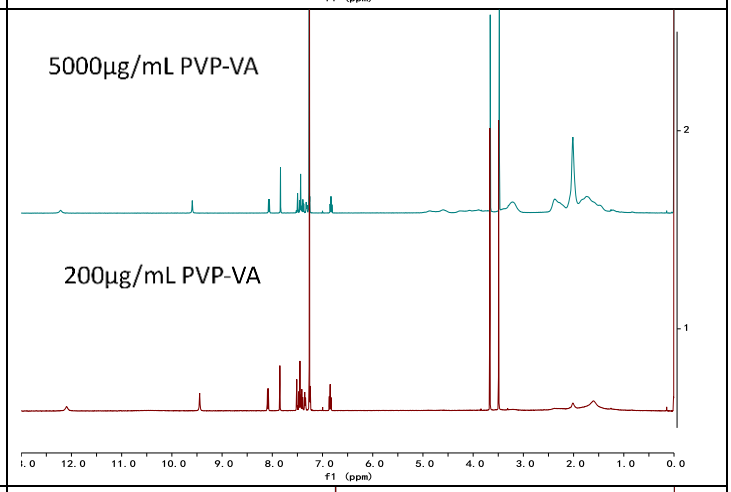
		500ug/mL FFA-TP	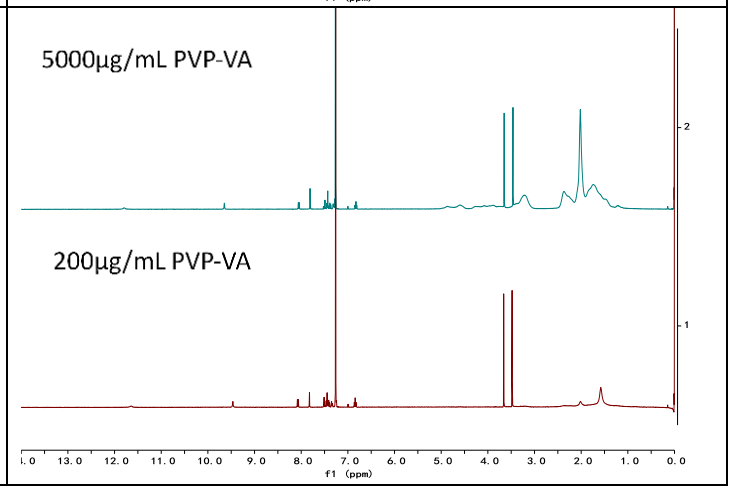

PUBLICATIONS

Journal Publications

[1] Qiu, S., et al., Role of polymers in solution and tablet-based carbamazepine cocrystal formulations. CrystEngComm, 2016. 18(15): p. 2664-2678.

[2] Guo, M., et al., Investigating the Influence of Polymers on Supersaturated Flufenamic Acid Cocrystal Solutions. Molecular Pharmaceutics, 2016. 13(9): p. 3292-3307.

[3] Guo, M., et al., Insight into Flufenamic Acid Cocrystal Dissolution in the Presence of a Polymer in Solution: from Single Crystal to Powder Dissolution. Molecular Pharmaceutics, 2017.

[4] Investigating Permeation Behavior of Flufenamic Acid Cocrystals using A Dissolution and Permeation System. Publication in preparation.

Conference Publications

[1] "Understanding the dissolution behaviors of Flufenamic acid cocrystals by investigating powder dissolution and single crystal dissolution", *4th Quality by Design Symposium,* Leicester.March 2017

[2] "Investigation of the Effect of Polymers on the Phase Transformation Flufenamic Acid Cocrystal", *4th Int. Pharm. Tech. Conference,* Leicester. November 2016.

[3] "Investigation of the Effect of Polymers on the Phase Transformation Flufenamic Acid Cocrystal", *4th Quality by Design Symposium*,Leicester. March 2016

[4] "Effects of polymers on solubility of Flufenamic acid-Nicotinamide cocrystal", *The 6th APS International PharmSci 2015*, Nottingham. March 2015.

Oral Presentations

[1] "Understanding the Effects of Polymeric Excipients on Recrystallization of Flufenamic Acid Cocrystals in solution", *East Midlands Universities Association (EMUA) postgraduate research student conference*; Loughborough University. September 2016.

[2] "Understanding the Effects of Polymeric Excipients on Recrystallization of Flufenamic Acid Cocrystals in solution", *Crystal Growth of Organic Material/ British Association of Crystal Growth 2016,* Leeds University. June 2016.

[3] "Investigating the role of polymers on solubility and dissolution rates of flufenamic acid cocrystals", *Crystal Growth of Organic Material/ British Association of Crystal Growth 2015*, Queen Mary, University of London. June 2015.

[4] "Mechanism of Flufenamic Acid Cocrystals Dissolution Behaviors in Presence of Polymers", *HLS postgraduate student conference*, De Montfort University. March 2015.